

# CONTRACTOR REPORT

SAND89-7068/1  
Unlimited Release  
UC-721

8524

RS-8232-21 70871

*dy1*

## Ground-Water Flow Modeling of the Culebra Dolomite

### Volume I: Model Calibration



8232-21/070871



00000001 -

A. M. LaVenue, T. L. Cauffman, J. F. Pickens  
INTERA Inc.  
6850 Austin Center Boulevard, Suite 300  
Austin, TX 78731

Prepared by Sandia National Laboratories Albuquerque, New Mexico 87185  
and Livermore, California 94550 for the United States Department of Energy  
under Contract DE-AC04-76DP00789

Printed October 1990

Issued by Sandia National Laboratories, operated for the United States Department of Energy by Sandia Corporation.

**NOTICE:** This report was prepared as an account of work sponsored by an agency of the United States Government. Neither the United States Government nor any agency thereof, nor any of their employees, nor any of their contractors, subcontractors, or their employees, makes any warranty, express or implied, or assumes any legal liability or responsibility for the accuracy, completeness, or usefulness of any information, apparatus, product, or process disclosed, or represents that its use would not infringe privately owned rights. Reference herein to any specific commercial product, process, or service by trade name, trademark, manufacturer, or otherwise, does not necessarily constitute or imply its endorsement, recommendation, or favoring by the United States Government, any agency thereof or any of their contractors or subcontractors. The views and opinions expressed herein do not necessarily state or reflect those of the United States Government, any agency thereof or any of their contractors.

Printed in the United States of America. This report has been reproduced directly from the best available copy.

Available to DOE and DOE contractors from  
Office of Scientific and Technical Information  
PO Box 62  
Oak Ridge, TN 37831

Prices available from (615) 576-8401, FTS 626-8401

Available to the public from  
National Technical Information Service  
US Department of Commerce  
5285 Port Royal Rd  
Springfield, VA 22161

NTIS price codes  
Printed copy: A13  
Microfiche copy: A01

SAND89-7068/1  
Unlimited Release  
Printed October 1990

Distribution  
Category UC-721

**GROUND-WATER FLOW MODELING  
OF THE CULEBRA DOLOMITE**

**VOLUME I: MODEL CALIBRATION\***

A.M. LaVenue, T.L. Cauffman, and J.F. Pickens  
INTERA Inc.  
6850 Austin Center Boulevard, Suite 300  
Austin, Texas 78731

**ABSTRACT**

This hydrogeologic modeling study has been performed as part of the regional hydrologic characterization of the Waste Isolation Pilot Plant (WIPP) site in southeastern New Mexico. The study has produced an estimation of the transmissivity and Darcy-velocity distributions in the Culebra Dolomite Member of the Permian Rustler Formation at the WIPP site. The results of this study are intended to support Sandia National Laboratories performance-assessment calculations.

The three-dimensional finite-difference code SWIFT II was employed for the numerical modeling, using a variable-fluid-density and single-porosity formulation. The spatial scale of the model, 21.3 km by 30.6 km, was chosen to allow simulation of regional-scale pumping tests conducted at the H-3 and H-11 hydropads and the WIPP-13 borehole, which are located south, southeast, and northwest, respectively, of the center of the WIPP site. The modeled area includes and extends beyond the controlled area defined by the WIPP-site boundaries.

The work performed in this study consisted of modeling the hydrogeology of the Culebra in two stages: steady-state modeling to develop the best estimate of the undisturbed head distribution (i.e., of the hydraulic conditions before excavation of the WIPP shafts, which began in 1981) and superimposed transient modeling of local hydrologic responses to excavation of the four WIPP shafts at the center of the WIPP site, as well as to various well tests. The transient modeling used the calculated steady-state freshwater heads as initial conditions.

\* The work described in this report was done for Sandia National Laboratories under Contract No. 32-1025.

The steady-state calibrated transmissivity field contains transmissivities that vary over seven orders of magnitude increasing westward toward Nash Draw. The most significant feature of the transmissivity field is a relatively high-transmissivity zone in the vicinity of wells H-17, P-17, and H-11. Modeled transmissivities within this zone are approximately  $5 \times 10^{-5} \text{ m}^2/\text{s}$ . The location of and transmissivities within the zone are similar to those proposed in a previous interim modeling report.

After calibration of the steady-state model, the major drilling and testing activities at the WIPP shafts and well locations were incorporated into the model. The transient simulation of the major hydraulic stresses in the Culebra dolomite extended from January 1, 1981 to June 16, 1989. Calibration of the model to the transient events required additional changes to the steady-state calibrated transmissivity field in order to reduce the differences between the calculated and observed transient heads. The major difference between the transient calibrated transmissivity field and the steady-state calibrated transmissivity field is the extension of the higher transmissivity zone near H-11 northward toward H-15.

The travel times for non-sorbing particles released within the steady-state flow field, using the transient calibrated model, were computed from selected locations within the model to the southern model (down-gradient) boundary. The predicted travel time from a release point within the Culebra that is coincident with the centroid of the waste panels to the southern WIPP-site boundary is  $1.4 \times 10^4$  yrs. Calculations were performed to assess the sensitivity of the above travel time to the grid-block transmissivities and the pressures assigned to the model boundaries.

## **EXECUTIVE SUMMARY**

**This hydrogeologic modeling study has been performed as part of the regional hydrologic characterization of the Waste Isolation Pilot Plant (WIPP) site in southeastern New Mexico. The study has produced an estimation of the transmissivity and Darcy-velocity distributions in the Culebra Dolomite Member of the Permian Rustler Formation at the WIPP site. The results of this study are intended to support Sandia National Laboratories performance-assessment calculations.**

**The three-dimensional finite-difference code SWIFT II was employed for the numerical modeling, using a variable-fluid-density and single-porosity formulation. The variable-fluid-density approach does not include changes in brine density within the model due to ground-water flow or due to local reactions, such as halite dissolution. The spatial scale of the model, 21.3 km by 30.6 km, was chosen to allow simulation of regional-scale pumping tests conducted at the H-3 and H-11 hydropads and the WIPP-13 borehole, which are located south, southeast, and northwest, respectively, of the center of the WIPP site. The modeled area includes and extends beyond the controlled area defined by the WIPP-site boundaries.**

**The work performed in this study consisted of modeling the hydrogeology of the Culebra in two stages: steady-state modeling to develop the best estimate of the undisturbed head distribution (i.e., of the hydraulic conditions before excavation of the WIPP shafts, which began in 1981) and superimposed transient modeling of local hydrologic responses to excavation of the four WIPP shafts at the center of the WIPP site, as well as to various well tests. Boundary conditions (prescribed constant fluid pressures and densities) were estimated using head and fluid-density data obtained from about 40 observation wells in the Culebra at and near the WIPP site. The transient modeling used calculated steady-state freshwater heads as initial conditions.**

**The initial spatial transmissivity distribution in the Culebra dolomite was obtained using the kriging code AKRIP developed at the Massachusetts Institute of Technology. The resulting transmissivity distribution contains low transmissivities ( $< 1 \times 10^{-7} \text{ m}^2/\text{s}$ )**

in the eastern model area, intermediate transmissivities ( $1 \times 10^{-6}$  to  $1 \times 10^{-4}$  m<sup>2</sup>/s) in the central part of the model area, and high transmissivities ( $> 1 \times 10^{-3}$  m<sup>2</sup>/s) in the western part of the model area representing Nash Draw. The initial steady-state model was calibrated to undisturbed head conditions so that the differences between the calculated and observed freshwater heads are consistent with the uncertainties associated with the observed heads. Calibration parameters were the prescribed-pressure boundary conditions and the transmissivities. Calibration was carried out by adding pilot points, or synthetic transmissivity data points, to the kriging data set in order to adjust the model's grid-block transmissivities. The GRASP II adjoint-sensitivity code, which processes the results from a SWIFT II flow simulation, guided the selection of locations for pilot points. The transmissivity assigned to the pilot points is based on the modeler's judgment, incorporating information on local geologic conditions and large-scale hydraulic-interference tests. Pilot points were sequentially added to the model during steady-state calibration until the differences between calculated and observed heads were consistent with the uncertainty of the observed steady-state heads.

The steady-state calibrated transmissivity field contains a relatively high-transmissivity zone in the vicinity of wells H-17, P-17, and H-11. Modeled transmissivities within this zone are approximately  $5 \times 10^{-5}$  m<sup>2</sup>/s. The location of and transmissivities within the zone are similar to those proposed in a previous interim modeling report.

After calibration of the steady-state model, the major drilling and testing activities at the WIPP shafts and well locations were incorporated into the model using the calculated steady-state heads as initial conditions for the transient simulation: (1) a simplified but complete shaft history since 1981, including the recent excavation of the air-intake shaft; (2) three pumping tests, bailing activities, and water-quality-sampling activities at the H-2 hydropad between 1981 and 1987; (3) the H-3 convergent-flow tracer test in 1984; (4) the H-3 step-drawdown test in 1985; (5) the H-3 multipad pumping test in 1985 and 1986; (6) the convergent-flow tracer test at the H-4 hydropad between 1982 and 1984; (7) the WIPP-13 multipad pumping test in 1987; (8) the H-11

multipad pumping test in 1988; (9) the water-quality-sampling activities at WIPP-19; and (10) the P-14 pumping test in 1989. The transient simulation of the above hydraulic stresses in the Culebra dolomite extended from January 1, 1981 to June 16, 1989.

Calibration of the model to the transient events required additional pilot points to be added to the steady-state calibrated transmissivity field in order to reduce the differences between the calculated and observed transient heads. The major difference between the transient calibrated transmissivity field and the steady-state calibrated transmissivity field is the extension of the higher transmissivity zone near H-11 northward toward H-15. The northerly extension was needed to reproduce the observed response at H-15 to pumping at H-11. Other smaller changes to the transmissivity field were also needed to calibrate the model to the other transient events included in the transient simulation.

The final calibrated transmissivity field, referred to as the transient calibrated transmissivities, reproduces the observed transient responses generated from the shaft events and the pumping tests used in the simulation reasonably well. However, the calculated drawdowns due to the excavation of the air-intake shaft (AIS) were generally less than the drawdowns observed at the H-1, WIPP-21, WIPP-22, and ERDA-9 boreholes. Sensitivity analyses to determine the effects of the shaft leakage indicated that the drawdowns at these boreholes are significantly improved after increasing the estimate of the leakage from the AIS by 50 percent (i.e., 0.05 L/s to 0.08 L/s). The minimum differences between the calculated and observed transient heads at these locations result when leakage from the AIS is increased by 50 percent and leakage from the exhaust shaft (EXS) is equal to 0.012 L/s from 1987 to mid-1989 (i.e., end of simulation time). These sensitivity calculations not only suggest a small amount of additional leakage from the AIS but also that leakage may be continuing at the EXS, the waste-handling shaft (WHS), the construction and salt handling (C&SH) shaft or a combination of all three since 1987. However, in the absence of actual observed leakage at either the EXS, WHS, or C&SH shaft, the proposed leakage at these locations can only be hypothesized.

Additional calculations were performed using GRASP II to determine the sensitivity of the calculated pressures to changes in the grid-block transmissivities and the pressures

assigned to the model boundaries. The results determined in these sensitivity calculations indicate that calculated pressures within the WIPP-site boundary are most sensitive to the specified boundary pressures and the grid-block transmissivities in the northwest region. However, the extent of data coverage and the magnitude of data uncertainty within the model restrict the flexibility one has in changing the transmissivities and specified boundary pressures in the northwest part of the model area. That is, even though the model is sensitive to the parameters in the northwest model region, the calibration to the steady-state heads in this area would be degraded if significant changes to either the transmissivities or boundary pressures were implemented.

The travel times for non-sorbing particles released within the steady-state flow field were computed from selected locations within the model to the southern model (down-gradient) boundary. By definition, the particle travel times are calculated using model-calculated Darcy velocities and an assumed matrix porosity of 16 percent. The predicted travel time from a release point within the Culebra that is coincident with the centroid of the waste panels to the southern WIPP-site boundary is  $1.4 \times 10^4$  yrs. GRASP II calculations were performed to assess the sensitivity of the above travel time to the grid-block transmissivities and the pressures assigned to the model boundaries. The highest sensitivities to the grid-block transmissivities occur along the ground-water travel path within the WIPP-site boundary. The maximum sensitivity value lies approximately 800 m east of the H-3 borehole. If the transmissivities specifically along the travel path are uniformly increased by 25 percent, which is reasonable given the uncertainty of the central transmissivities, the travel time to the southern WIPP-site boundary is predicted to decrease by 18 percent, or 2500 yrs, to  $1.16 \times 10^4$  yrs. Conversely, if the transmissivities along the travel path were uniformly decreased by 25 percent, the travel time is predicted to increase by 2500 yrs to  $1.66 \times 10^4$  yrs. However, the uncertainties associated with the transmissivities within this central part of the WIPP-site area are less than those within the northwest model region due to the higher number of observed transmissivity values from nearby boreholes and the calibration to H-3 and H-11 multipad pumping-test responses.

The sensitivities of the travel time to changes in the pressures assigned to the boundaries indicate that the travel time is most sensitive to the pressures assigned in



the northwest region of the model where, as previously mentioned, a significant flux of ground water enters the modeled system. An increase in the pressure assigned to this portion of the western boundary would increase the volume of ground water entering the system and the hydraulic gradient within the system. The increased gradient would reduce the travel time to the southern WIPP-site boundary. Increasing the pressure in the grid block with the highest sensitivity by 10 percent is predicted to result in a 2.3 percent decrease (approximately 325 yrs) in the predicted travel time to  $1.38 \times 10^4$  yrs. As mentioned above, however, changes to the northwest boundary pressures are restricted because of the head data in the northwest region.

The modeling study discussed in this report is based on the transmissivity data and freshwater-head data available as of June 1989. This study represents the culmination of more than one decade of data acquisition, data interpretation, and subsequent model simulation for the purpose of developing a comprehensive characterization of the regional hydrogeology of the Culebra dolomite of the Rustler Formation at the WIPP site. This characterization is intended to allow a thorough and well documented assessment of the Culebra flow system.

# CONTENTS

1.0	INTRODUCTION .....	1-1
1.1	Review of Model Calibration Techniques .....	1-2
1.2	General Approach Used in Present Study .....	1-4
1.2.1	The AKRIP Code.....	1-4
1.2.2	The SWIFT II Code .....	1-5
1.2.3	The GRASP II Code .....	1-5
2.0	SITE DESCRIPTION AND MODEL CONCEPTUALIZATION .....	2-1
2.1	Site Description .....	2-1
2.1.1	General .....	2-1
2.1.2	Stratigraphy .....	2-1
2.1.3	Regional Hydrogeology .....	2-4
2.1.4	Regional Dissolution in the Rustler Formation .....	2-7
2.2	Modeling History .....	2-12
2.3	Model Conceptualization .....	2-15
2.3.1	Data Base .....	2-16
2.3.2	Model Area .....	2-17
2.3.3	Model-Grid Description .....	2-19
2.3.4	Physical Model Constants .....	2-23
2.3.5	Transmissivity of the Culebra Dolomite .....	2-26
2.3.5.1	Data Base .....	2-26
2.3.5.2	Uncertainty of the Transmissivity Data .....	2-29
2.3.5.3	Estimation of Transmissivity Over the Model Region.....	2-29
2.3.6	Storativity of the Culebra Dolomite .....	2-32
2.3.6.1	Data Base .....	2-32
2.3.6.2	Model Storativity .....	2-36
2.3.7	Freshwater Heads in the Culebra Dolomite .....	2-37
2.3.7.1	Data Base .....	2-37
2.3.7.2	Estimation of the Undisturbed Hydrologic Conditions Over the Modeled Region .....	2-38
2.3.7.3	Hydraulic Stresses Since 1981 .....	2-43
2.3.7.4	Initial Boundary Conditions .....	2-43

## CONTENTS (Continued)

2.3.8	Formation-Fluid Densities .....	2-44
2.3.8.1	Data Base .....	2-44
2.3.8.2	Estimation of Formation-Fluid Densities Over the Modeled Region .....	2-46
3.0	SIMULATION OF FLOW UNDER UNDISTURBED HYDROLOGIC CONDITIONS (PRE-SHAFT) .....	3-1
3.1	Initial Parameter Values .....	3-1
3.2	Initial Steady-State Simulation .....	3-2
3.3	Calibration of the Steady-State Model .....	3-9
3.3.1	General Approach .....	3-9
3.3.2	Calibration of the Northern Model Area .....	3-12
3.3.3	Calibration of the Southwestern and Southeastern Model Areas .....	3-17
3.3.4	Calibration of the Central Model Area .....	3-21
3.3.5	The Steady-State Calibrated Transmissivity Field .....	3-27
3.3.6	The Calibrated Steady-State Heads .....	3-31
3.3.7	Calculated Particle Travel Times in the Model Region .....	3-39
4.0	EVENTS USED IN THE TRANSIENT SIMULATIONS .....	4-1
4.1	Simulation of the Shaft Histories .....	4-1
4.2	Simulation of Well Tests .....	4-11
4.2.1	Well Tests at the H-2 Hydropad .....	4-13
4.2.2	Well Tests at the H-3 Hydropad .....	4-16
4.2.2.1	Convergent-Flow Tracer Test at the H-3 Hydropad .....	4-16
4.2.2.2	Step-Drawdown Test at the H-3 Hydropad .....	4-16
4.2.2.3	H-3 Multipad Pumping Test .....	4-17
4.2.2.4	Water-Quality Sampling at the H-3 Hydropad .....	4-17
4.2.3	Convergent-Flow Tracer Test at the H-4 Hydropad .....	4-17
4.2.4	WIPP-13 Multipad Pumping Test .....	4-18
4.2.5	H-11 Multipad Pumping Test .....	4-18
4.2.6	Water-Quality Sampling at the WIPP-19 Borehole .....	4-18

## **CONTENTS (Continued)**

4.2.7	P-14 Pumping Test .....	4-19
5.0	<b>SIMULATION OF TRANSIENT RESPONSES RESULTING FROM SHAFT ACTIVITIES AND WELL TESTS .....</b>	<b>5-1</b>
5.1	Initial Transient Simulation Using the Steady-State Calibrated Model ..	5-2
5.2	Calibration to Transient Events .....	5-11
5.2.1	General Approach .....	5-11
5.2.2	Calibration to Shaft Leakage Rates .....	5-16
5.2.3	Calibration to the Well Tests at the H-3 Hydropad .....	5-23
5.2.4	Calibration to the H-11 Multipad Pumping Test .....	5-27
5.2.5	Calibration to the WIPP-13 Multipad Pumping Test .....	5-31
5.2.6	Calibration to the Excavation of the Air-Intake Shaft .....	5-39
5.2.7	Calibration to the P-14 Pumping Test .....	5-44
5.2.8	Calibration to Other Tests .....	5-48
5.3	The Transient Calibrated Heads .....	5-48
5.4	The Transient Calibrated Transmissivity Field .....	5-65
5.5	Calculated Particle Travel Times in the Model Region .....	5-72
6.0	<b>SENSITIVITY OF THE TRANSIENT CALIBRATED MODEL .....</b>	<b>6-1</b>
6.1	Sensitivity of Calculated Pressures to Model Transmissivities .....	6-1
6.2	Sensitivity of Calculated Pressures to Model Boundary Pressures.....	6-8
6.3	Sensitivity of the Predicted Ground-Water Travel Time .....	6-14
6.4	Sensitivity of the Calculated Pressures at Central WIPP-Site Boreholes to Shaft-Leakage Rates .....	6-20
6.5	Sensitivity of the Model Results to the Calibration Approach .....	6-25
7.0	<b>CONCLUSIONS .....</b>	<b>7-1</b>
8.0	<b>REFERENCES .....</b>	<b>8-1</b>

## FIGURES

1.1	Flow Chart Representing Adjoint-Sensitivity and Kriging Approach to Model Calibration .....	1-8
2.1	Geologic Column Representative of WIPP Area .....	2-2
2.2	WIPP Area .....	2-5
2.3	The Occurrence of Halite Beds Within the Rustler Formation .....	2-9
2.4	Stratigraphic Cross Section of the Rustler Formation West to East Across the WIPP Site .....	2-10
2.5	Approximate Boundaries of Ground-Water Flow Models in the WIPP Region .....	2-13
2.6	WIPP-Area and Model Boundaries.....	2-18
2.7a	WIPP-Area Boreholes and Model Grid .....	2-20
2.7b	Model Grid in the Central Model Region Showing Shaft and Borehole Locations .....	2-22
2.8	Center-of-Culebra Elevations in the Model Area .....	2-24
2.9	Culebra Log <sub>10</sub> Transmissivities at the WIPP-Area Boreholes .....	2-27
2.10a	Initial Kriged Log <sub>10</sub> Transmissivity Field.....	2-33
2.10b	Initial Standard Deviations of the Estimation Errors of Log <sub>10</sub> Transmissivity .....	2-34
2.11	Culebra Freshwater Heads at the WIPP-Area Boreholes.....	2-41
2.12	Culebra Freshwater-Head Contour Surface .....	2-42
2.13	Kriged Formation-Fluid Densities Used in Model .....	2-47
3.1	The Calculated Freshwater Heads of the Initial Simulation (Using AKRIP Initial Transmissivities and the Initial Boundary Conditions) .....	3-6
3.2	The Differences Between the Calculated and the Observed Freshwater Heads of the Initial Simulation.....	3-7
3.3	Pilot-Point Grid Used to Calibrate Northern Model Area .....	3-14
3.4	Normalized Sensitivities of Northern Borehole Pressure Differences to Changes in Transmissivities at Potential Pilot-Point Locations.....	3-15
3.5	Sensitivities of Southwestern Borehole Pressure Differences to Changes in Model Boundary Pressures .....	3-18

## FIGURES (Continued)

3.6	Normalized Sensitivities of Southwestern Borehole Pressure Differences to Changes in Transmissivities at Potential Pilot-Point Locations.....	3-19
3.7	Normalized Sensitivities of Central and Southern Borehole Pressure Differences to Changes in Transmissivities at Potential Pilot-Point Locations .....	3-22
3.8a	Normalized Sensitivities of Central Borehole Pressure Differences to Changes in Transmissivities at Potential Pilot-Point Locations.....	3-25
3.8b	Normalized Sensitivities of Central Borehole Pressure Differences After Adding Pair of Pilot-Points Near H-1 .....	3-26
3.8c	Normalized Sensitivities of Pressure Differences at the H-3, H-18, WIPP-13, and P-14 Boreholes to Changes in Transmissivities at Potential Pilot-Point Locations.....	3-28
3.9a	The Steady-State Calibrated Log <sub>10</sub> Transmissivities .....	3-29
3.9b	Steady-State Calibrated Log <sub>10</sub> Transmissivities Within the WIPP-Site Boundary .....	3-30
3.9c	Log <sub>10</sub> Transmissivity Differences Between Steady-State Calibrated and Initial Transmissivity Fields.....	3-32
3.10	Freshwater Heads of the Steady-State Calibrated Model.....	3-37
3.11	Darcy-Velocity Vectors of the Steady-State Calibrated Model.....	3-40
3.12	Calculated Particle Travel Paths and Travel Times in the Steady-State Calibrated Model .....	3-43
4.1	Characterization of the Skin Region Surrounding a Well.....	4-8
4.2	Concept of Skin Thickness for a Cartesian Grid Block.....	4-10
5.1a	Calculated and Observed Transient Freshwater Heads at H-1, H-2, and H-3 Using the Steady-State Calibrated Transmissivity Field .....	5-4
5.1b	Calculated and Observed Transient Freshwater Heads at H-4, H-6, and H-11 Using the Steady-State Calibrated Transmissivity Field.....	5-5

## FIGURES (Continued)

5.1c	Calculated and Observed Transient Freshwater Heads at H-14, H-15, and H-17 Using the Steady-State Calibrated Transmissivity Field.....	5-6
5.1d	Calculated and Observed Transient Freshwater Heads at DOE-1, DOE-2, and P-17 Using the Steady-State Calibrated Transmissivity Field.....	5-7
5.1e	Calculated and Observed Transient Freshwater Heads at WIPP-12, WIPP-13, and WIPP-18 Using the Steady-State Calibrated Transmissivity Field.....	5-8
5.1f	Calculated and Observed Transient Freshwater Heads at WIPP-19, WIPP-21, and WIPP-22 Using the Steady-State Calibrated Transmissivity Field.....	5-9
5.1g	Calculated and Observed Transient Freshwater Heads at WIPP-30, CB-1, and ERDA-9 Using the Steady-State Calibrated Transmissivity Field.....	5-10
5.2a	Calculated and Observed Leakage Rates at the C&SH and WHS Locations Used in the Initial Transient Simulation .....	5-12
5.2b	Calculated and Observed Leakage Rates at the EXS and AIS Locations Used in the Initial Transient Simulation .....	5-13
5.3a	Calculated and Observed Leakage Rates at the C&SH and WHS Locations After Calibrating to Observed Leakage .....	5-17
5.3b	Calculated and Observed Leakage Rates at the EXS and AIS Locations After Calibrating to Observed Leakage .....	5-18
5.4a	Calculated and Observed Transient Freshwater Heads at H-1, H-2, and H-3 After Calibrating to Observed Shaft Leakage .....	5-21
5.4b	Calculated and Observed Transient Freshwater Heads at WIPP-19, WIPP-21, and WIPP-22 After Calibrating to Observed Shaft Leakage .....	5-22
5.4c	Calculated and Observed Transient Freshwater Heads at H-11 and DOE-1 After Calibrating to Observed Shaft Leakage.....	5-24
5.5a	Normalized Sensitivities of H-3 Transient-Pressure Performance Measure to Changes in Transmissivities at Potential Pilot-Point Locations .....	5-25
5.5b	Calculated and Observed Transient Freshwater Heads at H-3 After Calibrating to the H-3 Well Tests.....	5-26

## FIGURES (Continued)

5.6a	Calculated and Observed Transient Freshwater Heads at H-14, H-15, and H-17 After Calibrating to the H-3 Well Tests.....	5-28
5.6b	Calculated and Observed Transient Freshwater Heads at DOE-1, P-17, and CB-1 After Calibrating to the H-3 Well Tests.....	5-29
5.7	Normalized Sensitivities of H-15 and DOE-1 Transient-Pressure Performance Measure to Changes in Transmissivities at Potential Pilot-Point Locations.....	5-30
5.8	Calculated and Observed Transient Freshwater Heads at H-11, H-15, and DOE-1 After Calibrating to the H-11 Multipad Pumping Test.....	5-32
5.9	Normalized Sensitivities of P-17 and CB-1 Transient-Pressure Performance Measure to Changes in Transmissivities at Potential Pilot-Point Locations.....	5-33
5.10a	Normalized Sensitivities of WIPP-12, WIPP-13, and WIPP-18 Transient-Pressure Performance Measure to Changes in Transmissivities at Potential Pilot-Point Locations.....	5-36
5.10b	Calculated and Observed Transient Freshwater Heads at WIPP-12, WIPP-13, and WIPP-18 After Adding Pilot Points near WIPP-13 .....	5-37
5.11	Normalized Sensitivities of Central Boreholes Steady-State Performance Measure to Changes in Transmissivities at Potential Pilot-Point Locations.....	5-38
5.12	Normalized Sensitivities of WIPP-30, WIPP-13, DOE-2, and H-6 Transient-Pressure Performance Measure to Changes in Transmissivities at Potential Pilot-Point Locations.....	5-40
5.13	Calculated and Observed Transient Freshwater Heads at H-6, DOE-2, and WIPP-30 After Calibrating to the WIPP-13 Multipad Pumping Test .....	5-41
5.14a	Calculated and Observed Transient Freshwater Heads at H-1, WIPP-21, and ERDA-9 After Calibrating to the WIPP-13 Multipad Pumping Test .....	5-42
5.14b	Calculated and Observed Transient Freshwater Heads at WIPP-19, H-2, and WIPP-22 After Calibrating to the WIPP-13 Multipad Pumping Test .....	5-43



## FIGURES (Continued)

5.15	Normalized Sensitivities of WIPP-21 Transient-Pressure Performance Measure to Changes in Transmissivities at Potential Pilot-Point Locations .....	5-45
5.16	Calculated and Observed Transient Freshwater Heads at WIPP-19 and ERDA-9 After Adding Pilot Points Between AIS and WIPP-21 .....	5-46
5.17	Calculated and Observed Transient Freshwater Heads at WIPP-19 After Adding Pilot Point West of WIPP-12 .....	5-47
5.18a	Calculated and Observed Transient Freshwater Heads at H-1, H-2, and H-3 Using the Transient Calibrated Transmissivity Field .....	5-49
5.18b	Calculated and Observed Transient Freshwater Heads at H-4, H-6, and H-11 Using the Transient Calibrated Transmissivity Field .....	5-50
5.18c	Calculated and Observed Transient Freshwater Heads at H-14, H-15, and H-17 Using the Transient Calibrated Transmissivity Field.....	5-51
5.18d	Calculated and Observed Transient Freshwater Heads at DOE-1, DOE-2, and P-14 Using the Transient Calibrated Transmissivity Field .....	5-52
5.18e	Calculated and Observed Transient Freshwater Heads at P-17, WIPP-12, and WIPP-13 Using the Transient Calibrated Transmissivity Field .....	5-53
5.18f	Calculated and Observed Transient Freshwater Heads at WIPP-18, WIPP-19, and WIPP-21 Using the Transient Calibrated Transmissivity Field.....	5-54
5.18g	Calculated and Observed Transient Freshwater Heads at WIPP-22, WIPP-25, and WIPP-30 Using the Transient Calibrated Transmissivity Field.....	5-55
5.18h	Calculated and Observed Transient Freshwater Heads at CB-1 and ERDA-9 Using the Transient Calibrated Transmissivity Field .....	5-56
5.19a	Calculated and Observed Leakage Rates at the C&SH and WHS Locations of the Transient Calibrated Model .....	5-57
5.19b	Calculated and Observed Leakage Rates at the EXS and AIS Locations of the Transient Calibrated Model .....	5-58
5.20	Freshwater Heads of the Transient Calibrated Model.....	5-60
5.21	Darcy-Velocity Vectors of the Transient Calibrated Model.....	5-61

## FIGURES (Continued)

5.22a	The Transient Calibrated Log <sub>10</sub> Transmissivities .....	5-67
5.22b	Transient Calibrated Log <sub>10</sub> Transmissivities Within the WIPP-Site Boundary .....	5-68
5.22c	Log <sub>10</sub> Transmissivity Differences Between the Transient Calibrated and Steady-State Calibrated Transmissivity Fields.....	5-69
5.23	Differences Between the Standard Deviations of the Initial and Transient Calibrated Kriged Log <sub>10</sub> Transmissivity Estimation Errors .....	5-71
5.24	Calculated Particle Travel Paths and Travel Times in the Transient Calibrated Model .....	5-73
5.25	Comparison of Particle Travel Paths Through the Steady-State Calibrated and Transient Calibrated Transmissivity Fields .....	5-75
6.1	Steady-State Pressures at Grid-Block Elevation for the Transient Calibrated Model.....	6-3
6.2	Dimensionless Sensitivities of the Sum of the Northwest Borehole Pressures at Grid-Block Elevation to Grid-Block Transmissivities.....	6-4
6.3	Dimensionless Sensitivities of the Sum of the Southern Borehole Pressures at Grid-Block Elevation to Grid-Block Transmissivities.....	6-6
6.4	Dimensionless Sensitivities of the Sum of the WIPP-Area Borehole Pressures at Grid-Block Elevation to Grid-Block Transmissivities.....	6-7
6.5	Dimensionless Sensitivities of the Sum of the Northwest Borehole Pressures at Grid-Block Elevation to Boundary Pressures .....	6-9
6.6	Dimensionless Sensitivities of the Sum of the Southern Borehole Pressures at Grid-Block Elevation to Boundary Pressures .....	6-11
6.7	Dimensionless Sensitivities of the Sum of the WIPP-Area Borehole Pressures at Grid-Block Elevation to Boundary Pressures .....	6-12
6.8	Dimensionless Sensitivities of Particle Travel Time to Grid-Block Transmissivities .....	6-16
6.9	Dimensionless Sensitivities in the Central Model Region of Particle Travel Time to Grid-Block Transmissivities.....	6-17
6.10	Dimensionless Sensitivities of Particle Travel Time to Boundary Pressures.....	6-19

## **FIGURES (Continued)**

6.11a	Calculated and Observed Transient Freshwater Heads at WIPP-21 and ERDA-9 and Increased Leakage Rate at the AIS Location .....	6-22
6.11b	Calculated and Observed Transient Freshwater Heads at H-1, WIPP-19, and WIPP-22 Using Increased AIS Leakage .....	6-23
6.12	Increased Leakage Rates at the EXS and AIS Locations .....	6-24
6.13a	Calculated and Observed Transient Freshwater Heads at H-1, WIPP-21, and ERDA-9 Using Increased AIS and EXS Leakage.....	6-26
6.13b	Calculated and Observed Transient Freshwater Heads at WIPP-19 and WIPP-22 Using Increased AIS and EXS Leakage.....	6-27

## TABLES

2.1	Summary of Modeling Investigations of the Rustler Formation or Culebra Dolomite Member in the WIPP-Site Region.....	2-14
2.2	Coordinates and Dimensions of the Model Area and the Grid Blocks.....	2-21
2.3	Physical Model Constants.....	2-25
2.4	Culebra Transmissivities and Their Uncertainties at the WIPP-Area Boreholes.....	2-28
2.5	Culebra Storativity at the WIPP-Area Boreholes .....	2-35
2.6	Culebra Undisturbed Equivalent Freshwater Heads and the Associated Uncertainties .....	2-39
2.7	Culebra Formation-Fluid Densities at the WIPP-Area Boreholes .....	2-45
3.1	Boundary Conditions for the Initial Simulation.....	3-3
3.2	Differences Between Calculated and Observed Freshwater Heads for the Initial Simulation .....	3-8
3.3	Differences Between Calculated and Observed Freshwater Heads After Steady-State Calibration of the Northern Model Area.....	3-16
3.4	Differences Between Calculated and Observed Freshwater Heads After Steady-State Calibration of the Southwestern Model Area.....	3-20
3.5	Differences Between Calculated and Observed Freshwater Heads After Adding a Pilot Point Between the P-17 and H-17 Boreholes.....	3-23
3.6	Final Boundary Conditions for the Model .....	3-33
3.7	Differences Between the Calculated and Observed Freshwater Heads for the Steady-State Calibrated Model .....	3-38
4.1	Abridged Shaft Events.....	4-2
4.2	Measured Leakage Rates at the WIPP Shafts.....	4-3
4.3	Initial Well Indices Assigned to Shafts.....	4-12
4.4	Initial Well Indices Assigned to Pumping Wells.....	4-14
5.1	Hydrogeologic Tests and Shaft Events Used in the Transient Simulations .....	5-3

## **TABLES (Continued)**

<b>5.2</b>	<b>Calibrated Well Indices to Shaft Leakage .....</b>	<b>5-19</b>
<b>5.3</b>	<b>Differences Between Calculated and Observed Freshwater Heads for the Transient Calibrated Model.....</b>	<b>5-62</b>
<b>5.4</b>	<b>Differences Between Calculated and Adjusted Undisturbed Freshwater Heads of the Central WIPP-Site Boreholes .....</b>	<b>5-64</b>
<b>5.5</b>	<b>Revised Undisturbed Freshwater Heads and the Differences Between the Model-Calculated and Revised Undisturbed Freshwater Heads.....</b>	<b>5-66</b>

## 1.0 INTRODUCTION

Regional site-characterization efforts have been conducted at the Waste Isolation Pilot Plant (WIPP), a U.S. Department of Energy facility in southeastern New Mexico, as part of the evaluation of the suitability of the bedded salt in the Salado Formation for isolation of defense transuranic wastes. The Culebra Dolomite Member of the Rustler Formation is the most transmissive, laterally-continuous, hydrogeologic unit above the Salado Formation and is considered to be the principal pathway for radionuclide transport in the subsurface, should an accidental breach of the repository occur. This report presents the approach to and results of development of a calibrated ground-water model for the Culebra dolomite on a regional scale (21.3 x 30.6 km) around the WIPP site. A companion report, Cauffman et al. (1990), presents and discusses the data base used in this model. This work was performed by INTERA Inc. under contract to Sandia National Laboratories (SNL). SNL is coordinating the site-characterization, experimental, and performance-assessment studies on behalf of the Department of Energy.

The objectives of this report are to:

- Summarize the hydrogeologic data base for the Culebra at the WIPP site (including Culebra elevations, transmissivities, storativities, formation-fluid densities, undisturbed equivalent freshwater heads, and hydrologic stresses and equivalent freshwater heads during the period 1981 to June 1989)
- Outline the calibration approach and steps to obtain a ground-water flow model of the Culebra dolomite calibrated to both undisturbed and transient head distributions
- Define flow paths and particle travel times within the modeled region using a particle-tracking code in conjunction with the Darcy-velocity distribution calculated for the calibrated Culebra flow model
- Perform a sensitivity analyses to determine the potential changes in the model calculated results for selected changes in various model parameters.

## 1.1 Review of Model Calibration Techniques

Numerical models for the simulation of hydrogeologic systems require the specification of system parameters for their solution. The initial estimates of these parameters are taken from field data and typically adjusted through the systematic comparison or matching of computed and historic ground-water head data from the site being modeled, a process referred to as history matching or model calibration. Over the last thirty years, numerous techniques have been developed to aid the modeler in the estimation of these parameters during model calibration. These techniques range from simplistic geostatistical algorithms to mathematically sophisticated inverse-problem solutions.

Geostatistical techniques including both linear and non-linear kriging, and co-kriging (Matheron, 1971, 1976; Delfiner, 1976; Delhomme, 1978, 1979; David, 1977, 1988; de Marsily, 1978, 1986; Olea, 1975a, 1975b; Journel and Huijbregts, 1978; Myers, 1982, 1984; Wackernagel, 1989; and others), facilitate the estimation of hydrogeologic parameter values and their uncertainties by assuming that the spatially variable distribution of the parameter values in the field can best be described as the realization of a random process. These techniques are generally used in the hydrologic community to estimate the parameter fields needed for numerical flow models, directly from available measurements. However, with the exception of automated inverse codes, there have been few attempts to develop techniques which aid the modeler in the adjustment of a kriged parameter field while calibrating a flow model.

One sensitivity technique, referred to as the first-order method (Benjamin and Cornell, 1970; Dettinger and Wilson, 1981), may be used during model calibration to identify those parameters to which a selected performance measure is most sensitive. The first-order method directly calculates the effect that parameter estimates have upon head estimates by determining sensitivity coefficients of the heads to changes in the parameter field. This direct technique was facilitated by the use of the adjoint approach for determining sensitivity coefficients (Chavent, 1971; Chavent et al., 1975; Neuman, 1980a; INTERA, 1983; Sykes and Wilson, 1984) and has been applied in a wide range of ground-water flow and transport problems (INTERA, 1984a, 1984b, 1984c; Metcalfe et al., 1985; Wilson and Metcalfe, 1985; Sykes et al., 1985; Samper and Neuman, 1986; LaVenue et al., 1989).

Rigorous inverse techniques that have been developed in the last ten years (Neuman, 1980b, 1982; Townley and Wilson, 1985; Carrera and Neuman, 1986a, 1986b; Yeh, 1986; and others) focus on various estimation techniques (i.e., weighted least squares, Kalman filter, maximum likelihood) which condition the transmissivity measurements upon both observed transmissivity data and head data and provide propagation of the parameter uncertainties to the head uncertainties. These techniques contain parameter-estimation algorithms which will adjust the parameter values automatically in order to minimize an objective function containing the calculated and observed heads. With few exceptions, these methods require the specification of zones within the modeled domain in which estimated parameters are constant (i.e., homogeneous). The selection of the zones can be somewhat arbitrary and generally requires an iterative process in which the optimum number of zones is determined. The parameter estimates and their uncertainties are model or zone-pattern specific and typically change if the zoning pattern changes.

Another requirement in the application of these inverse techniques involves the assignment of weights and uncertainty to prior information available on the parameters being estimated (e.g., transmissivity, storativity). Theoretically, prior information enables these inverse codes to provide much better parameter estimates than other more general methods. However, in practice the accurate determination of prior-information errors and proper weighting is rarely, if ever, possible. Since, as stated by Carrera and Neuman (1986b), the reliability of the parameter estimates is adversely affected by the lack of parameter constraints (e.g., prior information), the application of these inverse methods to poorly constrained problems should be cautioned.

In an attempt to circumvent the problems in applying the inverse techniques mentioned above, Hoeksema and Kitanidis (1984) and de Marsily et al. (1984) developed inverse solutions employing geostatistical algorithms. Hoeksema and Kitanidis (1984) extended a one-dimensional inverse code presented in Kitanidis and Vomvoris (1983) to two dimensions. They used a coupled co-kriging and maximum-likelihood approach to solve for grid-block estimates of transmissivities which were conditioned to the observed transmissivity and head data and consistent with their covariance and cross-covariance. De Marsily et al. (1984) employed an inverse



formulation to identify 'synthetic' transmissivity values at a selected number of fixed calibration points, referred to as pilot points, in order to match interference data at several boreholes. The locations of the pilot points were subjectively positioned in areas of high head gradients. By coupling the optimization algorithm to kriging, de Marsily demonstrated that it was possible to match the pressure records, preserve the local measured transmissivity values, and take account for the correlation structure of the observed parameters. An adjoint-sensitivity technique was also used to calculate the gradient of the objective function which was to be minimized.

## 1.2 General Approach Used in Present Study

An approach to model calibration similar to the inverse technique presented in de Marsily et al. (1984) has been used in this study to calibrate a ground-water flow model. The notable difference, relative to de Marsily's inverse formulation, derives from using adjoint-sensitivity techniques to identify the regions or locations where modification of the kriged transmissivity or prescribed head values on the boundaries will optimally improve the overall fit between measured and model-calibrated heads at selected wells. The present approach utilizes three primary codes, a kriging code, AKRIP, a ground-water flow and transport simulator, SWIFT II, and GRASP II, a code which calculates sensitivities of the SWIFT II simulation.

### 1.2.1 The AKRIP Code

The kriging package used during this study is a modified version of the M.I.T. kriging code, AKRIP (Kafritsas and Bras, 1981), a non-stationary kriging package which employs generalized covariances (Delfiner, 1976) during the estimation of a variable over space. AKRIP is capable of estimating variables which display an underlying spatial trend through the use of intrinsic random functions (polynomials) of order  $k$  (IRFK) where  $k$  is either 0, 1, or 2 (IRFK of 1, 2, or 3). AKRIP will calculate either point estimates or block-averaged estimates. For details on the procedure for using AKRIP to estimate a random variable over a selected region, the reader is referred to Kafritsas and Bras (1981) and Delfiner (1976).

The  $\log_{10}$  transmissivity values at each of the Culebra boreholes and an assigned uncertainty to these values were used as input to AKRIP. The block averaged  $\log_{10}$  transmissivity values were then estimated at each grid-block center of the discretized model accounting for the size of each grid block. The estimated  $\log_{10}$  transmissivities were then converted to linear conductivities and used in the SWIFT II model during flow simulations.

### 1.2.2 The SWIFT II Code

SWIFT II (Sandia Waste Isolation, Flow, and Transport Code) is a fully transient, three-dimensional, finite-difference code that solves the coupled equations for single-phase flow and transport in porous and fractured geologic media. The processes that SWIFT II is capable of simulating include fluid flow, heat transport, dominant-species miscible displacement (brine), and trace-species miscible displacement (radionuclide chains or other contaminants). The first three processes are coupled via porosity, fluid density, viscosity, and enthalpy. Together they provide the Darcy-velocity field required to model contaminant transport. Only the process of fluid flow is simulated in this study.

The SWIFT II code is supported by comprehensive documentation and extensive testing. The theory and implementation of SWIFT II are published in Reeves et al. (1986a) and the data-input guide in Reeves et al. (1986b). Finley and Reeves (1981) and Ward et al. (1984) present an extensive set of verification-validation tests for the code.

### 1.2.3 The GRASP II Code

GRASP II (Ground-Water Adjoint Sensitivity Program) computes measures of the behavior of a ground-water system (e.g., pressures at a location or several locations) and the system's performance for waste isolation (e.g., ground-water travel time), and estimates the sensitivities of these measures to system parameters (e.g., conductivities, transmissivities, boundary pressures). The computed measures are referred to as 'performance measures' and include weighted spatial sums of:

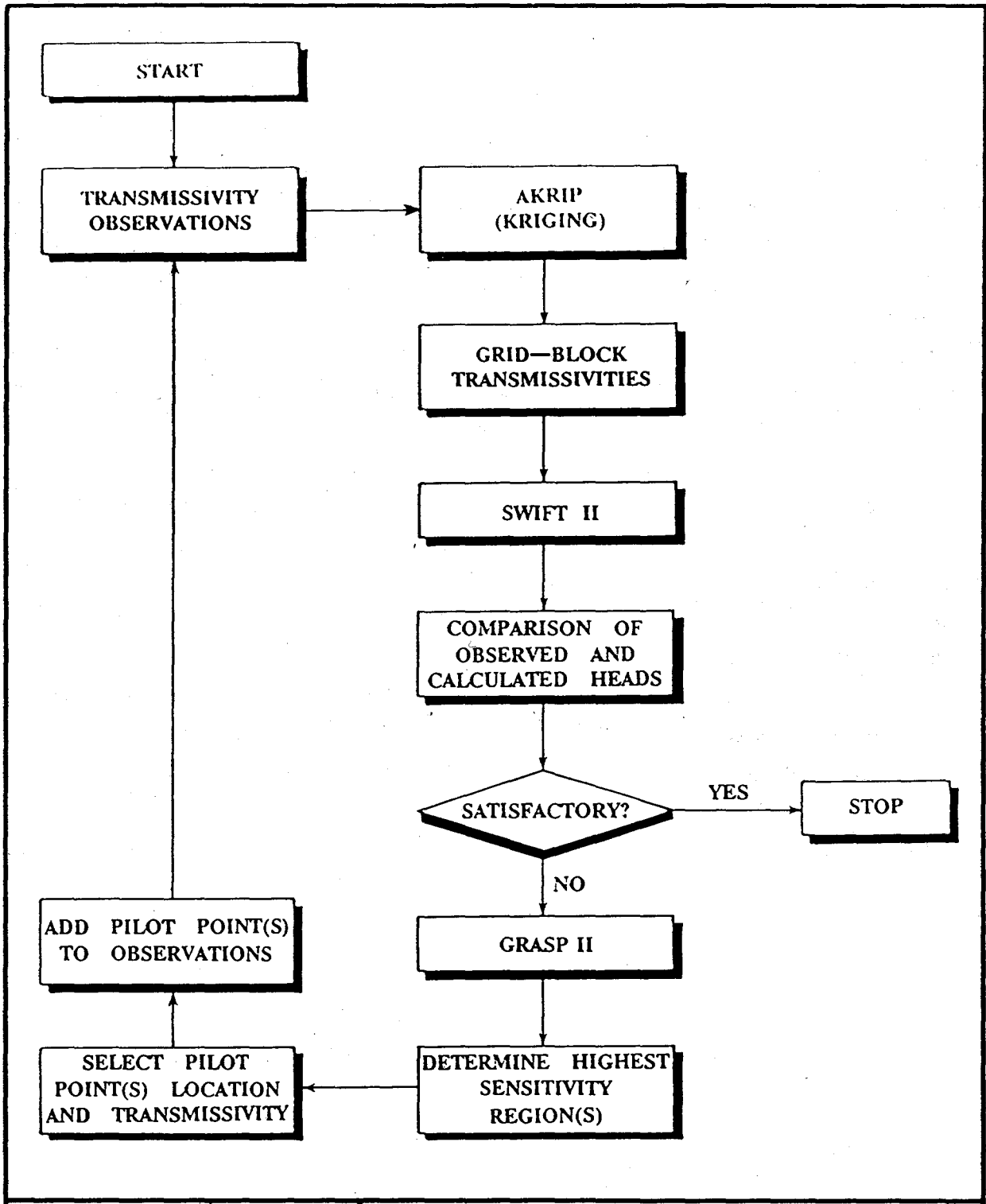
- **Ground-water pressures at selected locations**
- **Weighted squared deviations of computed and observed pressures at selected locations**
- **Local Darcy velocity components and magnitudes**
- **Boundary fluxes**
- **Ground-water travel time and distance along travel paths.**

The sensitivities are computed by the adjoint method (Chavent, 1971) and are exact derivatives of the performance measures with respect to the parameters for the modeled system, taken about the assumed parameter values. The system parameters available for use with GRASP II are:

- **Log<sub>10</sub> transmissivity assigned to a pilot point (see below)**
- **Grid-block conductivities**
- **Prescribed boundary pressures**
- **Recharge**
- **Source/sink rates.**

GRASP II presumes either steady-state or transient-state saturated ground-water flow conditions and post-processes the results from a SWIFT II flow simulation. The theory and verification of the transient flow sensitivity equations used in GRASP II are presented in RamaRao and Reeves (1990). The theory and verification for the steady-state flow sensitivity equations used in GRASP II are presented in Wilson et al. (1986).

The performance measures and their sensitivities can be employed in several ways. To assist in the characterization of a ground-water system, data-collection programs can be focused on those parameters and regions identified as having the largest influence on the system performance. Model calibration through the comparison of computed and observed steady-state or transient pressures can be expedited by the use of GRASP II, which is used to calculate the sensitivity of a steady-state or transient performance measure to changes in the transmissivity field. Changes of the transmissivity field are implemented through the use of kriging and the introduction of pilot points, or additional transmissivity data points, which are added to the set of observed transmissivity data. Pilot points are synthetic data points whose location is determined by GRASP II and whose magnitude is assigned by the modeler based on geologic and hydrogeologic information of the site. The GRASP II simulations identify regions where modification of the transmissivity values will directly improve the overall fit between observed and model-calculated heads at selected wells. The process of identifying subsequent pilot-point locations is repeated until the model is calibrated to both steady-state and transient conditions (Figure 1.1). Thus, the methodology provides an objective and quantitative approach to model calibration. It also allows for the judgement of the modeler in specifying the actual location and magnitude of parameter changes. Another advantage of the technique is that it permits simultaneous calibration to both steady-state and transient head distributions.



Drawn by	Date	Flow Chart Representing Adjoint-Sensitivity and Kriging Approach to Model Calibration
Checked by	Date	
Revisions	Date	

## 2.0 SITE DESCRIPTION AND MODEL CONCEPTUALIZATION

This chapter discusses the physical system and its discretized finite-difference representation. A description of the stratigraphy and regional hydrogeology is presented, based primarily on LaVenue et al. (1988), and is followed by several sections describing the modeling history, model data base, and initial model parameters as determined through a geostatistical analysis of the data base.

### 2.1 Site Description

#### 2.1.1 General

The WIPP site lies within the geologic region known as the Delaware Basin and specifically within the geographic region known as Los Medaños. Both the Delaware Basin and Los Medaños region occur within the southern section of the Pecos River portion of the Great Plains Physiographic Province. Los Medaños is a region of gently sloping terrain which rises eastward from the Pecos River to the western caprock of the Llano Estacado, located approximately 40 km to the northeast of the WIPP site (Mercer, 1983).

#### 2.1.2 Stratigraphy

The formations which crop out in and around the WIPP site range in age from Permian to Quaternary as shown in the geologic column of Figure 2.1. The Delaware Mountain Group represents the Permian Guadalupian Series and is composed of a sequence of fine-grained clastic rocks. In the WIPP area, the Delaware Mountain Group consists of the Brushy Canyon, Cherry Canyon, and Bell Canyon Formations. The Bell Canyon consists of interbedded sandstone and shale, which represent the fore-reef facies of a massive Permian reef known as the Capitan Limestone. The Ochoan Series rocks overlie the Guadalupian Series and contain a thick evaporitic sequence which accumulated in the Delaware Basin during late Permian time. The Castile Formation is the basal formation of the Ochoan Series and is composed principally of anhydrite and halite with some carbonates and sandstones. Overlying the Castile is the Salado Formation, which

SYSTEM	SERIES	GROUP	FORMATION	MEMBER
RECENT	RECENT		SURFICIAL DEPOSITS	
QUATERNARY	PLEISTOCENE		MESCALERO CALICHE	
			GATUNA	
TRIASSIC		DOCKUM	UNDIVIDED	
PERMIAN	OCHOAN		DEWEY LAKE RED BEDS	
			RUSTLER	Forty-niner
				Magenta
				Tamarisk
				Culebra
			Unnamed	
	SALADO	Upper		
		McNutt		
		Lower		
	CASTILE			
	GUADALUPIAN	DELAWARE MOUNTAIN	BELL CANYON	
CHERRY CANYON				
BRUSHY CANYON				

Drawn by	INTERA	Date	11/1/89
Checked by	M.L.	Date	11/1/89
Revisions		Date	
#H09700R869			11/1/89

Geologic Column Representative of WIPP Area  
(After Powers et al., 1978)

**INTERA** Technologies

Figure 2.1

contains the waste-storage panels of the WIPP repository. The Salado is composed of thick beds of halite interbedded with anhydrite, polyhalite, dolomite, and clay. More complete descriptions of the Salado Formation are found in Jones (1973, 1975). Overlying the Salado Formation is the Rustler Formation, which is the most water-transmissive formation in the area (Mercer, 1983).

The Rustler Formation has been divided into five separate members based upon lithology (Vine, 1963). They are, in ascending order: (1) an unnamed lower member composed of massive siltstone overlain by beds of halite, siltstone, and anhydrite; (2) the Culebra Dolomite Member; (3) the Tamarisk Member, composed of two zones of massive to bedded anhydrite separated by a sequence of halite and siltstones; (4) the Magenta Dolomite Member; and (5) the Forty-niner Member, composed of two anhydrite zones separated by a silty-halite unit, as in the Tamarisk. The Rustler Formation lithology presented above represents the lithological succession encountered in borehole P-18 which Snyder (1985) thinks to be a complete unaltered section. The Rustler lithology varies across the model area due to differences in depositional facies and locally to post-depositional dissolution of halite (Section 2.1.4). The Rustler Formation is conformably overlain by the Upper Permian Dewey Lake Red Beds, a series of interbedded siltstones and sandstones. These beds have prevalent vertical fractures that are generally gypsum filled.

In the eastern portion of the WIPP site, the Dewey Lake Red Beds are unconformably overlain by a Triassic clastic sequence deposited in a transitional depositional complex of fluvial, deltaic, and lacustrine environments. These units are collectively referred to as the Dockum Group.

Overlying the Dockum Group, where present, and the Dewey Lake Red Beds in the WIPP site area is a sequence of poorly sorted continental deposits of Quaternary age. These are, in ascending order, the Gatuña Formation, the Mescalero caliche, and recent alluvium and other surficial deposits. The Gatuña Formation consists of a sequence of pale reddish-brown terrestrial sandstones and conglomerates which were laid down after a maximum cycle of erosion within the Pecos River Valley during a much more humid pluvial time (Bachman, 1980). Izette and Wilcox (1982)



dated an ash bed in the upper portion of the Gatuña as middle Pleistocene (600,000 years before present [B.P.]) by mineralogy and fission-track dating.

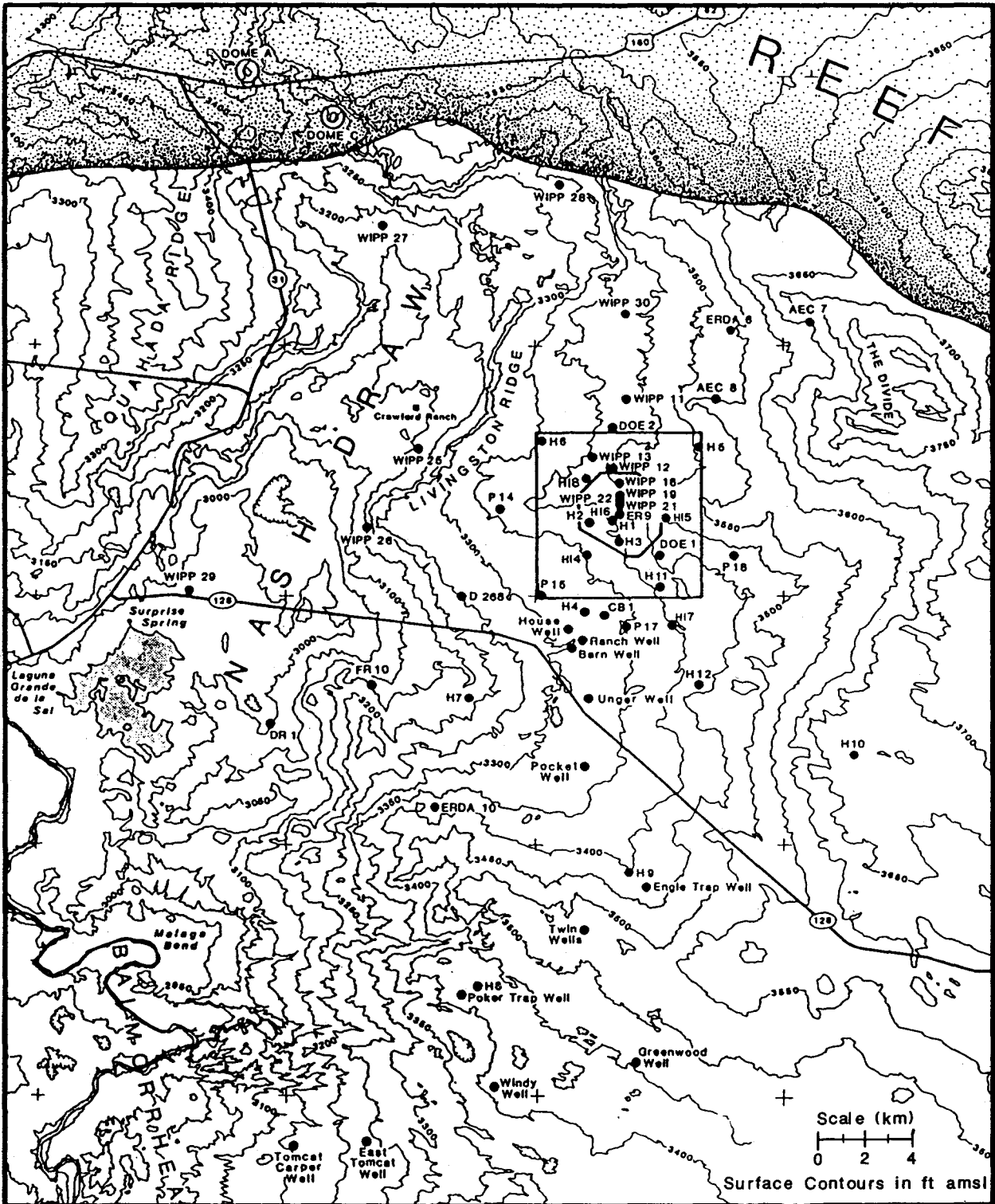
Overlying the Gatuña Formation is the Mescalero caliche, which is a pedogenic caliche formed in the C horizon of a paleosol during a tectonically and climatically stable period following the deposition of the Gatuña Formation (Bachman, 1980). The Mescalero caliche has been dated as being Pleistocene (510,000-410,000 years B.P.) through uranium-series disequilibrium techniques (Bachman, 1980). Overlying the caliche is a series of Holocene surficial deposits that consist of sheetlike deposits of surface sand, sand soil, and sand dunes.

### 2.1.3 Regional Hydrogeology

The discussion of the regional hydrogeology in this report is limited to the Rustler Formation and the uppermost Salado Formation. The hydrogeology of the individual hydrostratigraphic units is discussed in ascending order from the Rustler-Salado contact.

The Rustler-Salado contact is transmissive in some areas around the WIPP site (Mercer, 1983). In Nash Draw and areas immediately west of the WIPP site, the contact exists as a dissolution residue capable of transmitting water. Robinson and Lang (1938) referred to this residuum making up the contact as the "brine aquifer." As one moves eastward from Nash Draw toward Livingston Ridge (Figure 2.2), dissolution in the uppermost Salado, at the Rustler-Salado contact, and within the unnamed lower member of the Rustler Formation decreases and the transmissivity of this interval decreases.

Transmissivities for the Rustler-Salado contact range from  $2 \times 10^{-10}$  to  $9 \times 10^{-6}$  m<sup>2</sup>/s in Nash Draw and from  $3 \times 10^{-11}$  to  $5 \times 10^{-8}$  m<sup>2</sup>/s eastward from Livingston Ridge (Mercer, 1983). At well DOE-2, Beauheim (1986) attempted a slug test on the unnamed member and the Rustler-Salado contact and found that the permeability in this interval was too low to be tested effectively. In the waste-handling shaft, no water inflows from this interval were observed during excavation



Drawn by	INTERA	Date	11/1/89	WIPP Area
Checked by	M.L.	Date	11/1/89	
Revisions		Date		
#H09700R869		Date	11/1/89	
<b>INTERA Technologies</b>				Figure 2.2

and shaft mapping (Holt and Powers, 1984). At H-16, Beauheim (1987b) performed drill-stem tests of a 34-m interval including the unnamed-lower-member siltstone and the Rustler-Salado contact, and reported the transmissivity of this interval to be about  $3 \times 10^{-10} \text{ m}^2/\text{s}$ .

The Culebra dolomite is considered to be the most transmissive hydrogeologic unit in the WIPP-site area. Mercer (1983) describes ground-water flow within the Culebra as being southerly in Nash Draw and south to southwesterly beneath the Livingston Ridge surface. Reported values for transmissivity in the Culebra in the Nash Draw area range from  $2 \times 10^{-5}$  to  $1 \times 10^{-3} \text{ m}^2/\text{s}$  (Cauffman et al., 1990). Within the model area, the transmissivities range from  $1 \times 10^{-10}$  to  $1 \times 10^{-3} \text{ m}^2/\text{s}$ . Hydraulic gradients in the Culebra at the WIPP site generally range from  $1 \times 10^{-3} \text{ m/m}$  to  $4 \times 10^{-3} \text{ m/m}$ , based on the equivalent freshwater head distribution presented in Cauffman et al. (1990). As a general trend, total dissolved solids in Culebra ground waters increase from west to east across the WIPP site and the model area (Cauffman et al., 1990). An exception to this trend occurs at the WIPP-27 and WIPP-29 boreholes, where high TDS values occur due to contamination from potash mining and milling operations.

The Tamarisk Member of the Rustler separates the Culebra dolomite from the Magenta, and is composed of a sequence of halite and siltstones sandwiched between upper and lower anhydrites. The Tamarisk siltstone sequence has been tested at wells H-14 and H-16 (Beauheim, 1987b) and at DOE-2 (Beauheim, 1986). In all cases the hydraulic testing was unsuccessful due to the extremely low permeability of the unit. Mercer (1983) reported that in a few cases argillaceous zones within the Tamarisk Member have produced water at rates equivalent to the Magenta upon testing.

Ground water in the Magenta dolomite generally flows from the north toward the west-southwest (Mercer, 1983). In most areas east of Nash Draw, and east and south of the H-6 hydropad, the Magenta exists as a confined system with low transmissivity (less than or equal to  $4 \times 10^{-7} \text{ m}^2/\text{s}$ ). The difference between Magenta and Culebra hydraulic potentials generally increases eastward, with the Magenta having higher potentials. In areas of Nash Draw, the Magenta is generally

at water-table conditions and may be in hydraulic connection with other units in the Rustler Formation due to the absence of halite within the Nash Draw area. In other parts of Nash Draw, the Magenta is unsaturated. Magenta transmissivities range as high as  $4 \times 10^{-4}$  to  $6 \times 10^{-4}$  m<sup>2</sup>/s immediately east of Nash Draw (Mercer, 1983).

The uppermost member of the Rustler Formation, the Forty-niner Member, has claystones which are more transmissive than those in the Tamarisk Member. At well H-14, Beauheim (1987b) performed drill-stem tests upon the Forty-niner and determined that transmissivities were approximately an order of magnitude higher than in the Magenta at H-14. The average value of transmissivity calculated for the Forty-niner was  $6 \times 10^{-8}$  m<sup>2</sup>/s as opposed to  $6 \times 10^{-9}$  m<sup>2</sup>/s for the Magenta. Beauheim (1986) also tested the Forty-niner claystone in well DOE-2. Here again, he calculated slightly higher transmissivities for the Forty-niner claystone than for the Magenta. The average of the two transmissivities of the Forty-niner reported by Beauheim (1986) for DOE-2 is  $7.3 \times 10^{-9}$  m<sup>2</sup>/s. Drill-stem tests of the Forty-niner claystone at H-16 provided a transmissivity estimate of about  $6 \times 10^{-9}$  m<sup>2</sup>/s, lower than that of the Magenta at H-16 (Beauheim, 1987b).

#### 2.1.4 Regional Dissolution in the Rustler Formation

Dissolution within the upper Salado Formation and/or the Rustler Formation is observed both at the surface within Nash Draw, and in the subsurface at the WIPP site (Bachman, 1987). Nash Draw, located immediately west of the WIPP site (Figure 2.2), is a depression resulting from both dissolution and erosion. In Nash Draw, members of the Rustler are actively undergoing dissolution and locally contain caves, sinks, and tunnels typical of karst morphology in evaporitic terrane.

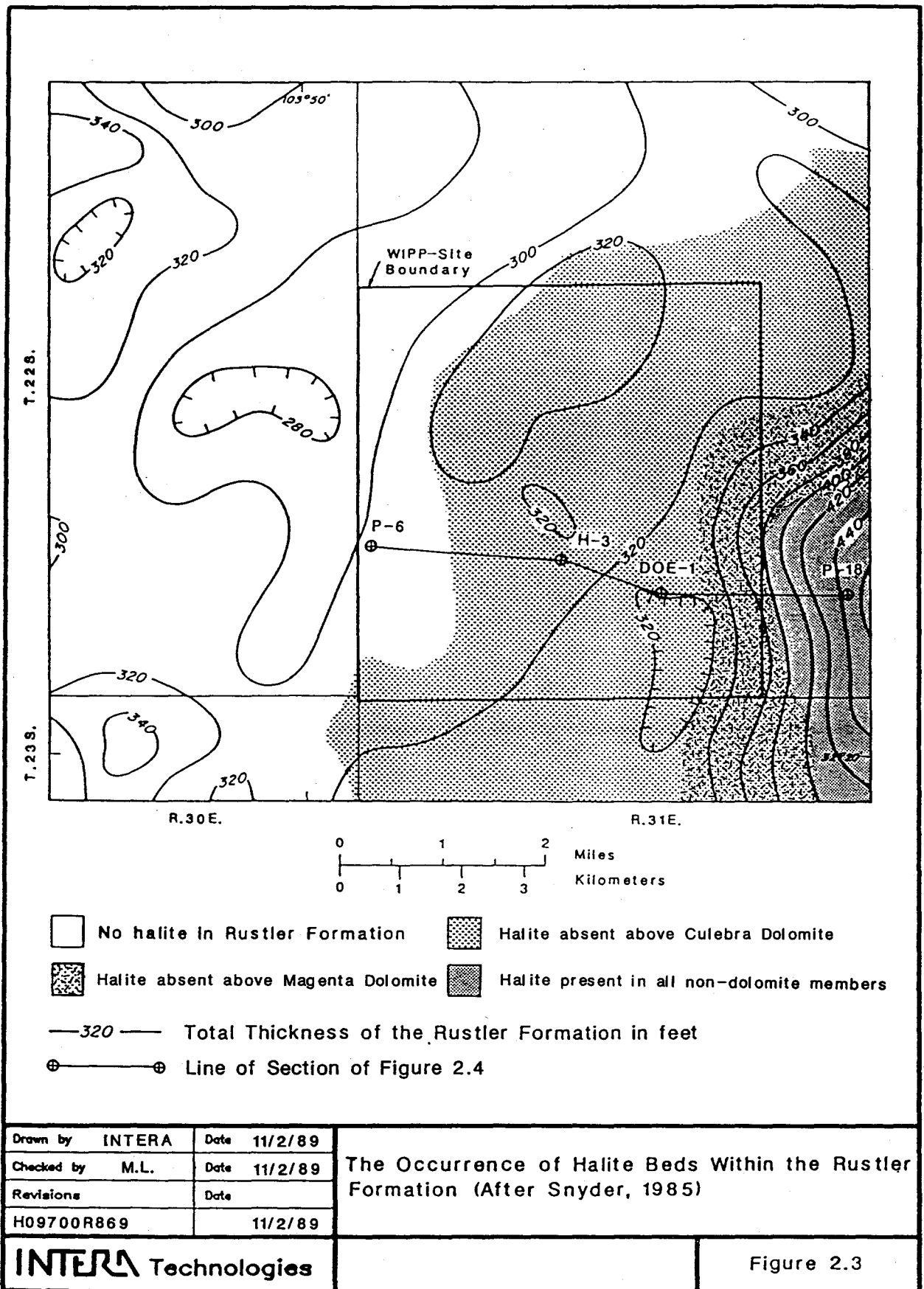
Based upon observations of outcrops, core, and detailed shaft mapping, the Culebra can be characterized, at least locally, as a fractured medium at the WIPP site (Chaturvedi and Rehfeldt, 1984; Holt and Powers, 1984). As the amount of fracturing and development of secondary porosity increases, the Culebra transmissivity generally increases (Chaturvedi and Channell, 1985). The fracturing and development of secondary porosity is thought to be a product of late-stage

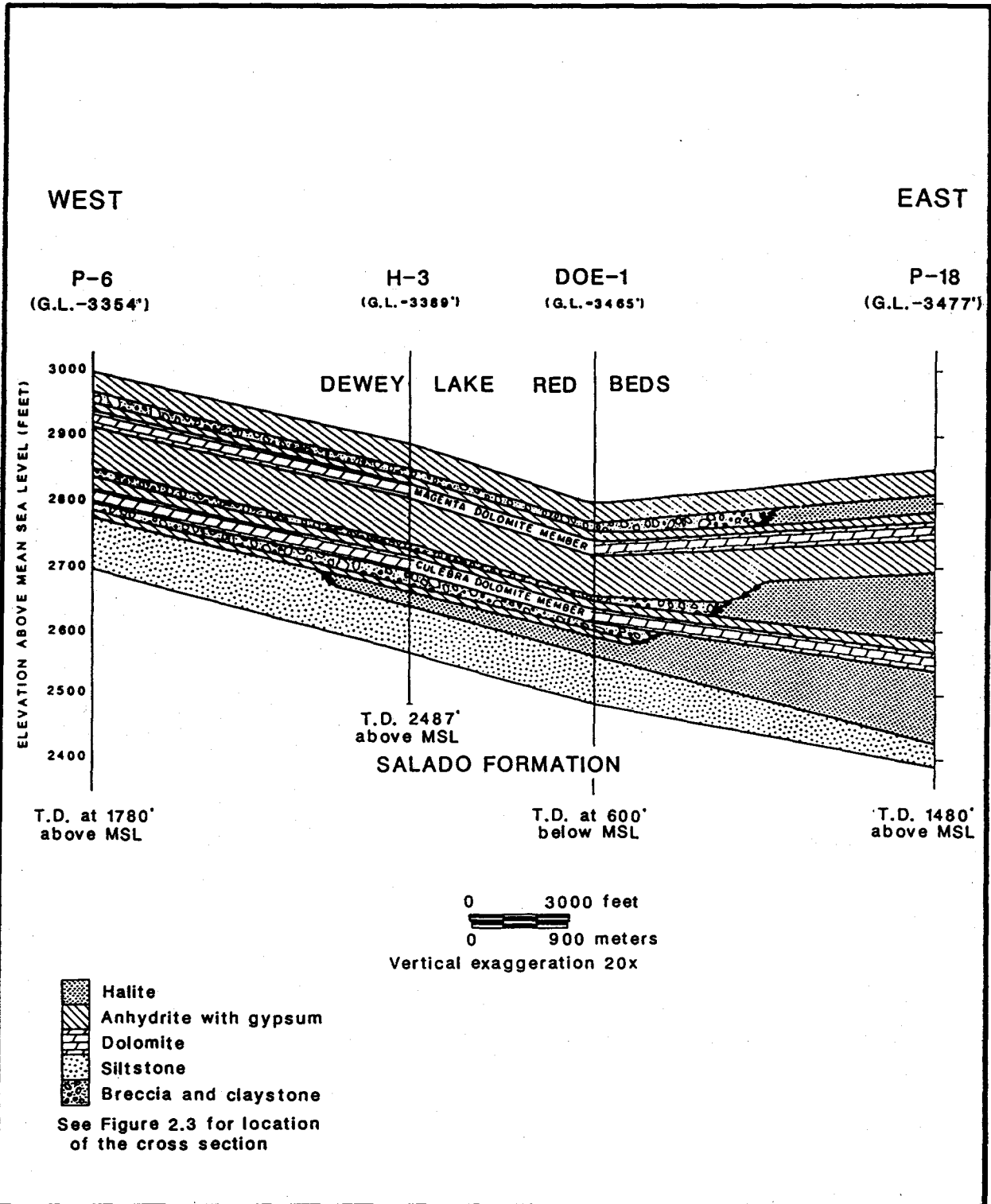
alteration and dissolution of the Rustler Formation. In general, as the amount of halite present in the Rustler decreases, the transmissivity of the dolomitic members increases as a result of halite removal and subsequent foundering and collapse of the more competent dolomitic members.

Bachman (1980) identified three types of dissolution occurring in the Delaware Basin: local, regional, and deep-seated. Of these, regional dissolution is the type which has the most potential to dictate or alter the flow characteristics of the Rustler Formation underlying the WIPP site. Regional dissolution occurs when chemically unsaturated water penetrates to permeable beds, where it migrates laterally, dissolving the soluble units it contacts. On a regional scale, the consequence of such dissolution appears to be removal of highly soluble rock types, such as halite, combined with displacement and fracturing of overlying rocks.

Snyder (1985) found evidence for the presence of an eastward-migrating dissolution front within the Rustler Formation at the WIPP site. In his study, Snyder concluded that the regional dissolution was greatest in the west and decreased eastward, as evinced by an increase in the number and thickness of halite beds and a corresponding thickening of the Rustler Formation (Figure 2.3). The stratigraphic level of the uppermost occurrence of salt is in the upper Rustler along the eastern margin of the WIPP site. Moving westward toward Nash Draw, the uppermost salt is found in progressively deeper horizons of the Rustler. This implies that, as a general trend, the eastward advancement of the dissolution front is greatest in the upper Rustler and decreases toward the Rustler-Salado contact. As the halite units are dissolved, insoluble residues remain, forming beds of mudstones, siltstones, and chaotic breccia with a clay matrix. As can be seen in a cross section taken between boreholes P-6, H-3, DOE-1, and P-18, (Figure 2.4), halite beds tend to thin and grade into residuum westward toward Nash Draw.

Although most investigators agree with the interpretation that a dissolution zone exists in the Rustler Formation at the WIPP site (Cooper and Glanzman, 1971; Powers et al., 1978; Mercer, 1983; Chaturvedi and Rehfeldt, 1984; Bachman, 1985; and Snyder, 1985), other investigators oppose this concept and think that the westward decrease of halite within the Rustler simply represents depositional limits





Drawn by INTERA	Date 1987/88
Checked by	Date
Revisions M.L.	Date 10/18/89
#H09700R869	10/18/89

Stratigraphic Cross Section of the Rustler Formation West to East Across the WIPP Site (After Chaturvedi and Channell, 1985)

**INTERA Technologies**

Figure 2.4

(Powers and Holt, 1984; and Holt and Powers, 1988). Lowenstein (1987) conducted a detailed analysis on core from wells DOE-2, WIPP-19, H-11, and H-12. The aim of the study was to distinguish between syndepositional features and post-depositional alteration features within the Rustler. Lowenstein could correlate structures, both syndepositional and post-depositional, over the study area and concluded that facies changes were not responsible for the westward decrease in halite within the Rustler in the study area. Lowenstein found evidence of late-stage alteration involving physical processes such as brecciation, slumping, fracturing, and faulting, as well as chemical processes such as rehydration of anhydrite to gypsum, precipitation of gypsum, and dissolution of halite, anhydrite, and gypsum. Thus, the study of Lowenstein (1987) supports the theory of a post-depositional dissolution of salt in the Rustler.

Holt and Powers (1984, 1988) performed detailed mapping in the waste-handing and exhaust shafts and reported no post-depositional features in any of the stratigraphic horizons. In addition, they found pronounced primary sedimentary features in several zones which had previously been identified as dissolution residues in several boreholes near the shafts (Holt and Powers, 1984). Recently, Holt and Powers (1988) expanded their earlier work by analyzing geophysical logs and re-examining Rustler cores from the WIPP-site area. This study presented a detailed depositional model for the Rustler Formation ranging from shallow lagoons and subtidal environments to shallow saline pans and environments marginal to the saline pan. Holt and Powers (1988) propose that parts of the Rustler formed when fresher water transgressed over the Salado, depositing clastics, carbonates, or subaqueous sulfates. As transgressing water evaporated, halite was deposited, forming lenticular units with the thickest part south and east of the WIPP site, in the depocenter (Holt and Powers, 1988). Halite in the halite and mudstone units at small to large scales was dissolved syndepositionally. After a transgression, and in some cases continuing after overlying sediments were deposited, halite was subjected to dissolution by less saline water. The latter would cause deformation and slumping in the overlying sediment. When the water table in the margins was lowered by subsidence or evaporation, halite was dissolved by meteoric water in the vadose zone and redeposited in the depocenter (Holt and Powers, 1988). The



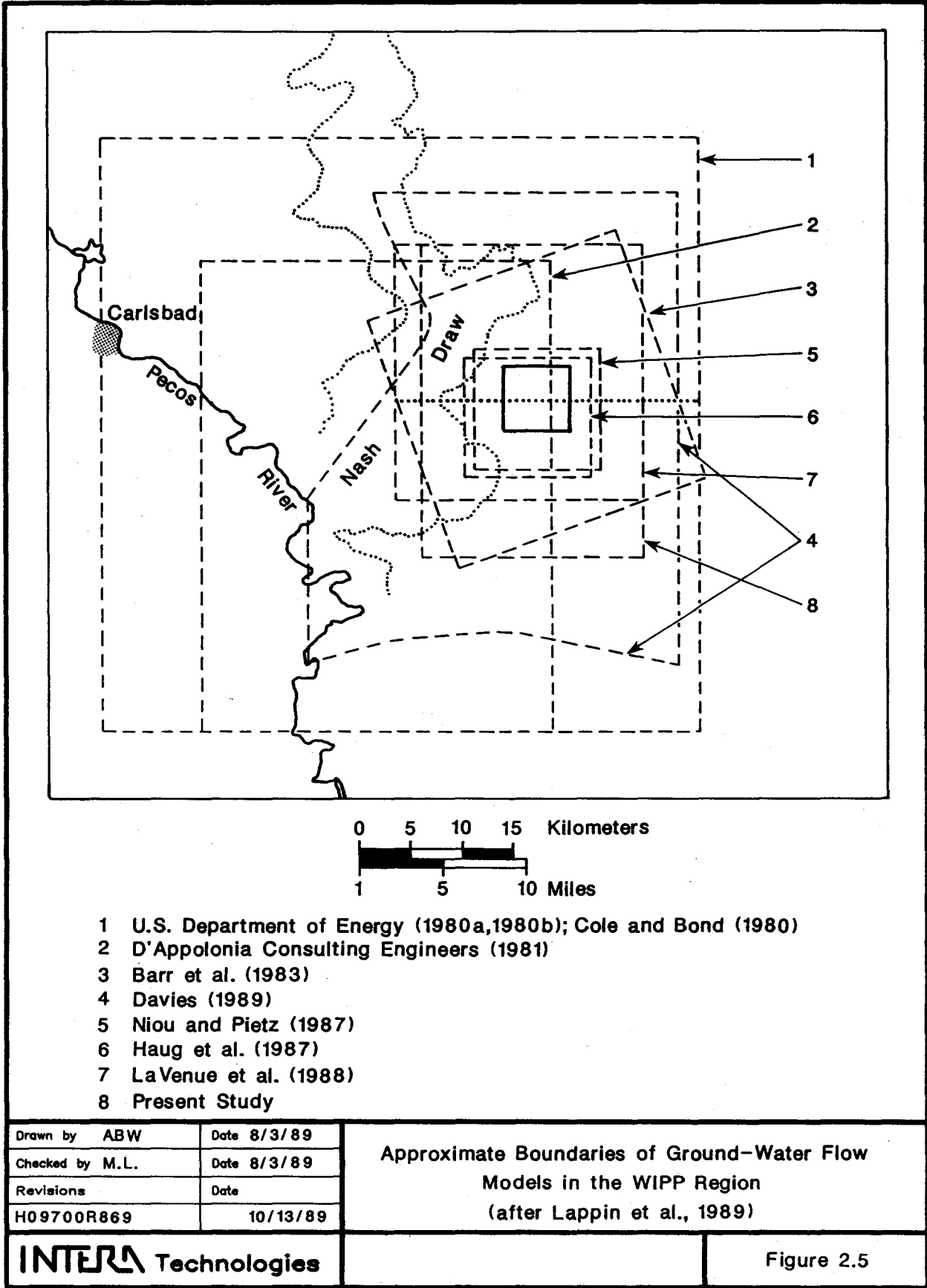
hydrologic implications of the Holt and Powers hypothesis have not yet been explored in detail and is subject to ongoing studies.

While it is commonly accepted that regional dissolution has been an active process within the Rustler in the past, there is some controversy over whether or not this dissolution is still active. Within the last 1.8 million years (Pleistocene), the climate in southeastern New Mexico has varied between periods of cold, moist continental glaciation and relatively warm and arid periods (Bachman, 1987). In Middle Pleistocene time, approximately 500,000 years B.P., southeastern New Mexico received precipitation which well exceeded the evapotranspiration. This period was followed by several hundred thousand years of a drier climate. In late Pleistocene time (approximately 75,000 to 10,000 years B.P.), rainfall was more prevalent than today and temperatures were lower (Bachman, 1987). Bachman thinks that most of the dissolution in the Rustler predates, or occurred during, Middle Pleistocene (Gatuña) time. However, he suggests that dissolution is ongoing in Nash Draw and areas very close to Livingston Ridge. Through the interpretation of radiocarbon data (Lambert, 1987) and stable isotopes (Lambert and Harvey, 1987), Lambert has suggested that recharge and subsequent dissolution of the Rustler ended after the more pluvial late Pleistocene (10,000 to 20,000 years B.P.).

## 2.2 Modeling History

Various ground-water modeling investigations have been performed which consider the Rustler Formation or the Culebra Dolomite Member for the WIPP-site region during the period 1976 to 1989. The conceptual model and the definitions of the parameter-value distributions have changed during this period as a result of continuing field investigations and expansion of the hydrogeologic data base. The regions encompassed in the modeling studies are illustrated in Figure 2.5 and a summary of the hydrogeologic unit modeled and whether the model was calibrated to steady-state conditions or to transient stresses is presented in Table 2.1. Lappin et al. (1989) present a review and discussion of the scope of each of these modeling studies.

The present study is the first that provides steady-state head calibration to undisturbed head conditions and transient head calibration to several large-scale



Reference	Hydrogeologic Unit Modeled	Head Calibration
U.S. Dept. of Energy (1980a,b)	Rustler	Steady State
D'Appolonia (1981)	Rustler	Steady State
Cole and Bond (1980)	Rustler	Steady State
Barr et al. (1983)	Culebra	Steady State
Davies (1989)	Culebra	Steady State
Niou and Pietz (1987)	Culebra	Transient
Haug et al. (1987)	Culebra	Steady State
LaVenué et al. (1988)	Culebra	Steady State
Present Study	Culebra	Combined Steady-State/Transient

Drawn by	Date
Checked by	Date
Revisions	Date

**Summary of Modeling Investigations of the Rustler Formation or Culebra Dolomite Member in the WIPP-Site Region**

**INTERA Technologies**

Table 2.1

pumping tests and the hydraulic stresses imposed by construction of the WIPP shafts. The studies by Haug et al. (1987) and LaVenue et al. (1988) utilized the model transmissivity distribution from calibration to the steady-state head distribution to investigate the model's suitability to simulate shaft effects and head changes resulting from large-scale pumping tests. However, these previous studies did not include extensive calibration efforts to improve the model's transmissivity distribution to simulate both steady-state and transient heads.

### 2.3 Model Conceptualization

The conceptual model used in this study assumes a two-dimensional steady-state flow system with spatially variable fluid densities and formation elevations. Steady-state conditions are assumed to approximate the hydrologic conditions in the Culebra prior to the excavation of the shafts. In general, hydrographs of the Culebra water levels prior to 1981 display either no significant fluctuations over time or a slight rise over time. Therefore, undisturbed heads selected from the hydrographs are assumed to represent quasi-steady state heads. Vertical flux is not considered in the model because of (1) the existence of low-permeability anhydrites above (the Tamarisk Member) and below (the unnamed lower member) the Culebra in the eastern and central model areas, and (2) responses to large-scale Culebra pumping tests performed in the WIPP-site area have not been observed in the Magenta dolomite. Even though there is a possibility of vertical flux occurring in Nash Draw (i.e., the western model area) and in the southwestern model area, the high transmissivities in these areas preclude vertical flux from having much of an effect upon the results of this study.

The steady-state and transient simulations discussed in Sections 3, 5, and 6 employ the steady-state and transient single-porosity flow equations (Equations 2.1 and 2.2 respectively) with variable fluid density.

$$\nabla \cdot [(\rho k / \mu)(\nabla p - \rho g \nabla z)] = 0 \quad (2.1)$$

$$- \partial(\phi \rho) / \partial t - \nabla \cdot [(\rho k / \mu)(\nabla p - \rho g \nabla z)] + q = 0 \quad (2.2)$$

where  $k = k(\underline{x})$  is permeability tensor,  $p = p(\underline{x},t)$  is pressure,  $z$  is the vertical coordinate,  $\rho = \rho(\underline{x})$  is fluid density,  $q$  is flux sources or sinks,  $g$  is the gravitational constant,  $\mu$  is fluid viscosity,  $\phi$  is rock porosity,  $\underline{x}$  is the position vector, and  $t$  is time. The fluid densities were not simulated but were spatially fixed; i.e., no transport of brine is calculated in the steady-state or transient model simulations, because the time constant to achieve steady-state conditions for Culebra formation-fluid densities in the WIPP region is considered much larger, e.g., several thousand years, than the time constant for flow, e.g., several years, (Section 2.3.8.2). However, the fluid densities are incorporated in the model calculation of formation pressures and Darcy velocities.

Sections 2.3.1 through 2.3.8 begin with a brief description of the data base used in this report. More detailed discussions of the data evaluation and analysis follow. A description of the basic model properties (e.g., boundaries, discretization, physical parameters, boundary conditions, etc.) is also included.

### 2.3.1 Data Base

For more than ten years, numerous field investigations at the WIPP site have focused on the Rustler Formation in general and the Culebra Dolomite Member in particular. The existing data for the Culebra include transmissivities, storativities, formation-fluid densities, depths to water, and pressures from the observation-well network. Construction activities at the WIPP site, such as the excavation of the shafts at the center of the site, have also provided hydrogeologic data. The majority of the hydrogeologic data are published in the following report series:

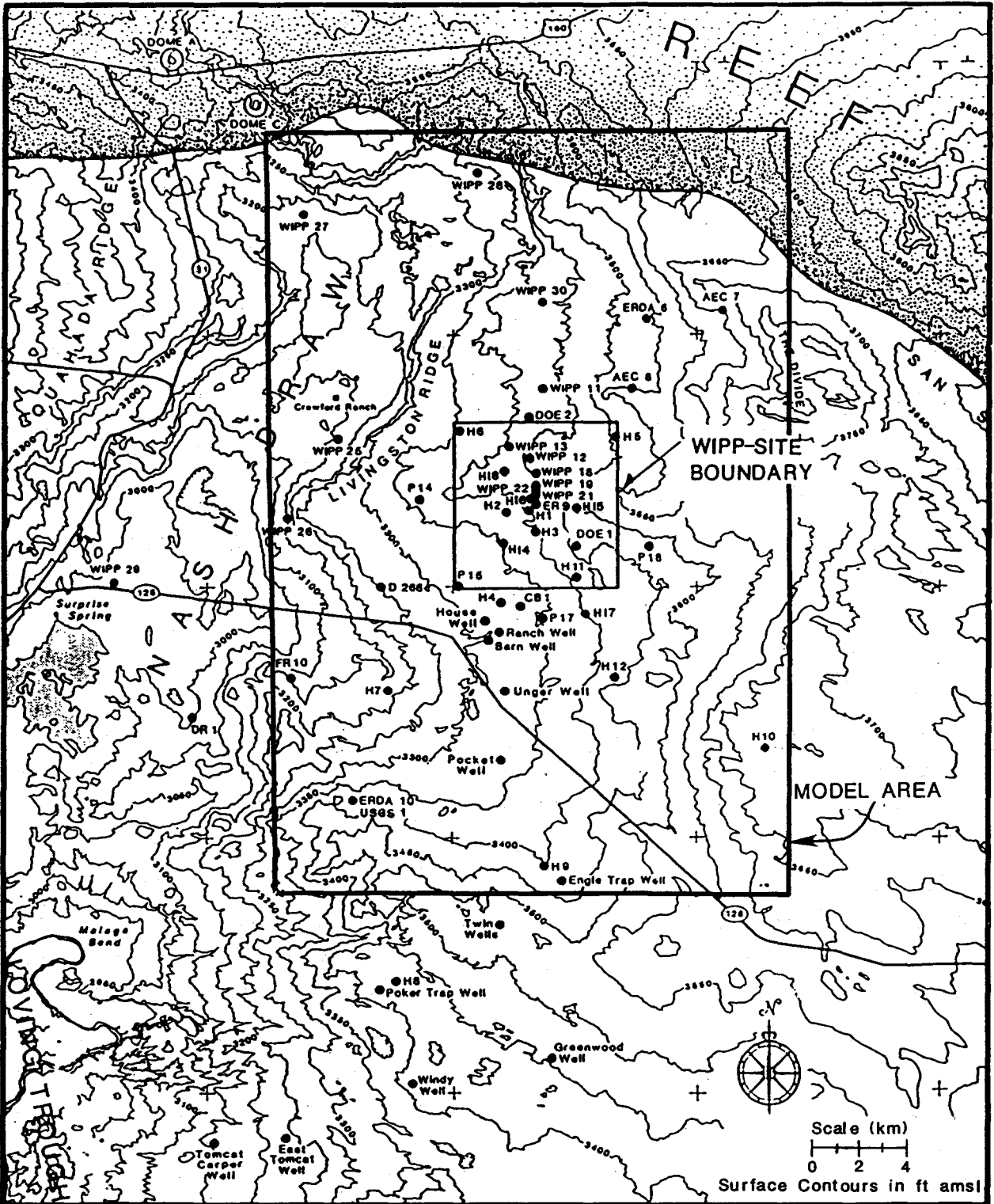
- Basic data reports (borehole-specific reports, e.g., Sandia National Laboratories and University of New Mexico, 1981; Gonzales, 1989; Richey, 1989)
- Hydrologic data reports (Hydro Geo Chem, 1985; INTERA and Hydro Geo Chem, 1985; INTERA, 1986; Saulnier et al., 1987; Stensrud et al., 1987, 1988a,b, 1990)
- Hydrogeologic interpretive reports (e.g., Mercer, 1983; Beauheim, 1986, 1987a,b,c, 1988, 1989; Saulnier, 1987; Avis and Saulnier, 1990)

- Water-quality data and geochemical interpretive reports (e.g., Mercer, 1983; Uhland and Randall, 1986; Uhland et al., 1987; Robinson, 1987; Randall et al., 1988; Lyon, 1989).

The data base used for this modeling study and a complete listing of data sources are presented in Cauffman et al. (1990). The report includes separate data bases for transmissivity, storativity, formation-fluid density, borehole locations, ground-surface and Culebra elevations, and freshwater heads and is considered to represent the most current information about the site. The data base was used in conjunction with geostatistical methods to assign the initial hydrogeologic parameters to each grid block in the model. Calibration procedures also utilized geostatistical methods to update the spatial distribution of hydrogeologic parameters in order to reduce the difference between calculated and observed heads.

### 2.3.2 Model Area

The model area used in this study is shown in Figure 2.6. It encompasses an area extending 21.3 km in the east-west and 30.6 km in the north-south directions. The selection of the locations of the boundaries of the model was a balance between placing them 1) far enough away from the central-model region to minimize the effect that the boundaries may have on the transient modeling results for the H-3, WIPP-13, and H-11 multipad pumping tests, and 2) not placing them so far away that no hydrologic information about the boundaries was available (i.e., too far away from regional boreholes). The western boundary lies within Nash Draw, which is believed to be a major conduit for ground-water flow toward the south. The other boundaries of the model do not coincide with physical hydrologic boundaries. However, the uncertainty of the specifications for the boundary conditions is minimized by utilizing hydrologic information from far-field wells (e.g., H-7b, H-9b, H-10b, H-12, WIPP-26, WIPP-27, WIPP-28, USGS-1, and USGS-4) close to the boundaries.



Drawn by INTERA	Date 1987/88
Checked by	Date
Revisions M.L.	Date 10/18/89
#H09700R869	10/18/89

WIPP-Area and Model Boundaries

**INTERA Technologies**

Figure 2.6

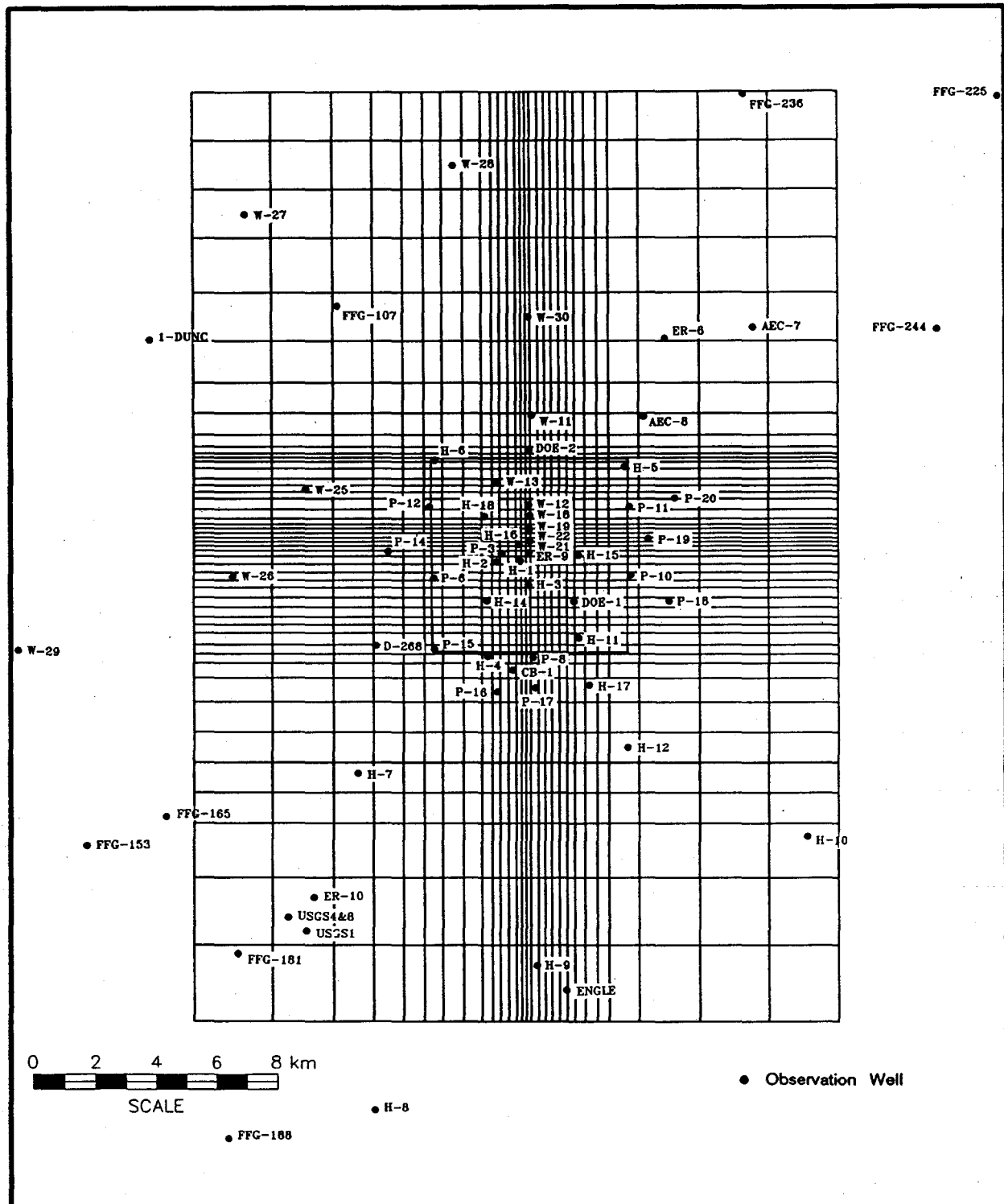
### 2.3.3 Model-Grid Description

The finite-difference grid used in this modeling study (Figure 2.7a) was selected to facilitate the successful reproduction of both steady-state and transient heads by reducing the numerical problems associated with coarse gridding. The horizontal dimensions of the grid are listed in Table 2.2 along with the Universal Transverse Mercator (UTM) coordinates of the corner points of the grid. The UTM system is an internationally recognized coordinate system providing uniform world coverage using metric units. A comprehensive discussion of the UTM system is provided in Gonzales (1989). The grid consists of 28 x 48 x 1 (x,y,z) grid blocks and has a much finer grid occurring in the central portion of the model in the vicinity of H-3, the shafts, H-11, and WIPP-13 (Figure 2.7b). The general "rule of thumb" used in developing the grid included not increasing adjacent grid-block sizes by more than a factor of two. Adopting this rule provides adequate resolution and numerical stability for transient flow modeling.

The vertical dimension of the finite-difference grid is taken from the thickness of the Culebra dolomite in the WIPP area. Several reports have documented the Culebra thicknesses observed in the WIPP-area boreholes (Jones, 1959, 1978; Sandia Laboratories and U.S. Geological Survey, 1979a,b,c,d,e,f, 1980a,b,c,d,e; Sandia National Laboratories, 1982; Sandia National Laboratories and D'Appolonia Consulting Engineers, 1982a,b,c, 1983a,b,c; Sandia National Laboratories and U.S. Geological Survey, 1980, 1981a,b, 1982, 1983a,b; Sandia National Laboratories and University of New Mexico, 1981; Mercer et al., 1987; Richey, 1989). The thickness of the Culebra, presented in Appendix B of Cauffman et al. (1990), ranges from 5.5 m at the H-2 borehole to 11.3 m in the vicinity of H-7. The mean thickness of 7.7 m was calculated from the available data and is assumed to be adequate for the vertical model dimension in this study.

The elevation of the Culebra dolomite has been documented in the reports referenced above on the WIPP-area boreholes. Appendix B of Cauffman et al. (1990) contains the ground-surface elevations and the depths to the Culebra from which the Culebra elevations at the borehole locations in the WIPP area were calculated. The elevations of the center of the Culebra over the model area range





Drawn by ABW	Date 10/30/89
Checked by M.L.	Date 10/31/89
Revisions	Date
H09700R869	10/31/89

WIPP-Area Boreholes and Model Grid

**INTERA** Technologies

Figure 2.7a

**UTM Coordinates of the Model-Area Corners:**

Southwest corner:	3 566 500 mN	602 700	mE
Southeast corner:	3 566 500 mN	624 000	mE
Northeast corner:	3 597 100 mN	624 000	mE
Northwest corner:	3 597 100 mN	602 700	mE

**Dimensions of the Model Area:**

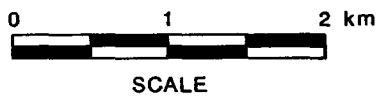
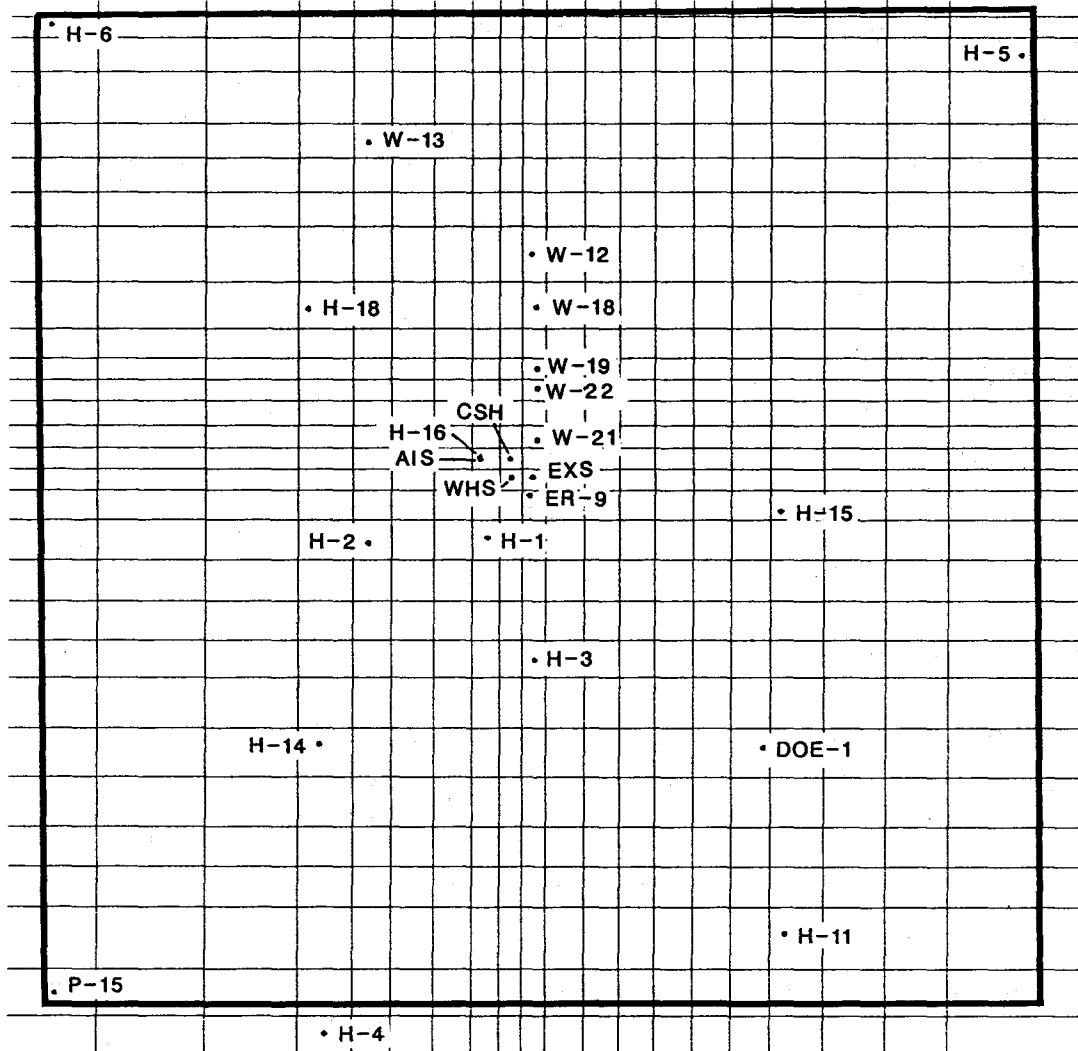
East - West:	21.3 km
North - South:	30.6 km
Area:	652. km <sup>2</sup>

**Grid-Block Dimensions (m):**

From West to East: 2600, 2000, 1300, 1000, 700, 600, 700, 600,  
 350, 250, 275, 250, 175, 150, 150, 250,  
 225, 225, 250, 250, 250, 350, 400, 400,  
 1000, 2000, 2300, 2300.

From South to North: 2500, 2200, 1800, 1000, 1000, 1000, 1000, 800,  
 500, 300, 300, 400, 260, 260, 320, 320,  
 320, 240, 260, 260, 260, 190, 140, 140,  
 140, 160, 140, 140, 190, 300, 360, 220,  
 220, 220, 340, 220, 140, 120, 220, 400,  
 700, 1000, 1400, 1600, 1800, 1600, 1600, 1600.

Drawn by	Date	<b>Coordinates and Dimensions of the Model Area and the Grid Blocks</b>
Checked by	Date	
Revisions	Date	
<b>INTERA Technologies</b>		Table 2.2



Drawn by	ABW	Date	1/24/90
Checked by	M.L.	Date	1/24/90
Revisions		Date	
H09700R869		1/24/90	

Model Grid in the Central Model Region  
Showing Shaft and Borehole Locations

**INTERA** Technologies

Figure 2.7b

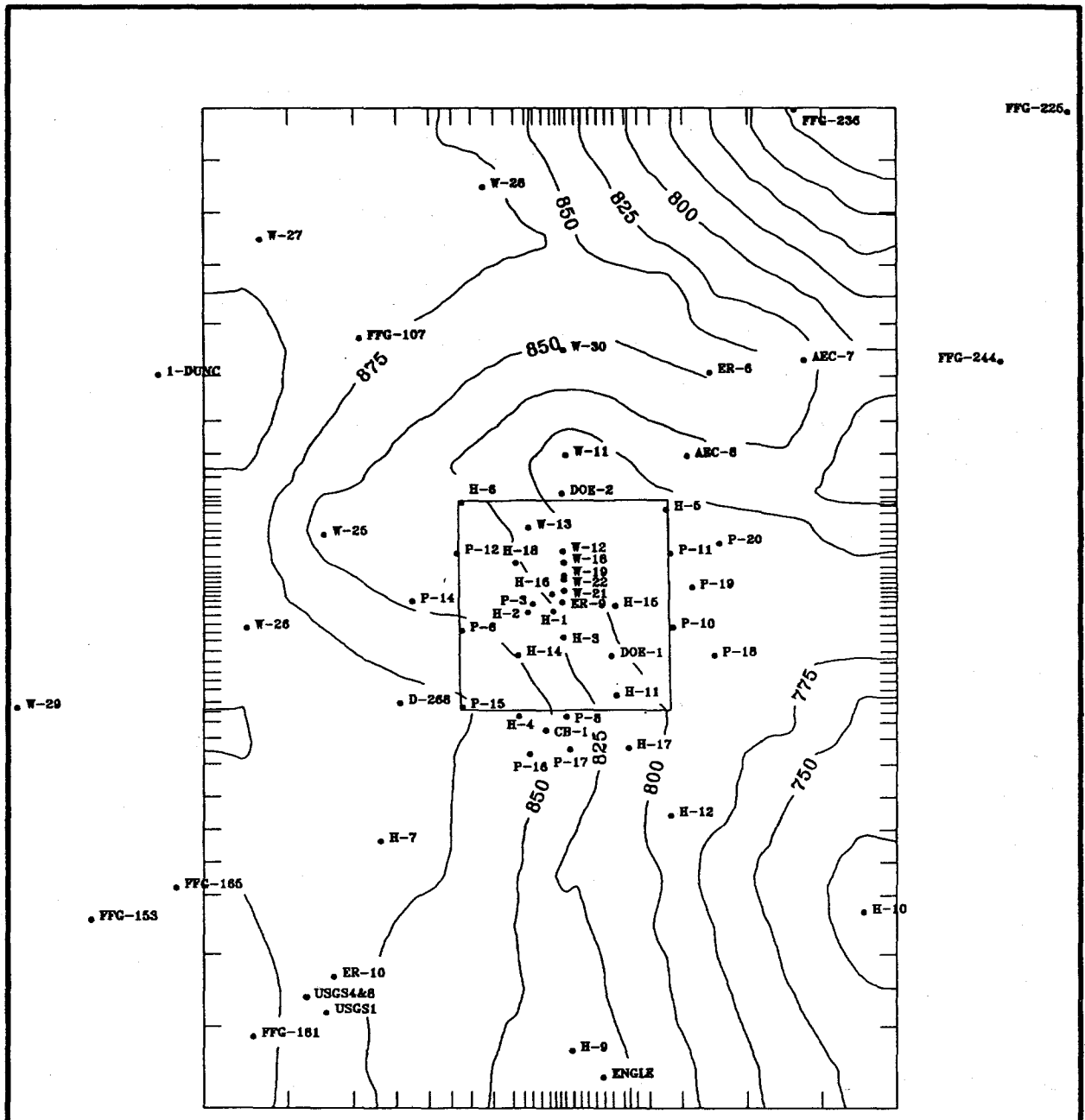
from 679 m above mean sea level (amsl) in the northeast model region to approximately 910 m in the northwest model region.

The Culebra-center elevations were estimated at each of the grid-block centers using AKRIP (Kafritsas and Bras, 1981), the MIT kriging program which utilizes generalized covariances. The kriged surface (Figure 2.8) is consistent with the observed elevation data containing higher elevations in the western part of the model area and lower elevations in the east and southeast. Generally, the Culebra dips slightly to the southeast. However, the dip increases locally within sections of the model area (e.g., the northeast corner of the model area).

#### 2.3.4 Physical Model Constants

SWIFT II requires the specification of a number of fluid- and rock-property constants that are used mainly in transient calculations. One of these parameters is the porosity of the rock. Matrix-porosity data of the Culebra dolomite were obtained from laboratory analyses on cores taken from several boreholes in the WIPP area (Kelley and Saulnier, 1990). The measured porosities range from 2.8 to 30 percent. A value of 16 percent was assumed representative for the model area. In addition, it is assumed that at the discretization scale of this model, double-porosity effects on calculated pressures are unimportant. This assumption was previously tested by comparing single- and double-porosity simulations and is presented in Haug et al. (1987) for a regional-scale model of the Culebra dolomite.

Other parameter constants that require specification include fluid temperature and viscosity, fluid and rock compressibilities, fluid thermal expansion coefficient, and fluid and rock heat capacities. Table 2.3 lists the values assigned to each of these constants in this modeling study and the pertinent references from which these parameters were taken. A detailed justification for the selection of these values is presented in Haug et al. (1987). However, note that since isothermal conditions are assumed to exist in the Culebra, the specification of some of the above parameters (e.g., thermal expansion and heat capacity) is a mere formality as a model-input data requirement and has no impact on the model results.



0 2 4 6 8 km  
SCALE

● Observation Well  
Elevations in m amsl  
Contour Interval: 25m

Drawn by ABW	Date 10/30/89
Checked by M.L.	Date 10/31/89
Revisions	Date
H09700R869	10/31/89

Center-of-Culebra Elevations in the Model Area

**INTERA** Technologies

Figure 2.8

Fluid Properties:

Temperature	= 25 °C	INTERA (1986)
Compressibility	= 4.53 x 10 <sup>-10</sup> m <sup>2</sup> /N (25 °C)	Langguth and Voigt (1980)
Thermal- Expansion Factor	= 2.07 x 10 <sup>-4</sup> °C <sup>-1</sup>	Kuchling (1982)
Heat Capacity	= 4.18 x 10 <sup>3</sup> J/kg °C	Kuchling (1982)
Viscosity	= 1.0 x 10 <sup>-3</sup> Pa s	Freeze and Cherry (1979)

References

Rock Properties:

Compressibility	= 1.1 x 10 <sup>-9</sup> m <sup>2</sup> /N	Freeze and Cherry (1979)
Heat Capacity	= 8.0 x 10 <sup>2</sup> J/kg °C	Kuchling (1982)
Density	= 2500 kg/m <sup>3</sup>	Kuchling (1982)

Transport Properties:

Longitudinal Dispersivity	= 50.0 m	Haug et al. (1987)
Transverse Dispersivity	= 2.5 m	Haug et al. (1987)
Molecular Diffusivity in Geologic Medium	= 1.6 x 10 <sup>-10</sup> m <sup>2</sup> /s	Bear (1972), Lerman (1979)

Other Properties:

Gravitational Constant	= 9.792 m/s <sup>2</sup>	D. Borns (Sandia National Laboratory, personal communication, 1989)
------------------------	--------------------------	---

Drawn by	Date
Checked by	Date
Revisions	Date

Physical Model Constants

**INTERA** Technologies

Table 2.3

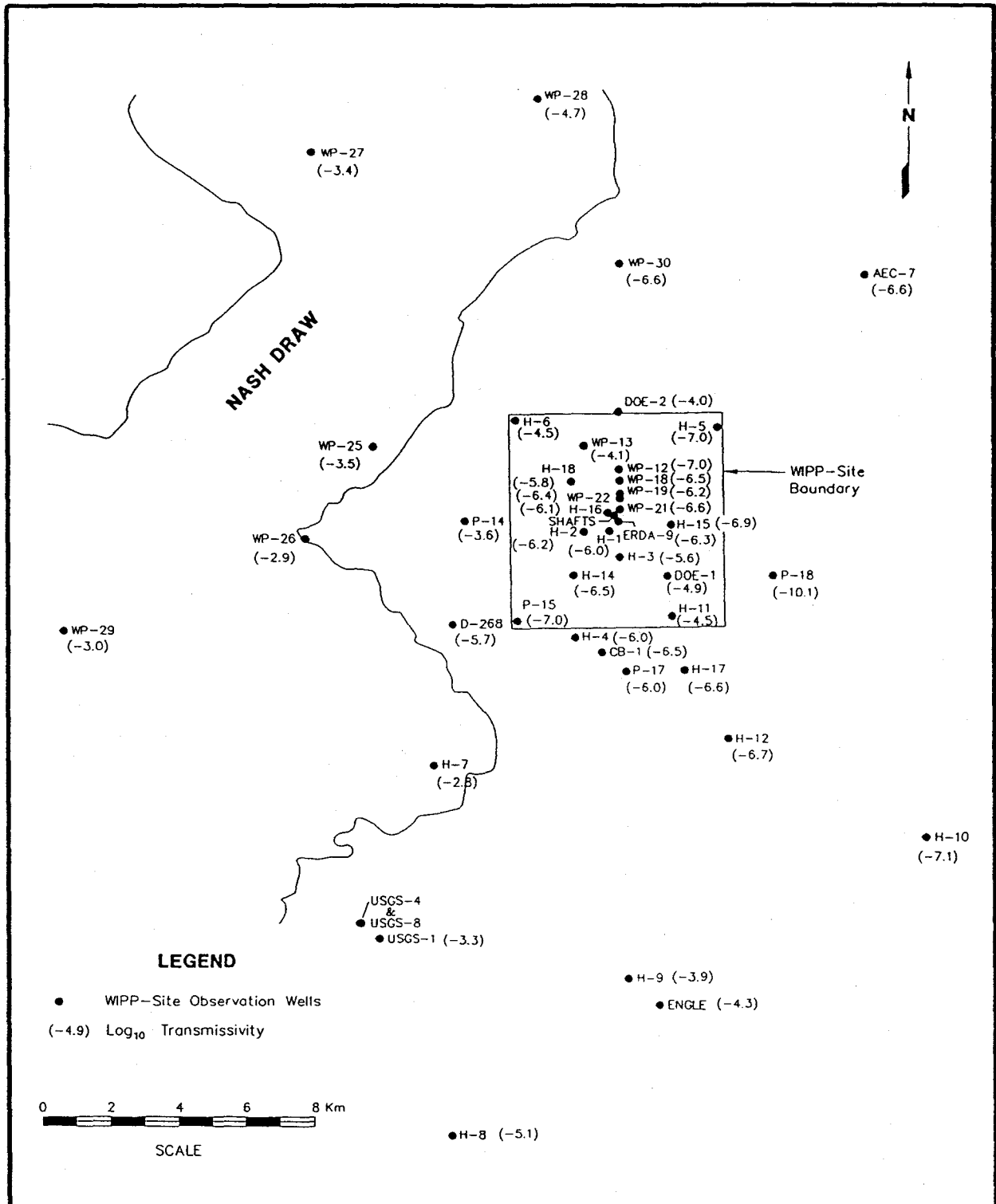
## 2.3.5 Transmissivity of the Culebra Dolomite

### 2.3.5.1 Data Base

The transmissivity data base for the Culebra dolomite (Appendix C of Cauffman et al., 1990) is derived from numerous hydraulic tests performed at the WIPP site. Values have been obtained from drill-stem tests (DST's), slug tests, and local and regional-scale pumping or interference tests. Transmissivity values interpreted from these tests extend over a range of seven orders of magnitude.

The large range in the transmissivities results from the heterogeneous nature of the Culebra dolomite. The area east of the WIPP site has, in general, lower transmissivities than regions west of the site. The large range in the transmissivities also reflects the volume of rock stressed during a hydrogeologic test which is both test and site specific. For example, at a single location the average transmissivity may vary with different types of tests, since the volume of rock actually hydraulically stressed in one type of test (e.g., slug) could be much smaller than the volume of rock stressed in another type of test (e.g., pumping). This difference in volume stressed may result in interpreted transmissivities that are representative of different spatial scales of the Culebra around the borehole. Therefore, the transmissivity data base has been evaluated in an attempt to determine representative values at a scale of tens of meters.

Appendix C of Cauffman et al. (1990) describes the rationale used to assign transmissivity values at each borehole in the modeling study. The transmissivity assigned to each hydropad or borehole was calculated by taking the mean of the  $\log_{10}$  of the published transmissivities at each location which were considered to represent the intermediate (i.e., scale of tens of meters) conditions. Regional interference transmissivity values were, therefore, not used in determining representative values at the boreholes, but were used to help guide the initial assignment of transmissivity values to the pilot points which were added during model calibration. The resulting transmissivities are illustrated in Figure 2.9 and listed in Table 2.4.



Drawn by	ABW	Date	11/2/89
Checked by	M.L.	Date	11/2/89
Revisions		Date	
H09700R869			11/2/89

**Culebra Log<sub>10</sub> Transmissivities at the WIPP-Area Boreholes (From Cauffman et al., 1990)**

**INTERA Technologies**

Figure 2.9



<u>Location</u>	<u>Transmissivity</u>		<u>Assigned</u>
	<u>(log<sub>10</sub> m<sup>2</sup>/s)</u>	<u>(m<sup>2</sup>/s)</u>	<u>Standard Deviation</u>
H-1	-6.03	9.4E-07	0.50
H-2	-6.20	6.3E-07	0.25
H-3	-5.61	2.5E-06	0.25
H-4	-6.00	1.0E-06	0.25
H-5	-7.01	9.7E-08	0.25
H-6	-4.45	3.6E-05	0.25
H-7	-2.81	1.5E-03	0.25
H-8	-5.05	8.8E-06	0.25
H-9	-3.90	1.3E-04	0.25
H-10	-7.12	7.5E-08	0.50
H-11	-4.51	3.1E-05	0.25
H-12	-6.71	1.9E-07	0.50
H-14	-6.48	3.3E-07	0.50
H-15	-6.88	1.3E-07	0.50
H-16	-6.11	7.7E-07	0.50
H-17	-6.64	2.3E-07	0.50
H-18	-5.78	1.7E-06	0.25
DOE-1	-4.93	1.2E-05	0.25
DOE-2	-4.02	9.6E-05	0.25
P-14	-3.56	2.8E-04	0.41
P-15	-7.04	9.2E-08	0.50
P-17	-5.97	1.1E-06	0.50
P-18	-10.12	7.5E-11	0.50
WIPP-12	-6.97	1.1E-07	0.50
WIPP-13	-4.13	7.4E-05	0.50
WIPP-18	-6.49	3.2E-07	0.50
WIPP-19	-6.19	6.5E-07	0.50
WIPP-21	-6.57	2.7E-07	0.50
WIPP-22	-6.40	4.0E-07	0.50
WIPP-25	-3.54	2.9E-04	0.25
WIPP-26	-2.91	1.2E-03	0.25
WIPP-27	-3.37	4.3E-04	0.25
WIPP-28	-4.68	2.1E-05	0.25
WIPP-29	-2.97	1.1E-03	0.25
WIPP-30	-6.60	2.5E-07	0.50
ERDA-9	-6.30	5.1E-07	0.50
CB-1	-6.52	3.0E-07	0.50
Engle	-4.34	4.6E-05	0.25
USGS-1	-3.26	5.5E-04	0.25
D-268	-5.69	2.0E-06	0.50
AEC-7	-6.55	2.8E-07	0.50

<small>Drawn by</small>	<small>Date</small>	<b>Culebra Transmissivities and Their Uncertainties at the WIPP-Area Boreholes</b>
<small>Checked by</small>	<small>Date</small>	
<small>Revisions</small>	<small>Date</small>	
<b>INTERA Technologies</b>		Table 2.4

### 2.3.5.2 Uncertainty of the Transmissivity Data

Differences in the uncertainty associated with the Culebra transmissivities stem from the variation in the type of hydraulic tests conducted to determine the transmissivity values. DST's, slug tests, and pumping tests were used to determine transmissivity values in the Culebra. Because each of these tests stress a different volume of rock, there are variations in the uncertainty associated with the transmissivity values determined from these tests. Thus, standard deviations ( $\sigma$ ) of the transmissivity values were assigned values based on the type of test used to obtain the value (Table 2.4). The assumed standard-deviation values are subjective estimates which are consistent with field-testing experience. For instance, a minimum standard deviation  $\sigma = 0.25 \log_{10} \text{ m}^2/\text{s}$  was assumed for pumping-test results and a standard deviation  $\sigma = 0.5 \log_{10} \text{ m}^2/\text{s}$  was considered to be appropriate for transmissivity values interpreted from the results of DST's or slug tests (Table 2.4). These assigned standard deviations are meant to represent the difference in uncertainties of the results of these tests on a scale of tens of meters. The standard deviations of the pumping test values are lower than those associated with DST or slug test values because the pumping test stresses a larger volume of rock.

If one assumes that the hydraulic tests have tested a representative rock volume and that the measurement error is normally distributed, the mean transmissivity  $\pm 2\sigma$  may be interpreted as a 95-percent confidence interval. Thus, the assumed minimum uncertainty of the pumping-test results is half an order of magnitude ( $2\sigma = 0.5 \log_{10} \text{ m}^2/\text{s}$ ), and for the other hydraulic tests it is one order-of-magnitude ( $2\sigma = 1.0 \log_{10} \text{ m}^2/\text{s}$ ). These uncertainties were used as input to the kriging code, AKRIP, in the estimation of the transmissivity distribution of the model area.

### 2.3.5.3 Estimation of Transmissivity Over the Model Region

The standard deviations of the transmissivity values were input into AKRIP to account for measurement errors or uncertainties in the input data. A brief description of the kriging equations solved by AKRIP is presented below along with a description of its application to the Culebra transmissivity data.

Kriging estimates parameter values,  $Y^*$ , over areal regions (S) by employing:

$$Y_m^*(S) = \sum_{i=1}^n \gamma_{mi} Y_i \quad (2.3)$$

where  $Y_i$  is the parameter value at observation point  $i$ , index  $i$  ranges over all  $n$  points  $\underline{x}_i$  within neighborhood of  $\underline{x}$  defined by the user, and kriging weights  $\gamma_{mi}$  represent the average weight between observation point,  $i$ , and the areal region of interest centered upon grid block  $m$ .

Taking an expectation, or mean value of the parameter of interest,  $Y$ ,  $E(Y) = \sum \alpha_k g^k(\underline{x})$ , and assuming any trend or drift present in the data may be characterized by a sum of polynomials  $g^k(\underline{x})$  of order  $k$ , with coefficients  $\alpha_k$ , kriging assumes that the data are correlated and that the generalized increments (Delfiner, 1976) are second-order stationary. That is, the mean and variance of the increments  $Y(\underline{x}_i) - Y(\underline{x}_i + h)$  are invariant with a translation in space. In this study, the covariance of the generalized increments (Delfiner, 1976), expressed as a generalized covariance function (GCF), is taken to have the form:

$$K(s) = c\delta |s| + a_1 |s| + a_3 |s|^3 + a_5 |s|^5 \quad (2.4)$$

where, assuming isotropy,  $s$  represents the magnitude of the separation between two points in the domain. The Kroenecker delta  $\delta$  is zero for all values of its argument except for  $s=0$ , where it equals unity. Constrained by the relations of Delfiner (1976), coefficients  $c$  and  $a_k$  represent application-dependent coefficients.

Determination of the kriging weights  $\gamma_{mi}$  for each interpolation area derive from a consideration of the "true" value  $Y_m$  and its relation to the interpolate  $Y_m^*$ . The weights  $\gamma_{mi}$  are chosen so that the kriging estimator is unbiased [ $E(Y_m^* - Y_m) = 0$ ] and has a minimum estimation variance [ $\text{var}(Y_m^* - Y_m) = \text{minimum}$ ] in the class of unbiased linear predictors (Journal and Huijbregts, 1978). Both the order  $k$  of the drift and coefficients  $c$  and  $a_k$  of the GCF are determined iteratively from a comparison of observed data  $Y_i$  with

kriged estimates  $Y_i^*$ , obtained successively at each observed location. The coefficients  $c$  and  $a_k$  must satisfy the requirements that, considering all the data, there be no systematic bias and that the kriging errors be consistent with the predicted variance (Kafritsas and Bras, 1981). Interestingly, all results are invariant to the value of the drift because the weights,  $\gamma_{mi}$ , are constrained such that they eliminate any non-stationary component of order less than  $k$  in the observed data.

For determination of the kriging weights  $\gamma_{mi}$ , and the kriging coefficients  $k$ ,  $c$ , and  $a_k$ , the analysis used a revised version of the computer code AKRIP (Kafritsas and Bras, 1981). The kriging coefficients are solved through a linear-regression procedure which is described in Delfiner (1976). Implemented as a preprocessor to SWIFT II, this code provided fixed values for density  $\rho(\underline{x})$ , and elevation  $z(\underline{x})$  at the centroid of each grid block. Interpolating the observed freshwater heads, it also provided boundary values for freshwater head,  $h_f(\underline{x})$ , at the extremities of the modeled region, where freshwater head relates to pressure by the relation  $p = \rho(h_f - z)$ . Finally, interpolating the  $\log_{10}$ -transmissivity field  $Y(\underline{x}) = \log_{10}[T(\underline{x})]$ , AKRIP provided the grid-block values of  $\log_{10}$ -transmissivity which were converted to conductivities and used in the SWIFT II model.

In this study, a local neighborhood is used during the estimation procedure of both the GCF coefficients and of the variable (i.e.,  $\log_{10}$  transmissivity) once the GCF has been determined. The neighborhood was defined as the ten nearest observed data points surrounding a particular grid block in the model area. Using this local neighborhood, a zero-order GCF was determined to best represent the structure of the  $\log_{10}$  transmissivity field. Equation 2.5 lists this GCF:

$$K(h) = -2.3 \times 10^{-4} |h| \quad (2.5)$$

where  $K(h)$  is the generalized covariance and  $h$  is the average distance between an observed data point and the center of the estimation area. A consistency check is normally performed on the theoretical GCF to verify that it is statistically consistent with the input data. A GCF that is consistent with the

input data should provide a reduced mean-square error near 1.0 (de Marsily, 1986). The GCF listed in Equation (2.5) gives a reduced mean square error of 1.5. However, Equation (2.5) preserves the input data at the observed points better than other GCF models that had better mean-square error values but contained a nugget. The zero order GCF implies that within local neighborhoods of the  $\log_{10}$ -transmissivity field, there is not a significant consistent trend.

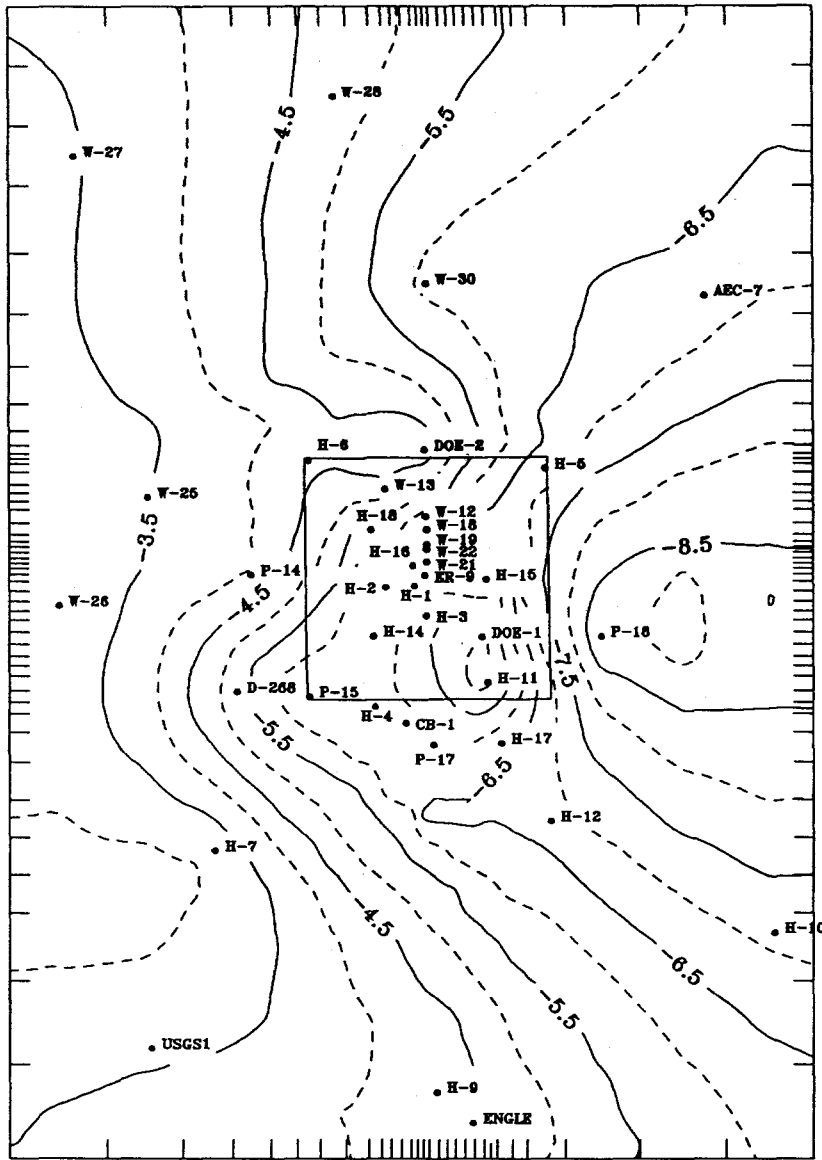
The initial grid-block  $\log_{10}$ -transmissivity estimates and the corresponding estimation errors calculated using the above GCF are shown in Figures 2.10a and 2.10b, respectively. These figures depict the higher transmissivity values in the western part ( $\log_{10}$  transmissivity from -3.0 to -3.5) of the model region and the lower values ( $\log_{10}$  transmissivity from -6.0 to -8.0) in the east. The lowest values of transmissivity occur along the eastern boundary and reflect the projection of the underlying local trends determined by AKRIP. The kriged  $\log_{10}$ -transmissivity values estimated for the grid blocks within the WIPP-site boundary vary from -4.1 at the grid block containing the H-6 borehole to -6.3 at the grid block containing the P-15 borehole. A local high occurs in the grid blocks within the vicinity of the H-11 and DOE-1 boreholes where the block estimates are between -4.5 and -5.0.

The estimation errors (as defined by one standard deviation) within the model region are highest near the northeast boundary due to the lack of data in the area. Here the errors have values of 1.5. Within the central portion of the model area, the errors of the estimates are between 0.5 and 0.75 of  $\log_{10}$  transmissivity.

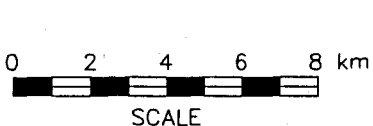
## 2.3.6 Storativity of the Culebra Dolomite

### 2.3.6.1 Data Base

The storativity data base (Appendix D of Cauffman et al., 1990) was evaluated to determine representative values at a scale of tens of meters. The rationale used in the evaluation is discussed in Cauffman et al. (1990). The final values assigned to borehole locations are listed in Table 2.5. The total number of



● Observation Well  
 Transmissivities in  $\log_{10} \text{ m}^2/\text{s}$   
 Contour Interval:  $0.5 \log_{10} \text{ m}^2/\text{s}$

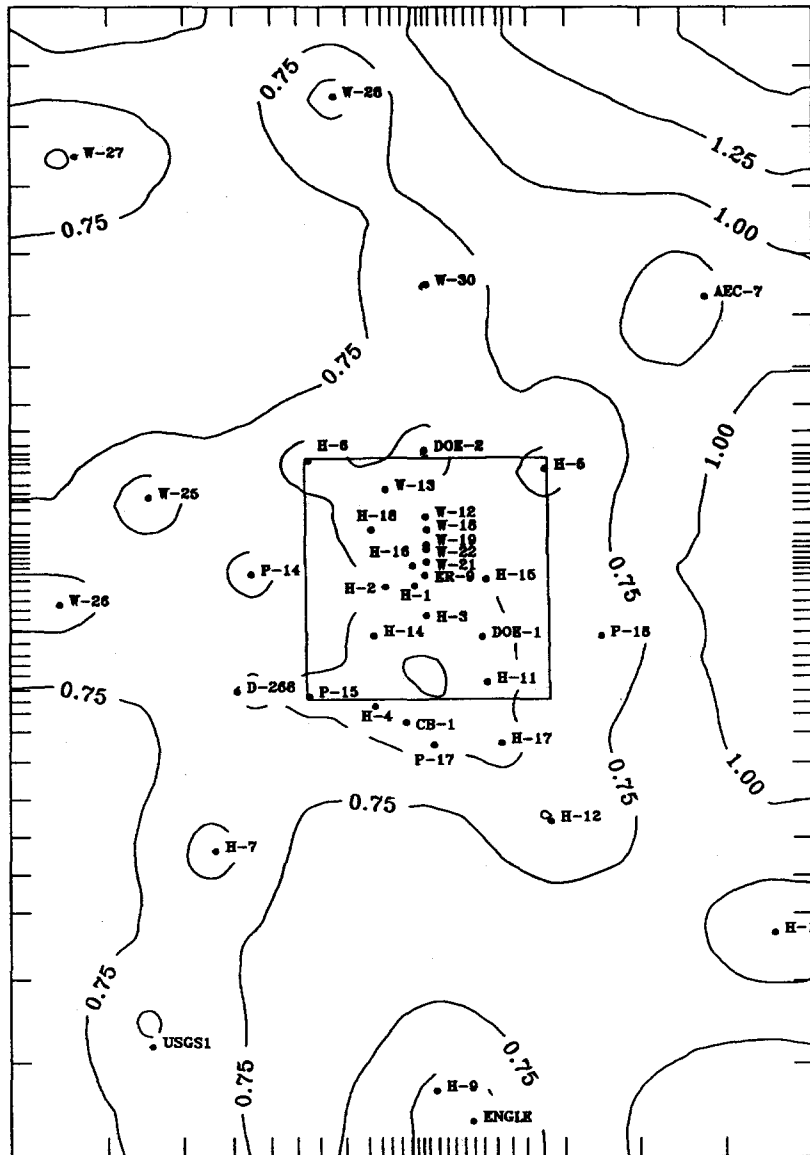


Drawn by	ABW	Date	10/30/89
Checked by	M.L.	Date	10/31/89
Revisions		Date	
H09700R869			10/31/89

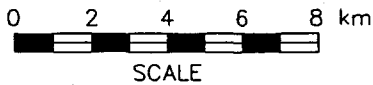
Initial Kriged  $\log_{10}$  Transmissivity Field

**INTERA** Technologies

Figure 2.10a



● Observation Well  
 Standard Deviations of the Kriging Estimation Errors of Log<sub>10</sub> T, T in m<sup>2</sup>/s  
 Contour Interval: 0.25



Drawn by	ABW	Date	10/30/89
Checked by	M.L.	Date	10/31/89
Revisions		Date	
H09700R869		10/31/89	

Initial Standard Deviations of the Estimation Errors of Log<sub>10</sub> Transmissivity

**INTERA** Technologies

Figure 2.10b

<u>Location</u>	<u>Storativity</u>	
	<u>(log S)</u>	<u>(S)</u>
H-2	-4.89	1.3E-05
H-4	-5.34	4.6E-06
H-5	-4.55	2.8E-05
H-6	-3.63	2.4E-04
H-9	-3.42	3.8E-04
H-11	-3.33	4.7E-04
H-16	-5.00	1.0E-05
P-14	-4.70	2.0E-05
WIPP-25	-2.00	1.0E-02
WIPP-26	-2.32	4.8E-03
WIPP-27	-6.00	1.0E-06
WIPP-28	-1.30	5.0E-02
USGS-1	-4.70	2.0E-05

Drawn by	Date	<b>Culebra Storativity at the WIPP-Area Boreholes</b>
Checked by	Date	
Revisions	Date	
<b>INTERA Technologies</b>		Table 2.5



storativity values is much less than the number of transmissivity values. The storativity values in the central model region have a mean of  $3 \times 10^{-5}$  and have a range that extends over two orders of magnitude ( $5 \times 10^{-6}$  to  $5 \times 10^{-4}$ ). West of the central model region, the estimated storativities are much higher. The storativities from these wells were not considered in assigning storativity values to the model because they were based only on single-well test interpretations.

### 2.3.6.2 Model Storativity

The rock compressibility used by SWIFT II in calculating storativity is not identical to the rock compressibility typically used in hydrogeological studies but is commonly used in the petroleum industry (Narasimhan and Kanehiro, 1980). The rock compressibility used in most hydrogeological studies is defined in terms of a bulk-volume compressibility whereas in the petroleum industry it is defined in terms of a pore-volume compressibility. SWIFT II calculates storativity as:

$$S = \phi \rho g b (\alpha + \beta) \quad (2.6)$$

where

$\phi$  = porosity

$\rho$  = fluid density

$b$  = aquifer thickness

$\alpha$  = rock compressibility

$\beta$  = fluid compressibility

The storativity value calculated for the transient modeling in this study is  $2 \times 10^{-5}$ , the same value used in the previous Haug et al. (1987) and LaVenue et al. (1988) studies. A single value was chosen due to the sparsity of storativity data. In addition, since transient pressures are much more sensitive to changes in the transmissivity, the storativity within the model was not changed during transient calibration.

## 2.3.7 Freshwater Heads in the Culebra Dolomite

### 2.3.7.1 Data Base

Data from the observation-well network in the Culebra were evaluated in this study to characterize the hydraulic conditions in the Culebra. Appendix G of Cauffman et al. (1990) presents the hydrographs plotted as equivalent freshwater head versus time. (The term "freshwater head" is utilized in this report and is equivalent to the term "freshwater elevation above mean sea level" because the head values are always related to mean sea level. It refers to the elevation of a column of fresh water with a fluid density of  $1 \text{ g/cm}^3$  that would exert a pressure at the elevation of the Culebra equal to the formation pore pressure.)

The freshwater-head data are calculated from either depth-to-water or downhole-pressure-transducer measurements. The procedure used and the information necessary to calculate the freshwater heads is also presented in Appendix G of Cauffman et al. (1990). In addition to the monitoring wells, transducers installed in the exhaust shaft, waste-handling shaft, and construction-and-salt-handling shaft at the WIPP site have monitored pressures at the Culebra-liner interface. From these hydrographs, estimates of the undisturbed hydraulic conditions and the transient responses due to shaft and site-characterization activities in the Culebra dolomite were assessed.

The calculation of the equivalent freshwater heads from depth-to-water and transducer measurements requires knowledge of the average borehole-fluid density. The estimation of the uncertainty in the borehole-fluid-density estimates and the corresponding uncertainty in the equivalent freshwater heads are discussed in Appendix F of Cauffman et al. (1990). In addition to the fluid-density uncertainty, sources of freshwater-head uncertainty include uncertainties in the reference elevation and the depth-to-water measurements, water-level variations exhibited in a well's hydrograph which may be the result of long-term natural head changes (trends) or, in some cases, changes of unknown origin, and shorter-term transients (residual effects) that are due to

the stress imposed on the Culebra interval by shaft activities, well testing, and/or water-quality sampling activities. Appendix G of Cauffman et al. (1990) lists the estimates of these individual uncertainties for each undisturbed freshwater-head estimate and combines all but the uncertainty due to trends to obtain a total uncertainty at each well, which is meant to correspond to the upper and lower bounds of the freshwater-head measurements. The uncertainty due to trends was not included in the overall freshwater-head uncertainty because the trends are poorly understood.

The term "observed freshwater heads" is used in this report to refer to equivalent freshwater heads that are determined from the depth-to-water and transducer measurements. The term "calculated freshwater heads" refers to heads calculated using SWIFT II.

#### 2.3.7.2 Estimation of the Undisturbed Hydrologic Conditions Over the Modeled Region

The undisturbed freshwater heads are assumed to be representative of a quasi-steady-state system relative to the time frame and magnitude of the WIPP-related hydraulic stresses. Haug et al. (1987) found that leakage from the Culebra into the WIPP shafts has occurred since the excavation of the first shaft (the construction and salt-handling shaft, 7/4/81-10/23/81). This leakage has caused drawdown responses at many of the observations wells at the WIPP site. For this reason, undisturbed freshwater heads are best determined from data collected before mid 1981. For wells in close proximity to the shafts for which no water-level data were recorded before the summer of 1981, undisturbed freshwater heads could not be estimated.

The determination of long-term mean formation pressures referred to as undisturbed pressures involved evaluating the hydrographs for the WIPP-site boreholes (Appendix G, Cauffman et al., 1990). We assume that the undisturbed pressures represent the quasi-steady-state pressure field that was present before the excavation of the shafts. Table 2.6 summarizes the estimates of undisturbed freshwater head for each of the wells and also lists the uncertainty associated with that value. The uncertainties listed in Table 2.6 are not symmetrical

<u>Location</u>	<u>Undisturbed Equivalent Freshwater Head (m amsl)</u>	<u>Uncertainty of Observed Head (m)</u>
H-1	923.3	+/-2.0
H-2	923.1	+1.8/-0.1
H-3	917.1	+1.9/-0.1
H-4	912.8	+/-0.6
H-5	934.0	+/-1.4
H-6	932.6	+/-1.0
H-7	912.5	+0.5/-0.1
H-8	912.1	+0.6/-0.1
H-9	907.6	+1.2/-0.1
H-10	921.4	+/-2.2
H-11	913.1	+1.5/-1.0
H-12	913.7	+1.2/-1.3
H-14	915.2	+0.7/-0.1
H-15	915.7	+2.8/-0.1
H-17	911.0	+/-0.9
H-18	932.1	+1.5/-1.1
DOE-1	914.2	+2.6/-2.2
DOE-2	935.3	+/-1.5
P-14	926.9	+/-0.9
P-15	916.8	+/-0.8
P-17	911.6	+/-0.7
WIPP-12	931.5	+1.3/-0.1
WIPP-13	934.0	+1.2/-1.3
WIPP-18	930.0	+/-1.2
WIPP-25	928.7	+/-1.0
WIPP-26	919.3	+0.4/-0.1
WIPP-27	938.1	+/-0.7
WIPP-28	937.2	+0.9/-1.2
WIPP-29	905.3	+0.3/-0.2
WIPP-30	935.3	+0.9/-1.3
CB-1	911.6	+0.7/-0.6
USGS-1	909.7	+0.4/-0.1
USGS-4	909.7	+/-0.1
USGS-8	911.1	+/-0.1
D-268	915.0	+0.4/-0.1
AEC-7	931.6	+/-2.3

Drawn by	Date	<b>Culebra Undisturbed Equivalent Freshwater Heads and the Associated Uncertainties</b>
Checked by	Date	
Revisions	Date	

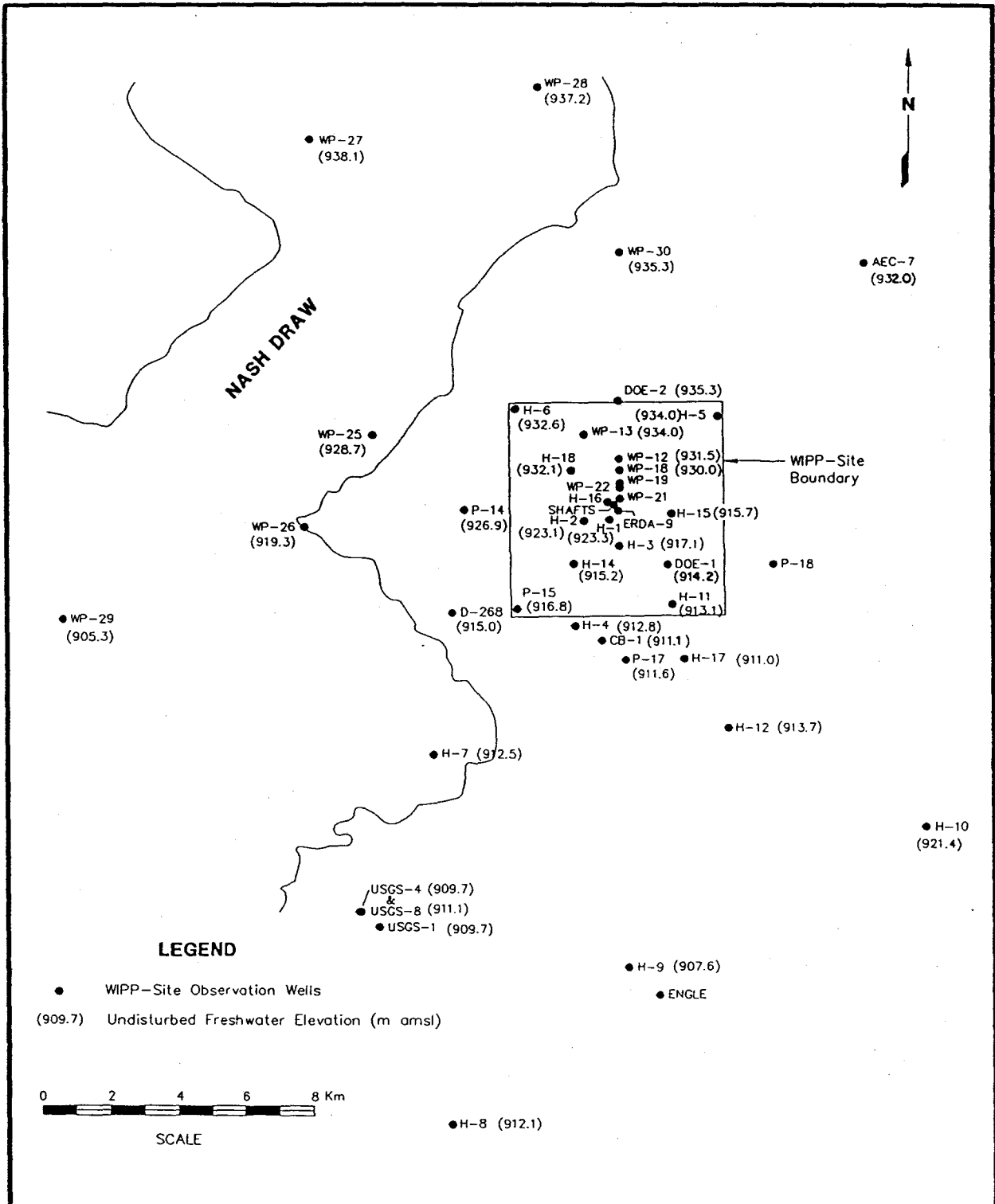
**INTERA** Technologies

Table 2.6

because of the unsymmetrical nature of the uncertainties of the borehole fluid density and the residual effects which contributed the most to the overall head uncertainties (Cauffman et al., 1990). Figure 2.11 shows the distribution of these values over the model area. The H-11, H-15, H-18, and DOE-1 undisturbed freshwater heads presented in Table 2.6 are slightly different from those presented in Cauffman et al. (1990) due to the addition of the estimated residual head (Table G.2, Cauffman et al., 1990) which attempts to account for any recovery which may still be occurring at these locations due to the cone of depression caused by the excavation of the shafts. Section 5.3 discusses this assumption in more detail and its effect on the differences between the calculated and observed freshwater heads.

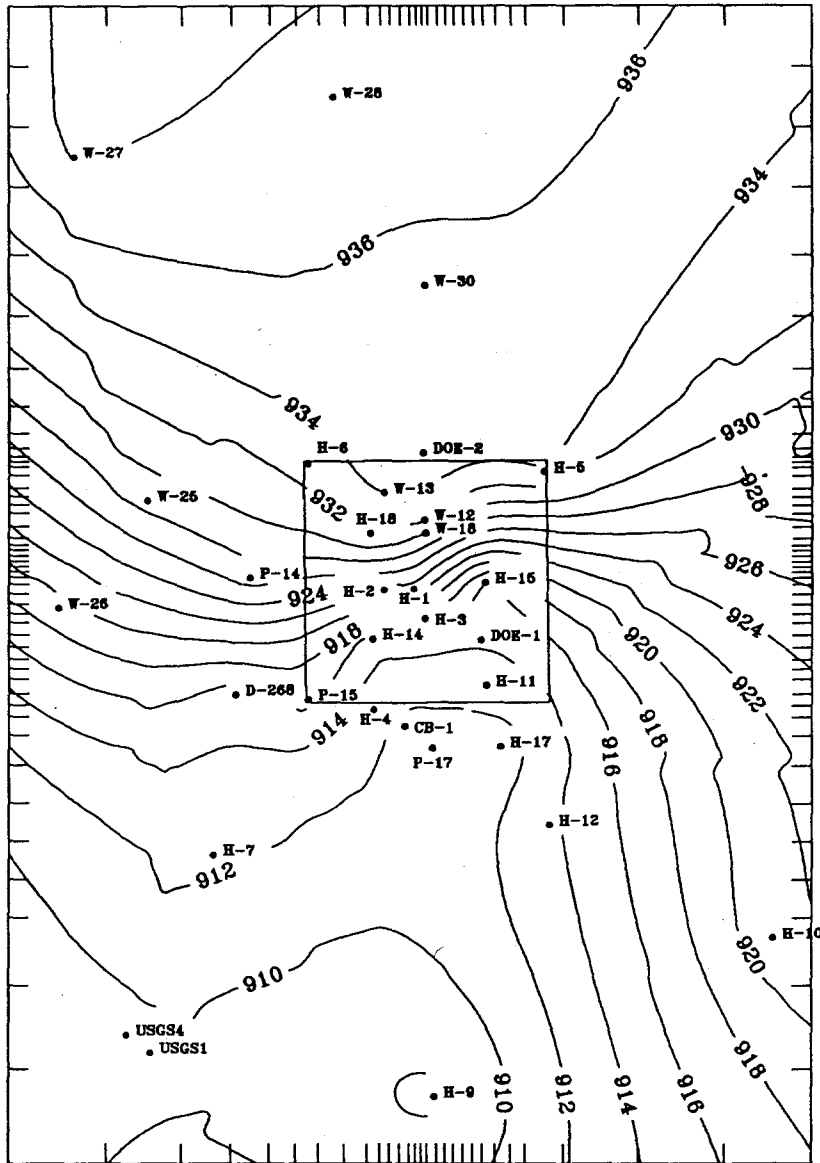
A contour of the undisturbed freshwater heads is illustrated in Figure 2.12. The freshwater heads reveal a predominantly southerly flow direction across the WIPP site. The heads within the southeastern portion of the modeled area reflect an approximately western flow direction. Low hydraulic gradients ( $1 \times 10^{-4}$  m/m) exist north and south of the WIPP site. The low gradient north of the WIPP site is defined by the minor head differences between the WIPP-28, WIPP-27, WIPP-30, DOE-2, H-5, and H-6 boreholes. The low gradient south of the WIPP site is defined by the minor head differences between the H-17, P-17, H-4, CB-1, H-12, H-7, and H-9 boreholes. Hydraulic gradients are higher ( $4 \times 10^{-3}$  m/m) in the north-central and central portions of the site. These higher gradients appear consistent with the lower transmissivities within this region. However, the initial transmissivity distribution with low transmissivities in the area of H-4, CB-1, P-17, and H-17 is not consistent with the observed low gradients immediately south of the southern site boundary. This implies that the estimated transmissivity field in this region does not adequately represent the actual transmissivities and will have to be modified during the calibration of the model in order to reproduce the observed heads.

It should also be noted that previous analyses conducted by Davies (1989) have indicated that the fluid-density distribution and the changes in elevation have a large effect upon the flow in low-hydraulic-gradient areas due to the pressure imposed by gravitational forces.

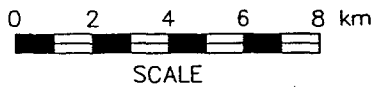


Drawn by	ABW	Date	11/2/89	<b>Culebra Freshwater Heads at the WIPP-Area Boreholes</b> (From Cauffman et al., 1990)
Checked by	M.L.	Date	11/2/89	
Revisions		Date		
H09700R869		11/2/89		

<b>INTERA</b> Technologies		Figure 2.11
----------------------------	--	-------------



• Observation Well  
 Freshwater Heads in m amsl  
 Contour Interval: 2m



Drawn by ABW	Date 10/30/89
Checked by M.L.	Date 10/31/89
Revisions	Date
H09700R869	10/31/89

Culebra Freshwater-Head Contour Surface

INTERA Technologies

Figure 2.12

### 2.3.7.3 Hydraulic Stresses Since 1981

Since the summer of 1981, the freshwater-head distribution in the Culebra dolomite has been influenced by drilling and excavating four shafts (waste-handling shaft, construction and salt-handling shaft, exhaust shaft, and air-intake shaft) at the center of the WIPP site (see chronology and discussion of shaft-construction activities in Appendix H of Cauffman et al., 1990). In addition, several wells have been drilled or re-completed in the model area and numerous well-testing activities, some of very long durations (e.g., H-4 tracer test), have been conducted since 1981 (Section 4). Consequently, the hydrologic conditions at the beginning of the H-3, WIPP-13, and H-11 multipad pumping tests cannot be considered to be undisturbed. Haug et al. (1987) illustrated the large drawdown cone caused by the different activities at the WIPP site since 1981. The center of the drawdown cone coincides with the location of the shafts. The diameter of the drawdown cone was about 7 km and the depth was about 33 m at the shaft location. The drawdowns at wells H-1 and H-2 reached maxima of about 12.2 m and 7.1 m, respectively (Haug et al., 1987).

The specification of these disturbances at the WIPP site, which are transient by their nature, was achieved using the wellbore submodel of SWIFT II (Reeves et al., 1986a). This submodel allows injection or withdrawal of water from the model at specified locations (i.e., at the shaft or well locations). Details of these events are discussed in Section 4. Similarly, the H-3, WIPP-13, and H-11 multipad pumping tests were specified using the above-mentioned wellbore submodel. These tests are also discussed in detail in Section 4.

### 2.3.7.4 Initial Boundary Conditions

The Culebra dolomite along the eastern boundary of the model area is characterized by extremely low transmissivities and negligible flow. The eastern boundary was therefore initially considered to be reasonably represented as a no-flow boundary. During steady-state calibration, however, pressures were eventually assigned to the eastern model boundary. Prescribed-pressure boundaries with prescribed formation-water densities were applied to the northern, southern, and western boundaries. Freshwater heads were estimated



at the outer edges of all grid blocks along the northern, southern, and western model boundaries using the heads specified in the steady-state calibrated model presented in LaVenue et al. (1988).

### 2.3.8 Formation-Fluid Densities

#### 2.3.8.1 Data Base

The formation-fluid-density data base (Appendix E of Cauffman et al., 1990) was compiled and evaluated to determine the most recent and most reliable fluid-density information available for the Culebra dolomite. The principal sources used in compiling the data base include:

- Hydrogeologic and hydrologic data reports (Mercer, 1983; INTERA and Hydro Geo Chem, 1985; INTERA, 1986; Saulnier et al., 1987; Stensrud et al., 1987, 1988a,b, 1990)
- Geochemistry reports (Robinson, 1987; Uhland and Randall, 1986; Uhland et al., 1987; Randall et al., 1988; Lyon, 1989)
- Unpublished INTERA and Hydro Geo Chem notes from field logbooks.

In Haug et al. (1987) and LaVenue et al. (1988), an attempt was made to determine which formation-fluid-density values are most representative of in-situ formation fluids. Unfortunately, several WIPP-area boreholes have not had sufficient pumping to remove drilling fluids still present in the formation around the boreholes. However, the fluid-density data base was evaluated and formation-fluid-density values believed to be the most representative of in-situ ground waters were determined. A detailed description of the methodology used in the evaluation of the representativeness of the fluid-density values is discussed in Haug et al. (1987).

The densities used in the present study (Table 2.7) are similar to those presented in LaVenue et al. (1988). The density values have been updated where necessary to provide the most representative values of in-situ ground-water densities (at 25° C) available at this time.

Location

Formation-Fluid Density

(g/cm<sup>3</sup>)

H-1	1.022
H-2	1.006
H-3	1.035
H-4	1.014
H-5	1.102
H-6	1.038
H-7b	0.999
H-8b	1.000
H-9b	1.000
H-10b	1.047
H-11	1.078
H-12	1.095
H-14	1.010
H-15	1.154
H-17	1.100
H-18	1.017
DOE-1	1.088
DOE-2	1.041
P-14	1.018
P-15	1.015
P-17	1.061
WIPP-13	1.046
WIPP-19	1.059
WIPP-25	1.009
WIPP-26	1.009
WIPP-28	1.032
WIPP-30	1.018
Engle	1.001
USGS-1	1.000
USGS-4	1.000
USGS-8	1.000

Drawn by	Date
Checked by	Date
Revisions	Date

Culebra Formation-Fluid Densities at the WIPP-Area Boreholes

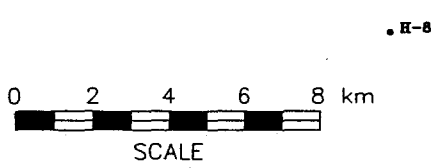
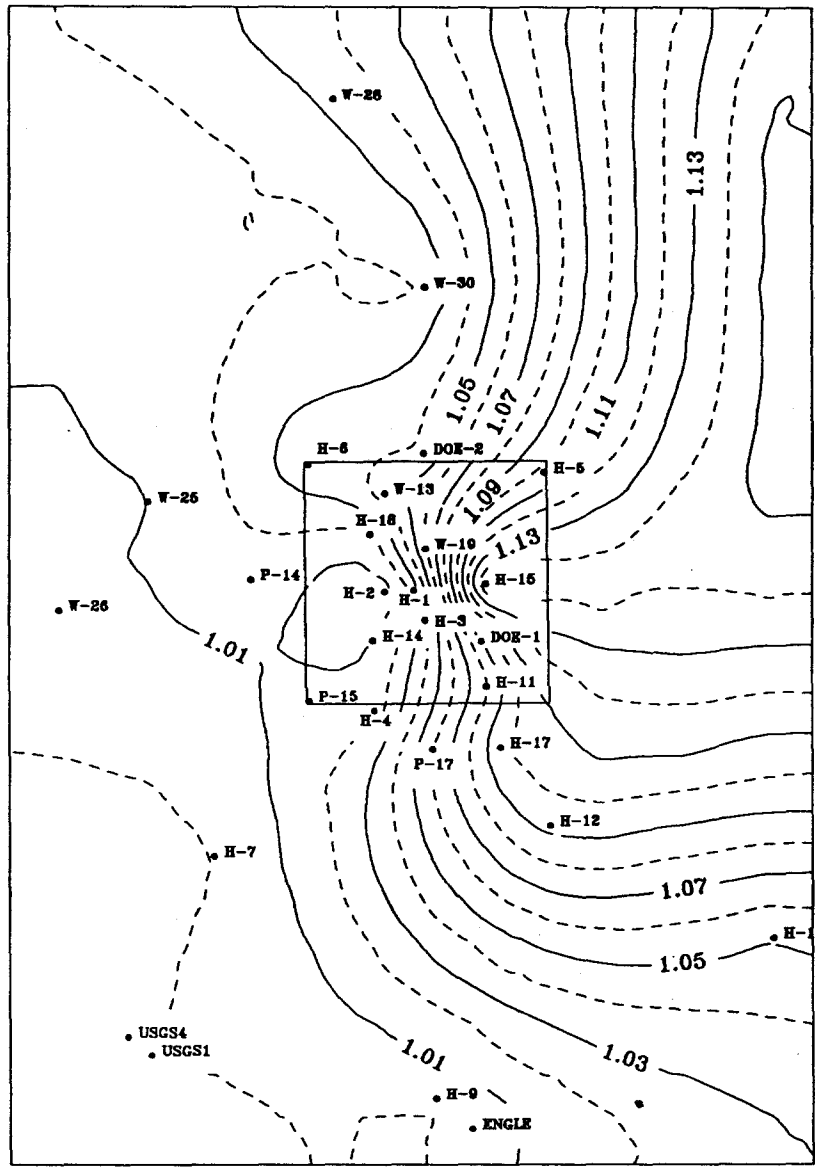
**INTERA** Technologies

Table 2.7

### 2.3.8.2 Estimation of Formation-Fluid Densities Over the Modeled Region

The fluid-density data deemed representative of the Culebra were used to estimate the formation-fluid densities over the model region. The kriging code, AKRIP, calculated the estimates of fluid densities which were assigned to the model grid blocks. Densities ranging from 1.00 to 1.03 g/cm<sup>3</sup> occur in a wide region extending from boreholes WIPP-28 to H-7b (Figure 2.13). Higher fluid densities were estimated east of this region with values ranging from 1.04 to 1.16 g/cm<sup>3</sup> along the eastern boundary. The area of the model with the highest uncertainty in fluid-density values occurs along the eastern boundary. Data in this area were estimated from the west-east trend in the observed values. Fluid-density values in the central region of the model area have lower uncertainties due to the larger number of boreholes located there.

At this point, several remarks should be made regarding the use of the estimated formation densities in the model. Geochemical investigations (Lambert and Harvey, 1987; Chapman, 1986; Lambert and Carter, 1987; and Lambert, 1987) suggest that the chemical constituents within the Culebra dolomite may not be at steady state with the present flow field. The time constant needed to achieve steady-state conditions for the Culebra formation-fluid density in the WIPP region is considered much larger, e.g., several thousand years, than the time constant for flow, e.g., several years. Therefore, using the observed formation-fluid densities as a calibration parameter during steady-state flow simulation would not be valid. For this reason, the formation-fluid densities estimated for each of the grid blocks were held constant for all model simulations. This allowed inclusion of the observed density distribution and the effects that variable densities have on the present-day flow field (i.e., calculated pressures and Darcy velocities).



● Observation Well  
 Formation-Water Densities in  $\text{g/cm}^3$   
 Contour Interval:  $0.01 \text{ g/cm}^3$

Drawn by ABW	Date 10/30/89
Checked by M.L.	Date 10/31/89
Revisions	Date
H09700R869	10/31/89

Kriged Formation-Fluid Densities Used in Model

**INTERA** Technologies

Figure 2.13

### 3.0 SIMULATION OF FLOW UNDER UNDISTURBED HYDROLOGIC CONDITIONS (PRE-SHAFT)

The first step in the simulation of ground-water flow in the Culebra dolomite was to define an initial set of parameters. Boundary conditions of the conceptual model and values of the system parameters (such as storativity, transmissivity, and various system constants as presented in Tables 2.2 to 2.7) were selected based on the documented data base. Using these data, a simulation was performed to assess how well the initial estimates of the system parameters reproduced the observed, undisturbed freshwater heads.<sup>1</sup> Subsequent changes to the initial estimates of the boundary conditions were made to reduce the differences between the calculated and observed heads in the northern and western model areas. Changes to the transmissivity field were then implemented as required to minimize the difference between the calculated and observed heads throughout the model region. The transmissivity changes were guided by the determination of high-sensitivity regions calculated by the GRASP II code (RamaRao and Reeves, 1990). High-sensitivity regions are defined as areas within the model area where changes in the transmissivity values will result in a significant reduction in the difference between calculated and observed freshwater heads. The model was considered calibrated to the undisturbed or steady-state conditions when the difference between the calculated and observed freshwater heads was consistent with the uncertainty assigned to each observed freshwater head. The results of the initial and final calibrated simulations for flow under undisturbed hydrologic conditions and a more detailed explanation of the technical approach are presented in the following subsections. The results for calibration to the transient events are presented in Section 5.

#### 3.1 Initial Parameter Values

The system parameters which comprise the components of the initial model conditions have been previously described in Section 2.3. The conceptual model, described in Section 2.3, is a two-dimensional, steady-state flow system with variable

---

1. As discussed in Section 2.3.7.1, "observed freshwater heads" refer to equivalent freshwater heads calculated from depth-to-water and transducer-pressure measurements.

fluid densities and formation elevations. The fluid densities were simulated as spatially fixed, i.e., no transport of brine is calculated in the steady-state model because the transport of brine is very slow compared to the time needed for pressure re-equilibration. Furthermore, no sources, sinks, or vertical flux are considered in this conceptual model for the undisturbed hydrologic conditions.

The initial model parameters are described in Section 2.3. The initial conductivities assigned to each model grid block are taken from the  $\log_{10}$  kriged transmissivity estimates obtained using AKRIP (Section 2.3.5.3). The initial boundary conditions (Table 3.1) were estimated from the the kriged density distribution (Section 2.3.8.2) and by extrapolating the pressures onto the model boundaries from the calibrated model presented in LaVenue et al. (1988). The eastern boundary was considered initially as a no-flow boundary. The transmissivities and the pressures prescribed for the model boundaries are the calibration parameters used in the simulations. However, because the assigned pressures are constrained by the observed freshwater-head data, the transmissivity distribution is considered the main calibration parameter.

### 3.2 Initial Steady-State Simulation

After establishing the initial boundary conditions and initial model parameters described above, the initial simulation of steady-state flow in the Culebra was performed. The results of this initial run are shown in Figures 3.1 and 3.2. Figure 3.1 illustrates the calculated freshwater heads derived from the calculated formation pressures and assigned fluid densities. The difference between the calculated and observed heads is shown in Figure 3.2.

Figure 3.2 illustrates that the calculated heads in the initial simulation do not reproduce the observed heads. The differences between the calculated and the observed heads have negative values (more than -4 m) in the north-central part of the modeled region and relatively positive values (more than 8 m) in the south-central part of the modeled region (Table 3.2). The negative values indicate the calculated head values are lower than the observed head values in the northern region. The positive differences of 0.9 m and 2.3 m that occur at WIPP-27 and

Model Indices			Grid-Block Center Elev	Specified Press @ Grid-Block Center (Pa)	Freshwater Head (m)	Fluid Density (kg/m <sup>3</sup> )
I	J	K	m			
-----						
Western Boundary						
-----						
1	1	1	908.7	8.961E+04	907.5	1000.0
1	2	1	912.1	6.121E+04	908.0	1000.4
1	3	1	902.0	1.699E+05	909.0	1001.2
1	4	1	899.0	2.120E+05	910.3	1001.6
1	5	1	897.4	2.306E+05	910.6	1002.0
1	6	1	898.9	2.198E+05	911.0	1000.8
1	7	1	898.5	2.277E+05	911.4	1002.0
1	8	1	900.6	2.110E+05	911.8	1003.2
1	9	1	900.4	2.149E+05	912.0	1004.2
1	10	1	900.2	2.208E+05	912.4	1004.8
1	11	1	900.0	2.267E+05	912.8	1005.3
1	12	1	899.8	2.326E+05	913.2	1005.8
1	13	1	899.5	2.384E+05	913.5	1006.3
1	14	1	899.3	2.424E+05	913.7	1006.8
1	15	1	899.0	2.482E+05	914.0	1007.2
1	16	1	898.4	2.580E+05	914.4	1007.6
1	17	1	897.8	2.678E+05	914.8	1008.1
1	18	1	897.1	2.786E+05	915.2	1008.4
1	19	1	895.9	2.943E+05	915.6	1008.7
1	20	1	893.7	3.197E+05	916.0	1009.0
1	21	1	890.8	3.559E+05	916.8	1009.3
1	22	1	888.2	3.892E+05	917.6	1009.5
1	23	1	886.2	4.157E+05	918.3	1009.6
1	24	1	884.5	4.402E+05	919.1	1008.8
1	25	1	891.8	3.755E+05	919.8	1009.0
1	26	1	891.0	3.912E+05	920.6	1009.1
1	27	1	890.3	4.049E+05	921.3	1009.4
1	28	1	889.7	4.186E+05	922.1	1009.4
1	29	1	889.0	4.333E+05	922.9	1006.4
1	30	1	888.2	4.480E+05	923.6	1006.4
1	31	1	887.5	4.627E+05	924.4	1006.5
1	32	1	887.4	4.705E+05	925.1	1006.5
1	33	1	888.1	4.715E+05	925.9	1009.1
1	34	1	888.6	4.735E+05	926.6	1009.2
1	35	1	889.5	4.735E+05	927.5	1009.2
1	36	1	890.8	4.676E+05	928.2	1009.4
1	37	1	891.8	4.656E+05	929.0	1009.4
1	38	1	892.6	4.646E+05	929.7	1009.5
1	39	1	893.7	4.617E+05	930.5	1009.5
1	40	1	896.0	4.460E+05	931.2	1009.7
1	41	1	901.3	4.020E+05	932.0	1000.1
1	42	1	908.0	3.559E+05	934.0	1000.1
1	43	1	915.2	2.903E+05	934.5	1000.1
1	44	1	913.6	3.207E+05	936.0	1000.1
1	45	1	901.6	4.578E+05	938.0	1000.1
1	46	1	886.8	6.125E+05	939.0	1000.2
1	47	1	888.4	6.066E+05	940.0	1000.2
1	48	1	889.9	6.213E+05	943.0	1020.2

Drawn by	M.L.	Date	11/2/89
Checked by	M.L.	Date	11/2/89
Revisions		Date	
H09700R869		11/2/89	

**Boundary Conditions for the Initial Simulation**

**INTERA** Technologies

Table 3.1

Model Indices			Grid-Block	Specified Press	Freshwater	Fluid
I	J	K	Center Elev	@ Grid-Block	Head	Density
			m	Center (Pa)	(m)	(kg/m <sup>3</sup> )

Southern Boundary

1	1	1	908.7	8.961E+04	907.5	1000.0
2	1	1	887.5	2.972E+05	907.5	1001.6
3	1	1	872.4	4.451E+05	907.5	1002.8
4	1	1	863.5	5.322E+05	907.5	1003.2
5	1	1	858.6	5.802E+05	907.5	1003.4
6	1	1	855.0	6.154E+05	907.5	1004.1
7	1	1	851.5	6.497E+05	907.5	1004.2
8	1	1	848.1	6.830E+05	907.5	1004.2
9	1	1	845.6	7.075E+05	907.5	1004.1
10	1	1	844.0	7.231E+05	907.5	1003.9
11	1	1	842.7	7.359E+05	907.5	1003.9
12	1	1	841.5	7.476E+05	907.5	1003.9
13	1	1	840.5	7.574E+05	907.5	1003.8
14	1	1	839.8	7.643E+05	907.5	1003.8
15	1	1	839.2	7.702E+05	907.5	1003.8
16	1	1	838.7	7.750E+05	907.5	1003.8
17	1	1	838.0	7.868E+05	908.0	1004.1
18	1	1	837.3	7.966E+05	908.3	1004.6
19	1	1	836.7	8.064E+05	908.7	1005.2
20	1	1	835.9	8.172E+05	909.0	1006.0
21	1	1	832.2	8.553E+05	909.2	1007.1
22	1	1	829.0	8.886E+05	909.4	1008.2
23	1	1	824.7	9.327E+05	909.6	1009.6
24	1	1	819.9	9.826E+05	909.9	1011.7
25	1	1	811.2	1.071E+06	910.2	1013.7
26	1	1	792.4	1.258E+06	910.5	1017.0
27	1	1	764.8	1.538E+06	911.5	1022.9
28	1	1	743.6	1.785E+06	915.5	1028.8

Drawn by	M.L.	Date	11/2/89
Checked by	M.L.	Date	11/2/89
Revisions		Date	
H09700R869		11/2/89	

Boundary Conditions for the Initial Simulation

**INTERA** Technologies

Table 3.1 (cont.)



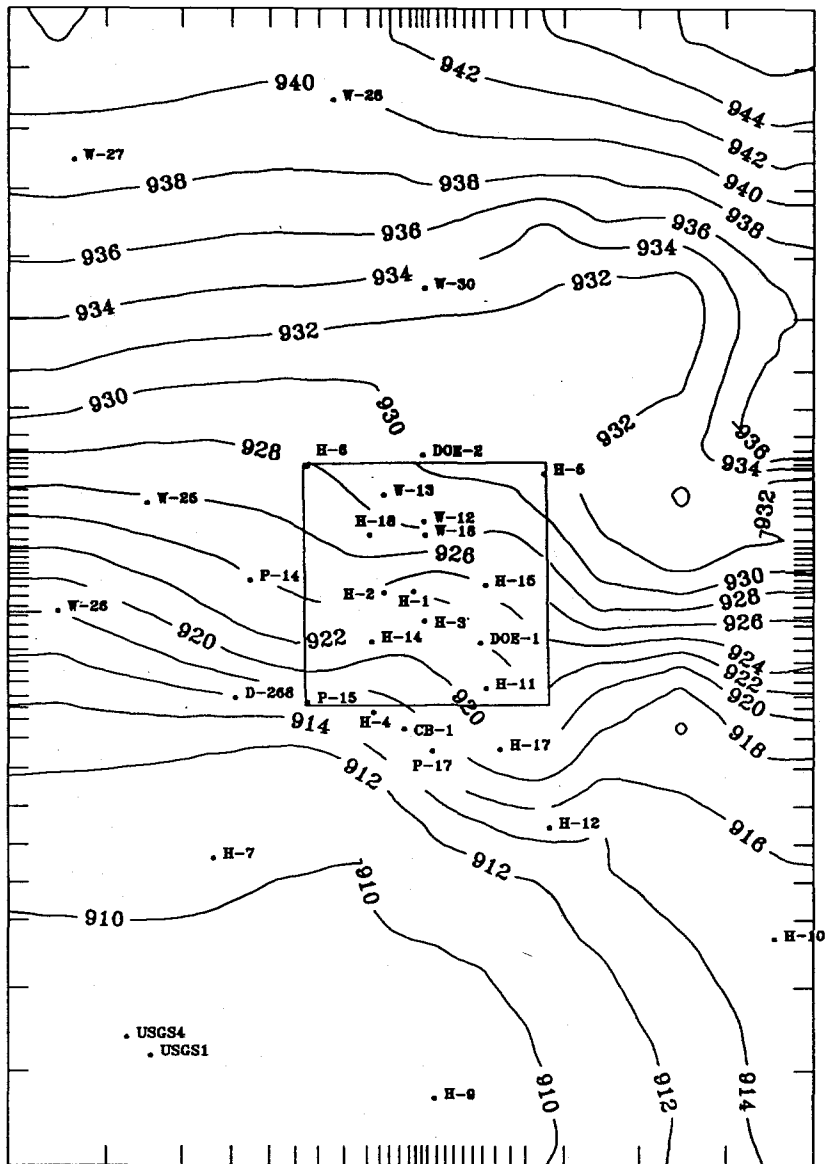
Model Indices			Grid-Block	Specified Press	Freshwater	Fluid
I	J	K	Center Elev	@ Grid-Block	Head	Density
			m	Center (Pa)	(m)	(kg/m <sup>3</sup> )
-----						
Northern Boundary						
-----						
1	48	1	889.9	6.213E+05	943.0	1020.2
2	48	1	886.8	6.389E+05	941.7	1023.8
3	48	1	885.8	6.438E+05	941.2	1027.1
4	48	1	886.5	6.350E+05	941.0	1031.0
5	48	1	872.8	7.711E+05	941.2	1034.4
6	48	1	870.7	7.937E+05	941.4	1037.4
7	48	1	866.7	8.338E+05	941.5	1040.0
8	48	1	860.3	8.984E+05	941.7	1043.1
9	48	1	853.9	9.631E+05	941.9	1046.6
10	48	1	849.7	1.005E+06	942.0	1049.5
11	48	1	845.8	1.044E+06	942.1	1051.4
12	48	1	841.8	1.084E+06	942.2	1053.3
13	48	1	838.4	1.119E+06	942.3	1055.0
14	48	1	835.8	1.144E+06	942.3	1056.7
15	48	1	833.4	1.169E+06	942.4	1057.8
16	48	1	830.1	1.201E+06	942.4	1059.1
17	48	1	826.1	1.241E+06	942.5	1060.5
18	48	1	822.3	1.278E+06	942.5	1062.5
19	48	1	818.2	1.319E+06	942.6	1064.3
20	48	1	813.9	1.363E+06	942.7	1066.4
21	48	1	809.4	1.407E+06	942.7	1068.5
22	48	1	804.1	1.460E+06	942.9	1070.9
23	48	1	797.8	1.522E+06	942.9	1073.6
24	48	1	790.4	1.596E+06	943.0	1077.2
25	48	1	776.9	1.729E+06	943.1	1081.1
26	48	1	749.3	2.001E+06	943.3	1088.2
27	48	1	703.8	2.450E+06	943.7	1104.1
28	48	1	677.9	2.710E+06	944.3	1126.8

Drawn by	M.L.	Date	11/2/89
Checked by	M.L.	Date	11/2/89
Revisions		Date	
H09700R869		11/2/89	

**Boundary Conditions for the Initial Simulation**

**INTERA** Technologies

Table 3.1 (cont.)

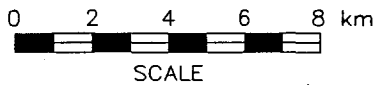


. H-8

● Observation Well

Freshwater Heads in m amsl

Contour Interval: 2m

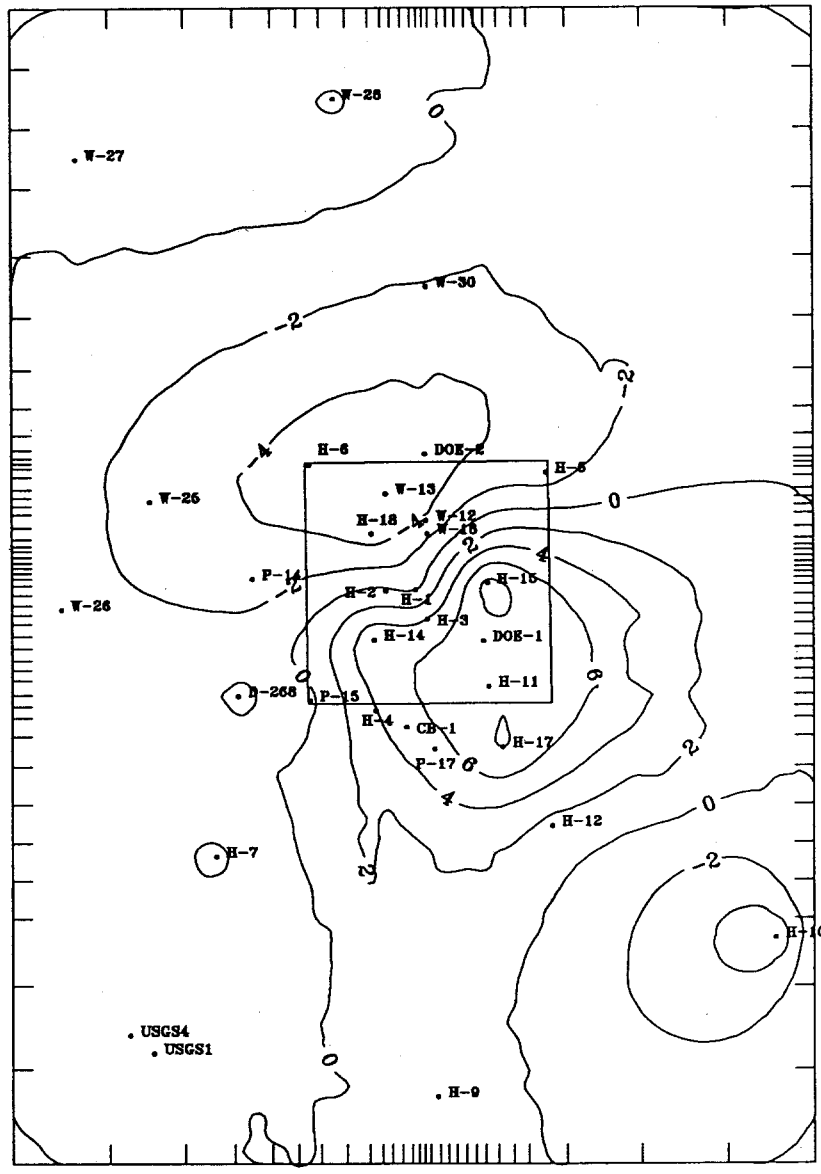


Drawn by ABW	Date 10/30/89
Checked by M.L.	Date 10/31/89
Revisions	Date
H09700R869	10/31/89

The Calculated Freshwater Heads of the Initial Simulation (Using AKRIP Initial Transmissivities and the Initial Boundary Conditions)

**INTERA** Technologies

Figure 3.1

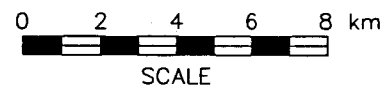


. H-8

● Observation Well

Freshwater-Head Differences in m

Contour Interval: 2m



Drawn by ABW	Date 10/30/89
Checked by M.L.	Date 10/31/89
Revisions	Date
H09700R869	10/31/89

The Differences Between the Calculated and the Observed Freshwater Heads of the Initial Simulation

**INTERA** Technologies

Figure 3.2

<u>Location</u>	<u>Difference Between Calculated and Observed Freshwater Head (m)</u>
H-1	-0.60
H-2	0.41
H-3	4.08
H-4	3.92
H-5	-3.08
H-6	-4.78
H-7	-2.26
H-9	0.96
H-10	-5.98
H-11	7.81
H-12	1.23
H-14	5.65
H-15	8.88
H-17	8.36
H-18	-4.92
P-14	-3.12
P-15	-0.66
P-17	5.09
WIPP-12	-4.07
WIPP-13	-5.49
WIPP-18	-2.38
WIPP-25	-3.09
WIPP-26	-1.29
WIPP-27	0.92
WIPP-28	2.31
WIPP-30	-2.08
CB-1	5.16
DOE-1	7.49
DOE-2	-4.98
D-268	0.37
USGS-1	-0.53
USGS-4	-0.53

Drawn by	Date	<b>Differences Between Calculated and Observed Freshwater Heads for the Initial Simulation</b>
Checked by	Date	
Revisions	Date	
<b>INTERA Technologies</b>		Table 3.2

WIPP-28, respectively, and the negative differences at H-6, WIPP-30, DOE-2, and H-5 indicate that the transmissivities in the area between these groups of boreholes are too low. High positive differences occur within the area bounded by H-3, H-4, H-11, H-15, P-17, CB-1, and H-17, indicating that the calculated heads at these wells are too high. The highest positive difference occurs at H-15 where the calculated head is 8.8 m higher than the observed head.

Changes to the initial transmissivity distribution and boundary conditions were used to improve the agreement between calculated and observed heads. The justification and methodology for the implementation of changes in the boundary conditions and transmissivity distributions is described in Section 3.3.

### 3.3 Calibration of the Steady-State Model

#### 3.3.1 General Approach

The general approach used to improve the agreement between the initial calculated heads and the observed heads employs "pilot points" or additional transmissivity data points which are added to the set of observed transmissivity data and used to alter the transmissivities within the model region through kriging. This approach greatly enhances one's ability to adjust the transmissivity within areas of a model with the minimum amount of effort and is derived from a technique discussed in de Marsily et al. (1984).

The locations of the pilot points are selected after using the GRASP II code to determine the highest sensitivity regions during a model-calibration step. GRASP II employs a coupled adjoint-sensitivity and kriging technique to calculate sensitivities (RamaRao and Reeves, 1990). Before the sensitivities are calculated, a calibration target or performance measure must be defined (e.g., such as reducing the differences between the calculated and observed heads in a local region of the model area). Although GRASP II uses pressures to compute a performance measure, the adequacy of the model calibration is discussed in terms of the differences between model-calculated and observed freshwater heads. The equation GRASP II uses to calculate the steady-state performance measure,

defined as the sum of the squared differences between calculated and observed pressures at selected wells, is:

$$\sum_{i=1}^N W_i (P_i - P_{ob_i})^2 \quad (3.1)$$

where

- N = Number of boreholes included in performance measure
- W = Weight assigned to selected boreholes
- P = Calculated pressure at grid-block elevation (Pa)
- P<sub>ob</sub> = Observed pressure at grid-block elevation (Pa)
- i = Subscript designating borehole identifier.

The selection of the boreholes used in the performance measure is made by the modeler and is generally guided by the magnitude of the steady-state head differences within a selected region. A default weight of 1.0 is assigned to the head difference at each borehole. A higher weight may be assigned to a borehole location to increase the importance of reducing the head difference at that location.

Once the boreholes to be used in the calculation of the performance measure are selected, GRASP II is employed to calculate the performance measure and determine the location at which the performance measure has the highest sensitivity to changes in the transmissivity field. Coupling both adjoint-sensitivity and kriging techniques permits GRASP II to compute sensitivity derivatives with respect to the pilot-point transmissivities. Before locating a pilot point, the present methodology first requires the specification of a superimposed grid of potential pilot-point locations upon the SWIFT II finite-difference grid. The location of the pilot-point grid is specified by the modeler and is not related to or restricted by the model's finite-difference grid. GRASP II determines the sensitivity of the performance measure to the log-transmissivity at each potential pilot-point location using the relation:

$$\frac{dJ}{dY_p} = \sum_{m=1}^N \gamma_{mp} (dJ/dY^*_m) \quad (3.2)$$

Here  $Y_p$  [equal to  $\log_{10}(T_p)$ ] is the sensitivity parameter, subscript  $p$  identifies a single point within the pilot-point grid, summation index  $m$  identifies the centroid of a SWIFT II grid block, and  $N$  is the number of grid blocks. It is evident from Equation 3.2 that  $\gamma_{mp}$  represents the derivative  $dY_m^*/dY_p$ .

GRASP II calculates the kriged transmissivity value and its estimation error at each pilot-point grid node, which represents a potential pilot-point location, in order to provide information to the modeler as to the limits within which the assigned pilot-point transmissivity may lie. GRASP II also calculates the sensitivity of the performance measure to changes in the transmissivity field that would result from adding a pilot point to the kriging data base. This requires the resolution of a new kriging system of equations for each potential pilot-point location, to determine the coefficients  $\gamma_{mp}$  needed in Equation 3.2, but not of the  $dJ/dY_m^*$  which are calculated only once for a given set of grid-block transmissivity values. A negative sensitivity indicates that the transmissivity at the pilot point should be increased to reduce the performance measure. A positive sensitivity, on the other hand, indicates that the transmissivity at the pilot point should be decreased to reduce the performance measure. One or more pilot points are then added to the kriging data base with locations coincident with the locations of the highest sensitivity. The  $\log_{10}$  transmissivity value of the pilot point is subjectively assigned using (1) geologic information, (2) interference values of transmissivity, and (3) the guideline that the magnitude of the estimated  $\log_{10}$  transmissivity value does not lie outside of the observed  $\log_{10}$  transmissivity distribution. This criterion restricts the assignment of pilot-point  $\log_{10}$  transmissivities which generate  $\log_{10}$  transmissivity estimates that are much lower or higher in magnitude than those observed in the field. An uncertainty value is also assigned to each pilot-point  $\log_{10}$  transmissivity consistent with the standard deviations of the initial  $\log_{10}$  transmissivity field estimates (Figure 2.10b). Changes to the transmissivity field are implemented by adding the newly selected pilot point to the kriging input data set and re-estimating the transmissivities in the model area. If the head differences at the boreholes selected for the performance measure are not reduced below their uncertainty values as a result of the changes to the transmissivity field then this process is repeated.

Model calibration is therefore performed on a step-by-step basis during which the magnitude of the performance measure is modified due to changes in the head differences or the selection of a different set of boreholes. In this study, the model was considered calibrated to steady-state conditions when the head difference at each borehole was consistent with the uncertainty of the observed undisturbed head.

The next three sections present the steady-state calibration of the model. The approach used in calibrating to the steady-state conditions consisted of initially focusing on regions of the model that lie outside of the WIPP-site boundary, and then calibrating to the steady-state heads within the WIPP-site boundary once the exterior model region is sufficiently calibrated. This approach is similar in theory to the modeling technique of using model-calculated heads determined in a regional model to provide boundary conditions for subsequent local-scale modeling.

The northern model region was calibrated first in order to adjust the ground-water flux into the system such that the differences between the calculated and observed heads at the boreholes north and west of the WIPP-site boundary were minimized. Section 3.3.2 describes the changes which were implemented to the transmissivity field during this calibration step. Because a large portion of the ground water entering the system through the northwest model region exits the model system through the southwestern boundaries, the southwestern model area was calibrated before focusing upon the central model area. Section 3.3.3 describes the changes to this part of the model in order to calibrate the calculated heads in this region properly. The central model region was calibrated last for the reasons cited above. The steps taken to calibrate the central model area are described in Section 3.3.4.

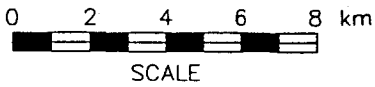
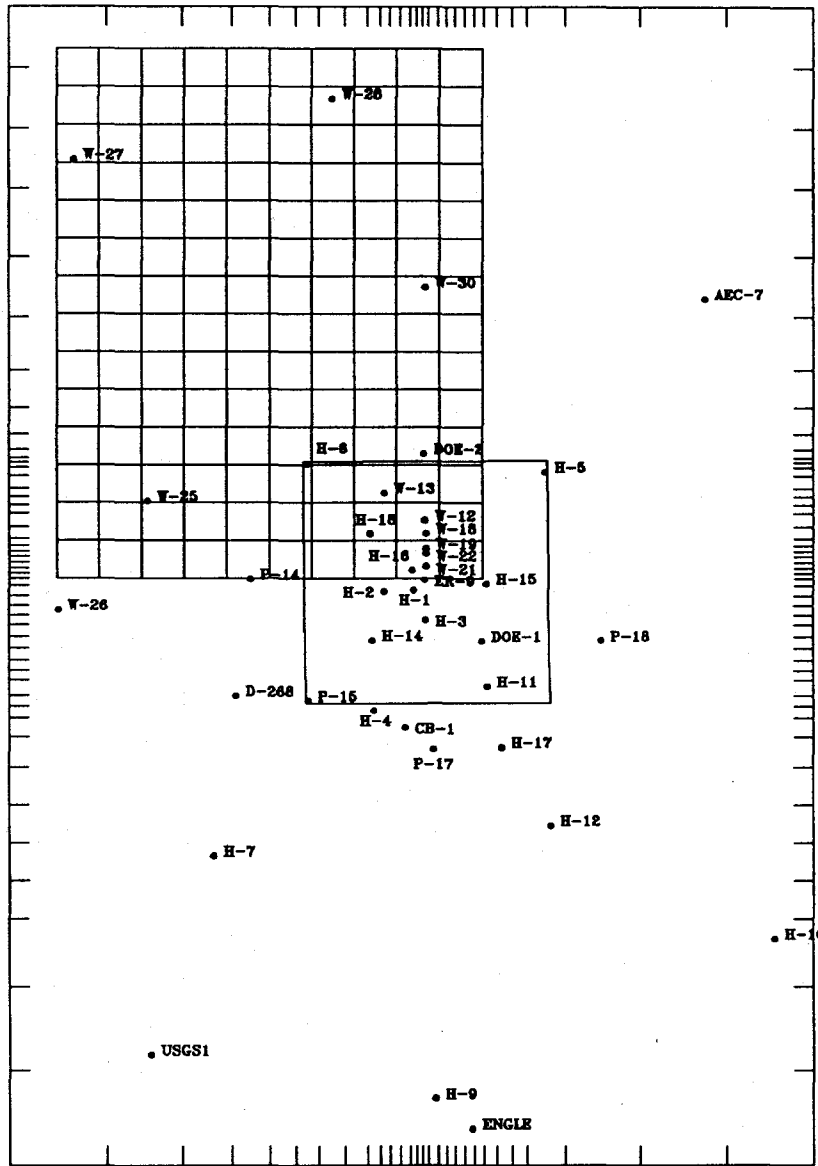
### 3.3.2 Calibration of the Northern Model Area

The first requirement during a calibration step involves defining a performance measure based on the difference between the calculated and measured heads. The initial head differences in the northern part of the model area are positive at WIPP-27 and WIPP-28 and negative downgradient at WIPP-25, WIPP-26,



WIPP-30, DOE-2, H-5, and H-6 (see Table 3.2). A performance measure consisting of the steady-state head differences for the above wells was used in GRASP II during this first step in the steady-state calibration.

In order to determine the region in which the performance measure was most sensitive to transmissivity changes, a 10 by 15 pilot-point grid was superimposed upon the northwest region of the model area (Figure 3.3). The sensitivities were then calculated by GRASP II and normalized with respect to the highest calculated sensitivity to facilitate the identification of the highest sensitivity region. Figure 3.4 contains the contoured surface generated from the normalized sensitivities. The area of highest absolute sensitivity (-0.9 contour) occurs just north of WIPP-25. Two pilot points were therefore placed in this area and the transmissivities of the entire model area were rekriged. The  $\log_{10}$  transmissivity assigned to these pilot points was successively increased by 0.5 until the estimated transmissivities at these grid blocks became approximately equal to the highest transmissivity observed in the field ( $-2.81 \log_{10} \text{ m}^2/\text{s}$ , at H-7). The total change in transmissivity at the pilot points was approximately a factor of 10. The  $\log_{10}$  transmissivities at these two pilot points were adjusted several times because subsequent GRASP II calculations continued to calculate the highest sensitivities at these locations. After rekriging using the new pilot points, the change in the transmissivity field ranged from  $0.5 \log_{10} \text{ m}^2/\text{s}$  near the pilot points (i.e., approximately within 1 to 2 km) to  $0.0 \log_{10} \text{ m}^2/\text{s}$  near the WIPP-25, WIPP-30, and H-6 boreholes. The performance measure was reduced considerably by the addition of these two pilot points. However, because the estimated transmissivities at the pilot-point locations were approximately the same as the highest observed value, the transmissivities assigned to these locations could no longer be increased. Therefore, a third pilot point was added within the area defined by the -0.9 contour of Figure 3.4 based upon a subsequent GRASP calculation. After increasing the transmissivity assigned to this pilot point by one-half order of magnitude (from  $-3.5$  to  $-3.0 \log \text{ m}^2/\text{s}$ ), the differences between the calculated and observed heads at the selected wells in the northern model area were sufficiently reduced (see Table 3.3).



• H-6

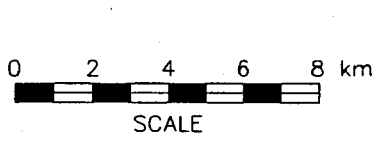
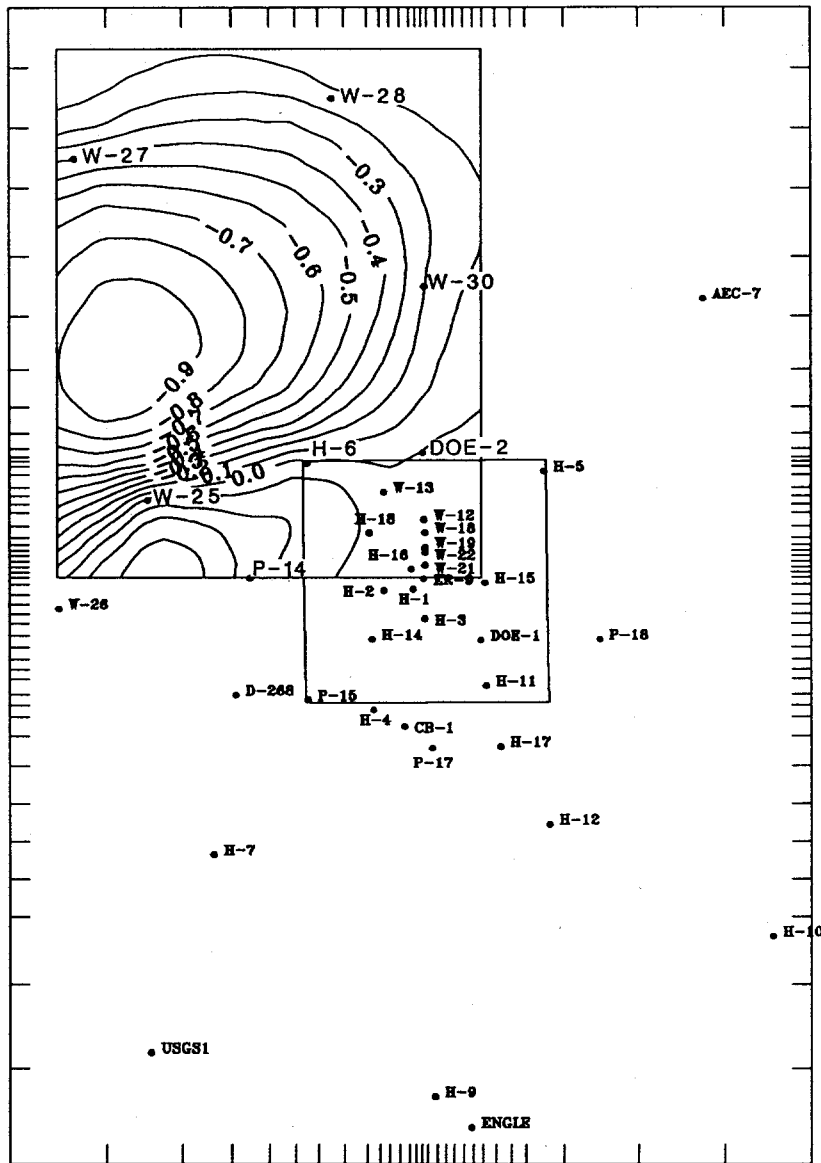
• Observation Well

Drawn by	ABW	Date	10/30/89
Checked by	M.L.	Date	10/31/89
Revisions		Date	
H09700R869		10/31/89	

Pilot-Point Grid Used to Calibrate  
Northern Model Area

**INTERA** Technologies

Figure 3.3



● Observation Well  
 Contour Interval: 0.1  
 Sensitivity Contours are Dimensionless

Drawn by	ABW	Date	10/30/89
Checked by	M.L.	Date	10/31/89
Revisions		Date	
H09700R869		10/31/89	

Normalized Sensitivities of Northern Borehole Pressure Differences to Changes in Transmissivities at Potential Pilot-Point Locations

**INTERA** Technologies

Figure 3.4

Location Difference Between Calculated  
and Observed Freshwater Head (m)

H-1	1.90
H-2	3.21
H-3	6.12
H-4	5.20
H-5	0.26
H-6	-0.63
H-7	-2.58
H-9	0.27
H-10	-9.27
H-11	9.51
H-12	0.96
H-14	7.85
H-15	11.00
H-17	9.59
H-18	-1.18
P-14	-0.25
P-15	0.40
P-17	6.27
WIPP-12	-0.30
WIPP-13	-1.51
WIPP-18	1.20
WIPP-25	0.15
WIPP-26	-0.29
WIPP-27	0.57
WIPP-28	1.45
WIPP-30	-0.62
CB-1	6.49
DOE-1	9.25
DOE-2	-1.10
D-268	1.11
USGS-1	-0.77
USGS-4	-0.77

Drawn by	Date	<b>Differences Between Calculated and Observed Freshwater Heads After Steady-State Calibration of the Northern Model Area</b>
Checked by	Date	
Revisions	Date	

**INTERA** Technologies

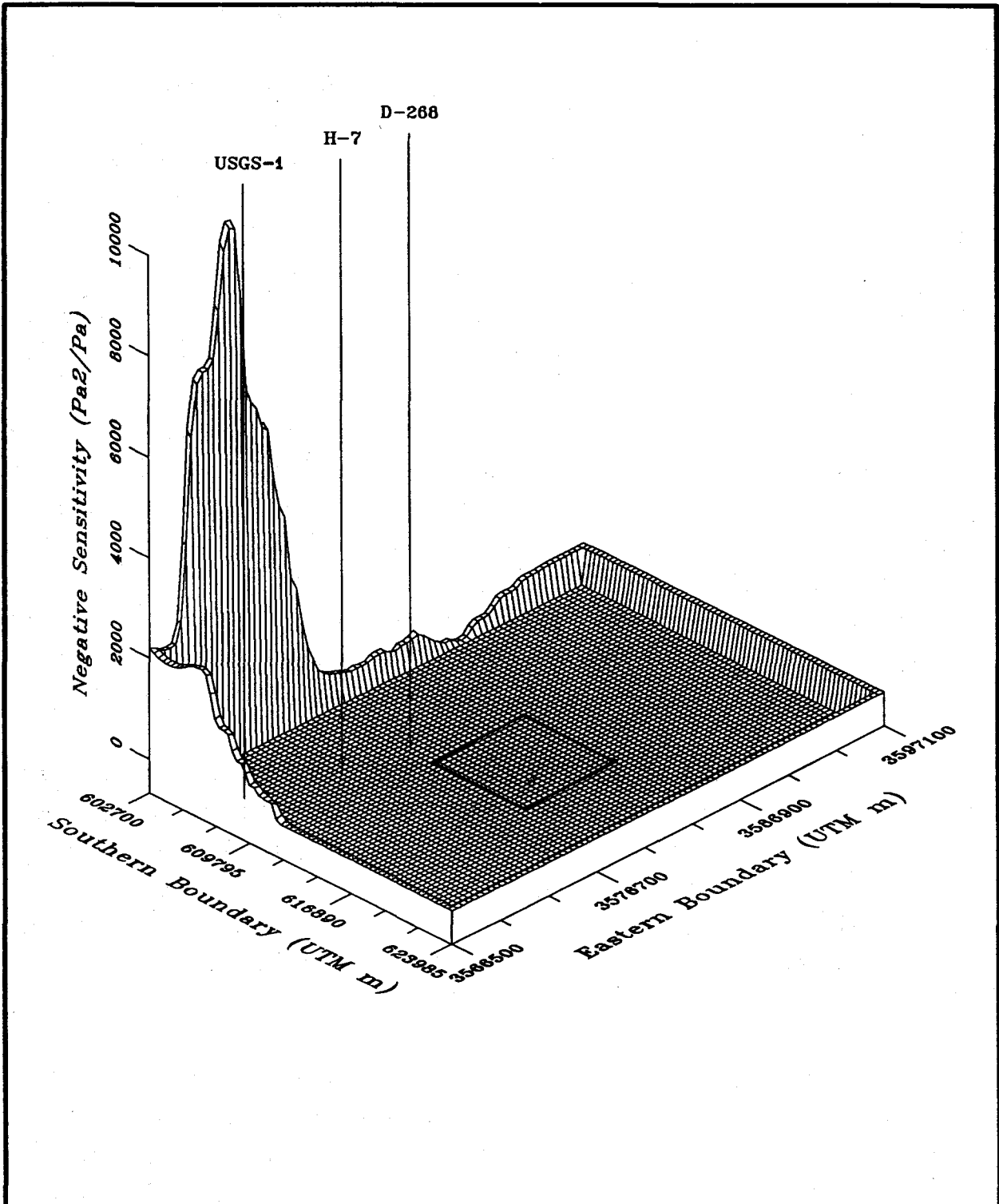
Table 3.3

### 3.3.3 Calibration of the Southwestern and Southeastern Model Areas

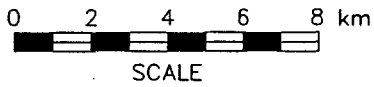
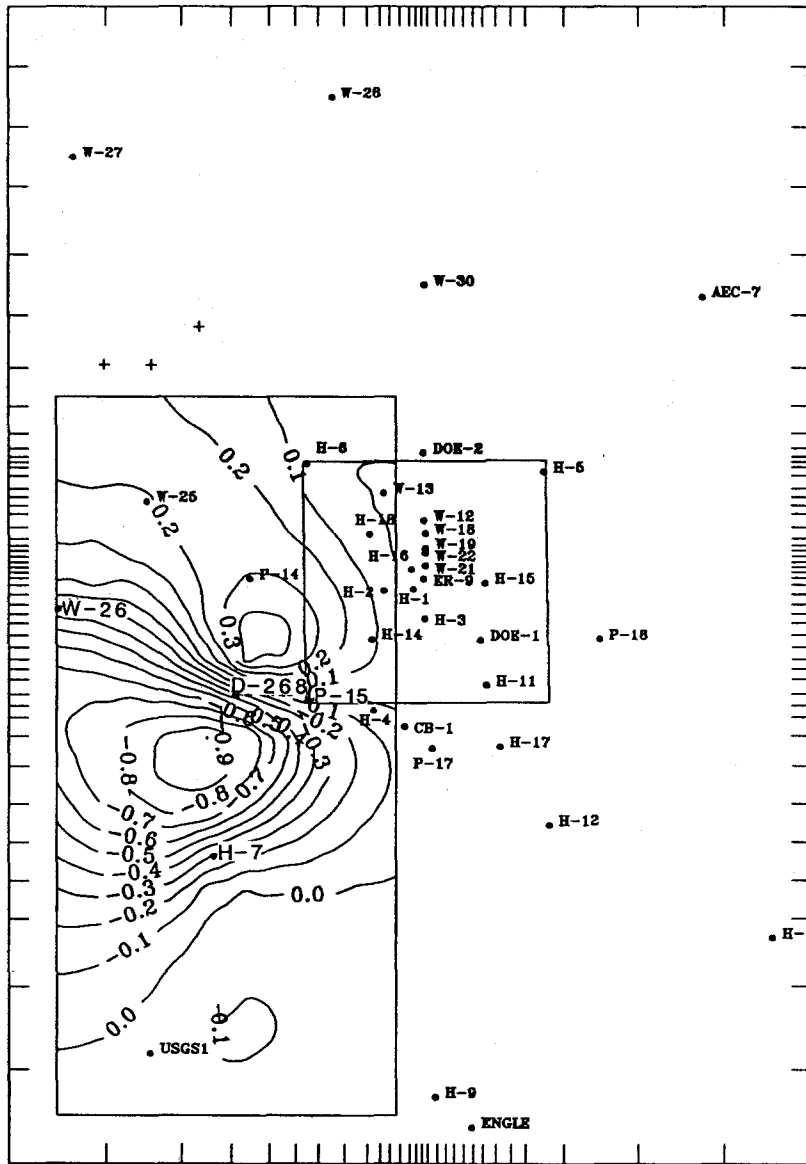
The head differences which existed after calibration of the northern model area are listed in Table 3.3. The differences in the calculated and observed heads at the H-7 (-2.6 m), D-268 (1.1 m), and USGS-1 (-0.8 m) boreholes were selected for the next performance measure. Two sensitivity runs were performed to determine whether changes to the boundary conditions on the southwestern model boundaries or changes to the transmissivity field should be implemented to reduce the head differences at the above boreholes. Figure 3.5 illustrates the sensitivity of the performance measure to the boundary pressures assigned to the model boundaries. The southernmost pressures assigned along the western boundary had the highest sensitivity and were subsequently increased by approximately  $9.7 \times 10^3 \text{ Pa}$  (1.0 m) to reduce the performance measure. The increase in boundary pressures reduced the head differences at H-7 and USGS-1 to -1.6 m, and 0.1 m, respectively. However, the head difference at D-268 was increased to 1.5 m. Therefore, efforts were focused upon changing the transmissivity field to further reduce the head difference at the D-268 location.

A 10 by 20 pilot-point grid superimposed on the southwestern model area was used for the calculation of sensitivities of the performance measure to changes in the transmissivity field. The GRASP II results illustrated in Figure 3.6 depict a high-negative-sensitivity region north of H-7. Two transmissivity pilot points were added in this region. An increase in transmissivity of approximately one-half order of magnitude at these pilot-point locations reduced the head differences at H-7, D-268, and USGS-1 to -1.5 m, 0.5 m, and 0.2 m, respectively.

The calibration efforts for the southwestern part of the model were ceased and the focus of the calibration turned to the southeastern model area where the head difference at the H-10 borehole was -9.3 m. At this point, the initial no-flow boundary along the eastern edge of the model region was replaced with a specified pressure boundary. This resulted in a reduction in the head difference at H-10 to -2.7 m (Table 3.4). Although this head difference is larger than the uncertainty for the H-10 borehole, further calibration at the southeastern part of the model area was deferred until calibration of the south-central model area (Section 3.3.4).



Drawn by	ABW	Date	10/30/89	Sensitivities of Southwestern Borehole Pressure Differences to Changes in Model Boundary Pressures
Checked by	M.L.	Date	10/31/89	
Revisions		Date		
H09700R869		10/31/89		
INTERA Technologies				Figure 3.5



- Observation Well
- + Pilot-Point Location
- Contour Interval: 0.1
- Sensitivity Contours are Dimensionless

Drawn by ABW	Date 11/2/89
Checked by M.L.	Date 11/2/89
Revisions	Date
H09700R869	11/2/89

Normalized Sensitivities of Southwestern Borehole Pressure Differences to Changes in Transmissivities at Potential Pilot-Point Locations

**INTERA** Technologies

Figure 3.6

<u>Location</u>	<u>Difference Between Calculated and Observed Freshwater Head (m)</u>
H-1	1.59
H-2	2.81
H-3	5.87
H-4	4.88
H-5	0.08
H-6	-0.86
H-7	-1.54
H-9	0.44
H-10	-2.73
H-11	9.33
H-12	1.49
H-14	7.41
H-15	10.80
H-17	9.60
H-18	-1.50
P-14	-1.12
P-15	-0.33
P-17	6.30
WIPP-12	-0.53
WIPP-13	-1.73
WIPP-18	0.96
WIPP-25	-0.12
WIPP-26	-0.70
WIPP-27	0.57
WIPP-28	1.44
WIPP-30	-0.69
CB-1	6.38
DOE-1	9.06
DOE-2	-1.29
D-268	0.46
USGS-1	0.16
USGS-4	0.16

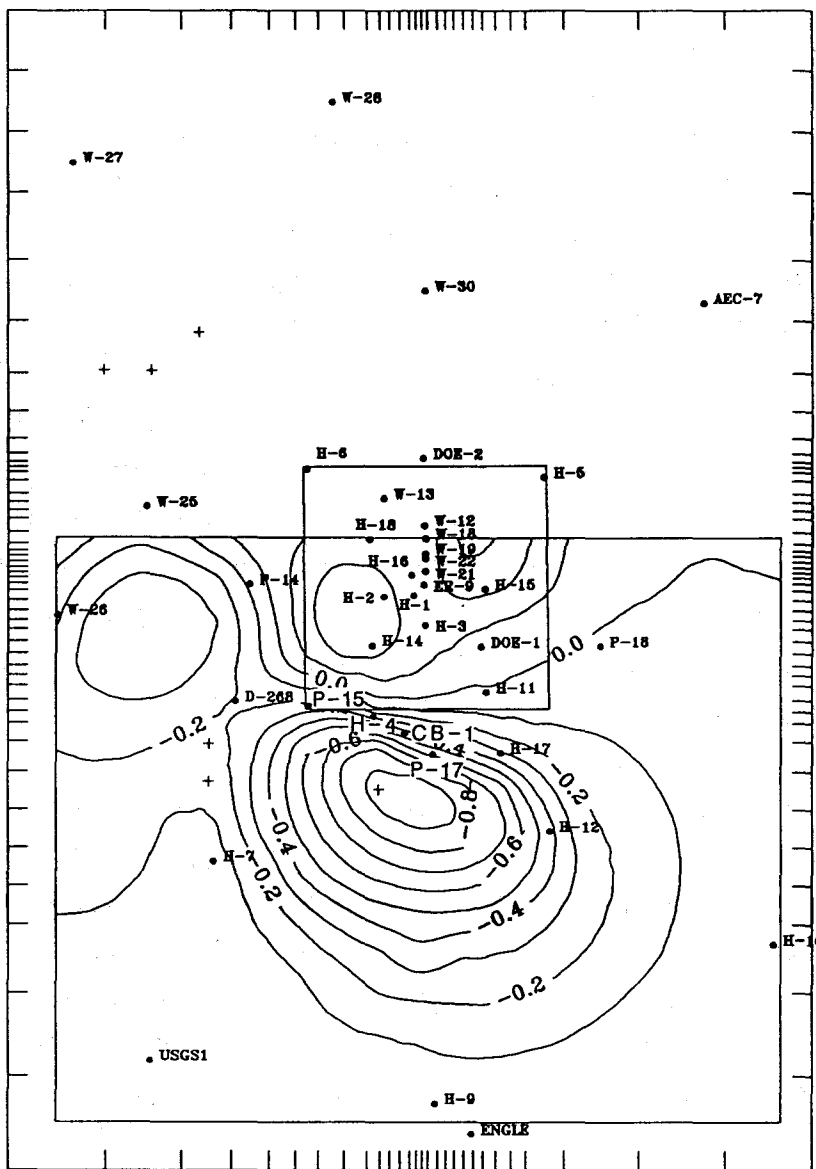
Drawn by	Date	Differences Between Calculated and Observed Freshwater Heads After Steady-State Calibration of the Southwestern Model Area
Checked by	Date	
Revisions	Date	
<b>INTERA Technologies</b>		Table 3.4



### 3.3.4 Calibration of the Central Model Area

Calibrating the central model area was conducted in several stages. The boreholes within the WIPP-site area and the H-4, H-12, H-17, P-14, P-17, and CB-1 boreholes comprised the performance measure during this first calibration step. The differences at these locations after calibrating the southwestern and southeastern portions of the model are listed in Table 3.4. A pilot-point grid was superimposed over the southern half of the model area. The GRASP II results, illustrated in Figure 3.7, depict a high-sensitivity region south of P-17. Two pilot points were added to this region and their transmissivities were ultimately increased one order of magnitude. After adding these pilot points to the transmissivity data base and re-kriging, the calculated heads were still high at H-11, H-14, H-15, H-17, and DOE-1. The same pilot-point grid was used to identify the location of the next pilot point. An area just south of the previous high-sensitivity region had the highest sensitivities. Therefore, another pilot point was added south of P-17 and was eventually assigned a transmissivity such that the grid-block transmissivity was increased 1.5 orders of magnitude. Once these changes were made, the head differences were again recalculated and the GRASP II results identified a high-sensitivity region between H-17 and P-17. The head differences after adding a pilot point between P-17 and H-17 and increasing the transmissivities in this area by approximately 1.5 orders of magnitude are listed in Table 3.5. The H-1, H-14, H-15, and H-17 boreholes all have differences that are too high. The remaining steps of the central model calibration focused on reducing the differences at these boreholes.

The next few calibration steps identified high-sensitivity regions within the WIPP-site area. This was due to the head differences at the H-1, H-14, and H-15 boreholes. Five pilot points were ultimately added during these steps to reduce the head differences. Each of the pilot-point locations was identified by GRASP II using a pilot-point grid that extended across the WIPP-site boundaries. The first pilot point added within the WIPP-site boundary was a lower transmissivity pilot point northwest of H-15 to reduce the head at the H-15 location. The other four pilot points can be grouped into two sets of pilot-point pairs of higher and lower transmissivities. By adding two pilot points, the magnitude of change needed to adjust the head differences is reduced relative to using only one pilot point. Both



0    2    4    6    8 km  
 SCALE

- Observation Well
- + Pilot-Point Location
- Contour Interval: 0.1
- Sensitivity Contours are Dimensionless

Drawn by ABW	Date 11/2/89	Normalized Sensitivities of Central and Southern Borehole Pressure Differences to Changes in Transmissivities at Potential Pilot-Point Locations
Checked by M.L.	Date 11/2/89	
Revisions	Date	
H09700R869	11/2/89	
<b>INTERA Technologies</b>		Figure 3.7

<u>Location</u>	<u>Difference Between Calculated and Observed Freshwater Head (m)</u>
H-1	-3.38
H-2	-0.38
H-3	-1.05
H-4	-0.50
H-5	-0.20
H-6	-0.88
H-7	-1.67
H-9	0.74
H-10	-2.78
H-11	0.74
H-12	0.23
H-14	2.76
H-15	3.26
H-17	2.38
H-18	-1.88
P-14	-1.14
P-15	-1.36
P-17	-0.61
WIPP-12	-1.17
WIPP-13	-1.79
WIPP-18	-0.46
WIPP-25	-0.12
WIPP-26	-0.69
WIPP-27	0.57
WIPP-28	1.43
WIPP-30	-0.71
CB-1	-0.49
DOE-1	0.74
DOE-2	-1.32
D-268	0.25
USGS-1	0.17
USGS-4	0.17

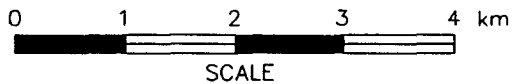
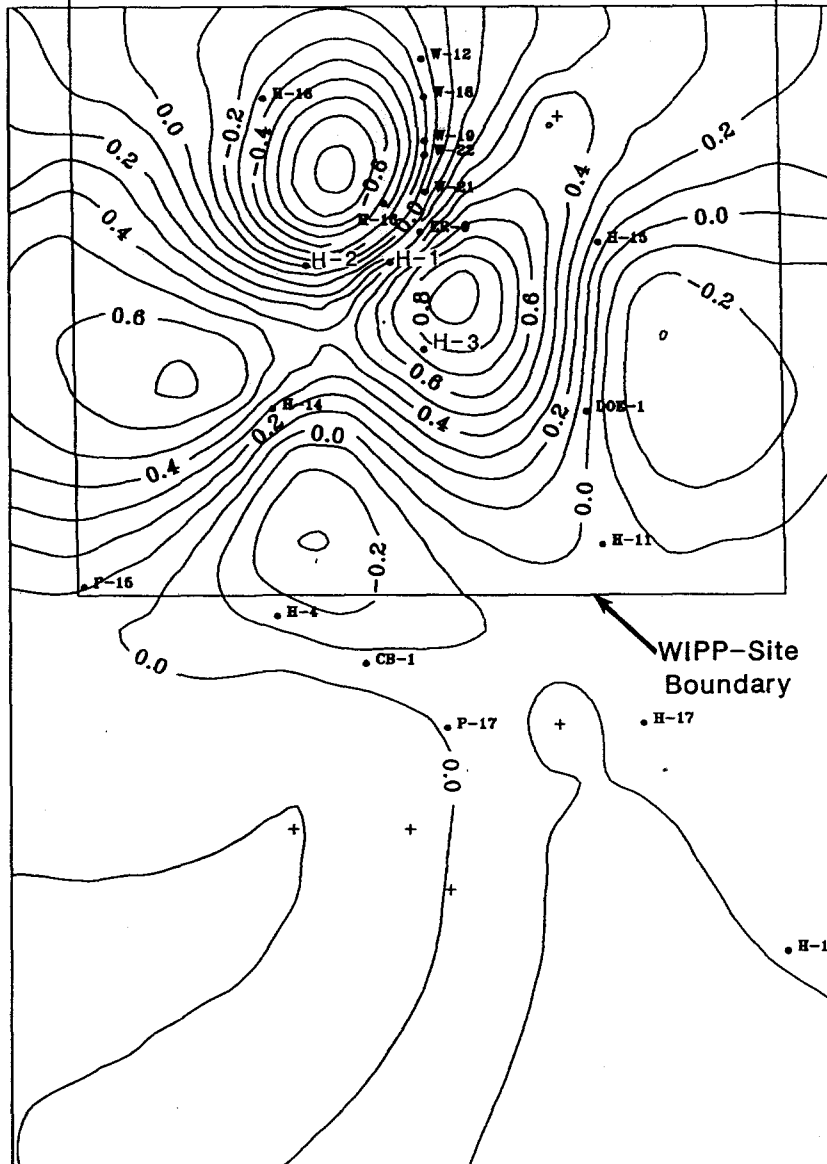
Drawn by	Date	Differences Between Calculated and Observed Freshwater Heads After Adding a Pilot Point Between the P-17 and H-17 Boreholes
Checked by	Date	
Revisions	Date	
<b>INTERA Technologies</b>		Table 3.5

sets were added simultaneously during the calibration step. This occurred because GRASP II identified both a high-negative-sensitivity region and a high-positive-sensitivity region that could be used to reduce the head differences at the selected boreholes.

The first pair of pilot points was added northwest and southeast of borehole H-1, which had a negative head difference (i.e., the calculated head was lower than the observed head). The normalized sensitivities determined by GRASP II are shown on Figure 3.8a. There was a high-negative-sensitivity region northwest of H-1 and a high-positive-sensitivity region southeast of H-1. A pilot point was added to each of these regions. The pilot point to the northwest had its transmissivity increased by one-half order of magnitude to allow more flow to the H-1 area while the pilot point to the southeast had its transmissivity decreased by one-half order of magnitude, to reduce the flow from the H-1 area. These two effects caused the calculated head at H-1 to rise, thereby reducing the head difference at this location.

The second pair of pilot points added within the WIPP-site boundary roughly center upon the H-14 borehole. GRASP II sensitivities (Figure 3.8b) indicated that a pair of pilot points should be added to the model to reduce the head difference at H-14. A lower transmissivity pilot point, at which the transmissivity was decreased by one-half order of magnitude, is located northwest of H-14 and a higher transmissivity pilot point, at which the transmissivity was increased by one-half order of magnitude, is located to the southeast. These pilot points reduced the calculated head, and thereby the head difference, in the vicinity of H-14.

When the transmissivities were modified in the H-14 area, the calculated head became 2.2 m less than the observed head at the P-15 borehole. A GRASP II run suggested adding a pair of pilot points north and south of P-15 to reduce the head difference at this location. A higher transmissivity pilot point was located northwest of P-15 and a lower transmissivity pilot point was added to the south. The transmissivities at both of these locations were adjusted by one-half order of magnitude. The calculated head value at P-15 was increased by 1.2 m after this change to the transmissivity field.



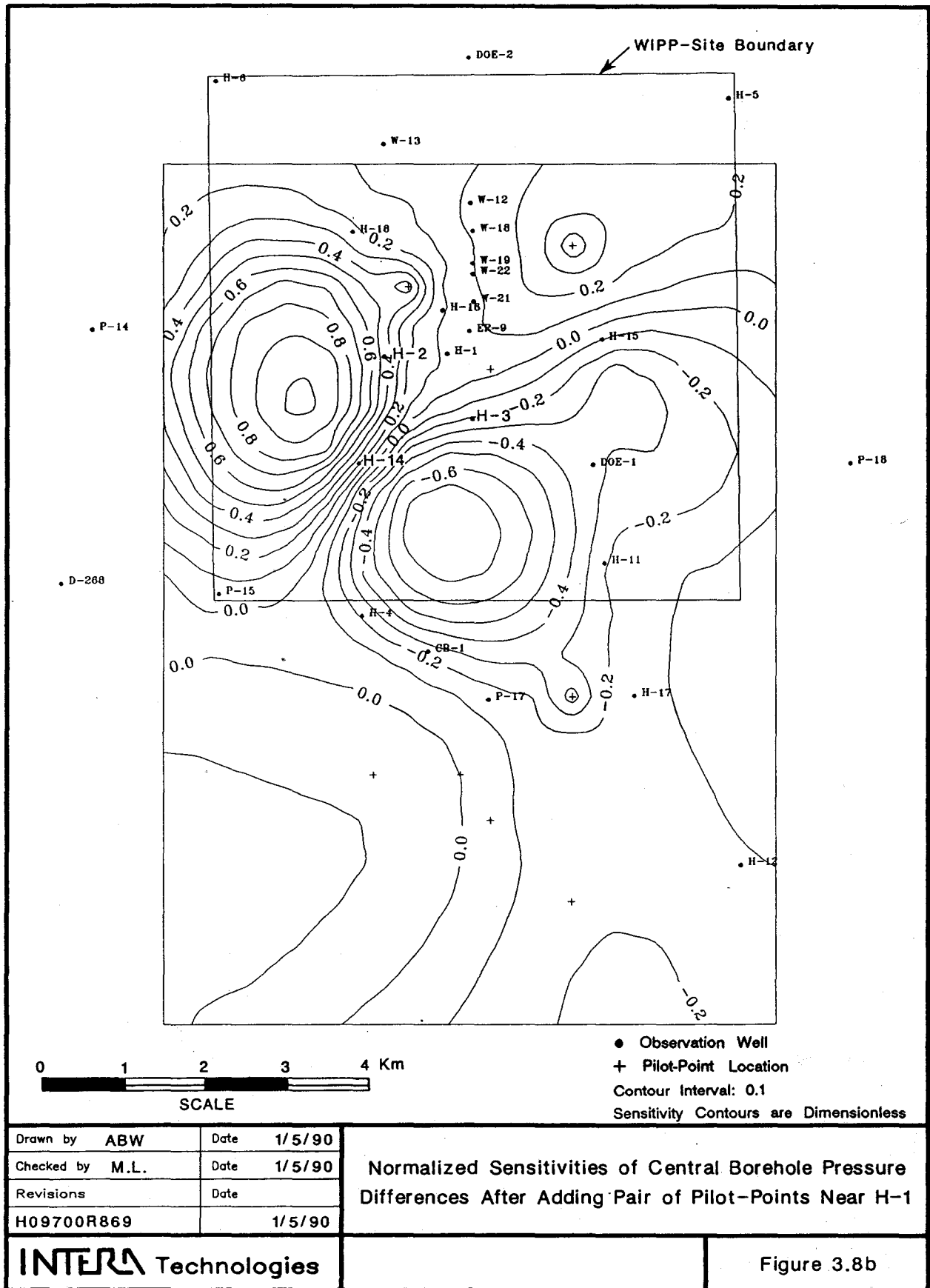
- Observation Well
- + Pilot-Point Location
- Contour Interval: 0.1
- Sensitivity Contours are Dimensionless

Drawn by ABW	Date 10/30/89
Checked by M.L.	Date 10/31/89
Revisions	Date
H09700R869	10/31/89

Normalized Sensitivities of Central Borehole Pressure Differences to Changes in Transmissivities at Potential Pilot-Point Locations

**INTERA** Technologies

Figure 3.8a

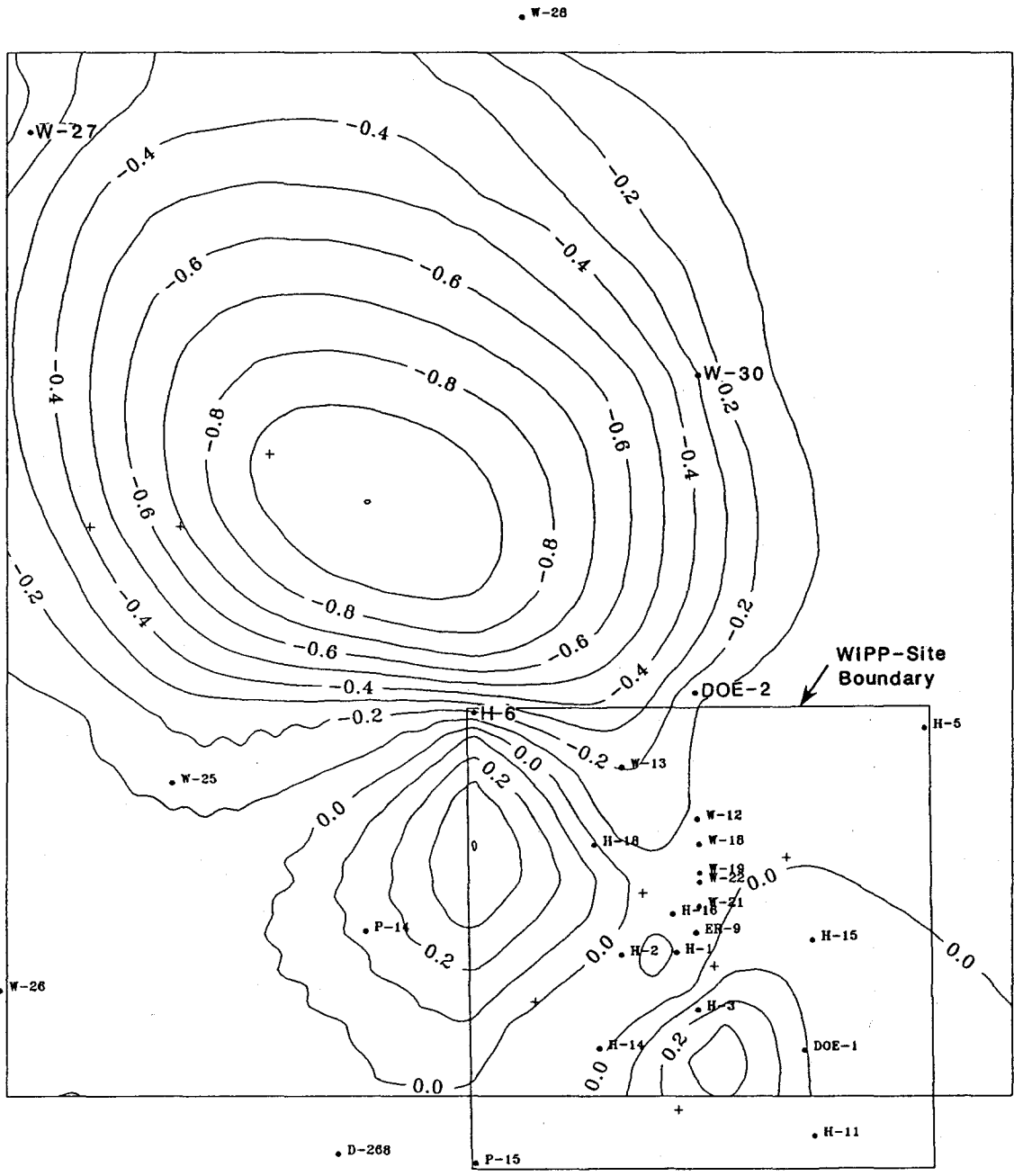


The next step of the steady-state calibration was to decrease the head differences at H-3, H-18, WIPP-13, and P-14. The changes to the transmissivity field discussed above had generated calculated heads at these boreholes of 1.9 m, 1.6 m, 1.4 m, and 1.4 m, respectively, below the observed head values. GRASP II identified a high-sensitivity region northwest of H-6 (Figure 3.8c). Two higher transmissivity pilot points were located in this area and adjusted by 0.75 order of magnitude. These pilot points increased the flow through the northern WIPP-site boundary and decreased the negative head differences at the above boreholes.

The last step required during steady-state calibration focused on reducing the calculated head at H-17. The calculated head was 3.3 m higher than the observed head. GRASP II identified a high-sensitivity region west-southwest of H-12. Two pilot points were added to this area. The transmissivities assigned to these two pilot points had to be significantly increased above the highest observed transmissivity to reduce the head difference at H-17. In order to reduce the magnitude of the assigned transmissivities, these two pilot points were separated by several kilometers to generate a broader feature. A third pilot point was also added just south of H-17 to further reduce the head at this location. In addition, GRASP II identified the southeastern boundary pressures as significant to reducing the H-17 head difference. The boundary pressures assigned to the grid blocks in this area were decreased between  $5 \times 10^3$  Pa and  $1.5 \times 10^4$  Pa (i.e., 0.5 and 1.5 m). The head difference at H-17 was reduced to 1.5 m and the head difference at H-10 was improved to -1.6 m after these changes.

### 3.3.5 The Steady-State Calibrated Transmissivity Field

The transmissivities that are considered to reproduce the observed steady-state freshwater-head distribution adequately, hereafter referred to as the steady-state calibrated (SSC) transmissivity field, and all the pilot points added during steady-state calibration, are shown in Figure 3.9a. Figure 3.9b represents the SSC transmissivities within the WIPP-site boundary. The SSC transmissivity field contains the same broad features as the initial transmissivity field (Figure 2.10a), namely, increasing transmissivity from east to west and locally high transmissivity around H-11 and DOE-1. The major differences between the initial transmissivity



0 1 2 3 Km  
SCALE

● Observation Well  
+ Pilot-Point Location  
Contour Interval: 0.1  
Sensitivity Contours are Dimensionless

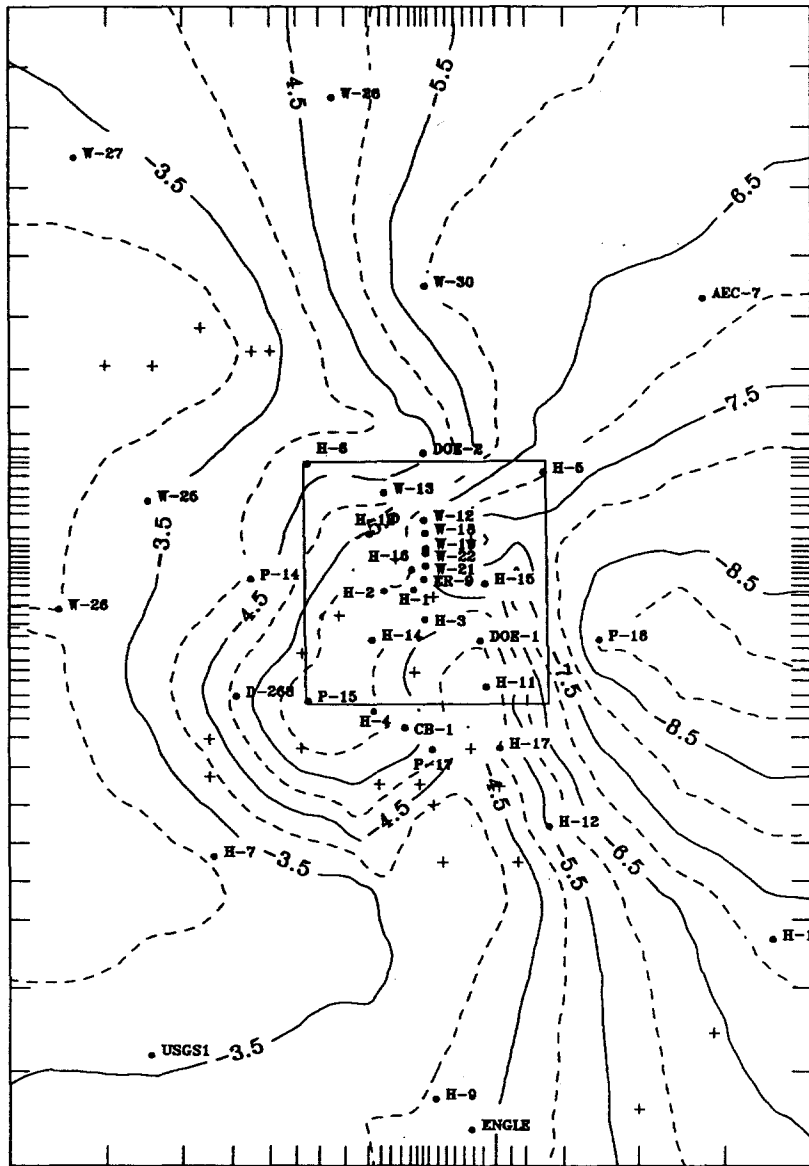
Drawn by	ABW	Date	1/5/90
Checked by	M.L.	Date	1/5/90
Revisions		Date	
H09700R869		1/5/90	

Normalized Sensitivities of Pressure Differences at the H-3, H-18, WIPP-13, and P-14 Boreholes to Changes in Transmissivities at Potential Pilot-Point Locations

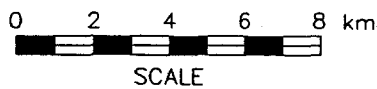
**INTERA** Technologies

Figure 3.8c





● Observation Well  
 + Pilot-Point Location  
 Transmissivities in log<sub>10</sub> m<sup>2</sup>/s  
 Contour Interval: 0.5 log<sub>10</sub> m<sup>2</sup>/s

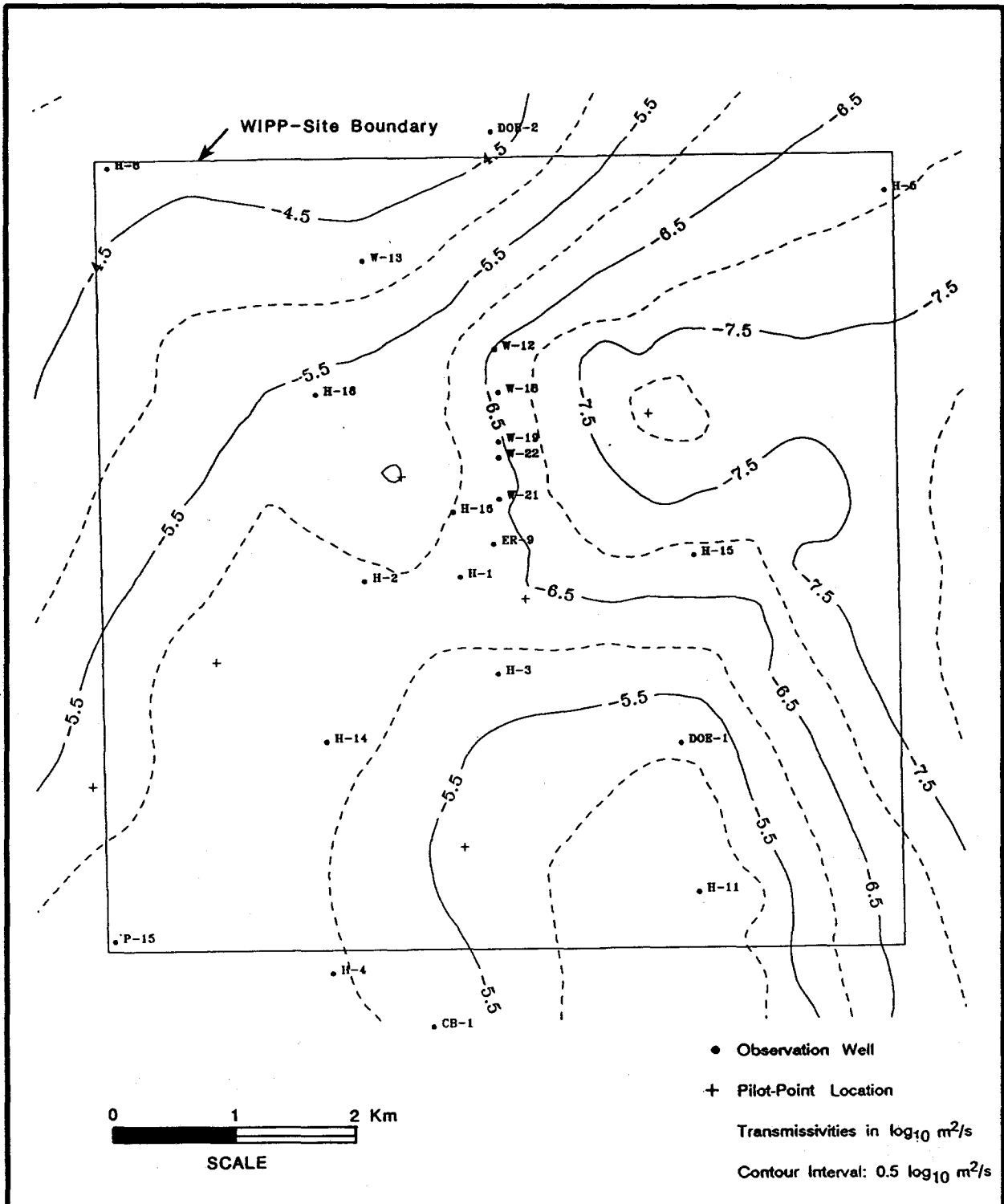


Drawn by ABW	Date 10/30/89
Checked by M.L.	Date 10/31/89
Revisions	Date
H09700R869	10/31/89

The Steady-State Calibrated Log<sub>10</sub> Transmissivities

**INTERA** Technologies

Figure 3.9a



Drawn by M.L.	Date 1/8/90
Checked by M.L.	Date 1/8/90
Revisions	Date
H09700R869	1/8/90

Steady-State Calibrated  $\log_{10}$  Transmissivities  
Within the WIPP-Site Boundary

**INTERA Technologies**

Figure 3.9b

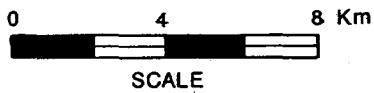
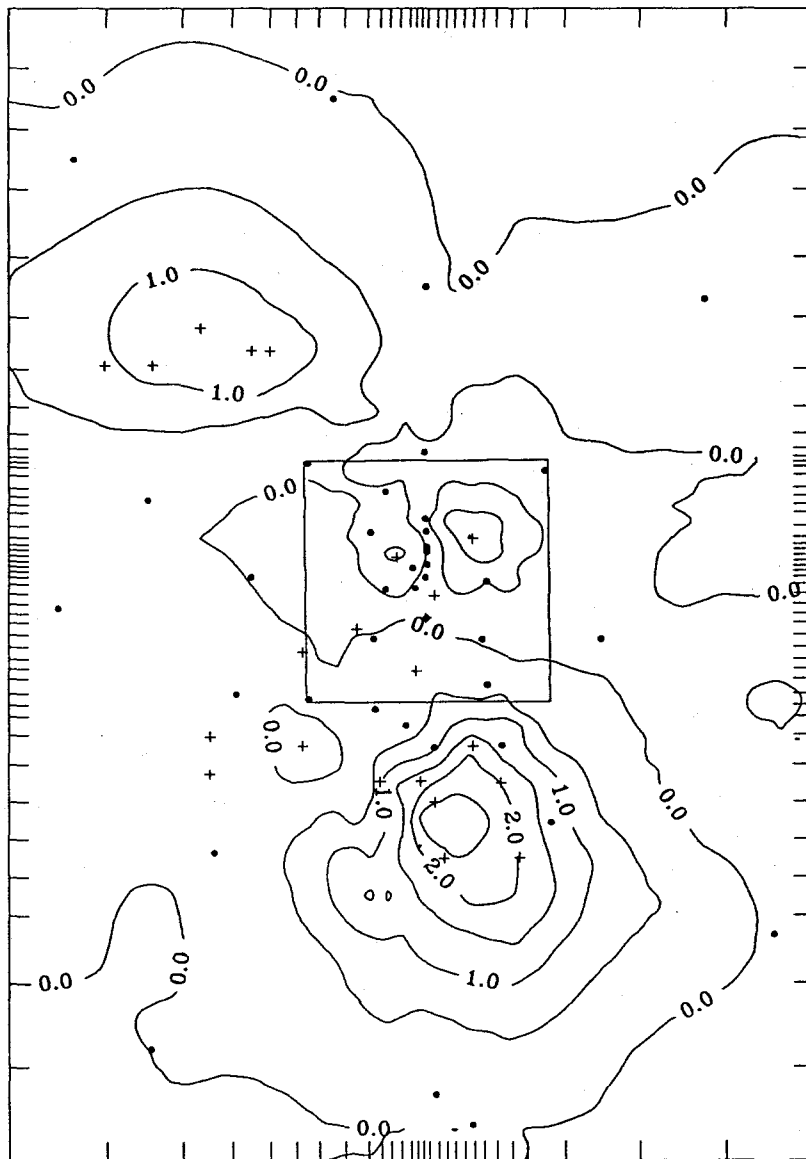
field and the SSC transmissivity field occur in the northwest and south-central model areas (Figure 3.9c). The transmissivities in the northwest model area are 0.5 to 1.0 orders of magnitude higher than the initial transmissivities. Such transmissivity changes are considered reasonable because their relative locations are along the northeast-southwest axis of Nash Draw. The higher transmissivity feature located south of H-11 and extending southwest of H-12 is the most noted change in the SSC transmissivity field. Here, the transmissivities range from  $2 \times 10^{-4} \text{ m}^2/\text{s}$  to  $1 \times 10^{-5} \text{ m}^2/\text{s}$ , which is an increase of between 0.5 to 1.5 orders of magnitude relative to the initial transmissivities. These transmissivity changes were necessary in order to calibrate to the heads observed at H-15, DOE-1, and H-1.

### 3.3.6 The Calibrated Steady-State Heads

The calibrated steady-state heads were calculated using the final boundary conditions, listed in Table 3.6, and the SSC transmissivity field described in Section 3.3.5. Figure 3.10 shows the steady-state calibrated heads over the model region. The calculated head distribution is quite similar to the observed distribution (Figure 2.12). The gradients in the calibrated head distribution agree with the gradients defined by the undisturbed heads, i.e., low gradients north and south of the WIPP-site boundary and an increased gradient within the WIPP-site boundary.

The head differences (the calculated heads minus the observed heads) for the steady-state calibrated model are listed in Table 3.7. The differences between the calculated and observed heads at boreholes in the vicinity of H-11 are small. The maximum head difference in this area occurs at H-3, where the calculated head is 2.1 m lower than the observed head. It should be noted that most of the head differences listed in Table 3.7 were subsequently modified during the transient-calibration efforts because of the necessary adjustments in the transmissivity field to reduce the differences between the calculated and observed transient responses. The transient calibration is presented in Section 5.

The Darcy velocities of the calibrated steady-state model were calculated by SWIFT II using the SSC transmissivity distribution (Figure 3.9a), the steady-state



● Observation Well  
 + Pilot-Point Location  
 Contour Interval: 0.5 log<sub>10</sub> m<sup>2</sup>/s

Drawn by ABW	Date 1/5/90
Checked by M.L.	Date 1/5/90
Revisions	Date
H09700R869	1/5/90

Log<sub>10</sub> Transmissivity Differences Between Steady-State Calibrated and Initial Transmissivity Fields

**INTERA** Technologies

Figure 3.9c

Model Indices			Grid-Block Center Elev	Specified Press @ Grid-Block Center (Pa)	Freshwater Head (m)	Fluid Density (kg/m <sup>3</sup> )
I	J	K	m			

Western Boundary

1	1	1	908.7	1.014E+05	908.7	1000.0
1	2	1	912.1	7.297E+04	909.2	1000.4
1	3	1	902.0	1.817E+05	910.2	1001.2
1	4	1	899.0	2.150E+05	910.6	1001.6
1	5	1	897.4	2.316E+05	910.7	1002.0
1	6	1	898.9	2.218E+05	911.2	1000.8
1	7	1	898.5	2.307E+05	911.7	1002.0
1	8	1	900.6	2.081E+05	911.5	1003.2
1	9	1	900.4	2.149E+05	912.0	1004.2
1	10	1	900.2	2.208E+05	912.4	1004.8
1	11	1	900.0	2.267E+05	912.8	1005.3
1	12	1	899.8	2.326E+05	913.2	1005.8
1	13	1	899.5	2.384E+05	913.5	1006.3
1	14	1	899.3	2.424E+05	913.7	1006.8
1	15	1	899.0	2.482E+05	914.0	1007.2
1	16	1	898.4	2.580E+05	914.4	1007.6
1	17	1	897.8	2.678E+05	914.8	1008.1
1	18	1	897.1	2.786E+05	915.2	1008.4
1	19	1	895.9	2.943E+05	915.6	1008.7
1	20	1	893.7	3.197E+05	916.0	1009.0
1	21	1	890.8	3.559E+05	916.8	1009.3
1	22	1	888.2	3.892E+05	917.6	1009.5
1	23	1	886.2	4.157E+05	918.3	1009.6
1	24	1	884.5	4.402E+05	919.1	1008.8
1	25	1	891.8	3.755E+05	919.8	1009.0
1	26	1	891.0	3.912E+05	920.6	1009.1
1	27	1	890.3	4.049E+05	921.3	1009.4
1	28	1	889.7	4.186E+05	922.1	1009.4
1	29	1	889.0	4.333E+05	922.9	1006.4
1	30	1	888.2	4.480E+05	923.6	1006.4
1	31	1	887.5	4.627E+05	924.4	1006.5
1	32	1	887.4	4.705E+05	925.1	1006.5
1	33	1	888.1	4.715E+05	925.9	1009.1
1	34	1	888.6	4.735E+05	926.6	1009.2
1	35	1	889.5	4.735E+05	927.5	1009.2
1	36	1	890.8	4.676E+05	928.2	1009.4
1	37	1	891.8	4.656E+05	929.0	1009.4
1	38	1	892.6	4.646E+05	929.7	1009.5
1	39	1	893.7	4.617E+05	930.5	1009.5
1	40	1	896.0	4.460E+05	931.2	1009.7
1	41	1	901.3	4.020E+05	932.0	1000.1
1	42	1	908.0	3.559E+05	934.0	1000.1
1	43	1	915.2	2.903E+05	934.5	1000.1
1	44	1	913.6	3.305E+05	937.0	1000.1
1	45	1	901.6	4.676E+05	939.0	1000.1
1	46	1	886.8	6.213E+05	939.9	1000.2
1	47	1	888.4	6.066E+05	940.0	1000.2
1	48	1	889.9	6.213E+05	943.0	1020.2

Drawn by	M.L.	Date	11/2/89
Checked by	M.L.	Date	11/2/89
Revisions		Date	
H09700R869		11/2/89	

Final Boundary Conditions for the Model

INTERA Technologies

Table 3.6

Model Indices			Grid-Block Center Elev	Specified Press @ Grid-Block Center (Pa)	Freshwater Head (m)	Fluid Density (kg/m <sup>3</sup> )
I	J	K	m			

-----  
Eastern Boundary  
-----

28	1	1	743.6	1.768E+06	913.8	1033.2
28	2	1	727.2	1.970E+06	918.0	1042.2
28	3	1	713.3	2.183E+06	925.9	1051.3
28	4	1	715.4	2.154E+06	925.0	1065.1
28	5	1	722.6	2.079E+06	924.6	1077.6
28	6	1	729.2	2.016E+06	924.7	1090.2
28	7	1	735.4	1.956E+06	924.8	1101.7
28	8	1	739.9	1.913E+06	924.9	1109.1
28	9	1	745.2	1.862E+06	925.0	1115.4
28	10	1	747.0	1.845E+06	925.1	1119.1
28	11	1	748.5	1.832E+06	925.2	1121.7
28	12	1	749.9	1.819E+06	925.3	1124.7
28	13	1	751.2	1.807E+06	925.4	1127.5
28	14	1	752.2	1.797E+06	925.4	1129.5
28	15	1	753.7	1.784E+06	925.5	1131.8
28	16	1	782.4	1.503E+06	925.5	1134.1
28	17	1	782.3	1.505E+06	925.6	1136.4
28	18	1	780.6	1.521E+06	925.6	1138.3
28	19	1	786.5	1.464E+06	925.7	1139.9
28	20	1	787.2	1.458E+06	925.7	1143.2
28	21	1	787.8	1.453E+06	925.8	1144.7
28	22	1	788.4	1.447E+06	925.8	1145.9
28	23	1	788.8	1.444E+06	925.9	1146.8
28	24	1	789.2	1.441E+06	926.0	1146.3
28	25	1	789.6	1.437E+06	926.0	1147.0
28	26	1	790.1	1.433E+06	926.1	1147.8
28	27	1	790.5	1.429E+06	926.1	1148.5
28	28	1	791.0	1.425E+06	926.2	1149.2
28	29	1	791.5	1.420E+06	926.2	1150.7
28	30	1	792.3	1.413E+06	926.3	1151.7
28	31	1	805.5	1.284E+06	926.3	1153.0
28	32	1	807.2	1.272E+06	926.8	1154.0
28	33	1	808.4	1.265E+06	927.2	1154.8
28	34	1	809.7	1.256E+06	927.6	1155.4
28	35	1	811.5	1.242E+06	928.0	1155.9
28	36	1	812.2	1.240E+06	928.5	1157.0
28	37	1	813.4	1.231E+06	928.8	1156.7
28	38	1	779.1	1.570E+06	929.1	1156.5
28	39	1	780.2	1.562E+06	929.4	1156.4
28	40	1	782.3	1.547E+06	929.9	1156.1
28	41	1	786.2	1.516E+06	930.7	1155.6
28	42	1	792.5	1.470E+06	932.3	1155.1
28	43	1	801.4	1.404E+06	934.4	1155.1
28	44	1	800.5	1.438E+06	937.0	1155.8
28	45	1	773.8	1.729E+06	940.0	1154.9
28	46	1	740.3	2.081E+06	942.5	1155.1
28	47	1	707.9	2.426E+06	945.3	1152.7
28	48	1	677.9	2.738E+06	947.2	1146.3

Drawn by	M.L.	Date	11/2/89
Checked by	M.L.	Date	11/2/89
Revisions		Date	
H09700R869		11/2/89	

Final Boundary Conditions for the Model

**INTERA** Technologies

Table 3.6 (cont.)

Model Indices			Grid-Block	Specified Press	Freshwater	Fluid
I	J	K	Center Elev m	@ Grid-Block Center (Pa)	Head (m)	Density (kg/m <sup>3</sup> )
-----						
Southern Boundary						
-----						
1	1	1	908.7	1.014E+05	908.7	1000.0
2	1	1	887.5	2.972E+05	907.5	1001.6
3	1	1	872.4	4.451E+05	907.5	1002.8
4	1	1	863.5	5.322E+05	907.5	1003.2
5	1	1	858.6	5.802E+05	907.5	1003.4
6	1	1	855.0	6.154E+05	907.5	1004.1
7	1	1	851.5	6.497E+05	907.5	1004.2
8	1	1	848.1	6.830E+05	907.5	1004.2
9	1	1	845.6	7.075E+05	907.5	1004.1
10	1	1	844.0	7.231E+05	907.5	1003.9
11	1	1	842.7	7.359E+05	907.5	1003.9
12	1	1	841.5	7.476E+05	907.5	1003.9
13	1	1	840.5	7.574E+05	907.5	1003.8
14	1	1	839.8	7.643E+05	907.5	1003.8
15	1	1	839.2	7.702E+05	907.5	1003.8
16	1	1	838.7	7.750E+05	907.5	1003.8
17	1	1	838.0	7.819E+05	907.5	1004.1
18	1	1	837.3	7.888E+05	907.5	1004.6
19	1	1	836.7	7.946E+05	907.5	1005.2
20	1	1	835.9	8.025E+05	907.5	1006.0
21	1	1	832.2	8.387E+05	907.5	1007.1
22	1	1	829.0	8.700E+05	907.5	1008.2
23	1	1	824.7	9.121E+05	907.5	1009.6
24	1	1	819.9	9.591E+05	907.5	1011.7
25	1	1	811.2	1.044E+06	907.5	1013.7
26	1	1	792.4	1.238E+06	908.5	1017.0
27	1	1	764.8	1.513E+06	909.0	1022.9
28	1	1	743.6	1.768E+06	913.8	1033.2

Drawn by	M.L.	Date	11/2/89
Checked by	M.L.	Date	11/2/89
Revisions		Date	
H09700R869		11/2/89	

**Final Boundary Conditions for the Model**

**INTERA** Technologies

Table 3.6 (cont.)

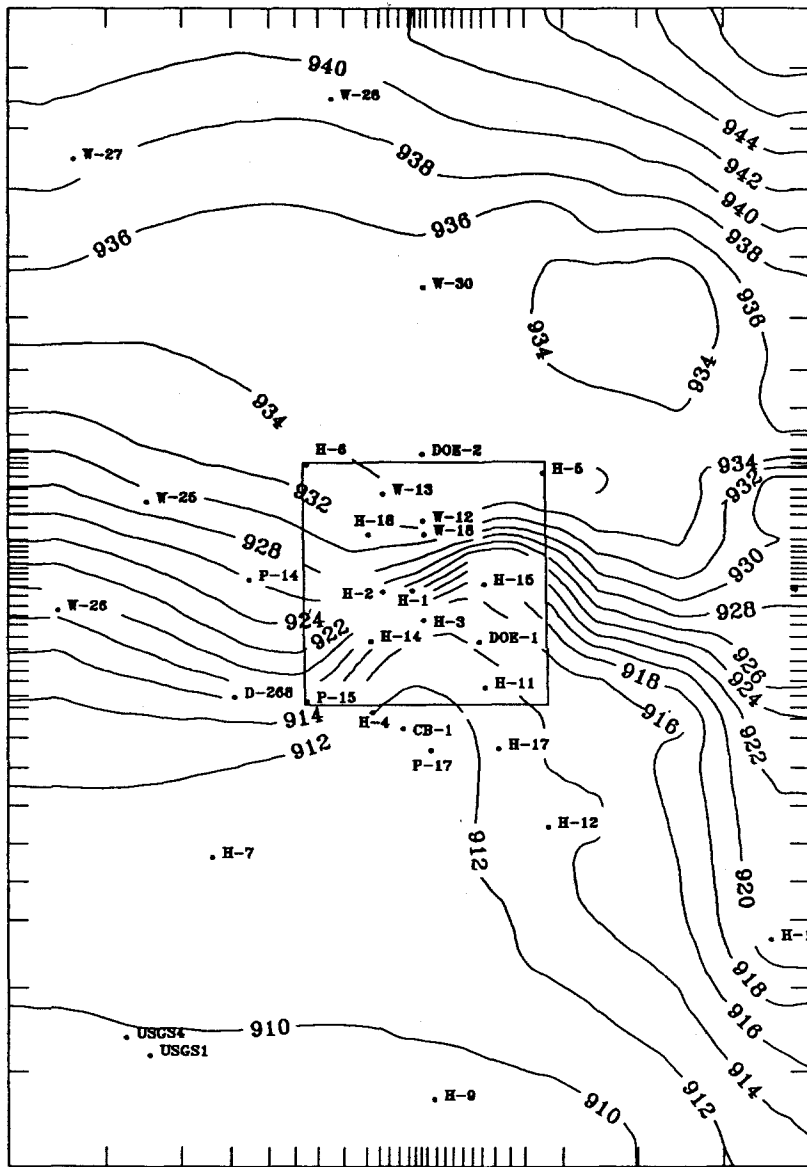
Model Indices			Grid-Block	Specified Press	Freshwater	Fluid
I	J	K	Center Elev	@ Grid-Block	Head	Density
			m	Center (Pa)	(m)	(kg/m <sup>3</sup> )

Northern Boundary

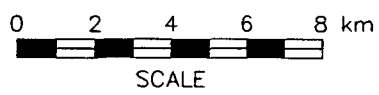
1	48	1	889.9	6.213E+05	943.0	1020.2
2	48	1	886.8	6.389E+05	941.7	1023.8
3	48	1	885.8	6.438E+05	941.2	1027.1
4	48	1	886.5	6.350E+05	941.0	1031.0
5	48	1	872.8	7.711E+05	941.2	1034.4
6	48	1	870.7	7.937E+05	941.4	1037.4
7	48	1	866.7	8.338E+05	941.5	1040.0
8	48	1	860.3	8.984E+05	941.7	1043.1
9	48	1	853.9	9.631E+05	941.9	1046.6
10	48	1	849.7	1.005E+06	942.0	1049.5
11	48	1	845.8	1.044E+06	942.1	1051.4
12	48	1	841.8	1.084E+06	942.2	1053.3
13	48	1	838.4	1.119E+06	942.3	1055.0
14	48	1	835.8	1.144E+06	942.3	1056.7
15	48	1	833.4	1.169E+06	942.4	1057.8
16	48	1	830.1	1.201E+06	942.4	1059.1
17	48	1	826.1	1.241E+06	942.5	1060.5
18	48	1	822.3	1.278E+06	942.5	1062.5
19	48	1	818.2	1.319E+06	942.6	1064.3
20	48	1	813.9	1.363E+06	942.7	1066.4
21	48	1	809.4	1.407E+06	942.7	1068.5
22	48	1	804.1	1.460E+06	942.9	1070.9
23	48	1	797.8	1.522E+06	942.9	1073.6
24	48	1	790.4	1.596E+06	943.0	1077.2
25	48	1	776.9	1.729E+06	943.1	1081.1
26	48	1	749.3	2.001E+06	943.3	1088.2
27	48	1	703.8	2.450E+06	943.7	1104.1
28	48	1	677.9	2.738E+06	947.2	1146.3

Drawn by M.L.	Date 11/2/89	<b>Final Boundary Conditions for the Model</b>
Checked by M.L.	Date 11/2/89	
Revisions	Date	
H09700R869	11/2/89	
<b>INTERA Technologies</b>		<b>Table 3.6 (cont.)</b>





• Observation Well  
 Freshwater Heads in m amsl  
 Contour Interval: 2m



Drawn by ABW	Date 10/30/89	<b>Freshwater Heads of the Steady-State Calibrated Model</b>
Checked by M.L.	Date 10/31/89	
Revisions	Date	
H09700R869	10/31/89	
<b>INTERA Technologies</b>		<b>Figure 3.10</b>

<u>Location</u>	<u>Difference Between Calculated and Observed Freshwater Head (m)</u>
-----------------	---

H-1	-1.30
H-2	1.20
H-3	-2.12
H-4	-0.99
H-5	1.08
H-6	0.07
H-7	-1.67
H-9	0.86
H-10	-1.62
H-11	-0.22
H-12	-0.23
H-14	0.90
H-15	1.57
H-17	1.52
H-18	-1.16
P-14	-1.31
P-15	-0.77
P-17	-1.37
WIPP-12	-0.05
WIPP-13	-0.79
WIPP-18	0.81
WIPP-25	-0.02
WIPP-26	-0.98
WIPP-27	0.45
WIPP-28	1.09
WIPP-30	-0.56
CB-1	-1.15
DOE-1	-0.40
DOE-2	-0.27
D-268	0.89
USGS-1	0.21
USGS-4	0.21

Drawn by	Date	<b>Differences Between the Calculated and Observed Freshwater Heads for the Steady-State Calibrated Model</b>
Checked by	Date	
Revisions	Date	
<b>INTERA Technologies</b>		Table 3.7

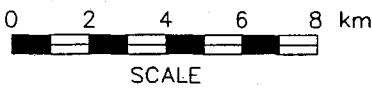
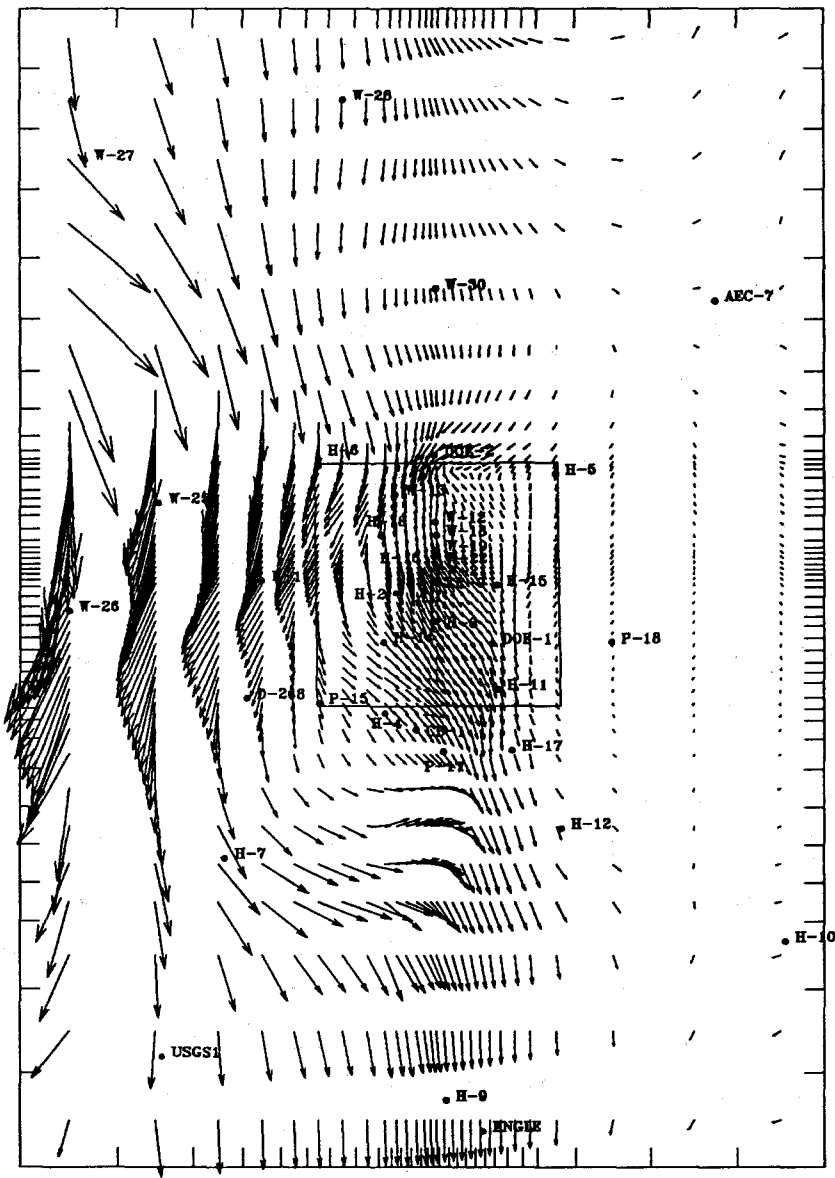
pressure field (Note: the calibrated equivalent freshwater head distribution (Figure 3.10) is determined from calculated pressures at formation depth), the prescribed fluid-density distribution (Figure 2.13), and the center-of-Culebra elevations (Figure 2.8). The Darcy velocities are defined as the specific discharge per unit cross-sectional area normal to the direction of the flow. The Darcy-velocity distribution, shown in Figure 3.11, should be interpreted as an indicator for the flow directions and the relative magnitude of ground-water flux along the different flow paths.

It is evident from Figure 3.11 that the largest flux of ground water enters the system along the northwestern model boundary and flows predominantly south toward WIPP-25. Flow in the northern part of the WIPP site is generally from north to south. A large portion of the ground water within the WIPP-site boundaries enters the high-transmissivity zone in the vicinity of H-11 and exits the modeled region from the central part of the southern boundary.

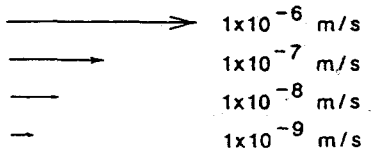
Within the modeled region, the Darcy-velocity vectors range in value over six orders of magnitude. The lowest velocities occur east of the WIPP site, where the magnitude of the velocity vectors is approximately  $1 \times 10^{-12}$  m/s (Figure 3.11). The highest velocities occur in the central portion of Nash Draw along the western boundary of the model, where the velocities are between  $5 \times 10^{-8}$  to  $5 \times 10^{-7}$  m/s. Within the WIPP-site boundary, the Darcy-velocity magnitudes are approximately  $1 \times 10^{-11}$  to  $1 \times 10^{-10}$  m/s. The velocities increase to between  $1 \times 10^{-10}$  to  $1 \times 10^{-9}$  m/s in the high-transmissivity zone south of H-11. The increase in velocity is lower than expected from the increased transmissivities in this region because the gradient within the area south of H-11 is much lower than that to the north at the WIPP-site center. The velocity vectors in the northeast quadrant of the model area, near DOE-2, and west of H-12 are greatly affected by the Culebra-elevation changes that occur in these areas.

### 3.3.7 Calculated Particle Travel Times in the Model Region

In a steady-state flow field, calculated particle travel times are good indicators of the potential travel times of the ground water due strictly to the changes in transmissivity and hydraulic gradient over a particular area. By definition,



**Darcy-Velocity Vector Scale**



Drawn by ABW	Date 11/2/89
Checked by M.L.	Date 11/2/89
Revisions	Date
H09700R869	11/2/89

Darcy-Velocity Vectors of the Steady-State  
Calibrated Model

**INTERA Technologies**

Figure 3.11

particle travel times are calculated using the Darcy velocities and a selected porosity. The processes of dispersion, transport in fractures, matrix diffusion, and sorption are not included in the travel-time calculations presented in this study. The travel times which would be determined by including these processes could be very different from those presented in this study. For example, the travel time of a reactive contaminant in a double-porosity system will depend upon the sorptive interaction of the contaminant and the formation fluid and the interaction between the fractures and the matrix. In addition, changes in the formation fluid densities should be expected over the time frame considered in this particle-tracking exercise. No attempt has been made to account for these changes.

The particle travel times should be interpreted relative to the assumption of spatially constant porosity and the uncertainties associated with the transmissivities and the hydraulic gradients. For instance, spatially-varying porosities along the flow path could dramatically reduce the travel time if the porosities are significantly lower than the 16 percent porosity value used in the present travel-time calculation (e.g., selection of a fracture porosity). In this study, a significant portion of the uncertainties of the transmissivities in the WIPP-site area can be derived from the estimation errors of the transmissivity field (Figure 2.10b). The uncertainties of the observed head values must also be considered. The uncertainties of the observed heads (Table 2.6) originate mainly from the uncertainties in the borehole-fluid densities and the trends observed in the hydrographs for the WIPP-area boreholes (Cauffman et al., 1990).

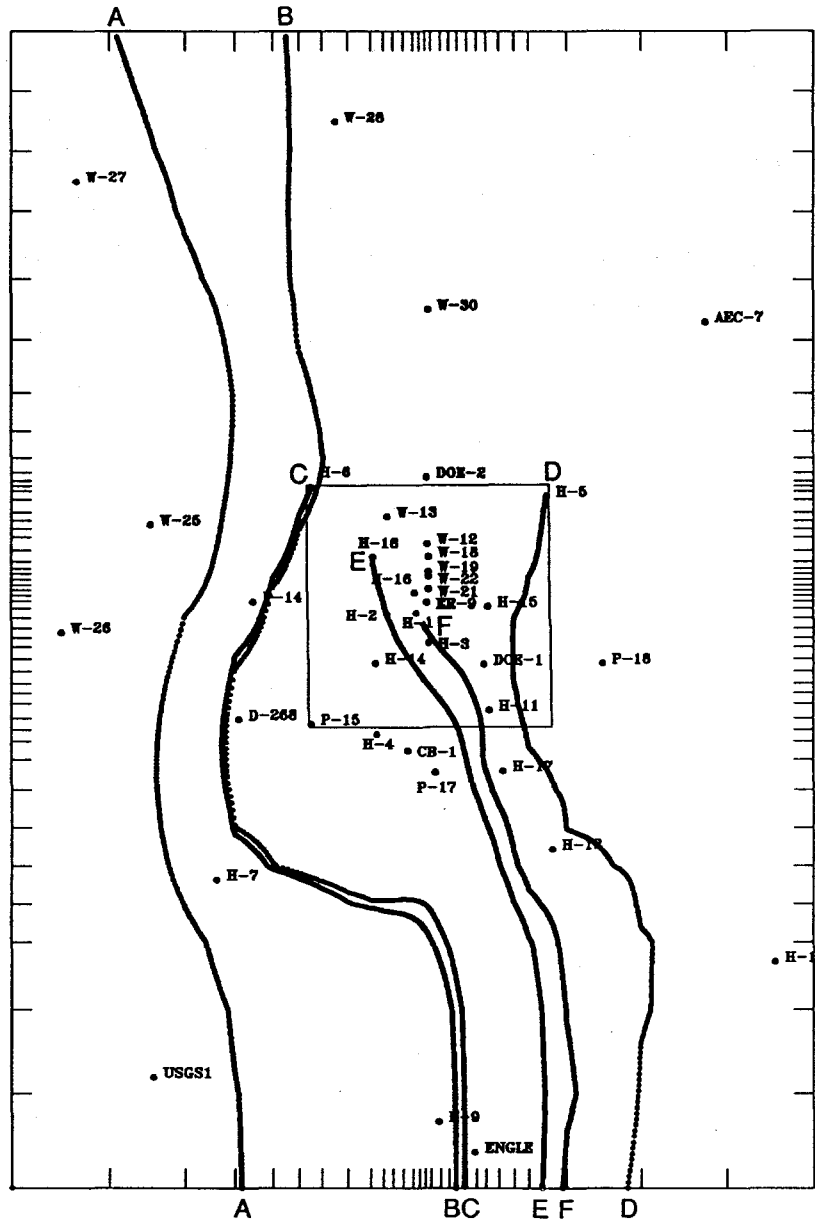
The particle travel times are presented to illustrate the range in travel times for the calibrated steady-state model using the steady-state calibrated transmissivities and a spatially constant porosity of 16 percent. In addition, these travel-time values will provide a basis for comparison with the travel times determined using the transient calibrated transmissivity field.

Calculations were performed for the release of six particles in the flow field defined by the steady-state calibrated heads. Of these six, two were released along the western half of the northern boundary to determine the travel times within the model area representing Nash Draw. The four other particles were released within the WIPP-site boundary at locations coincident with H-5, H-6,

H-18, and a point corresponding to the centroid of the underlying repository which was considered the base-case release point in Reeves et al. (1987). Figure 3.12 illustrates the particle travel paths for all six particles. The paths are consistent with the velocity vectors illustrated in Figure 3.11. The shortest travel times occur in the western part of the model area where Particles A and B have travel times of approximately  $4.5 \times 10^3$  and  $2.4 \times 10^4$  years, respectively, to the southern model boundary. Both of these particles traveled directly south in the area representing Nash Draw where the Darcy velocities range from  $5 \times 10^{-8}$  to  $5 \times 10^{-7}$  m/s. Particle B initially travels southward but is redirected southwest near H-6 and eventually travels southeast away from H-7 exiting the southern model boundary near H-9.

The travel path of Particle C, originating at H-6, is oriented southwest because the ground-water flow in this area is oriented away from the relatively low transmissivities south of H-6. The travel path is essentially the same as Particle B exiting the southern model boundary near H-9 with a total particle travel time of  $1.5 \times 10^4$  years. Particle D was released from a location coincident with H-5 and exits the model area from the southern boundary in  $2.9 \times 10^6$  years. The calculated travel time for Particle D is long because of the low calculated Darcy velocities ( $1 \times 10^{-11}$  to  $1 \times 10^{-10}$  m/s) near the eastern WIPP-site boundary and because Particle D does not enter the high-velocity zone between H-17 and P-17 which is generated by the high-transmissivity zone described in Section 3.3.5.

Particles E and F were released in the central part of the WIPP site. The release point for Particle E is coincident with H-18. This particle then travels southeast between H-3 and H-14, enters the high-velocity zone between H-17 and P-17 and reaches the southern model boundary in  $7.6 \times 10^4$  years. Particle F was released in the Culebra from a point coincident with the centroid of the underlying repository area. This release point was used as the base-case release point in Reeves et al. (1987). The calculated particle travel time for Particle F to reach the southern WIPP-site boundary is approximately  $2.1 \times 10^4$  years, which is about one-fifth of the total travel time to the southern model boundary ( $1.2 \times 10^5$  years).



Calculated Particle Travel Times

- Particle A =  $4.5 \times 10^3$  years
- Particle B =  $2.4 \times 10^4$  years
- Particle C =  $1.5 \times 10^4$  years
- Particle D =  $2.9 \times 10^6$  years
- Particle E =  $7.6 \times 10^4$  years
- Particle F =  $1.2 \times 10^5$  years

Drawn by	ABW	Date	10/31/89
Checked by	M.L.	Date	10/31/89
Revisions		Date	
H09700R869		10/31/89	

Calculated Particle Travel Paths and Travel Times  
in the Steady-State Calibrated Model

**INTERA** Technologies

Figure 3.12

The travel time determined for Particle F to reach the southern WIPP-site boundary is approximately 1.6 times longer than the travel time to the southern WIPP-site boundary presented in LaVenue et al. (1988). The increase in particle travel time is primarily due to the lower ground-water velocities south of H-3 generated by the lower transmissivities in the vicinity of H-11 estimated in this study relative to those presented in LaVenue et al. (1988). It should be noted that transmissivity changes required during transient calibration affected the travel times of the particles released within the WIPP-site boundary. The adjusted travel times are presented in Section 5.5.



## 4.0 EVENTS USED IN THE TRANSIENT SIMULATIONS

The events included in the transient simulations mainly consist of those activities which have caused intermediate to large-scale hydraulic stresses on the Culebra. Many other well-testing and water-quality-sampling activities have been conducted at the WIPP site and could be implemented in the transient simulation. In general, most of these are of short duration with relatively small impacts on the hydrologic conditions in the Culebra. We have selected tests of longer duration which have stressed the Culebra within the WIPP-site boundary. These tests cannot be simulated adequately by simply assuming that initially undisturbed hydraulic conditions exist. The shaft disturbances (i.e., shaft activities) were simulated in order to obtain the proper initial hydrologic conditions in the Culebra dolomite at the beginning of the selected well tests. Descriptions of the shaft activities and the well tests that were used in the model are presented in the following sections.

### 4.1 Simulation of the Shaft Histories

The major shaft events considered to have had the greatest impact on the Culebra are summarized in Table 4.1. These events are described in detail in Appendix H of Cauffman et al. (1990). The events listed in Table 4.1 have caused the shaft inflow from the Culebra to vary. Unfortunately, measured shaft-inflow data from the Culebra are very sparse. Very few inflow measurements have been made in the exhaust shaft (EXS), the construction and salt-handling (C&SH) shaft, and the air-intake shaft (AIS) (Table 4.2). While inflow into the waste-handling shaft (WHS) has been measured more frequently than inflow into the other shafts, most of the measurements were taken during the short period from 1986 through 1987. There is sufficient information regarding drilling-fluid levels during shaft excavation to allow for the specification of pressures for most of the time periods in which shaft excavation was conducted. For example, the pressures imposed upon the Culebra due to drilling fluid levels during the excavation of the C&SH and air-intake shafts have been estimated in Stevens and Beyeler (1985) and Avis and Saulnier (1990), respectively. Thus, both pressure and rate information must be used to simulate the shaft histories if adequate representation of the shaft events and their effect upon the Culebra is to be made.

<u>SHAFT</u>	<u>EVENT</u>	<u>DATE</u>
C&SH	3.68 m dia penetrates Culebra	8/81
C&SH	Liner on Culebra	12/81
WHS	1.83 m dia penetrates Culebra	1/82
EXS	0.20 m dia penetrates Culebra	10/83
EXS	Enlarged dia to 0.28 m	12/83
EXS	Enlarged dia to 1.83 m	1/84
WHS	Enlarged dia to 6.55 m	2/84
WHS	Liner on Culebra	4/84
WHS	Grouting Culebra	8/84
EXS	Enlarged dia to 4.27 m	10/84
EXS	Liner on Culebra	12/84
EXS	Grouting Culebra (1st round)	7/85
EXS	Grouting Culebra (2nd round)	11/86
C&SH	Grouting Culebra	6/87
EXS	Grouting Culebra (3rd round)	7/87
WHS	Grouting Culebra	11/87
AIS	0.25 m dia penetrates Culebra	1/88
AIS	Enlarged dia to 0.37 m	2/88
AIS	Enlarged dia to 6.17 m	6/88
AIS	Steel plate liner on Culebra	11/88

Drawn by	Date
Checked by	Date
Revisions	Date

Abridged Shaft Events

Date	Inflow Rate * (L/s)	Reference
=====	=====	=====

Construction & Salt-Handling Shaft:

09/13/81	0.110	Deshler & McKinney (1988)
07/03/82	0.019	Gonzales (1989) **
09/28/82	0.036	Gonzales (1989)
10/02/82	0.025	Gonzales (1989)
10/02/82	0.025	Gonzales (1989)
10/02/82	0.025	Gonzales (1989)
10/02/82	0.019	Gonzales (1989)
10/02/82	0.025	Gonzales (1989)
10/08/82	0.043	Gonzales (1989)

Waste-Handling Shaft:

03/10/82	0.022	Gonzales (1989)
07/03/82	0.019	Deshler & McKinney (1988)
09/28/82	0.032	Deshler & McKinney (1988)
10/02/82	0.025	Deshler & McKinney (1988)
10/08/82	0.038	Deshler & McKinney (1988)
06/84	0.032	Roberts (1985)
10/84	0.001	U.S. DOE (1986)
01/02/86	0.025	Deshler & McKinney (1988)
01/15/86	0.027	Deshler & McKinney (1988)
01/15/86	0.030	Deshler & McKinney (1988)
01/23/86	0.030	Deshler & McKinney (1988)
01/30/86	0.023	Deshler & McKinney (1988)
02/03/86	0.027	Deshler & McKinney (1988)
02/03/86	0.028	Deshler & McKinney (1988)
02/05/86	0.021	Deshler & McKinney (1988)
02/12/86	0.028	Deshler & McKinney (1988)
02/13/86	0.028	Deshler & McKinney (1988)
02/17/86	0.028	Deshler & McKinney (1988)
02/19/86	0.028	Deshler & McKinney (1988)
02/20/86	0.019	Deshler & McKinney (1988)
02/28/86	0.021	Deshler & McKinney (1988)
03/07/86	0.021	Deshler & McKinney (1988)
03/13/86	0.019	Deshler & McKinney (1988)
03/17/86	0.027	Deshler & McKinney (1988)
03/18/86	0.019	Deshler & McKinney (1988)
03/21/86	0.028	Deshler & McKinney (1988)
03/26/86	0.019	Deshler & McKinney (1988)
04/02/86	0.018	Deshler & McKinney (1988)
04/03/86	0.025	Deshler & McKinney (1988)

Drawn by	M.L.	Date	11/2/89	Measured Rustler Leakage Rates at the WIPP Shafts
Checked by	M.L.	Date	11/2/89	
Revisions		Date		
H09700R869		11/2/89		
<b>INTERA</b> Technologies				Table 4.2

Date	Inflow Rate * (L/s)	Reference
Waste-Handling Shaft (cont.) :		
04/07/86	0.014	Deshler & McKinney (1988)
04/08/86	0.017	Deshler & McKinney (1988)
04/10/86	0.017	Deshler & McKinney (1988)
04/15/86	0.016	Deshler & McKinney (1988)
04/16/86	0.020	Deshler & McKinney (1988)
04/18/86	0.019	Deshler & McKinney (1988)
04/24/86	0.018	Deshler & McKinney (1988)
04/25/86	0.020	Deshler & McKinney (1988)
04/25/86	0.017	Deshler & McKinney (1988)
05/15/86	0.014	Deshler & McKinney (1988)
05/19/86	0.014	Deshler & McKinney (1988)
05/22/86	0.014	Deshler & McKinney (1988)
05/28/86	0.015	Deshler & McKinney (1988)
06/02/86	0.013	Deshler & McKinney (1988)
06/06/86	0.008	Deshler & McKinney (1988)
06/06/86	0.008	Deshler & McKinney (1988)
06/12/86	0.010	Deshler & McKinney (1988)
06/19/86	0.009	Deshler & McKinney (1988)
06/24/86	0.014	Deshler & McKinney (1988)
07/01/86	0.008	Deshler & McKinney (1988)
10/13/86	0.008	Deshler & McKinney (1988)
10/28/86	0.011	Deshler & McKinney (1988)
11/06/86	0.013	Deshler & McKinney (1988)
11/11/86	0.012	Deshler & McKinney (1988)
11/20/86	0.016	Deshler & McKinney (1988)
11/26/86	0.015	Deshler & McKinney (1988)
12/04/86	0.015	Deshler & McKinney (1988)
12/29/86	0.016	Deshler & McKinney (1988)
01/29/87	0.011	Deshler & McKinney (1988)
03/13/87	0.010	Deshler & McKinney (1988)
03/20/87	0.006	Deshler & McKinney (1988)
04/03/87	0.013	Deshler & McKinney (1988)
04/08/87	0.013	Deshler & McKinney (1988)
04/22/87	0.012	Deshler & McKinney (1988)
04/19/87	0.010	Deshler & McKinney (1988)
05/07/87	0.020	Deshler & McKinney (1988)
05/08/87	0.004	Deshler & McKinney (1988)
05/15/87	0.011	Deshler & McKinney (1988)
05/22/87	0.012	Deshler & McKinney (1988)
06/11/87	0.011	Deshler & McKinney (1988)
06/18/87	0.011	Deshler & McKinney (1988)
06/30/87	0.010	Deshler & McKinney (1988)
07/07/87	0.009	Deshler & McKinney (1988)

Drawn by M.L.	Date 11/2/89	Measured Rustler Leakage Rates at the WIPP Shafts
Checked by M.L.	Date 11/2/89	
Revisions	Date	
H09700R869	11/2/89	

<b>INTERA</b> Technologies	Table 4.2 (cont.)
----------------------------	-------------------

Date	Inflow Rate * (L/s)	Reference
Waste-Handling Shaft (cont.):		
07/16/87	0.010	Deshler & McKinney (1988)
07/23/87	0.010	Deshler & McKinney (1988)
07/29/87	0.009	Deshler & McKinney (1988)
08/05/87	0.010	Deshler & McKinney (1988)
08/06/87	0.008	Gonzales (1989)
08/20/87	0.009	Deshler & McKinney (1988)
08/26/87	0.010	Deshler & McKinney (1988)
09/11/87	0.010	Deshler & McKinney (1988)
09/16/87	0.015	Deshler & McKinney (1988)
10/01/87	0.010	Deshler & McKinney (1988)
10/07/87	0.010	Deshler & McKinney (1988)
10/08/87	0.010	Deshler & McKinney (1988)
10/16/87	0.012	Deshler & McKinney (1988)
10/30/87	0.011	Deshler & McKinney (1988)
11/04/87	0.012	Deshler & McKinney (1988)

Exhaust Shaft:

11/30/83	0.026	Deshler & McKinney (1988)
12/21/83	0.030	Deshler & McKinney (1988)
01/85	0.022	Deshler & McKinney (1988)

Air-Intake Shaft:

02/07/88	0.030	Deshler & McKinney (1988)
10/28/88	0.056	Avis & Saulnier (1990)
06/01/89	0.047	INTERA ***
06/07/89	0.047	INTERA
06/12/89	0.047	INTERA

\* The majority of the inflow rates reflect combined flow from the Magenta and Culebra dolomites. For a complete description of the inflow measurements see the appropriate references.

\*\* Gonzales (personal communication, 1989).

\*\*\* INTERA logbook field notes.

Drawn by	M.L.	Date	11/2/89	Measured Rustler Leakage Rates at the WIPP Shafts
Checked by	M.L.	Date	11/2/89	
Revisions		Date		
H09700R869		11/2/89		
INTERA Technologies				Table 4.2 (cont.)

In order to simulate each shaft history, a sink/source at each shaft location was included in the model. Technically, this was done by placing a pumping/injection well in each of the grid blocks that coincides with the location of a shaft. The shaft's pressure and/or leakage-rate histories were simulated using both the pressure-controlled and rate-controlled modes of the wellbore submodel (Reeves et al., 1986a). In the pressure-controlled mode, the leakage or injection rate is automatically adjusted by SWIFT II during the simulation so that the prescribed pressures are maintained in the grid block containing a shaft. The rate is directly specified in the rate-controlled mode and the bottom-hole pressure is adjusted by SWIFT II during the simulation.

The approach used for the simulation of the shafts consisted of specifying bottom-hole pressures at each shaft until it was completed (i.e., excavation was complete and a liner was emplaced and grouted) at which time a rate or series of rates was specified for the duration of the simulation time. Since several reaming events occurred at each shaft during excavation (Table 4.1), the inflow rate to the open boreholes would vary due to an increase in the surface area of the borehole exposed to atmospheric pressure. The pressure-controlled mode was favored over the rate-controlled mode during shaft excavation because it allowed for the implementation of the excavation events while utilizing the information regarding the various pressures imposed upon the Culebra during excavation. Pressures were specified at the C&SH shaft from August to December of 1981 based on the pressure imposed upon the Culebra determined from drilling-fluid levels. A rate was specified at the C&SH shaft after this time based on the inflow measurements obtained in 1982. Similarly, the WHS and EXS had specified pressures from January to August 1984 and from October 1983 to July 1985, respectively. Rates were then specified at these boreholes based on the measured leakage rates taken after shaft completion. The AIS is the only shaft which had only specified pressures over the length of the simulation as its excavation began in 1988 and it has not yet been grouted.

During the time periods in which pressures were specified at the shafts (i.e., before excavation was complete), available measured inflow rates were used to provide a check for the calculated inflow which is a function of the gradient between the formation pressure and the pressure within the shaft and is proportional to a well

index assigned to the shaft. A well index represents the transmitting capability of the region surrounding a borehole or shaft. Each of the shafts and pumping wells is assigned a well index based on the diameter of the borehole, the dimensions of the grid block containing the shaft or pumping well, and the transmissivity of a skin which is considered to be the local region surrounding the borehole. If the calculated rates were significantly different from the rates observed, the well index assigned to the shaft would be modified until the calculated and observed inflow rates agreed. The following paragraphs contain more information regarding the theory, equations, and implementation of the well indices.

The region surrounding a well is called the skin (see Figure 4.1). The ability of this region to transmit fluid may be either degraded or enhanced relative to that of the undisturbed formation, depending on well completion. This transmitting capability of the skin is characterized by the well index, WI, which is generally defined by the relation

$$q = (WI/\mu)\Delta p \quad (4.1)$$

where  $q$  is the flow rate in  $m^3/s$ ,  $\Delta p$  is the pressure drop across the skin region in Pa, and  $\mu$  is viscosity in Pa·s. For specific values of viscosity,  $\mu_0$ , and fluid density,  $\rho_0$ , the well index may be defined in terms of head drop rather than pressure drop:

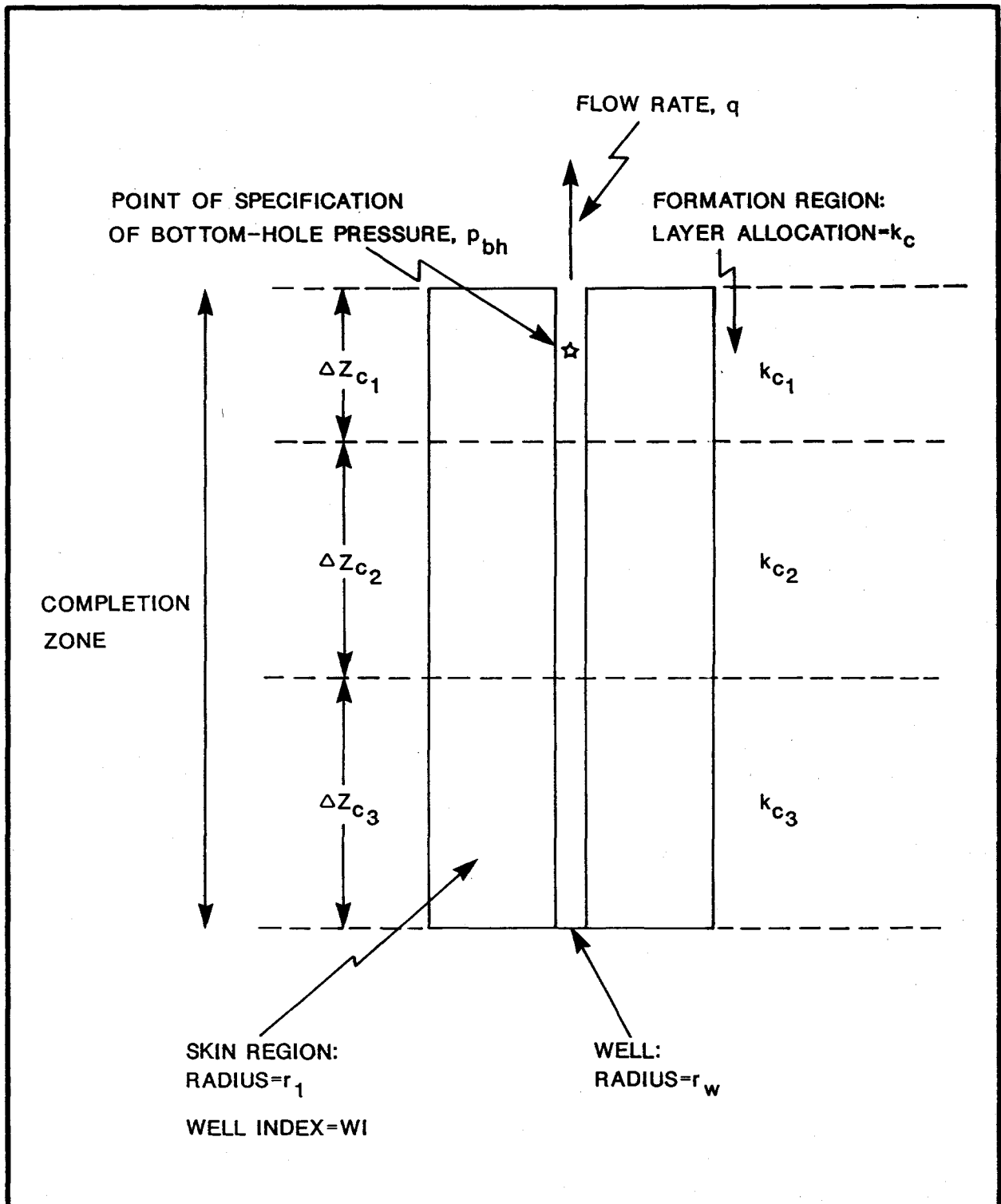
$$q = WI_0\Delta H \quad (4.2)$$

where  $WI_0$  is measured in  $m^2/s$  and is defined by

$$WI_0 = \rho_0 g WI / \mu_0 \quad (4.3)$$

where  $g$  is the gravitational constant. The SWIFT II code requires  $WI_0$  as input, where  $\rho_0$  and  $\mu_0$  are defined in terms of reference values of pressure, temperature, and concentration.

For injection or production wells, the well index may be estimated by a one-dimensional, steady-state solution of the flow equation which yields



Drawn by	ABW	Date	10/31/89
Checked by	M.L.	Date	10/31/89
Revisions		Date	
H09700R869		10/31/89	

Characterization of the Skin Region  
Surrounding a Well  
(After Reeves et al., 1986a)

**INTERA** Technologies

Figure 4.1



$$WI_0 = 2\pi K_s \sum_i \Delta z_i / \ln(r_1/r_w) \quad (4.4)$$

where  $K_s$  is the hydraulic conductivity of the skin, index  $i$  ranges over all layers in which the well is completed,  $\Delta z$  is the thickness of the individual layer,  $r_1$  is the skin radius, and  $r_w$  is the well radius. This equation is directly applicable for radial coordinates since radius  $r_1$  is defined as the position of the first nodal point in that case.

For Cartesian coordinates the well index is no longer directly comparable to physical parameters (i.e., skin radius and permeability) due to the fact that the skin radius,  $r_1$ , is not defined directly, but is specified in terms of the average grid-block radius,  $r_a$ , where

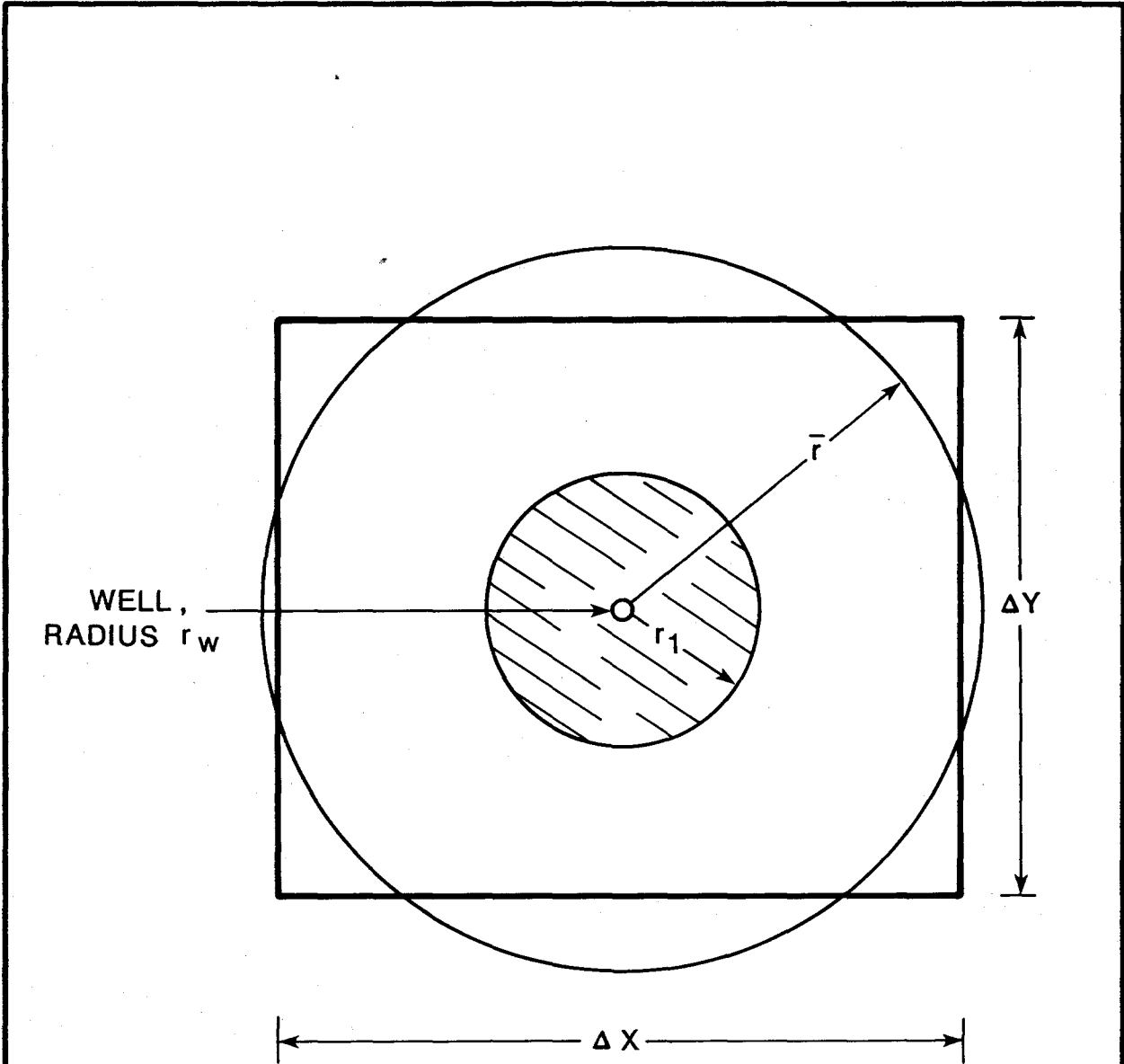
$$r_a = (\Delta x \Delta y / \pi)^{1/2} \quad (4.5)$$

where  $\Delta x$  and  $\Delta y$  are the grid-block dimensions. Schematically, the assumed relation between the skin radius and this average block radius is shown in Figure 4.2. Mathematically, this relation is given by

$$\ln(r_1/r_w) = r_w [1 + (r_a/r_w) [\ln(r_a/r_w) - 1] / (r_a - r_w)] \quad (4.6)$$

In this case, the pressure drop  $\Delta p$  of Equation (4.1) is the difference between the well and the grid-block pressures, and radius  $r_1$  is taken to be the location of the radially averaged pressure of the cone of influence between radii  $r_w$  and  $r_a$ .

In this study, the skin transmissivity assigned to the shafts was initially set equal to the steady-state calibrated transmissivity of the grid block containing the shaft. Increasing the transmissivity of the skin implies that the local region surrounding the borehole has a greater capacity to transmit fluid relative to the rest of the grid block. This condition could occur if the borehole intersected fractures. Conversely, a reduction in the transmissivity of the skin denotes a decrease in the transmitting capability of the local region surrounding the borehole relative to the rest of the grid block. This condition could occur for the shafts as a result of grouting and sealing activities.



WELL,  
RADIUS  $r_w$

$\Delta Y$

$\Delta X$

$\bar{r}$  = Radius of Equivalent Circle with Area of  $\Delta x \cdot \Delta y$

$r_1$  = The Distance to the Average Pressure of the Cone  
of Influence Between  $r_w$  and  $\bar{r}$

Drawn by	ABW	Date	10/31/89
Checked by	M.L.	Date	10/31/89
Revisions		Date	
H09700R869		10/31/89	

Concept of Skin Thickness for a  
Cartesian Grid Block  
(After Reeves et al., 1986a)

**INTERA** Technologies

Figure 4.2

By modifying the transmissivity of the skin, the well index was adjusted in order to represent the grouting and lining activities that have occurred at three of the four shafts. Table 4.3 lists the well indices assigned to the shafts in the initial transient simulation. It was assumed that once a liner was emplaced over the Culebra interval, the transmissivity of the skin decreased by a factor of two. Furthermore, the transmissivity was assumed to be reduced two orders of magnitude from the pre-lined value after grouting had occurred. However, if leakage into a shaft was observed after grouting occurred, the well index assigned during the time period of the observed leakage was increased back to the value assigned prior to grouting. The increase in the well index was performed in order to account for the ineffective grouting of a shaft. The well index assigned to the C&SH shaft and WHS was lowered to  $1 \times 10^{-15} \text{ m}^2/\text{s}$  after the grouting program conducted in 1987 designed to end the leakage into these shafts had occurred. A well index of  $1 \times 10^{-15} \text{ m}^2/\text{s}$  essentially reduces the inflow to the shafts to 0.0 L/s. A comparison of the reductions in, or actual values assigned to, the permeability of the skin to the permeability of intact cement is not presented due to the fact that in a discretized, two-dimensional Cartesian system, the well index, and therefore the skin permeability, is merely a fitting parameter used to adjust the pressures or rates at a production or injection well. Therefore, comparisons of the values used for the skin or the well index in this study to physical parameters such as the permeability of the grout used during shaft completion should be strictly qualitative.

#### 4.2 Simulation of Well Tests

The hydraulic heads of the Culebra dolomite have not only been disturbed by the shaft activities discussed in the previous subsection but also by numerous well tests. Important for the hydraulic conditions in the central part of the model area were the tests performed at H-2, H-3, H-4, H-11, WIPP-13, WIPP-19, and P-14. Consequently, the tests on these wells or hydropads that were considered to be relevant and for which sufficient data were available were implemented in the model. The following subsections discuss the tests that were considered important.

Well indices were assigned to each of the pumping wells used in the transient simulation of this study. Because the transient responses at the pumping wells and

<u>Shaft</u>	<u>Well Index (m<sup>2</sup>/s)</u>	<u>Time Period</u>
C&SH	1.3x10 <sup>-6</sup>	08/07/81 - 12/06/81
	1.3x10 <sup>-8</sup>	12/06/81 - 06/01/87
	1.0x10 <sup>-15</sup>	06/01/87 - 06/01/89
WHS	9.8x10 <sup>-7</sup>	01/30/82 - 02/01/84
	1.5x10 <sup>-6</sup>	02/01/84 - 04/05/84
	7.4x10 <sup>-7</sup>	04/05/84 - 08/20/84
	1.5x10 <sup>-8</sup>	08/20/84 - 12/16/85
	7.4x10 <sup>-7</sup>	12/16/85 - 11/01/87
EXS	1.0x10 <sup>-15</sup>	11/01/87 - 06/01/89
	4.7x10 <sup>-7</sup>	10/05/83 - 01/10/84
	7.4x10 <sup>-7</sup>	01/10/84 - 10/15/84
	9.5x10 <sup>-7</sup>	10/15/84 - 12/04/84
	4.8x10 <sup>-7</sup>	12/04/84 - 07/15/85
AIS	9.5x10 <sup>-9</sup>	07/15/85 - 06/01/89
	9.6x10 <sup>-7</sup>	01/01/88 - 01/08/88
	1.0x10 <sup>-6</sup>	01/08/88 - 02/02/88
	2.2x10 <sup>-6</sup>	02/02/88 - 06/01/89

Drawn by	Date
Checked by	Date
Revisions	Date

Initial Well Indices Assigned to Shafts

the observation wells have been thoroughly analyzed, information concerning the skins associated with each well is available. For instance, Beauheim has published several reports (Beauheim, 1987a, 1987c, 1989) in which he analyzed the measured responses to the three multipad pumping tests conducted at H-3, WIPP-13, and H-11. In these reports he discusses the values of transmissivity and storativity which provide the best fits to the responses at the pumping wells and the many observation wells. Another parameter he presents is the skin factor used to match the measured drawdowns at the pumping well. The skin factor provides an indication of the degree of hydraulic connection of the pumping well to the surrounding formation. A large negative skin factor indicates that the wellbore is directly intersected by fractures (Beauheim, 1987a) which may act as additional production surfaces to the well. Qualitatively, this means that the response at this well would appear to have come from a wellbore with a much larger radius. Conversely, a positive skin factor indicates the well behaves hydraulically like a well with a smaller radius (Beauheim, 1987a).

The skin factors have been qualitatively used while assigning well indices to the pumping wells discussed in this section. The skin permeabilities for the wells with high negative skin factors (H-3, H-11, and WIPP-13) have all been increased relative to the transmissivity of the grid block containing the well. Table 4.4 lists the well indices initially assigned to the pumping wells used in this study. The scale of the model requires a hydropad (i.e., a location which may have several wells, within 50 m of each other) to be represented by a single well in a grid block and, therefore, Table 4.4 only lists one well at a hydropad.

#### 4.2.1 Well Tests at the H-2 Hydropad

The H-2 hydropad has an extensive history of slug, pumping, and tracer tests (Cauffman et al., 1990). Only tests conducted since 1981 were considered for this modeling study, however, because earlier tests are not likely to have had a significant influence on the hydrologic conditions in the Culebra dolomite relative to the effects of the shaft beginning in 1981.

The following major tests were conducted at the H-2 hydropad in the period 1981 to 1987:

<u>Well</u>	<u>Well Index (m<sup>2</sup>/s)</u>
H-2	7.2x10 <sup>-7</sup>
H-3	4.5x10 <sup>-2</sup>
H-4	8.3x10 <sup>-7</sup>
H-11	1.8x10 <sup>-4</sup>
WIPP-13	8.3x10 <sup>-1</sup>
WIPP-19	7.5x10 <sup>-7</sup>
P-14	9.4x10 <sup>-5</sup>

Drawn by	Date	<b>Initial Well Indices Assigned to Pumping Wells</b>
Checked by	Date	
Revisions	Date	
<b>INTERA Technologies</b>		Table 4.4

- A pumping test at H-2b2 (October 13-16, 1983) with an average pumping rate of  $2.45 \times 10^{-2}$  L/s (calculated for a 72-hour pumping period)
- A second pumping test at H-2b2 (November 8-17, 1983) with an average pumping rate of  $1.78 \times 10^{-2}$  L/s
- Bailing at H-2b1, H-2b2, and H-2c between June 7, 1984 and July 2, 1984. The volumes of ground water removed from the different boreholes during the different tests totalled about 6300 L. This corresponds to an average production rate of  $3.83 \times 10^{-3}$  L/s during this time period
- A third pumping test at H-2b2 (July 17 - August 2, 1984). During eight pumping periods, about 2600 L were removed from that borehole. This corresponds to an average pumping rate of  $1.83 \times 10^{-3}$  L/s during the time period
- Pumping at H-2a for water-quality sampling (April 4 - 21, 1986) with an average pumping rate of  $2.36 \times 10^{-2}$  L/s
- Pumping at H-2a for water-quality sampling (July 23 - August 12, 1987) with an average pumping rate of  $1.89 \times 10^{-2}$  L/s.

Numerous additional tests or similar activities were performed since 1981, but because they did not last more than 3 or 4 days, they were not considered to be important enough to be implemented into the model. Also, recirculation tracer tests performed at the H-2 hydropad were not considered because these tests did not represent a net removal of ground water from the Culebra.

The well history at the H-2 hydropad was complicated by drilling activities (e.g., H-2b2 in summer 1983), well reconditioning (e.g., all wells at the H-2 hydropad in winter 1983/1984), and packer movements and transducer installations (e.g., H-2b1 in July 1984). Sufficient data were not available to enable incorporation of these activities into the model. Thus, only the six tests outlined above were implemented into the model using the SWIFT II wellbore submodel (rate-controlled mode).

## 4.2.2 Well Tests at the H-3 Hydropad

### 4.2.2.1 Convergent-Flow Tracer Test at the H-3 Hydropad

After completion of the H-3 hydropad early in 1984, the first major test conducted at that hydropad was a convergent-flow tracer test (Hydro Geo Chem, 1985; Kelley and Pickens, 1986). The activities associated with this test included well development, a pumping test designed to evaluate the transmissivity of the Culebra dolomite at the H-3 hydropad, and the pumping period corresponding to the convergent-flow tracer test. The first two pumping periods (well development) were very short and, therefore, were not incorporated into the model.

The first pumping period that was incorporated into the model lasted from April 23 through May 7, 1984. An average production rate of  $2.5 \times 10^{-1}$  L/s was used. On May 7, the pumping rate was lowered in order to prepare for the convergent-flow tracer test which had to be performed under regulated flow conditions. A pumping rate of about  $1.9 \times 10^{-1}$  L/s was maintained between May 7 and June 3, 1984. From June 3 until the end of the test on June 12, 1984, moderately higher pumping rates were recorded. An average pumping rate of  $2.2 \times 10^{-1}$  L/s was selected for modeling purposes for this latter period.

In summary, the convergent-flow tracer test was implemented as a pumping test using  $2.5 \times 10^{-1}$  L/s for the time period from April 23 to May 7;  $1.9 \times 10^{-1}$  L/s from May 7 to June 3; and  $2.2 \times 10^{-1}$  L/s from June 3 to June 12, 1984.

### 4.2.2.2 Step-Drawdown Test at the H-3 Hydropad

A step-drawdown test, which increased the pumping rate in a step-wise manner, was performed at H-3b2 between June 20 and July 10, 1985 (INTERA, 1986). This test was simulated in the model using the following average pumping periods and rates:



June 20	-	June 24, 1985	:	$1.29 \times 10^{-1}$ L/s
June 24	-	June 28, 1985	:	$2.50 \times 10^{-1}$ L/s
June 28	-	July 5, 1985	:	$3.00 \times 10^{-1}$ L/s
July 5	-	July 10, 1985	:	$3.21 \times 10^{-1}$ L/s

These four pumping periods with the corresponding pumping rates were implemented using the rate-controlled mode of the SWIFT II wellbore submodel.

#### 4.2.2.3 H-3 Multipad Pumping Test

The pumping period of the H-3 multipad pumping test was from October 15, 1985 through December 16, 1985 (INTERA, 1986). Using the H-3b2 well as the pumping well, an average of about  $3.08 \times 10^{-1}$  L/s was removed over a time period of 62 days. The H-3 multipad pumping test was incorporated into the model using the rate-controlled mode of the SWIFT II wellbore submodel.

#### 4.2.2.4 Water-Quality Sampling at the H-3 Hydropad

H-3b3 was pumped as part of the water-quality sampling program (WQSP) in January and February 1985, August 1987, and February and March 1989. The following average pumping periods and rates were used in the model:

January 29	-	February 4, 1985	:	$1.89 \times 10^{-1}$ L/s
August 7	-	August 24, 1987	:	$2.02 \times 10^{-1}$ L/s
February 14	-	March 2, 1989	:	$2.90 \times 10^{-1}$ L/s

#### 4.2.3 Convergent-Flow Tracer Test at the H-4 Hydropad

A long-term tracer test was conducted at the H-4 hydropad from October 24, 1982 to October 15, 1984 (Hydro Geo Chem, 1985; Kelley and Pickens, 1986). The withdrawal well was H-4c. The pumping rate during the tracer test can be generally divided into two separate flow periods. The first flow rate of about  $1.67 \times 10^{-2}$  L/s started October 24, 1982 and continued until June 10, 1983. At that time, the pumping rate was doubled to  $3.33 \times 10^{-2}$  L/s and maintained until

August 9, 1983. Thereafter, the pumping rate fluctuated around  $3.1 \times 10^{-2}$  L/s until June 20, 1984. Slightly higher pumping rates, with an estimated average of  $3.33 \times 10^{-2}$  L/s, were recorded from June 20, 1984 until the end of the tracer test on October 15, 1984. Similar to the other well tests, the H-4 convergent-flow tracer test was implemented into the model using the rate-controlled mode of the SWIFT II wellbore submodel.

#### 4.2.4 WIPP-13 Multipad Pumping Test

The WIPP-13 multipad pumping test consisted of a 36-day constant-rate pumping period. The test began on January 12, 1987, with WIPP-13 being pumped continuously at approximately 1.93 L/s until February 17, 1987 (Stensrud et al., 1987). The actual pumping rate varied slightly over the 36-day period from 1.88 L/s to 2.0 L/s.

Four periods were used in the model to implement the WIPP-13 pumping test. From January 12 to January 27, a pumping rate of 1.89 L/s was used. The second period was from January 27 to February 4 and had a pumping rate of 1.94 L/s. The highest pumping rate of 1.99 L/s was implemented from February 4 to February 11. The fourth period lasted from February 11 until February 17 and had a pumping rate of 1.97 L/s. These four pumping periods were implemented into the model using the rate-controlled mode of the SWIFT II wellbore submodel.

#### 4.2.5 H-11 Multipad Pumping Test

The H-11 multipad pumping test began on May 5, 1988. Pumping continued for 63 days ending on July 7, 1988. The average pumping rate during the test was  $3.82 \times 10^{-1}$  L/s. The H-11 multipad pumping test was incorporated into the model using the rate-controlled mode of the SWIFT II wellbore submodel.

#### 4.2.6 Water-Quality Sampling at the WIPP-19 Borehole

WIPP-19 was pumped as part of the WQSP in January and February 1988, and in August 1988. These two pumping events were incorporated in the model when transient calibration efforts were focused on the responses at WIPP-19 due to

excavation of the AIS. The following pumping periods and rates were implemented into the model using the rate-controlled mode of the SWIFT II wellbore submodel:

January 26 - February 12, 1988 :  $1.7 \times 10^{-2}$  L/s  
August 17 - August 29, 1988 :  $2.0 \times 10^{-2}$  L/s

#### 4.2.7 P-14 Pumping Test

The P-14 pumping test began on February 14, 1989. Pumping continued for 3 days ending on February 17, 1989. The average pumping rate during the test was 3.6 L/s. The P-14 test was implemented to the model using the rate-controlled mode of the SWIFT II wellbore submodel. The P-14 test was included because it stressed an area of the model (i.e., western-central) in which there exists little regional hydraulic-interference test data (e.g., the WIPP-25 borehole responded to the pumping at P-14).

## 5.0 SIMULATION OF TRANSIENT RESPONSES RESULTING FROM SHAFT ACTIVITIES AND WELL TESTS

The purpose of this modeling study was to determine the transmissivity field which best represents the undisturbed and transient heads observed at the WIPP site as part of the site-characterization activities being conducted by Sandia National Laboratories. A ground-water model calibrated to both undisturbed conditions and the large-scale hydraulic stress tests is more defensible for estimation of the Darcy-velocity distribution and particle travel times within the WIPP-site boundaries. Therefore, the transient behavior of the Culebra dolomite in response to the shaft excavations, the H-3, WIPP-13, and H-11 multipad pumping tests, and the other pumping events discussed in Section 4 was simulated. The following sections present the model calibration to the heads measured during the activities described in Section 4.

The observed transient data are presented in terms of freshwater heads which require knowledge of representative borehole-fluid densities (Cauffman et al., 1990). Because borehole-fluid density is an uncertain parameter, a vertical line with a horizontal tic mark has been used in the figures showing the plotted transient hydrographs to express the maximum uncertainty in the transient freshwater heads calculated from the densities discussed in Cauffman et al. (1990). The vertical line indicates the maximum uncertainty associated with the freshwater-head value, while the horizontal tic mark corresponds to the best estimate of the freshwater-head value (Section 2.3.7.2).

Simulating transient events requires a definition of the time scale at which the major characteristics of measured responses may be adequately reproduced. Taking into account the length of time to be simulated (more than 8 years) and the frequency of the observed head measurements (see Cauffman et al., 1990), it was assumed that a minimum time step of one day was appropriate for the SWIFT II simulations. In order to optimize the efficiency of the transient simulations, the minimum time step was only used at the beginning of a new activity, e.g., at the start of a test or after drilling a shaft. Similar to the common practice of reducing monitoring frequency during a hydraulic test, the length of subsequent time steps was increased (e.g., 2, 4, 8, 16 days). An arbitrary value of 32 days was chosen for the maximum time-step size.

## **5.1 Initial Transient Simulation Using the Steady-State Calibrated Model**

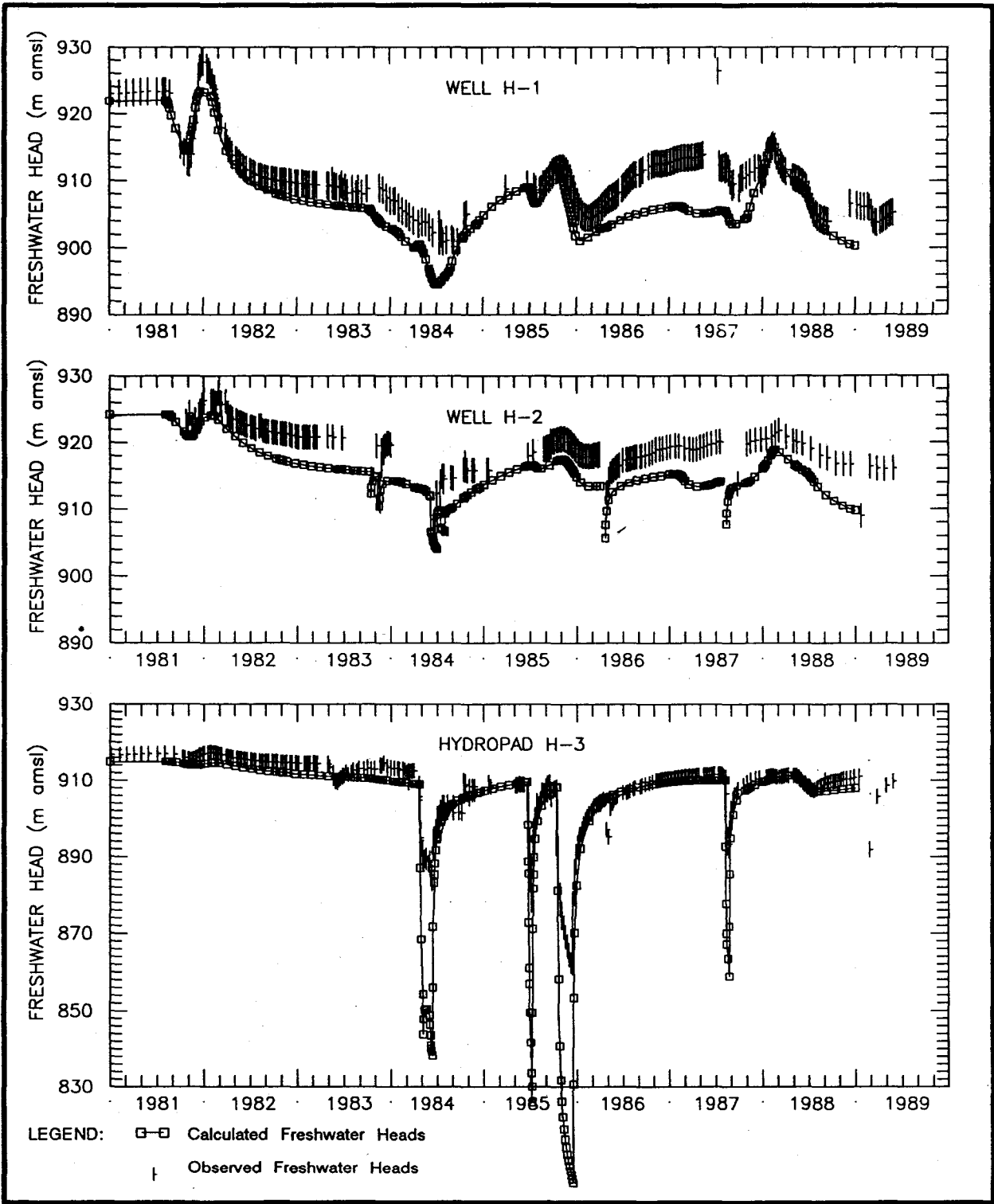
The transient simulations in this modeling study include the entire shaft history extending from its beginning in July 1981 to the present (mid-1989). Table 5.1 lists the hydrologic tests conducted at the pumping wells and the events at the shafts used in the transient simulations. For convenience, January 1, 1981 was selected as the beginning of the simulation time scale. All of the transient simulations utilize the calculated heads of the calibrated steady-state model (Figure 3.10) as the initial condition. The initial or base-case transient simulation also used the transmissivities and boundary conditions of the calibrated steady-state model. This section briefly describes the initial transient simulation. The results of the transient calibration, performed to improve the results determined in the initial simulation, are presented in Sections 5.2.1 through 5.2.6.

Figures 5.1a through 5.1g contain the results of the initial transient simulation for H-1, H-2, H-3, H-4, H-6, H-11, H-14, H-15, H-17, DOE-1, DOE-2, P-17, WIPP-12, WIPP-13, WIPP-18, WIPP-19, WIPP-21, WIPP-22, WIPP-30, CB-1, and ERDA-9. The H-5 borehole is not included because it did not respond to any of the events used in the model. The calculated heads illustrated in Figures 5.1a through 5.1g, in general, are similar to the observed heads. The shape of the calculated responses are also similar to the observed but the absolute magnitudes are somewhat different. For instance, the calculated drawdowns during the pumping tests at H-3 (Figure 5.1a) and during pumping at WIPP-13 (Figure 5.1e) are over a factor of two greater than the observed drawdowns at these two locations while the calculated drawdown at H-11 (Figure 5.1b) is a factor of two less than the drawdown observed while pumping. The calculated responses at other observation wells due to pumping at H-3, H-11, and WIPP-13 (i.e., H-1, H-2, H-6, H-14, H-15, H-17, DOE-1, DOE-2, P-17, WIPP-12, WIPP-18, and WIPP-30) also require some improvement. For instance, the calculated response at H-15 (Figure 5.1c) due to H-11 pumping is a poor representation of the observed response, as are the calculated responses at WIPP-12, WIPP-18, WIPP-19, WIPP-21, WIPP-22, WIPP-30, and ERDA-9 (Figures 5.1e through 5.1g) due to WIPP-13 pumping and/or the shaft effects.

<u>Time Period</u>	<u>Well/Shaft</u>	<u>Event</u>
08/07/81 - 12/06/81	C&SH	Construction
12/06/81 - 10/01/83	C&SH	Lined and Grouted
01/30/82 - 02/01/84	WHS	Construction
10/24/82 - 10/14/84	H-4	Pumping for Tracer Test
10/05/83 - 01/10/84	EXS	Construction
10/13/83 - 10/16/83	H-2	Pumping
11/08/83 - 11/17/83	H-2	Pumping
01/10/84 - 10/15/84	EXS	Enlarged dia. to 4.3 m
02/01/84 - 04/05/84	WHS	Enlarged dia. to 6.5 m
04/05/84 - 08/20/84	WHS	Lined and Grouted
04/23/84 - 06/13/84	H-3	Pumping for Tracer Test
06/07/84 - 07/02/84	H-2	Bailing at H-2
07/17/84 - 08/02/84	H-2	Pumping
10/15/84 - 12/04/84	EXS	Liner on Culebra
06/20/85 - 07/10/85	H-3	Pumping (Step Drawdown)
10/15/85 - 12/16/85	H-3	Pumping (Multipad Test)
04/04/86 - 04/21/86	H-2	Pumping
01/12/87 - 02/17/87	WIPP-13	Pumping (Multipad Test)
06/01/87 - 06/01/89	C&SH	Grouted
07/23/87 - 08/12/87	H-2	Pumping (Water Qual.Samp)
08/07/87 - 08/24/87	H-3	Pumping (Water Qual.Samp)
11/01/87 - 06/01/89	WHS	Grouted
01/01/88 - 11/01/88	AIS	Construction
05/05/88 - 07/07/88	H-11	Pumping (Multipad Test)
11/01/88 - 06/01/89	AIS	Steel Liner Emplaced
02/13/89 - 03/02/89	H-3	Pumping (Water Qual.Samp)
02/14/89 - 02/17/89	P-14	Pumping

Drawn by	Date	<b>Hydrogeologic Tests and Shaft Events Used in the Transient Simulations</b>
Checked by	Date	
Revisions	Date	
<b>INTERA Technologies</b>		Table 5.1



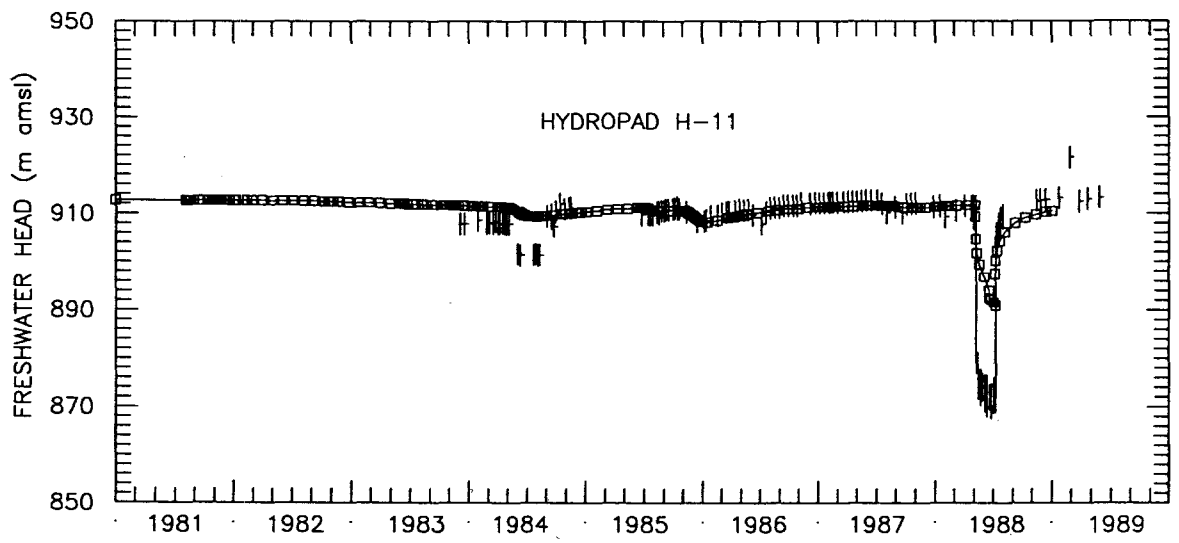
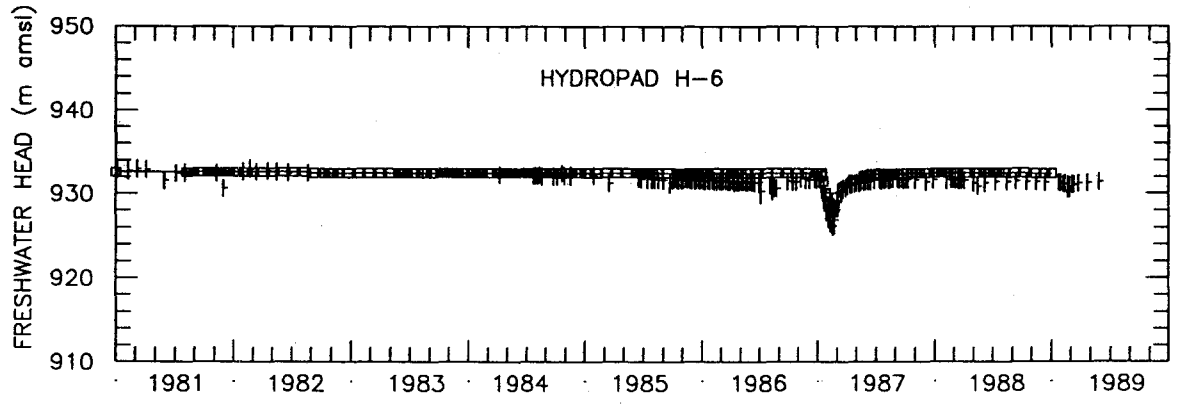
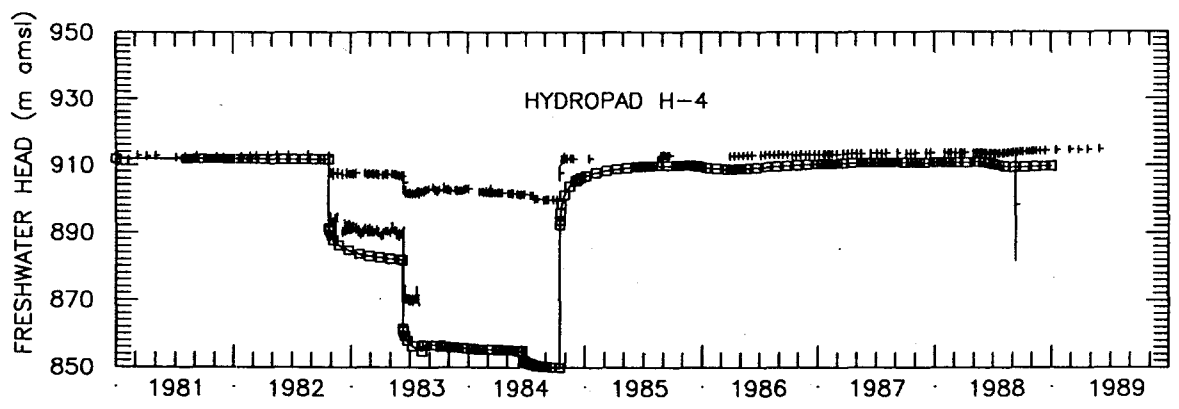
LEGEND:  $\square$ — $\square$  Calculated Freshwater Heads  
 | Observed Freshwater Heads

Drawn by	M.L.	Date	10/30/89
Checked by	ABW	Date	10/31/89
Revisions		Date	
H09700R869		10/31/89	

Calculated and Observed Transient Freshwater Heads at H-1, H-2, and H-3 Using the Steady-State Calibrated Transmissivity Field

**INTERA** Technologies

Figure 5.1a



LEGEND: □—□ Calculated Freshwater Heads  
 † Observed Freshwater Heads

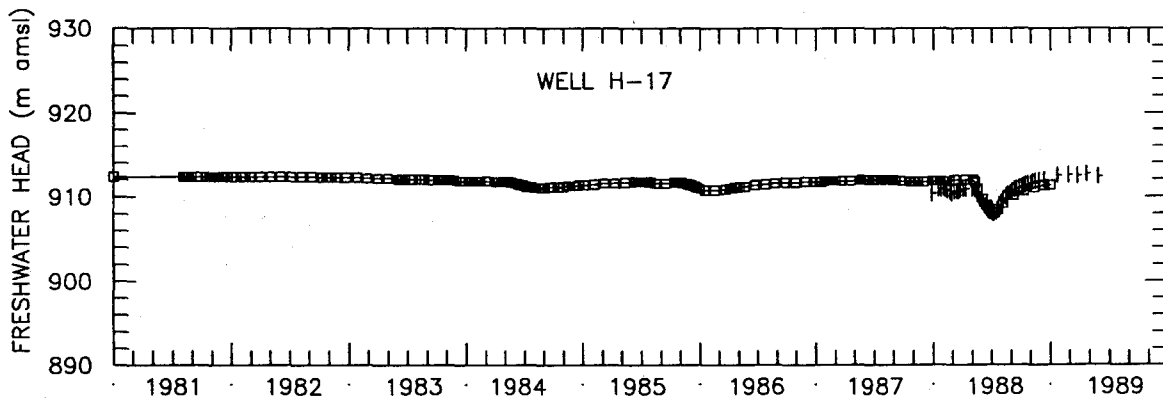
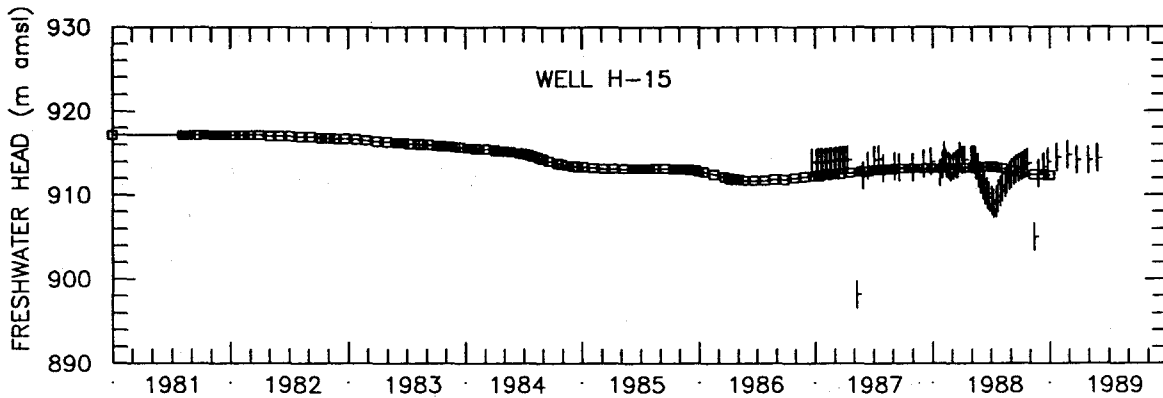
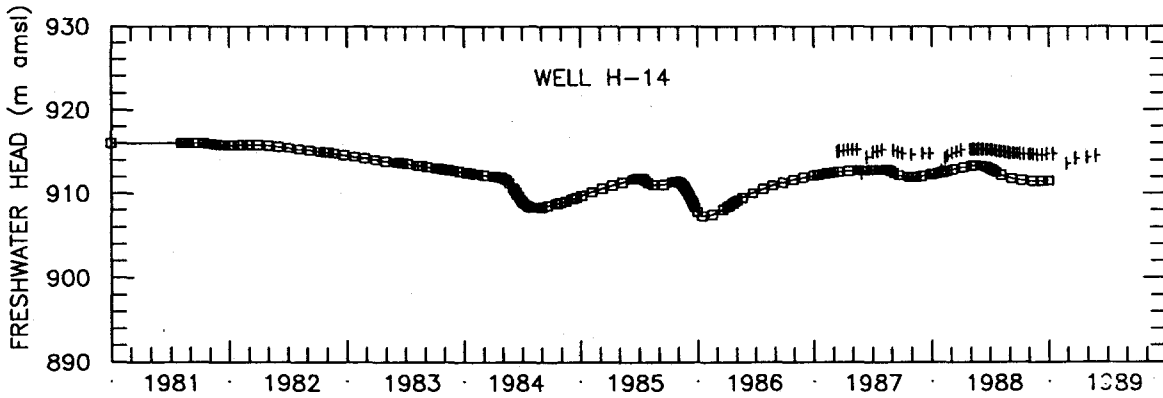
Drawn by	ABW	Date	10/30/89
Checked by	M.L.	Date	10/31/89
Revisions		Date	
H09700R869		10/31/89	

Calculated and Observed Transient Freshwater Heads at H-4, H-6, and H-11 Using the Steady-State Calibrated Transmissivity Field

**INTERA** Technologies

Figure 5.1b





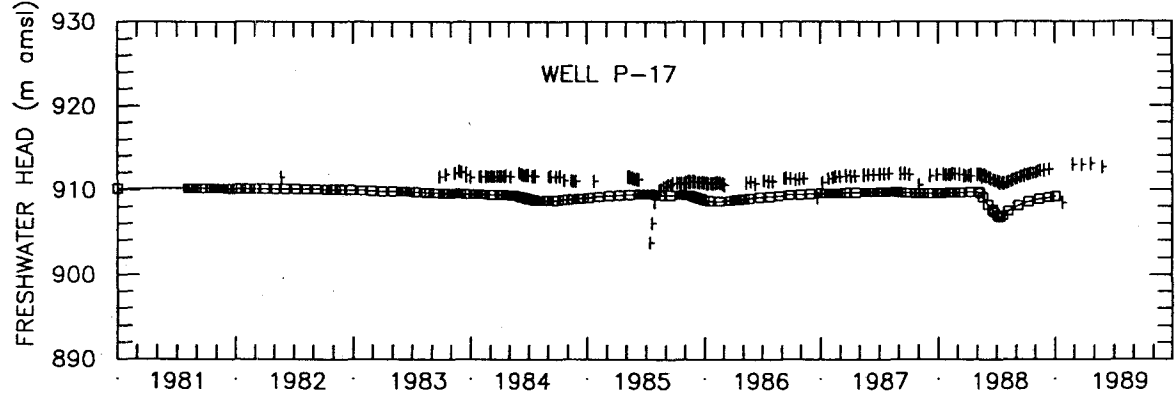
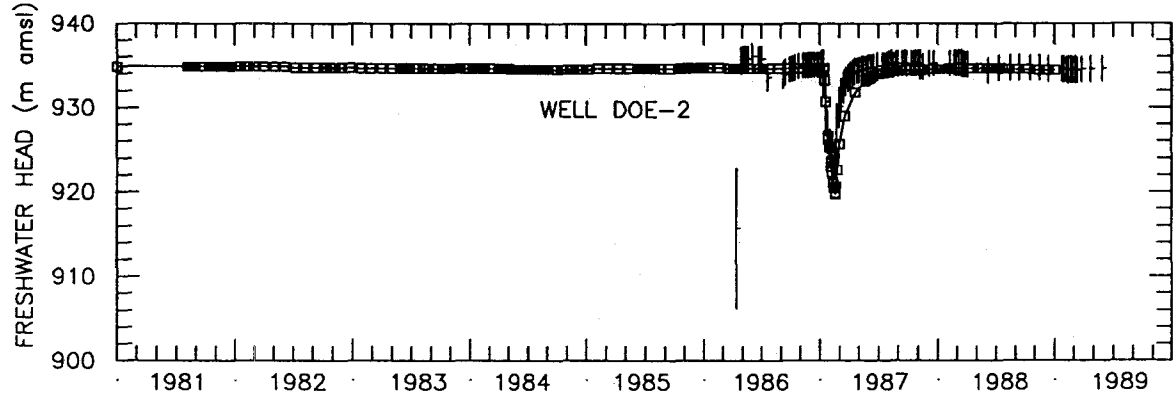
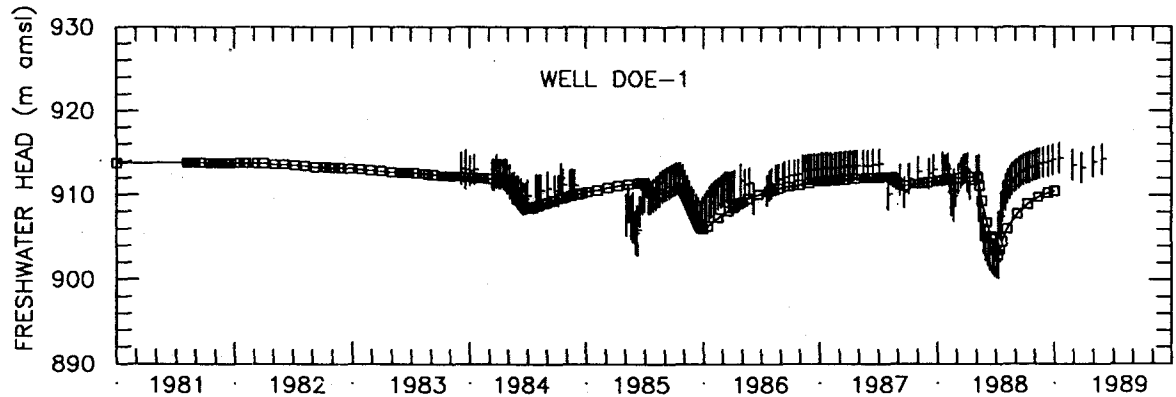
LEGEND:  $\square$ - $\square$  Calculated Freshwater Heads  
 | Observed Freshwater Heads

Drawn by ABW	Date 10/30/89
Checked by M.L.	Date 10/31/89
Revisions	Date
H09700R869	10/31/89

Calculated and Observed Transient Freshwater Heads  
 at H-14, H-15, and H-17 Using the Steady-State  
 Calibrated Transmissivity Field

**INTERA** Technologies

Figure 5.1c



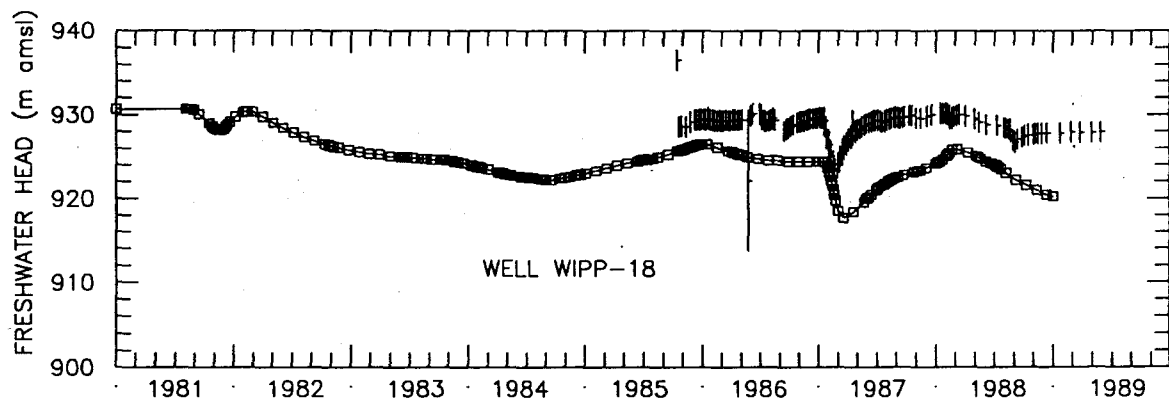
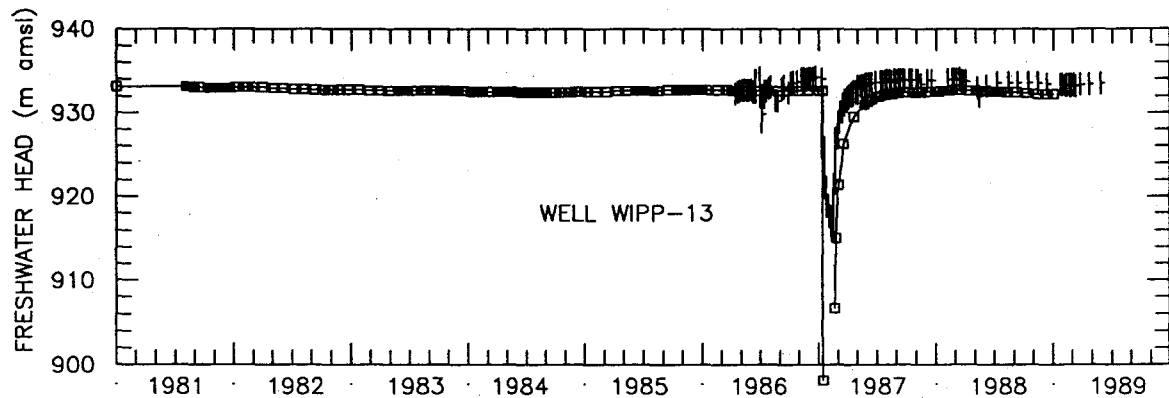
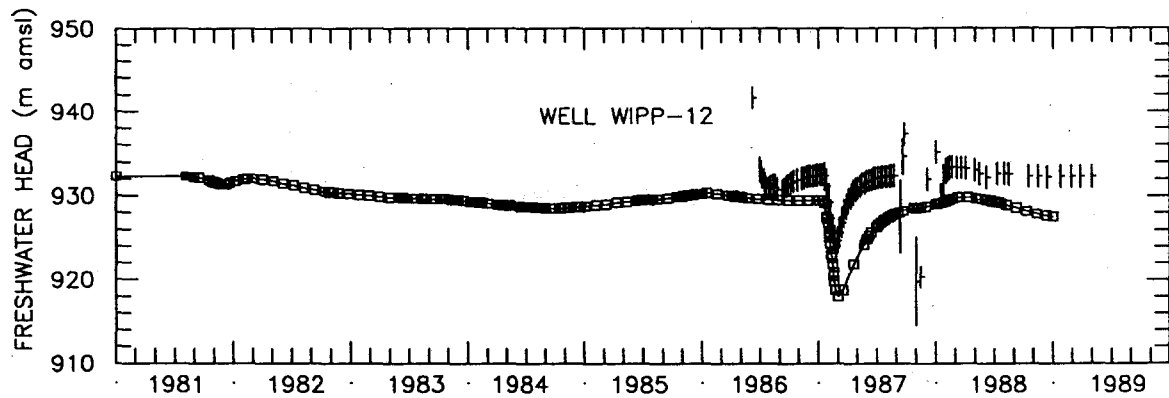
LEGEND: □—□ Calculated Freshwater Heads  
 | Observed Freshwater Heads

Drawn by ABW	Date 10/30/89
Checked by M.L.	Date 10/31/89
Revisions	Date
H09700R869	10/31/89

Calculated and Observed Transient Freshwater Heads at DOE-1, DOE-2, and P-17 Using the Steady-State Calibrated Transmissivity Field

**INTERA** Technologies

Figure 5.1d



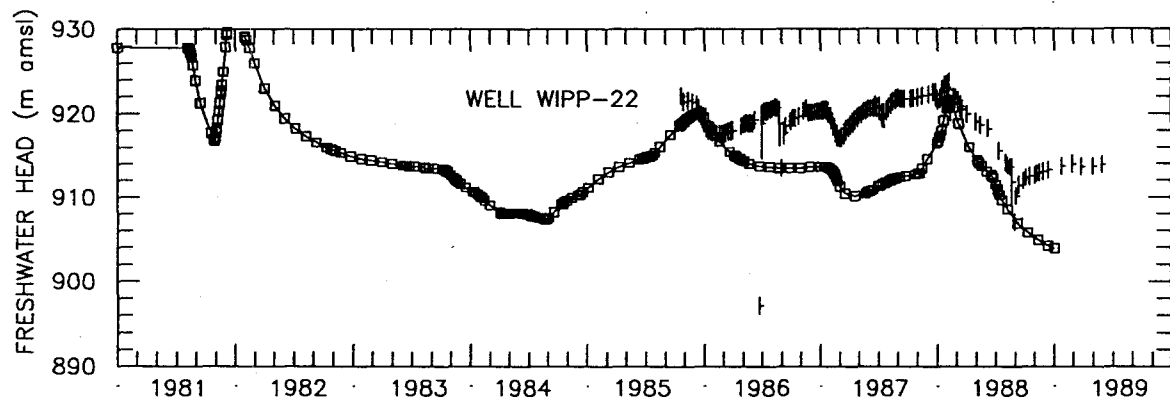
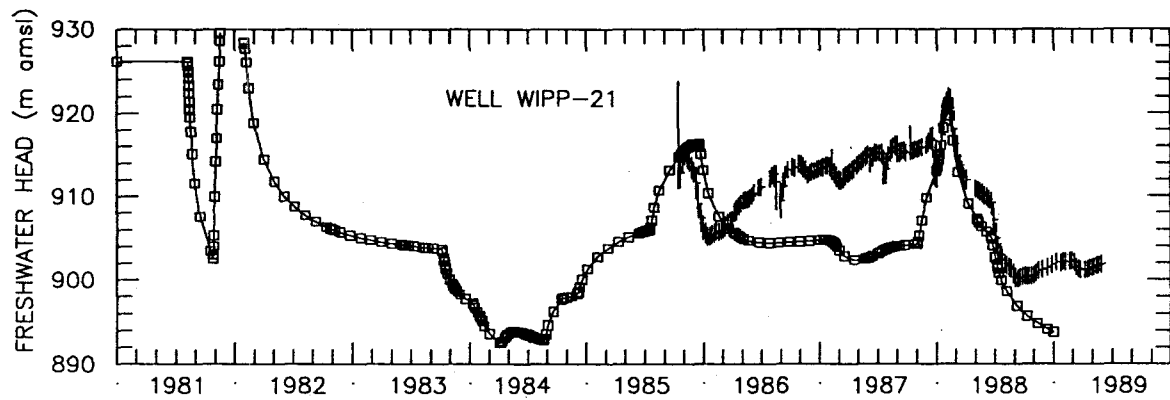
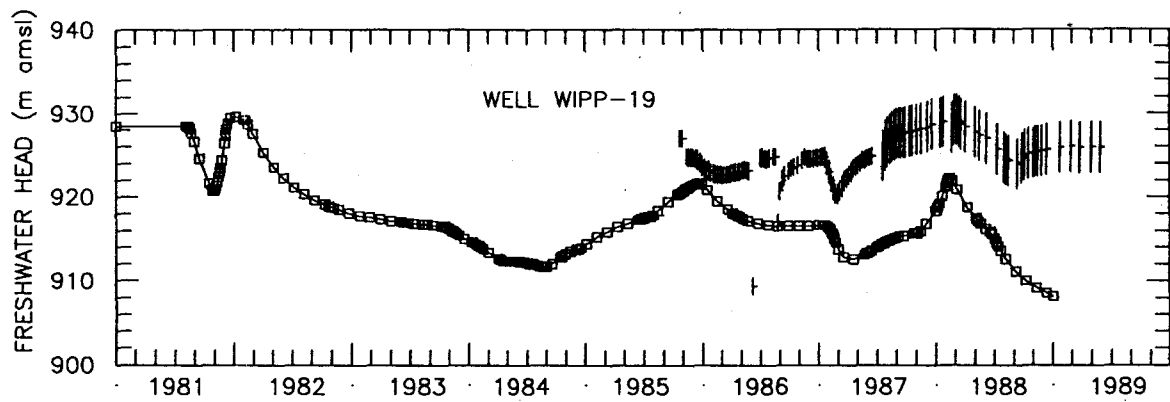
LEGEND: □—□ Calculated Freshwater Heads  
 † Observed Freshwater Heads

Drawn by ABW	Date 10/30/89
Checked by M.L.	Date 10/31/89
Revisions	Date
H09700R869	10/31/89

Calculated and Observed Transient Freshwater Heads at WIPP-12, WIPP-13, and WIPP-18 Using the Steady-State Calibrated Transmissivity Field

**INTERA** Technologies

Figure 5.1e



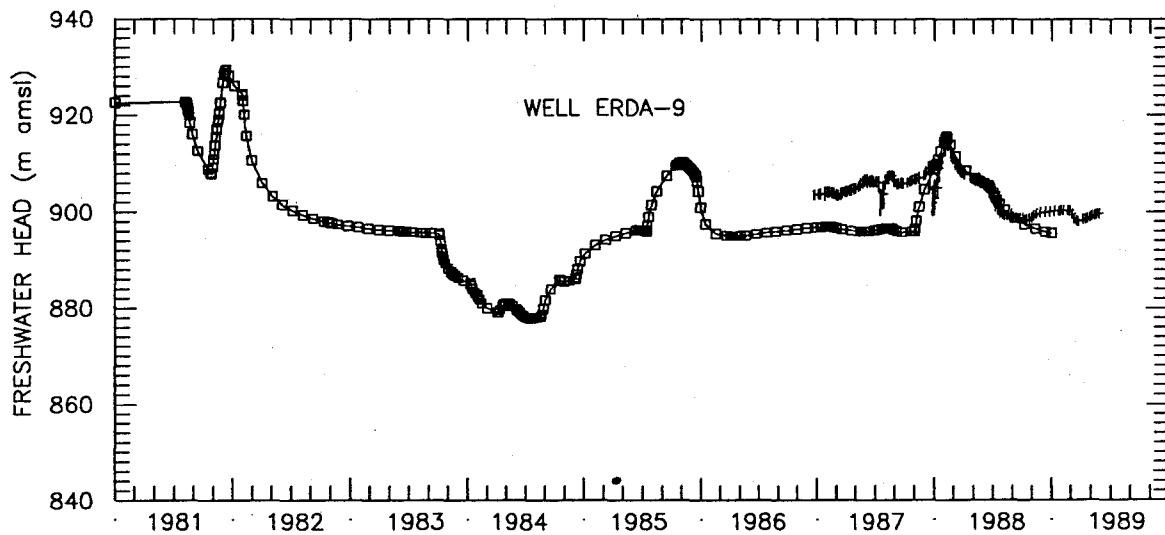
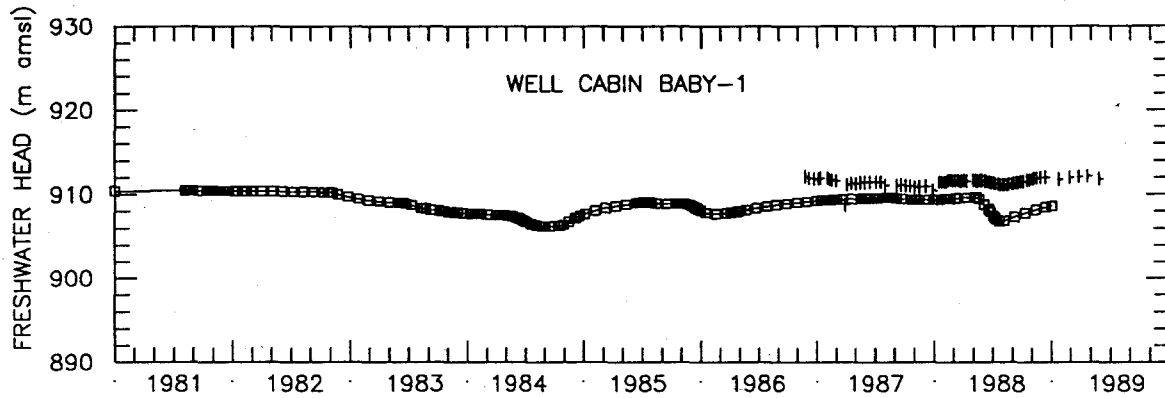
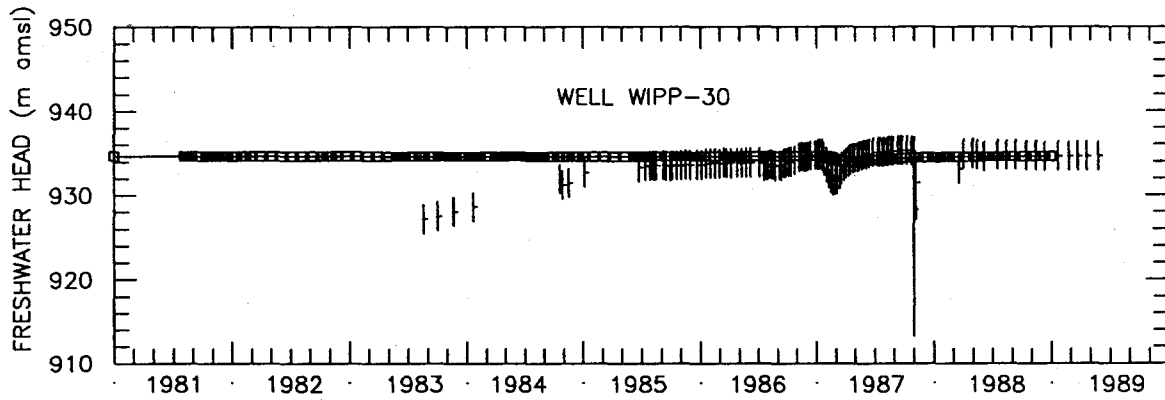
LEGEND:  $\square$  Calculated Freshwater Heads  
 | Observed Freshwater Heads

Drawn by ABW	Date 10/30/89
Checked by M.L.	Date 10/31/89
Revisions	Date
H09700R869	10/31/89

Calculated and Observed Transient Freshwater Heads  
 at WIPP-19, WIPP-21, and WIPP-22 Using the  
 Steady-State Calibrated Transmissivity Field

**INTERA** Technologies

Figure 5.1f



LEGEND: □-□ Calculated Freshwater Heads  
 | Observed Freshwater Heads

Drawn by ABW	Date 10/30/89
Checked by M.L.	Date 10/31/89
Revisions	Date
H09700R869	10/31/89

Calculated and Observed Transient Freshwater Heads  
 at WIPP-30, CB-1, and ERDA-9 Using  
 the Steady-State Calibrated Transmissivity Field

**INTERA** Technologies

Figure 5.1g

The calculated leakage rates for the four shafts are illustrated in Figures 5.2a and 5.2b. The rates illustrated in these figures were calculated by SWIFT II using the pressure-controlled mode. (As discussed in Section 4.1, a combination of specified pressures and specified rates were used to simulate the shafts' inflows. However, this approach was not finalized until after the initial transient simulation and, therefore, only the calculated rates of the pressure-controlled mode are shown in Figures 5.2a and 5.2b.) The measured leakage rates are shown as asterisks on these figures. The calculated rates at the exhaust shaft (EXS) agree well with the measured leakage rates. The calculated leakage at the waste-handling shaft (WHS) and air-intake shaft (AIS) need to be reduced by a factor of two, while the construction and salt handling (C&SH) shaft leakage needs to be increased in order to match the measured leakage.

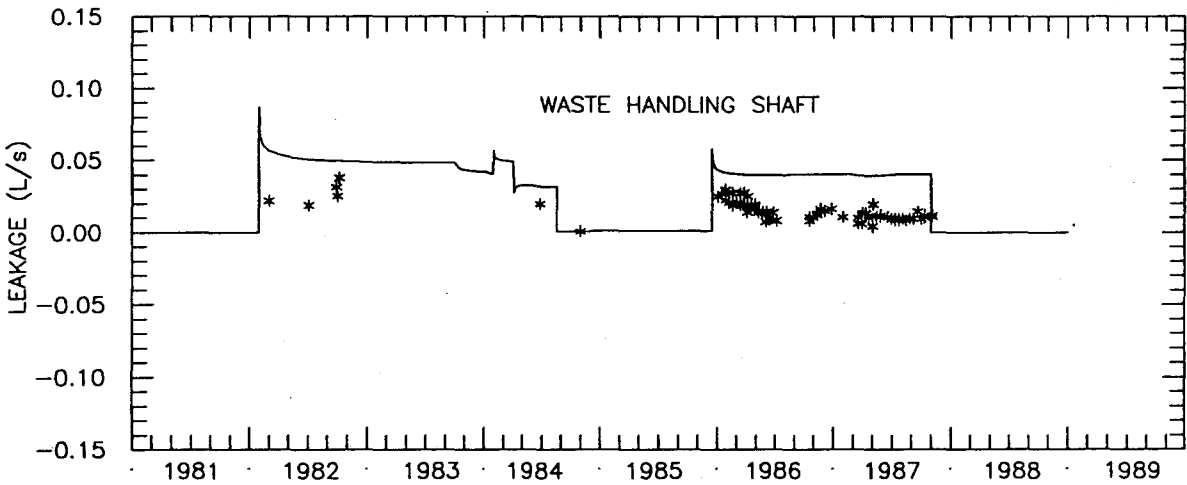
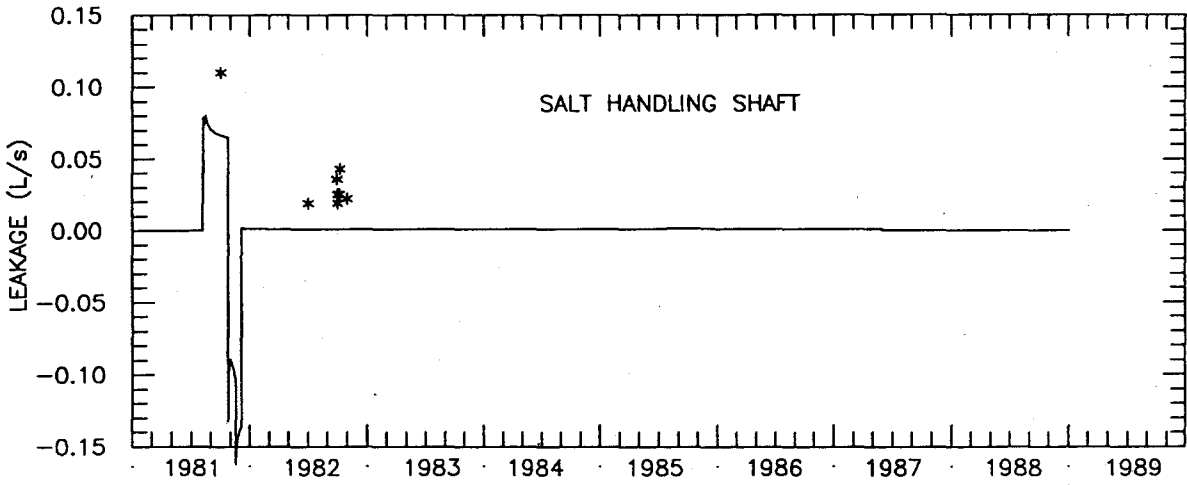
The total simulated time during transient calibration (presented in Sections 5.2.1 through 5.2.6) is slightly less than the total simulation time of the final transient simulation (presented in Sections 5.2.7 through 5.2.8). This is due to the addition of several events later in the calibration process which were not initially incorporated into the model (i.e., the WQSP pumping of H-3 in 1989, the WQSP pumping of WIPP-19 in 1988, and the P-14 pumping test).

## 5.2 Calibration to Transient Events

### 5.2.1 General Approach

Transient calibration requires an iterative procedure which includes changing local transmissivities to improve the calculated transient results while maintaining the calibrated steady-state fit to the observed heads. GRASP II was used during transient calibration to guide the location of additional pilot points needed to reduce the differences between the calculated and observed transient heads.

Before a transient performance measure may be calculated, the hydrographs at each borehole (Cauffman et al., 1990) must be reduced to a set of head values defined at each time step of the SWIFT II transient simulation. This reduction of the hydrographs permits the calculation of a transient performance measure from



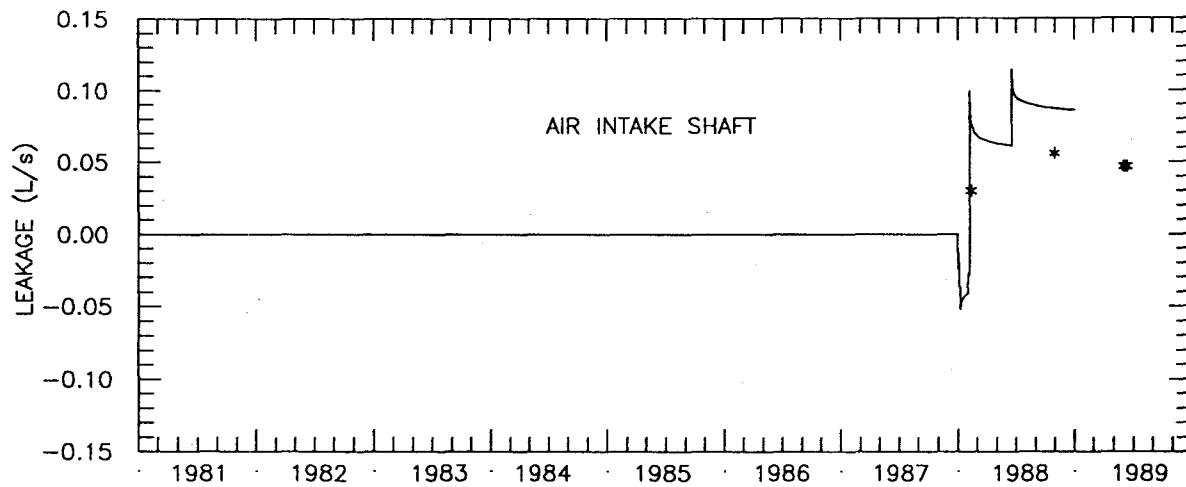
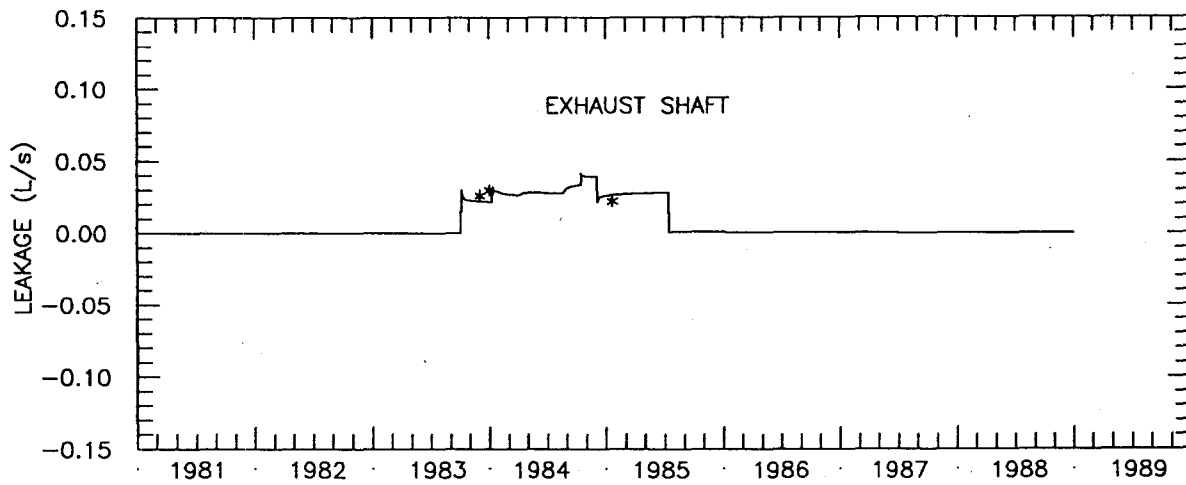
LEGEND: — Calculated Leakage Rate  
 \* Measured Leakage Rate

Drawn by ABW	Date 10/30/89
Checked by M.L.	Date 10/31/89
Revisions	Date
H09700R869	10/31/89

Calculated and Observed Leakage Rates at the C&SH and WHS Locations Used in the Initial Transient Simulation

**INTERA** Technologies

Figure 5.2a



LEGEND: — Calculated Leakage Rate  
 \* Measured Leakage Rate

Drawn by	ABW	Date	10/30/89
Checked by	M.L.	Date	10/31/89
Revisions		Date	
H09700R869		10/31/89	

Calculated and Observed Leakage Rates at the EXS and AIS Locations Used in the Initial Transient Simulation

**INTERA** Technologies

Figure 5.2b



the calculated and observed head differences at each time step of the simulation for selected boreholes. A pre-processor, PONS, was used for the reduction of the hydrographs. The head values which constitute each borehole's hydrograph and the time steps of the SWIFT II simulation are input to PONS which then averages all of the observed head values within each time step. If a borehole does not have any observed head values over a given period of time, PONS does not assign any value to that borehole for the time steps covering that period.

Performance measures defined during the transient calibration are similar to those used during the steady-state calibration. The main difference stems from the selection of a time window over which the differences between the observed and calculated heads are determined. The equation used to calculate the transient performance measure, which is defined as the sum of the squared differences between calculated and observed pressures (NOTE: GRASP II computes the performance measure using pressures at grid-block elevation while the adequacy of the calibration of the model is discussed using freshwater head differences), at selected wells over a selected time period is:

$$\sum_{t_1}^{t_2} \sum_{i=1}^N W_{i,t} (P_{i,t} - P_{ob_{i,t}})^2 \quad (5.1)$$

where

- $t_1$  = Beginning of the time window
- $t_2$  = End of the time window
- $N$  = Number of boreholes included in the performance measure
- $W$  = Weight assigned to selected boreholes for a given time,  $t$
- $P$  = Calculated pressure at grid-block elevation (Pa)
- $P_{ob}$  = Observed pressure at grid-block elevation (Pa)
- $i$  = Subscript designating borehole identifier

The time window is selected from and must coincide with the time steps used in the transient simulation. In addition to the selection of the time window, the locations or boreholes to be included in the difference calculation must also be specified. This allows for the selection of short transient events (e.g., water-

quality sampling) in which a response is only observed at a single location or long-term events (e.g., multipad pumping tests) in which responses are observed at several locations.

Depending on the length of the time window and whether a selected borehole has observed heads at each of the time steps during the time window, the number of differences used for the calculation of the transient performance measure could be much higher than the number used in determining the steady-state performance measure. This is because only one undisturbed head value at a borehole is used as a calibration target in the steady-state calibration whereas there are often many observed head values used as calibration targets in the transient calibration.

During transient calibration, it is often necessary to improve the fit between calculated and observed responses to transient events without degrading the fit to steady-state or undisturbed heads. GRASP II allows one to couple steady-state and transient performance measures in order to improve the transient fit while minimizing the effect upon the steady-state results. This requires that the contribution from both the steady-state and transient differences to the coupled performance measure be approximately equal. Since transient performance measures are generally several orders of magnitude greater than the steady-state performance measures (because values are calculated for each time step in the time window), weights may be used (Equations (3.1) and (5.1)) to insure the contribution from the steady-state differences to the coupled performance measure is approximately equal to the contribution from the transient differences.

Similar to steady-state model calibration, transient calibration is performed on a step-by-step basis in which the transient performance measure is constantly changing due to changes in the head differences, the selection of a different set of boreholes for inclusion in the performance-measure calculation, or the definition of a new time window.

The following sections present the calibration of the model to the major transient events conducted at the WIPP site. The transient events were considered in the following order during transient model calibration:

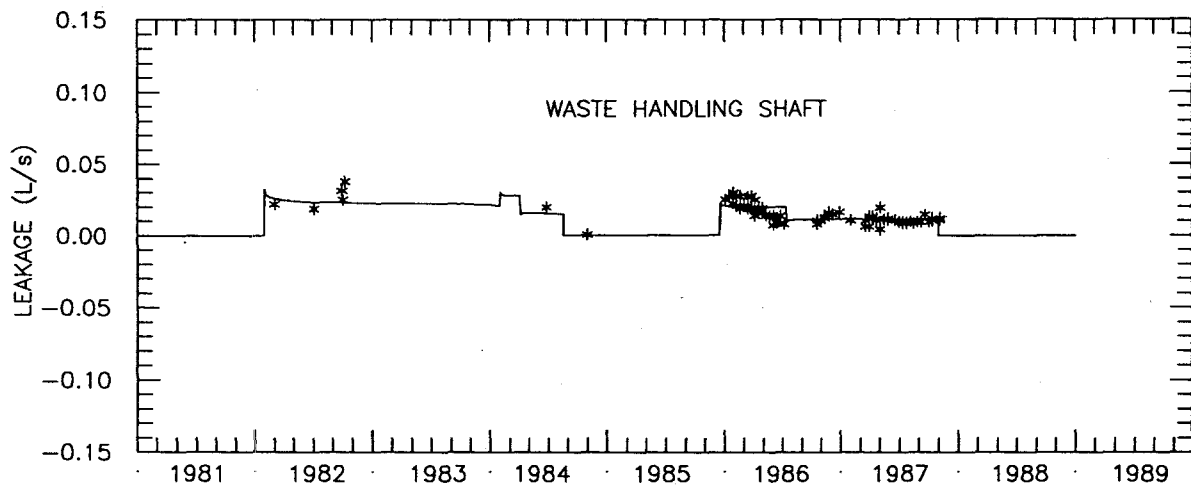
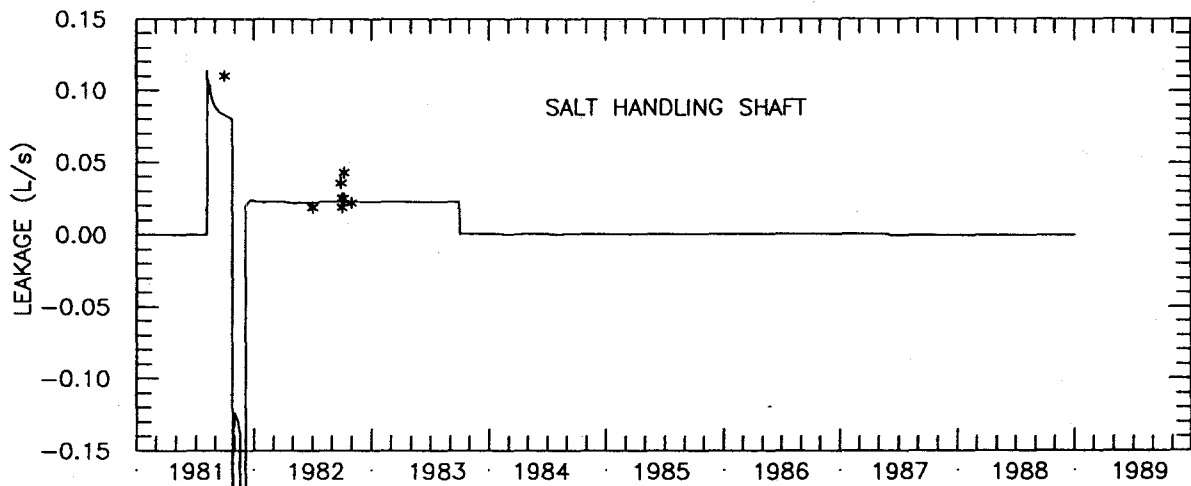
- Responses to the early shaft events
- Responses to the H-4 tracer test, the H-3, H-11, and WIPP-13 multipad pumping tests, and the P-14 pumping test
- Responses to excavation of the air-intake shaft
- Responses to the WIPP-19 WQSP pumping.

The travel times presented in Section 3.3.7 were then recalculated using the transient calibrated transmissivity field and are discussed in Section 5.5.

#### 5.2.2 Calibration to Shaft Leakage Rates

The first step in calibrating the model to the transient events focused on reproducing the measured leakage rates at the shafts. To improve the agreement between the measured and calculated leakage at each of the shafts, the well index initially assigned to each shaft was modified and rates were directly specified in the model for times after a shaft was completed (i.e., lined and grouted). The changes to the well indices were needed to reduce the differences between the calculated inflow and the observed inflow during the specified-pressure time periods (Section 4.1), which implies that the initial estimates of the skin transmissivities used in the calculation of the well indices were not representative of the properties of the local region surrounding the shafts.

Figures 5.3a and 5.3b illustrate the final calibration run to the observed leakage rates. The agreement between the observed and calculated values is much better than in the initial simulation. The well indices assigned to the C&SH shaft were raised to increase the leakage in late 1981 (Table 5.2). A rate of 0.032 L/s was specified from December 1981 (after lining and grouting) until October 1983 based on the measurements taken during that time period (Figure 5.3a). After October 1983, the leakage was reduced to 0.005 L/s based on an inspection conducted in November 1983 which found that several capped drainage pipes produced small amounts of accumulated water after being closed for several weeks



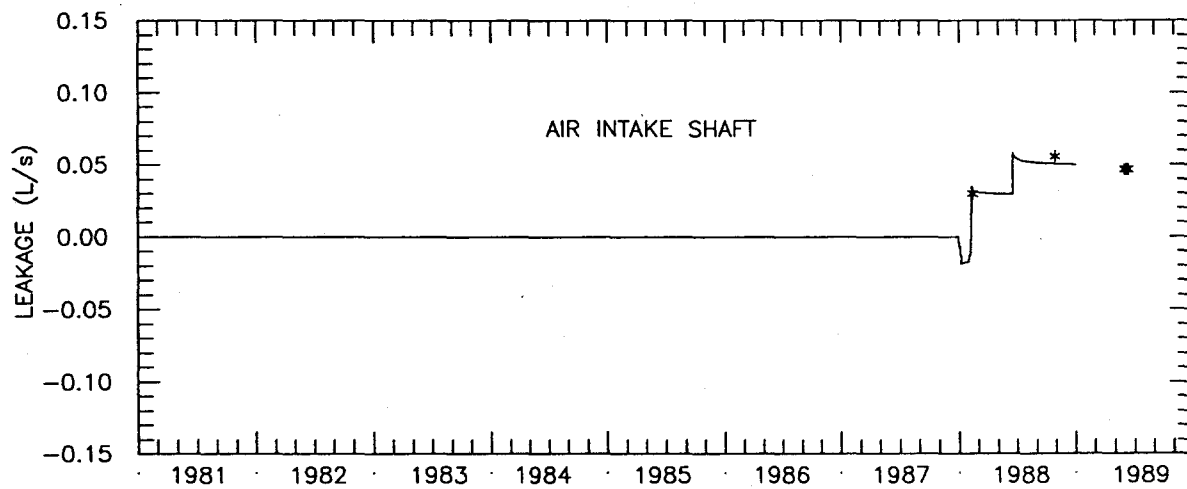
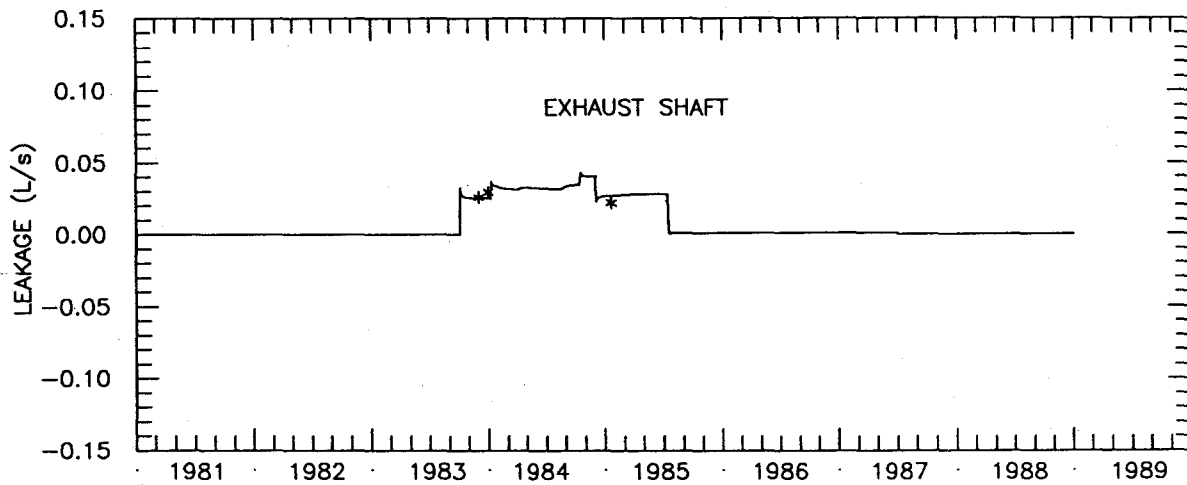
LEGEND: — Calculated Leakage Rate  
 \* Measured Leakage Rate

Drawn by	ABW	Date	10/30/89
Checked by	M.L.	Date	10/31/89
Revisions		Date	
H09700R869		10/31/89	

Calculated and Observed Leakage Rates at the  
 C&SH and WHS Locations After  
 Calibrating to Observed Leakage

**INTERA** Technologies

Figure 5.3a



LEGEND: — Calculated Leakage Rate  
 \* Measured Leakage Rate

Drawn by	ABW	Date	10/30/89
Checked by	M.L.	Date	10/31/89
Revisions		Date	
H09700R869		10/31/89	

Calculated and Observed Leakage Rates at the  
 EXS and AIS Locations After  
 Calibrating to Observed Leakage

**INTERA** Technologies

Figure 5.3b

<u>Shaft</u>	<u>Well Index (m<sup>2</sup>/s)</u>	<u>Time Period</u>
C&SH	2.2x10 <sup>-6</sup>	08/07/81 - 12/06/81
	5.5x10 <sup>-7</sup>	12/06/81 - 10/01/83
	1.0x10 <sup>-8</sup>	10/01/83 - 06/01/87
	1.0x10 <sup>-15</sup>	06/01/87 - 06/01/89
WHS	3.5x10 <sup>-7</sup>	01/30/82 - 02/01/84
	5.3x10 <sup>-7</sup>	02/01/84 - 04/05/84
	2.7x10 <sup>-7</sup>	04/05/84 - 08/20/84
	1.5x10 <sup>-8</sup>	08/20/84 - 12/16/85
	2.7x10 <sup>-7</sup>	12/16/85 - 07/15/86
	1.3x10 <sup>-7</sup>	07/15/86 - 11/01/87
	1.0x10 <sup>-15</sup>	11/01/87 - 06/01/89
EXS	4.7x10 <sup>-7</sup>	10/05/83 - 01/10/84
	7.4x10 <sup>-7</sup>	01/10/84 - 10/15/84
	9.5x10 <sup>-7</sup>	10/15/84 - 12/04/84
	4.8x10 <sup>-7</sup>	12/04/84 - 07/15/85
	9.5x10 <sup>-9</sup>	07/15/85 - 06/01/89
AIS	3.4x10 <sup>-7</sup>	01/01/88 - 01/08/88
	3.6x10 <sup>-7</sup>	01/08/88 - 02/02/88
	7.6x10 <sup>-7</sup>	02/02/88 - 06/01/89

Drawn by	Date
Checked by	Date
Revisions	Date

Calibrated Well Indices to Shaft Leakage

**INTERA** Technologies

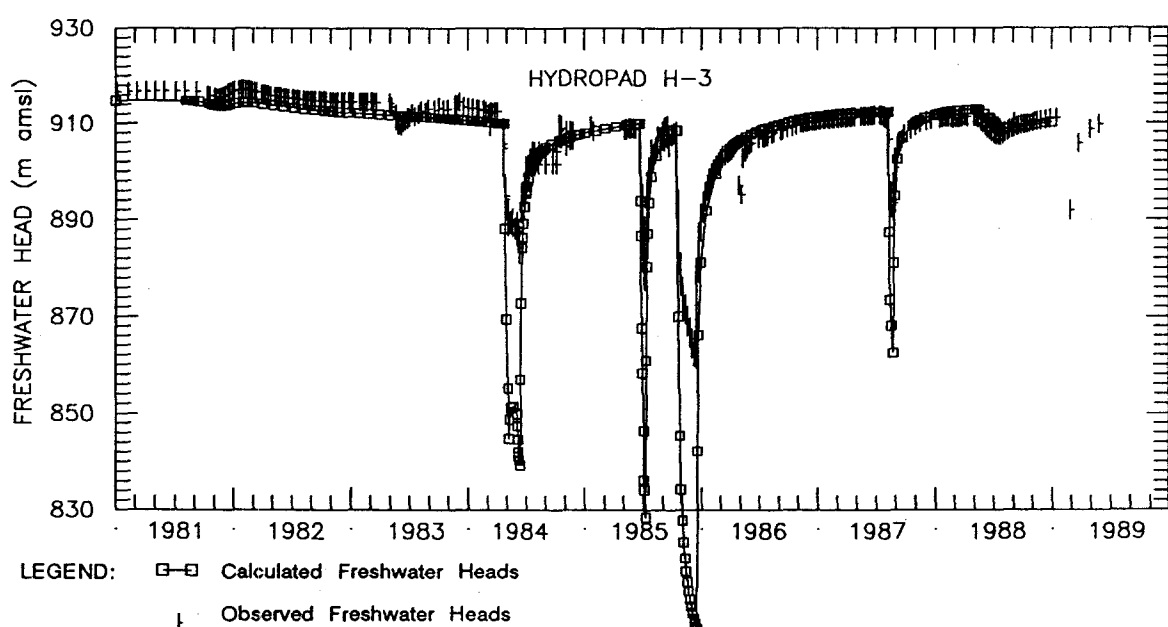
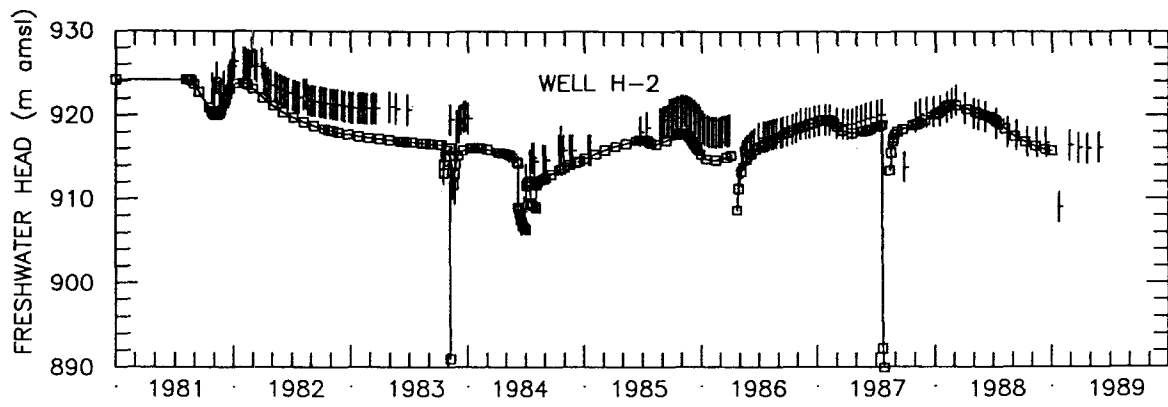
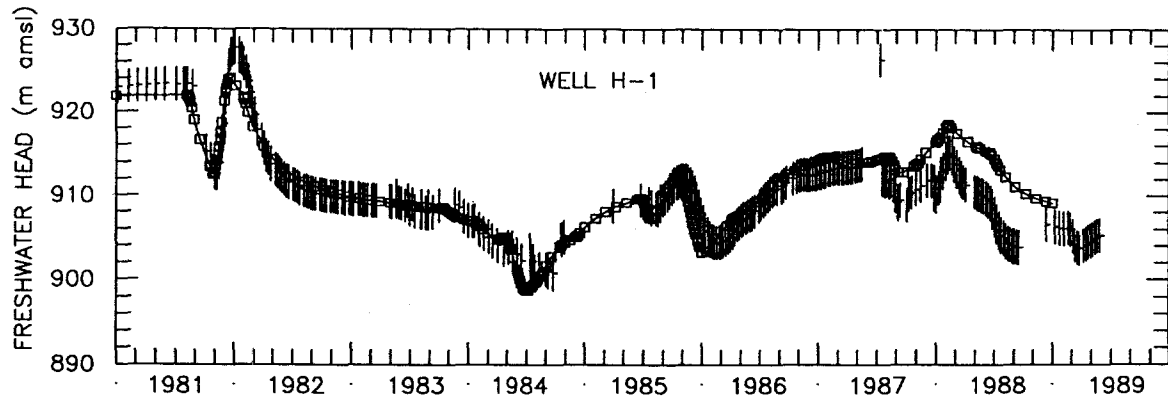
Table 5.2

(M. Gonzales, Sandia National Laboratories, personal communication, 1989). In June 1987, the leakage was effectively set to zero due to extensive reconditioning of the shaft during this time.

Calculated leakage rates in the initial simulation at the WHS were a factor of two too high. The modified well indices assigned to the WHS reduced the leakage such that the agreement between the calculated and observed values before shaft completion is very good (Figure 5.3a). A series of specified rates were used after shaft completion to represent the measured rates in the model. In August 1984, the WHS was grouted and a leakage measurement of  $9.4 \times 10^{-4}$  L/s was made in October 1984 (U.S. Department of Energy, 1986). This value was used in the model from August 1984 to January 1986. A series of measurements made from 1986 through 1987 provided enough information to specify two rates to represent this time period. A rate of 0.022 L/s was used from January to July, 1986 based on the measured data, after which time a lower rate of 0.015 L/s was used until November 1987. After November 1987, leakage at the WHS was effectively set to zero because a major grouting program performed during November is assumed to have ended the leakage.

A factor of three reduction in the skin transmissivity was used at the AIS (Table 5.2) to reduce the initial leakage rates which were a factor of two higher than the observed rates (Figure 5.2b). The lower well indices reduced the differences between the observed and calculated leakage rates at this location (Figure 5.3b).

The effects of calibrating to the observed leakage rates is evident from examination of the calculated responses for the surrounding boreholes. The differences between the calculated and observed transient heads at H-1 and H-2 were improved by matching the measured shaft leakage rates (Figure 5.4a). The magnitudes of the calculated drawdowns at WIPP-19, WIPP-21, and WIPP-22 (Figure 5.4b) were much closer to the observed than the initial simulation drawdowns. However, there is still some improvement necessary at these boreholes, as discussed in subsequent sections.



LEGEND:  $\square$  Calculated Freshwater Heads  
 | Observed Freshwater Heads

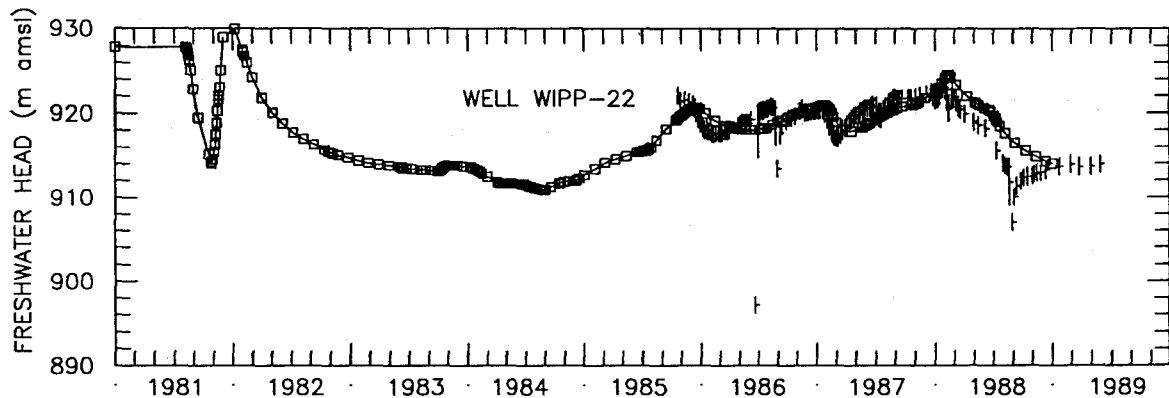
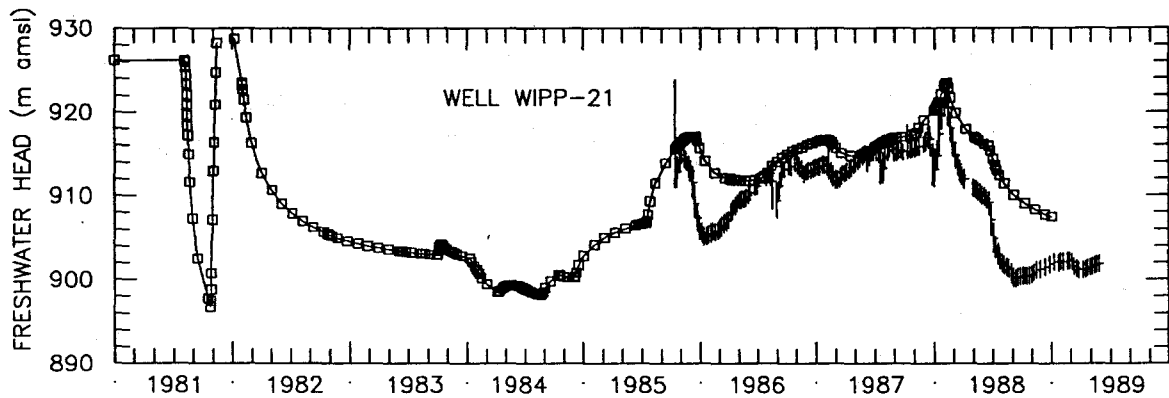
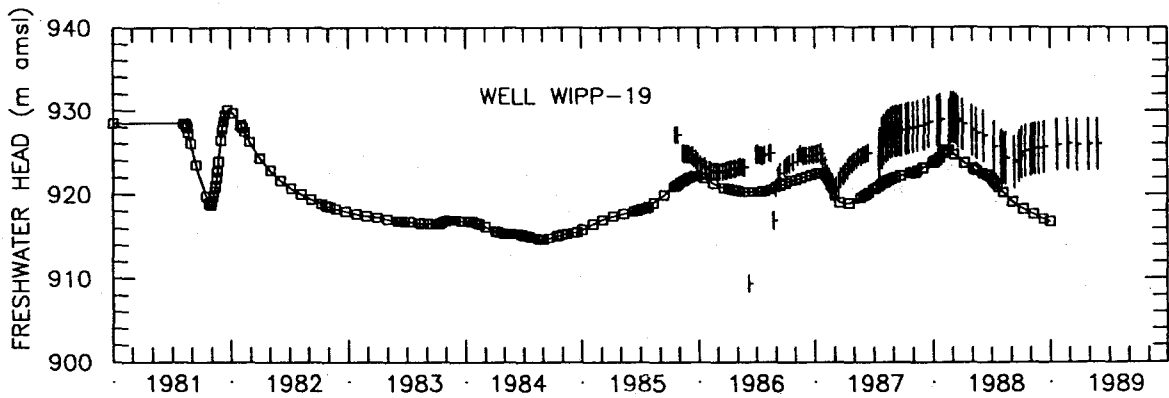
Drawn by	ABW	Date	10/30/89
Checked by	M.L.	Date	10/31/89
Revisions		Date	
H09700R869		10/31/89	

Calculated and Observed Transient Freshwater Heads at H-1, H-2, and H-3 After Calibrating to Observed Shaft Leakage

**INTERA** Technologies

Figure 5.4 a





LEGEND: □-□ Calculated Freshwater Heads  
 † Observed Freshwater Heads

Drawn by	ABW	Date	10/30/89
Checked by	M.L.	Date	10/31/89
Revisions		Date	
H09700R869		10/31/89	

Calculated and Observed Transient Freshwater Heads at WIPP-19, WIPP-21, and WIPP-22 After Calibrating to Observed Shaft Leakage

**INTERA** Technologies

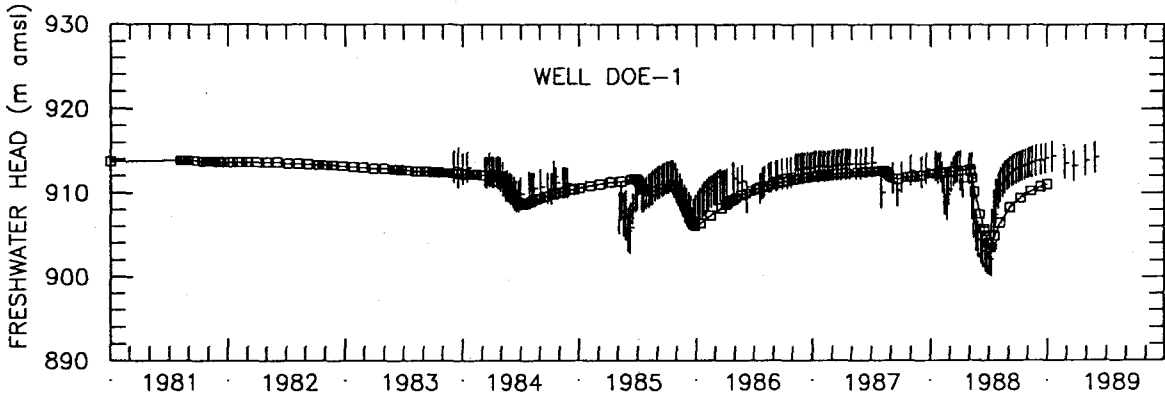
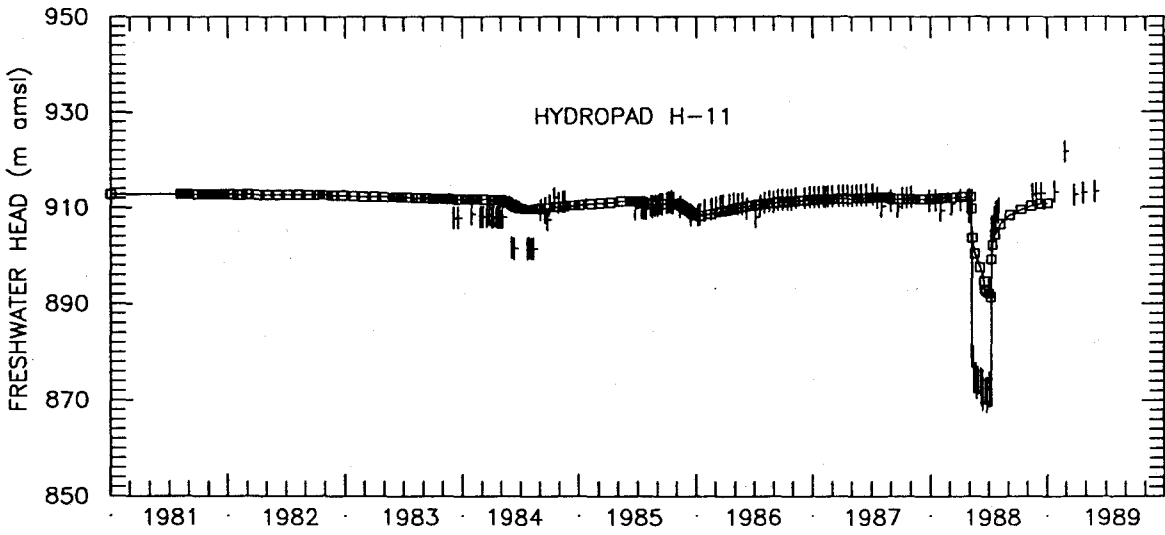
Figure 5.4b

### 5.2.3 Calibration to the Well Tests at the H-3 Hydropad

The well tests conducted at the H-3 hydropad from 1984 through 1989 are discussed in Section 4.2.2. The calculated and observed transient responses at the H-1, H-2, and H-3 locations after model calibration to the shaft leakage rates are illustrated in Figure 5.4a. The calculated drawdowns at the H-3 hydropad during the well tests conducted during this time period are greater than two times the observed drawdowns. The observed data at H-1 and H-2 exhibit drawdown and recovery in response to the H-3 well tests. At these boreholes, the calculated drawdowns agree well with the observed drawdowns. The calculated recovery rate at H-2 is slower than the observed recovery.

Responses to the H-3 multipad pumping test conducted in late 1985 were observed at H-11 and DOE-1 (Figure 5.4c). The calculated drawdowns at DOE-1 and H-11 match the observed drawdowns quite well (NOTE: WQSP pumping at DOE-1 in April 1985 was not simulated). However, as in the responses at H-2 to H-3 testing, the calculated recoveries at both wells are slower than the observed recoveries.

The well index assigned to the H-3 borehole was initially adjusted in order to reduce the calculated drawdown at H-3. However, it was determined that the calculated drawdown at H-3 was insensitive to increases in the well index. Therefore, GRASP II was employed to locate the region in which changes to the transmissivity field would result in a decrease in the calculated drawdown. The steady-state head differences and the transient-head differences at H-3 were coupled in the calculation of the performance measure. The time window specified for fitting the H-3 drawdown extended from the beginning of 1984 to the end of 1986, which included all three of the major pumping events conducted at H-3. A pilot-point grid was superimposed over the central WIPP-site area. The GRASP II results identified a high-negative-sensitivity region just south of H-3 (Figure 5.5a). The transmissivities were increased by adding a pilot point in this area which reduced the differences between the calculated and observed drawdowns at H-3 considerably (Figure 5.5b) and did not significantly affect the steady-state head differences of the central model boreholes, with the exception of H-1. The change in transmissivity degraded the steady-state fit at H-1 from -1.0 to -2.4 m. However, the increase at the H-1 location was reduced during the calibration to the WIPP-13 multipad test (Section 5.2.5).



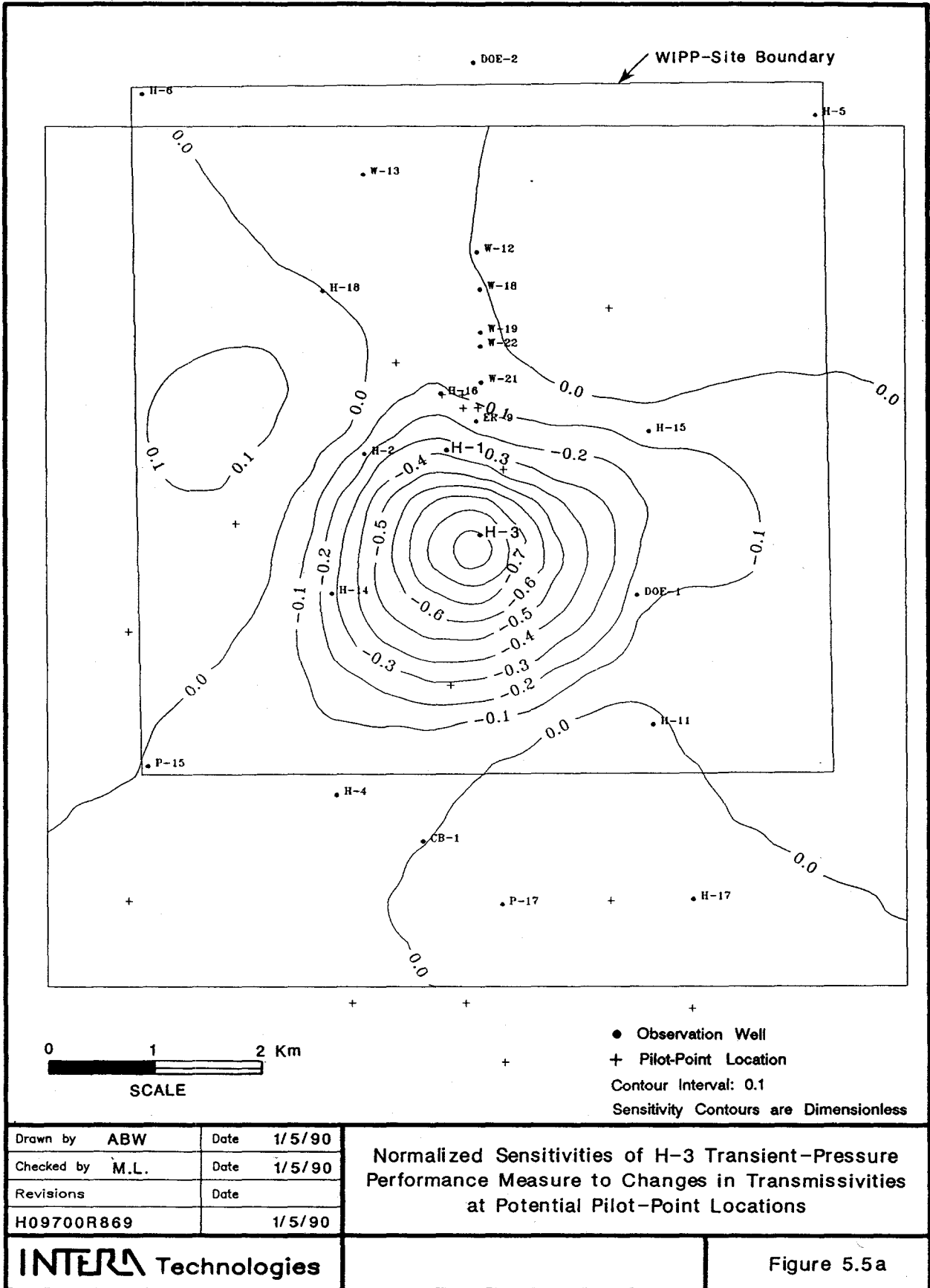
LEGEND:   
 □—□ Calculated Freshwater Heads   
 † Observed Freshwater Heads

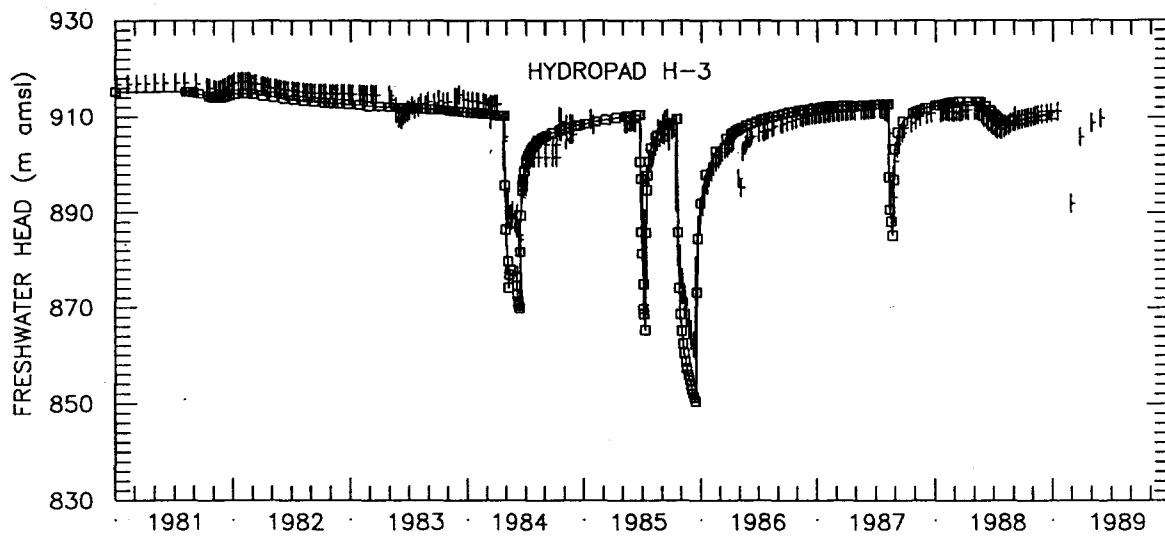
Drawn by	ABW	Date	10/30/89
Checked by	M.L.	Date	10/31/89
Revisions		Date	
H09700R869		10/31/89	

Calculated and Observed Transient Freshwater Heads at H-11 and DOE-1 After Calibrating to Observed Shaft Leakage

**INTERA** Technologies

Figure 5.4c





LEGEND: □—□ Calculated Freshwater Heads  
 +—+ Observed Freshwater Heads

Drawn by	ABW	Date	10/30/89
Checked by	M.L.	Date	10/31/89
Revisions		Date	
H09700R869		10/31/89	

Calculated and Observed Transient Freshwater Heads at H-3 After Calibrating to the H-3 Well Tests

**INTERA** Technologies

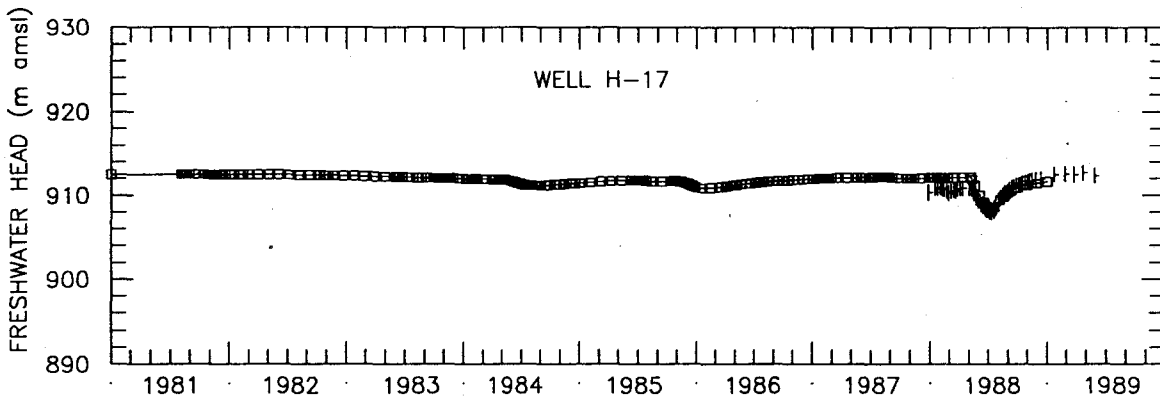
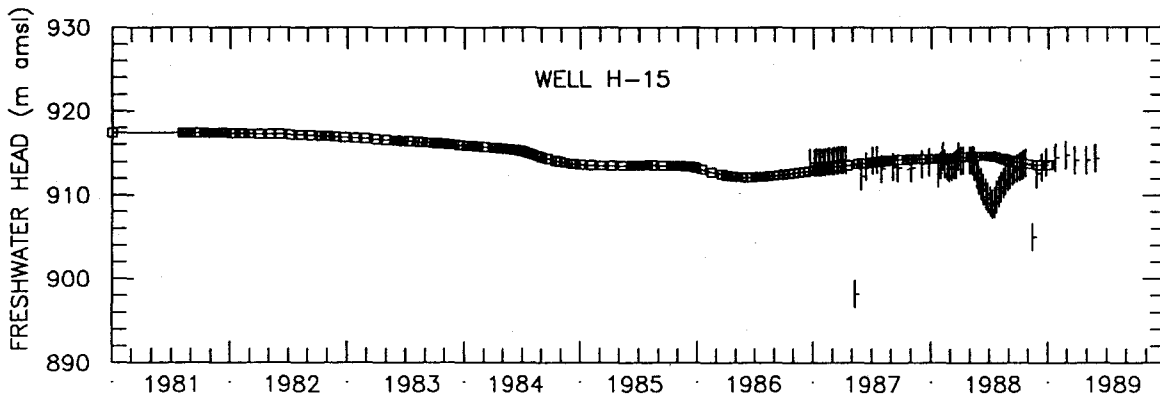
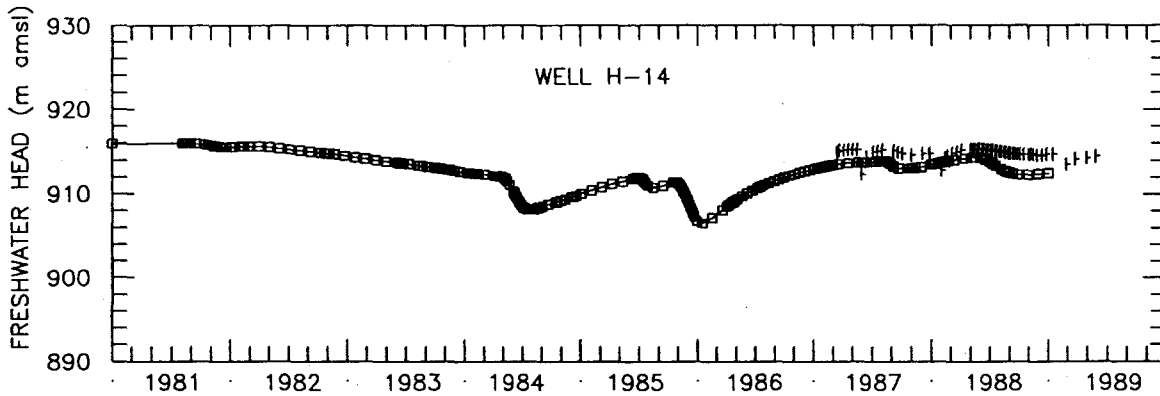
Figure 5.5b

#### 5.2.4 Calibration to the H-11 Multipad Pumping Test

The H-11 multipad pumping test conducted from May to July 1988 is described in Section 4.2.5. The calculated drawdown due to pumping at H-11 is shown in Figure 5.4c to be approximately one-half the observed drawdown at H-11. This implies that the transmissivity of the skin surrounding the H-11 borehole should be lower than the average grid-block transmissivity and that the well index must be decreased.

The calculated drawdowns at the surrounding boreholes which responded to H-11 pumping are illustrated in Figures 5.5b, 5.6a, and 5.6b. The relative magnitudes and timing of the calculated drawdowns compare well with the observed transient freshwater heads at the H-3, H-17, and DOE-1 locations. However, the calculated recoveries are slower than the observed recoveries at the DOE-1 and H-3 locations. Wells H-14, H-15, P-17, and CB-1 also responded to pumping at H-11. With the exception of H-15, the calculated drawdowns are generally greater than the observed drawdowns at these locations. For example, the maximum observed drawdowns at H-14 and P-17 are approximately 1 m. However, the calculated drawdowns at H-14 and P-17 are about 3 and 4 m, respectively. The observed drawdown at the H-15 borehole is approximately 6 m while the calculated drawdown is minimal. This implies that the transmissivities between H-11, H-14, and P-17 are probably too high and the transmissivities between H-11 and H-15 are probably too low.

After adjusting the H-11 well index to increase the drawdown at the H-11 hydropad, the responses at the observation wells did not significantly improve. Therefore, a pilot-point grid covering the central WIPP-site area was used in conjunction with GRASP II to determine the location(s) at which changes to the transmissivity field would improve the difference between the observed and calculated responses. The response at the H-15 borehole was chosen as the first calibration target. The performance measure consisted of the H-15 and DOE-1 transient head differences from the beginning of the H-11 pumping test in May 1988 to the beginning of 1989. GRASP II identified a high-negative-sensitivity region just south of H-15 (Figure 5.7) and a high-positive-sensitivity region



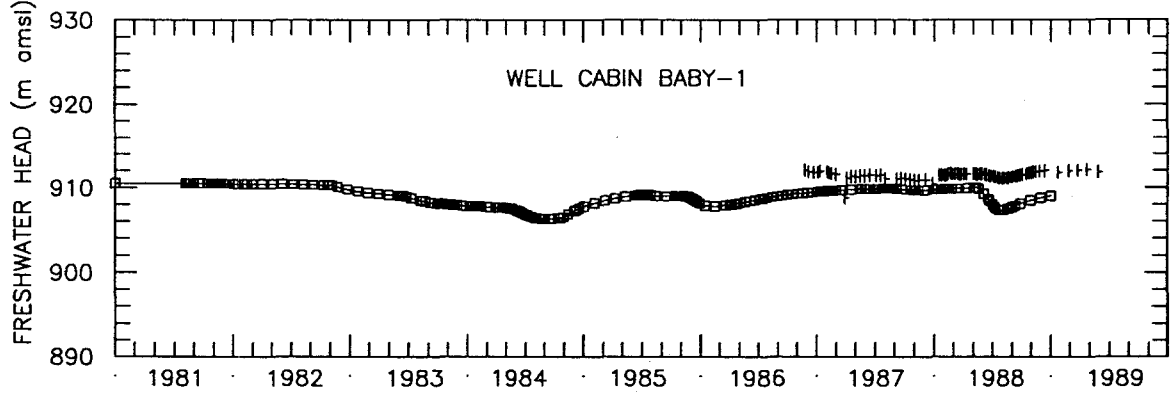
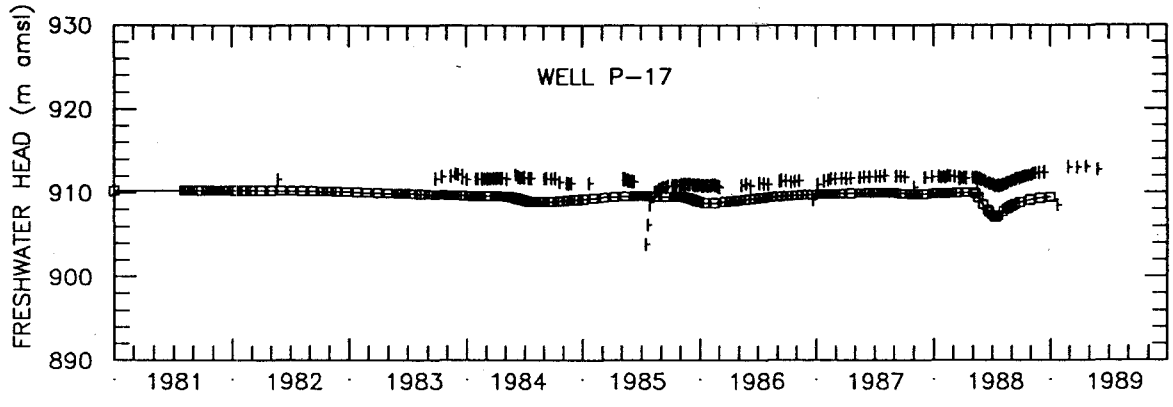
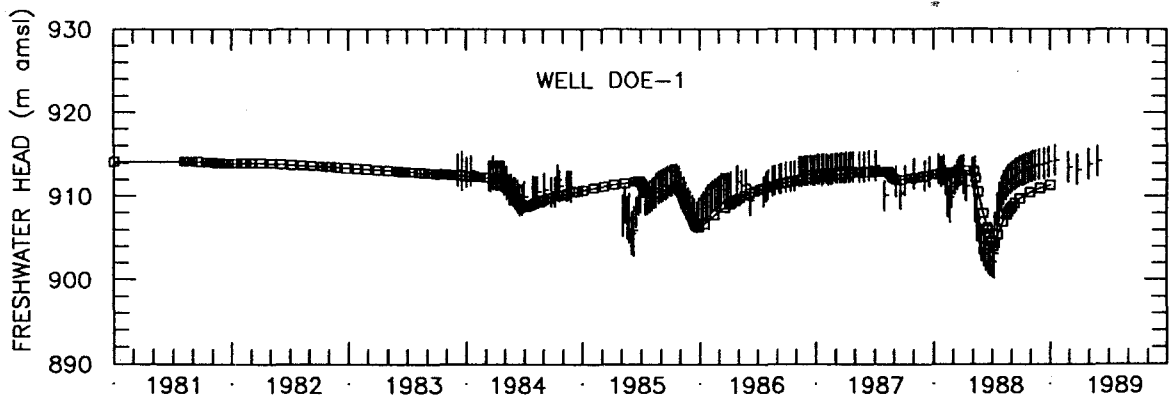
LEGEND: □—□ Calculated Freshwater Heads  
 † Observed Freshwater Heads

Drawn by ABW	Date 10/30/89
Checked by M.L.	Date 10/31/89
Revisions	Date
H09700R869	10/31/89

Calculated and Observed Transient Freshwater Heads at H-14, H-15, and H-17 After Calibrating to the H-3 Well Tests

**INTERA** Technologies

Figure 5.6a



LEGEND: □—□ Calculated Freshwater Heads  
 † Observed Freshwater Heads

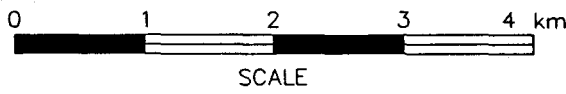
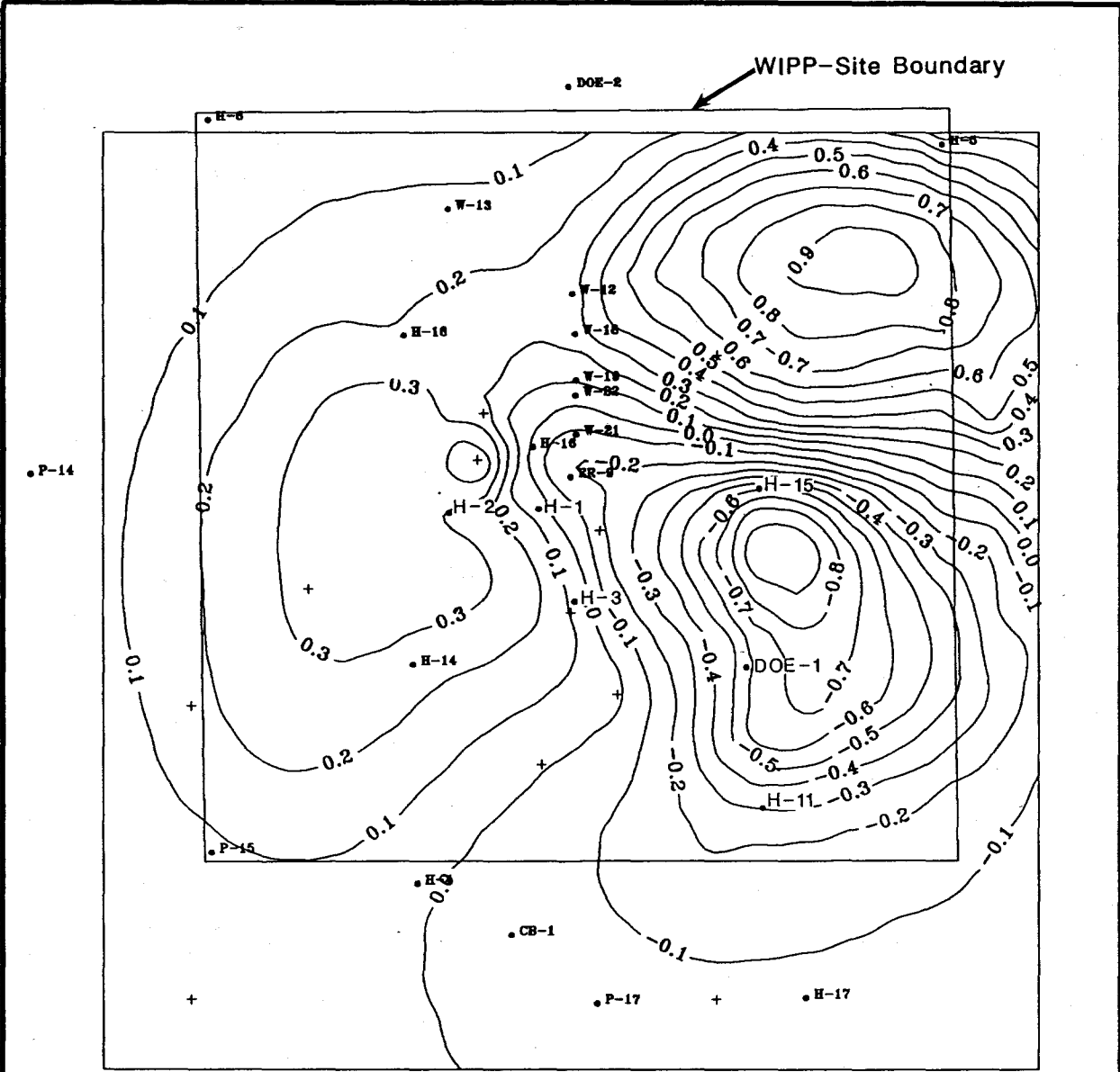
Drawn by	ABW	Date	10/30/89
Checked by	M.L.	Date	10/31/89
Revisions		Date	
H09700R869		10/31/89	

Calculated and Observed Transient Freshwater Heads at DOE-1, P-17, and CB-1 After Calibrating to the H-3 Well Tests

**INTERA** Technologies

Figure 5.6b





- Observation Well
- + Pilot-Point Location
- Contour Interval: 0.1
- Sensitivity Contours are Dimensionless

Drawn by ABW	Date 10/30/89
Checked by M.L.	Date 10/31/89
Revisions	Date
H09700R869	10/31/89

Normalized Sensitivities of H-15 and DOE-1 Transient-Pressure Performance Measure to Changes in Transmissivities at Potential Pilot-Point Locations

**INTERA** Technologies

Figure 5.7

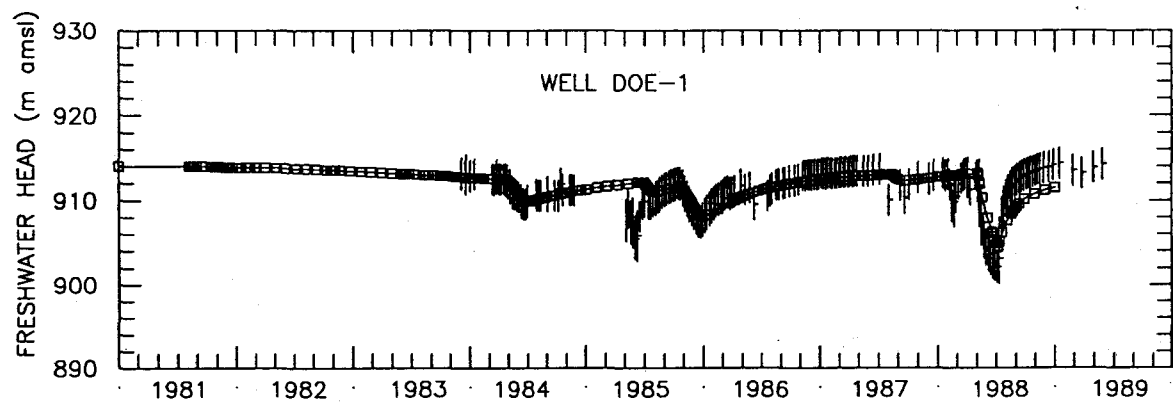
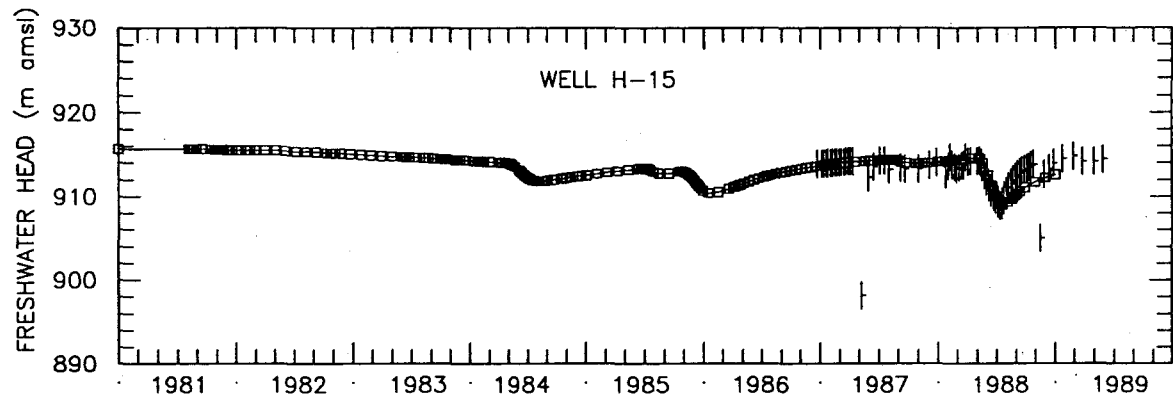
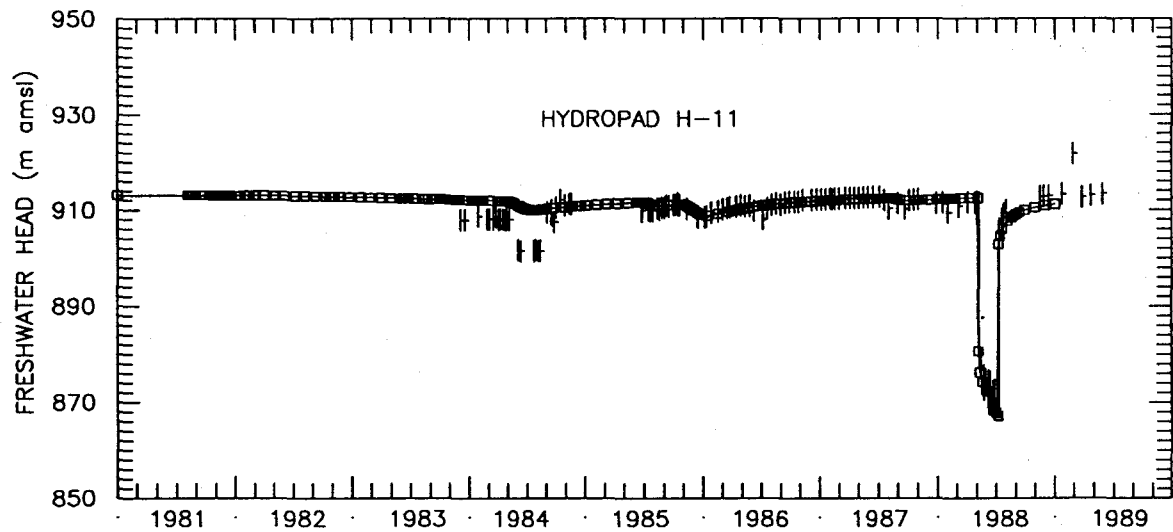
southwest of H-5. Pilot points were added only to the high-sensitivity region south of H-15 because increasing the transmissivities between H-15 and H-11 to improve the drawdown at H-15 due to H-11 pumping is consistent with hydrogeologic intuition. Two pilot points were added to the H-15/H-11 region increasing the transmissivities approximately 1.0 order of magnitude. While this improved the drawdown at H-15, the differences between the observed and measured drawdowns were not sufficiently reduced a subsequent GRASP II run identified the grid block containing the H-15 borehole as the optimum location for another pilot point. Figure 5.8 illustrates the transient heads at the H-11, H-15, and DOE-1 boreholes after these changes were implemented to the transmissivity field. The magnitudes of the calculated drawdowns agree well with those of the observed drawdowns. The calculated recovery at H-15 is slower than the observed recovery.

The addition of the higher transmissivity pilot points south of H-15 extended the high-transmissivity feature within and south of the H-11 area toward H-15. The higher transmissivities also lowered the steady-state head difference at H-15 from 2.0 m to 0.3 m with virtually no change in the steady-state head differences at H-11, DOE-1, H-17, or P-17.

An attempt was made to improve the transient fit at the P-17 and CB-1 boreholes (Figure 5.6b). A performance measure was selected consisting of these two borehole's transient head differences during the H-11 pumping test. Two pilot points were located between H-11 and these two boreholes based on the GRASP II results (Figure 5.9). The transmissivities at these pilot points was decreased by one-half order of magnitude. The improvement at these wells was minimal; therefore, the calibration efforts were redirected at improving the transient fit at the central WIPP wells to the WIPP-13 pumping test.

#### 5.2.5 Calibration to the WIPP-13 Multipad Pumping Test

The WIPP-13 pumping test, conducted from January to February 1987, is described in Section 4.2.4. At this point in the calibration, the calculated and observed drawdowns for the boreholes in the vicinity of WIPP-13 were essentially



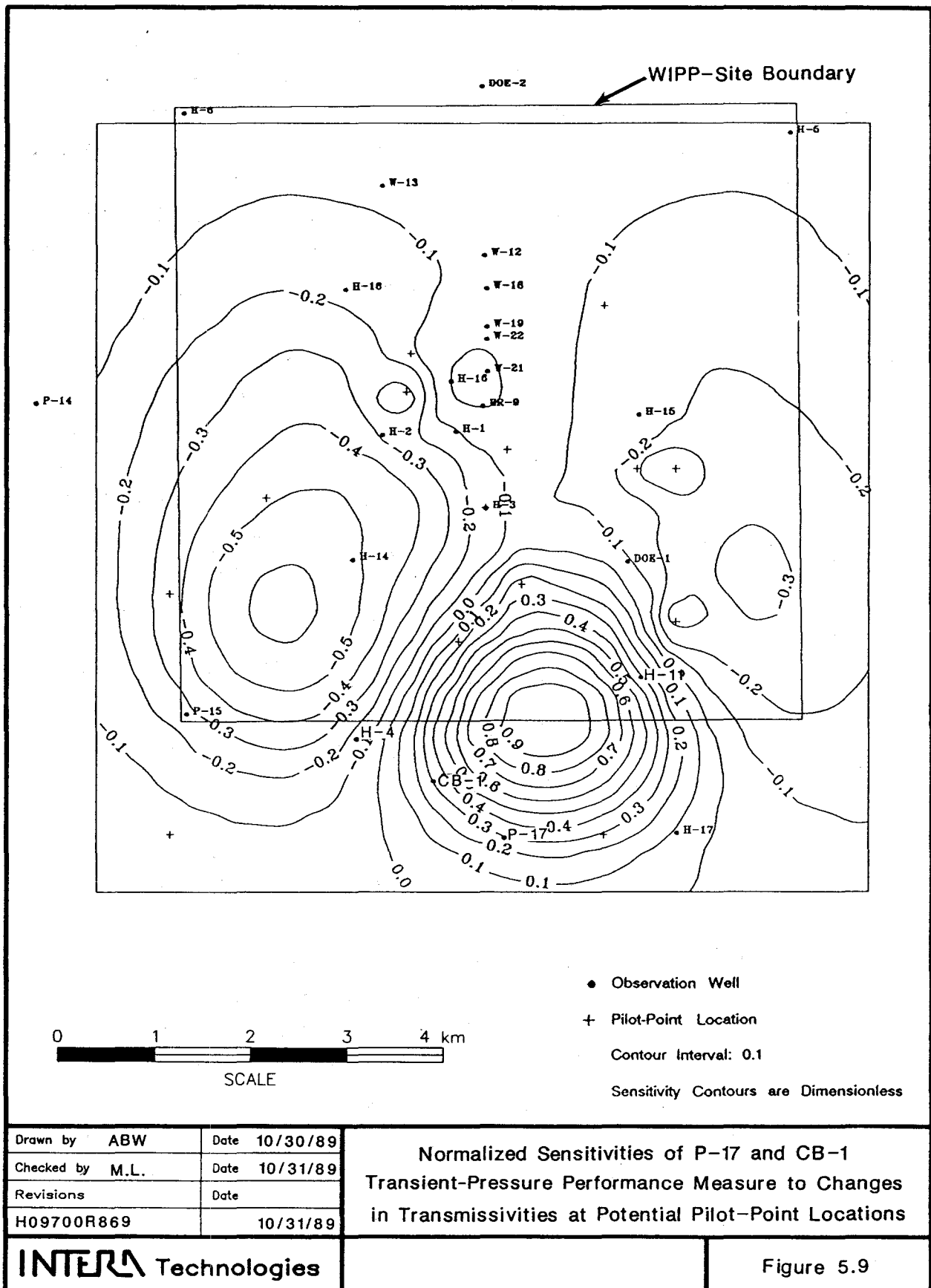
LEGEND: Calculated Freshwater Heads  
 Observed Freshwater Heads

Drawn by	ABW	Date	10/30/89
Checked by	M.L.	Date	10/31/89
Revisions		Date	
H09700R869		10/31/89	

Calculated and Observed Transient Freshwater Heads at H-11, H-15, and DOE-1 After Calibrating to the H-11 Multipad Pumping Test

**INTERA** Technologies

Figure 5.8



the same as those shown for the initial transient simulations because the changes implemented to the transmissivity field in the H-3/H-15 area did not affect the transmissivities in the WIPP-13 area. This is because of the local kriging neighborhood (ten nearest boreholes) used while estimating a grid-block's transmissivity. The pilot points added during calibration to the H-3 and H-11 multipad pumping tests were not close enough to the WIPP-13 area to become part of the WIPP-13 neighborhood and, therefore, did not affect the estimated transmissivities in this region. Thus, the initial transient simulation figures (Figures 5.1a through 5.1g) are referred to first in this section because they are representative of the calculated heads for the northern WIPP-site boreholes during this stage of the calibration efforts.

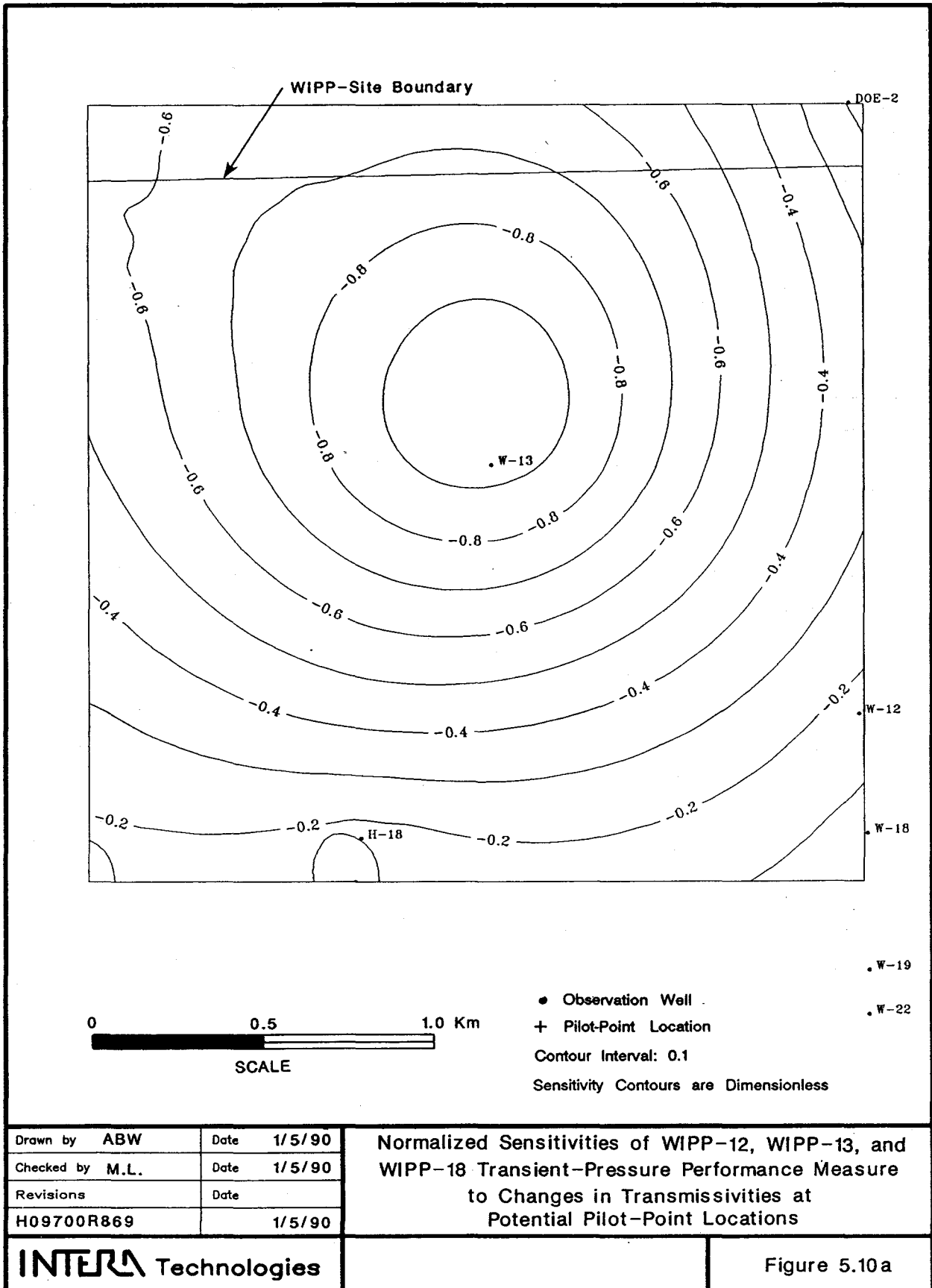
The calculated drawdown at the WIPP-13 borehole during the WIPP-13 multipad pumping test was much greater than the observed drawdown, implying that the well index assigned to WIPP-13 needed to be adjusted (Figure 5.1e). The calculated drawdowns at the H-6, DOE-2, WIPP-12, and WIPP-18 boreholes are illustrated in Figures 5.1b, 5.1d, and 5.1e. The relative magnitudes and timing of the calculated drawdowns and recoveries compare well with the observed transient freshwater heads at these locations. This implies that the calibrated transmissivities between these boreholes and WIPP-13 are probably representative of the actual transmissivities.

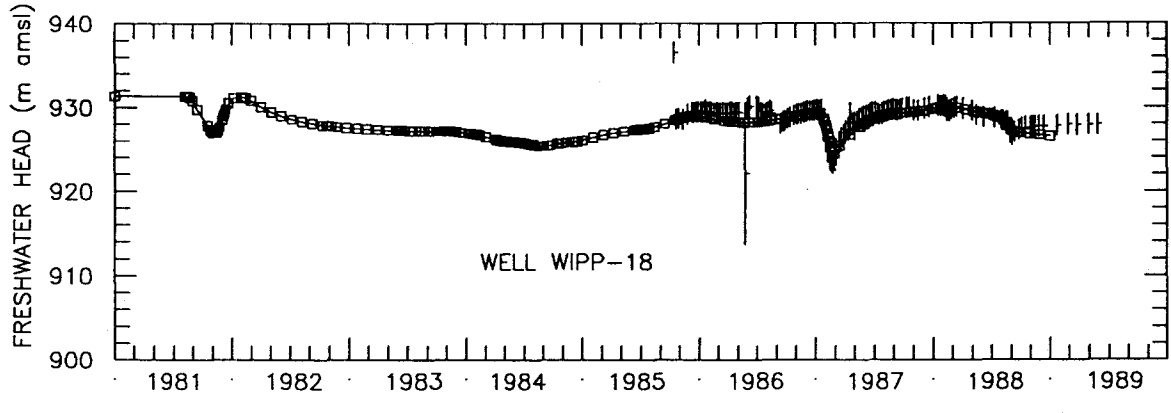
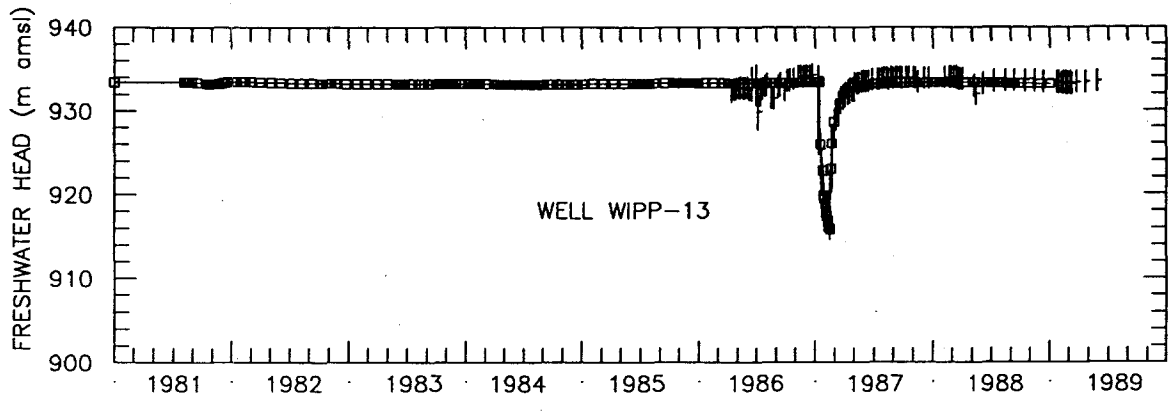
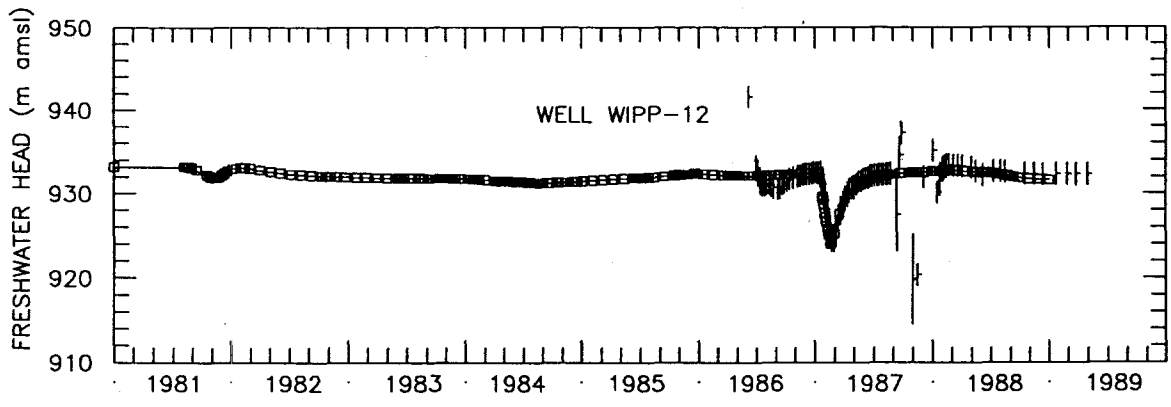
Wells WIPP-19, WIPP-21, WIPP-22, and WIPP-30 also responded to pumping at WIPP-13. The calculated and observed transient freshwater heads at these locations are shown in Figures 5.1f and 5.1g. With the exception of WIPP-30, the calculated drawdowns generally agree reasonably well with the observed drawdowns at these locations. However, the calculated recoveries are much slower than the observed recoveries, implying that the actual transmissivity distribution between WIPP-13 and the WIPP wells noted above is slightly different from that used in the initial transient simulation. The calculated drawdown at WIPP-30 is much less than the observed drawdown. The relatively low transmissivities within the WIPP-30 region form a barrier to flow which reduces the magnitude of its response to pumping at WIPP-13.

After increasing the well index assigned to the WIPP-13 borehole, a performance measure consisting of the transient head differences at WIPP-12, WIPP-13, and WIPP-18 during the WIPP-13 pumping test was selected for a GRASP II simulation to determine the optimum location for changes in the transmissivity field. GRASP II identified a high-negative-sensitivity region within the vicinity of WIPP-13 (Figure 5.10a). Two pilot points were added to increase the transmissivities in this area. One was added within the WIPP-13 grid block and the other was located just north of the WIPP-13 grid block. The calculated drawdowns and recoveries at the WIPP-12, WIPP-13, and WIPP-18 boreholes were improved after increasing the transmissivities in this area (Figure 5.10b). The calculated drawdown and recovery at WIPP-13 agrees well with the observed. The same is true for the WIPP-12 and WIPP-18 boreholes where there is excellent agreement between the calculated and observed transient heads.

The increase in transmissivity in the WIPP-13 area also increased the flow toward the center of the site, causing the steady-state head differences to become worse in the central site area. The maximum differences between the calculated and observed heads occurred at H-2, H-14, and WIPP-18, where the values were 2.0, 1.8, and 1.7 m, respectively. A performance measure consisting of the steady-state differences at the central boreholes was used to re-establish the steady-state calibration. GRASP II identified a high-positive-sensitivity area southeast of H-18 and a high-negative-sensitivity area west of H-3 (Figure 5.11). The high-positive-sensitivity region southeast of H-18 suggests lowering the transmissivities in this area to restrict ground-water flow from the north, thereby lowering the steady-state differences at H-2, H-14, and WIPP-18. The high-negative-sensitivity region suggests raising the transmissivities west of H-3 to increase the flow away from H-2 and H-14 to reduce the steady-state head differences.

A lower transmissivity pilot point was added southeast of H-18 which reduced the steady-state head differences. However, the lower transmissivities in this region degraded the transient fits at WIPP-18, WIPP-19, and WIPP-22. Therefore, the lower transmissivity pilot point was removed and a higher transmissivity pilot point was added west of H-3. The steady-state head differences were reduced to 0.8, 1.7, and 1.4 m at the H-2, H-14, and WIPP-18 boreholes, respectively.





LEGEND: □—□ Calculated Freshwater Heads  
 † Observed Freshwater Heads

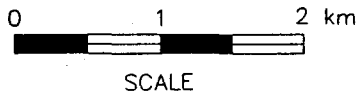
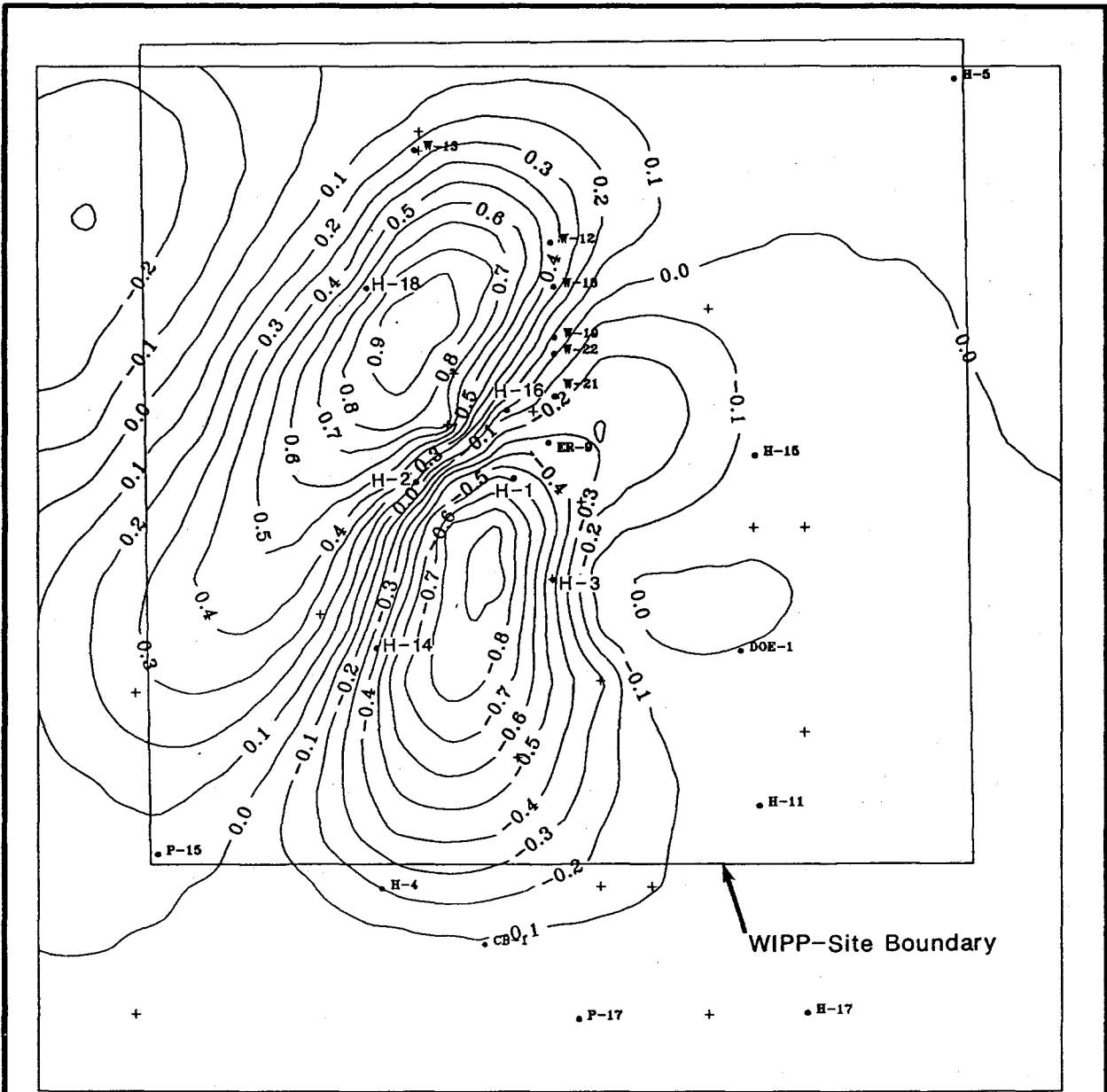
Drawn by ABW	Date 10/30/89
Checked by M.L.	Date 10/31/89
Revisions	Date
H09700R869	10/31/89

Calculated and Observed Transient Freshwater Heads at WIPP-12, WIPP-13, and WIPP-18 After Adding Pilot Points near WIPP-13

**INTERA** Technologies

Figure 5.10b





- Observation Well
- + Pilot-Point Location
- Contour Interval: 0.1
- Sensitivity Contours are Dimensionless

Drawn by ABW	Date 11/2/89
Checked by M.L.	Date 11/2/89
Revisions	Date
H09700R869	11/2/89

**Normalized Sensitivities of Central Boreholes  
Steady-State Performance Measure to Changes in  
Transmissivities at Potential Pilot-Point Locations**

**INTERA Technologies**

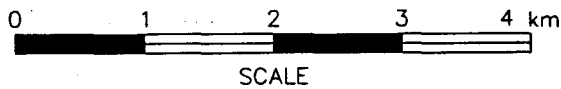
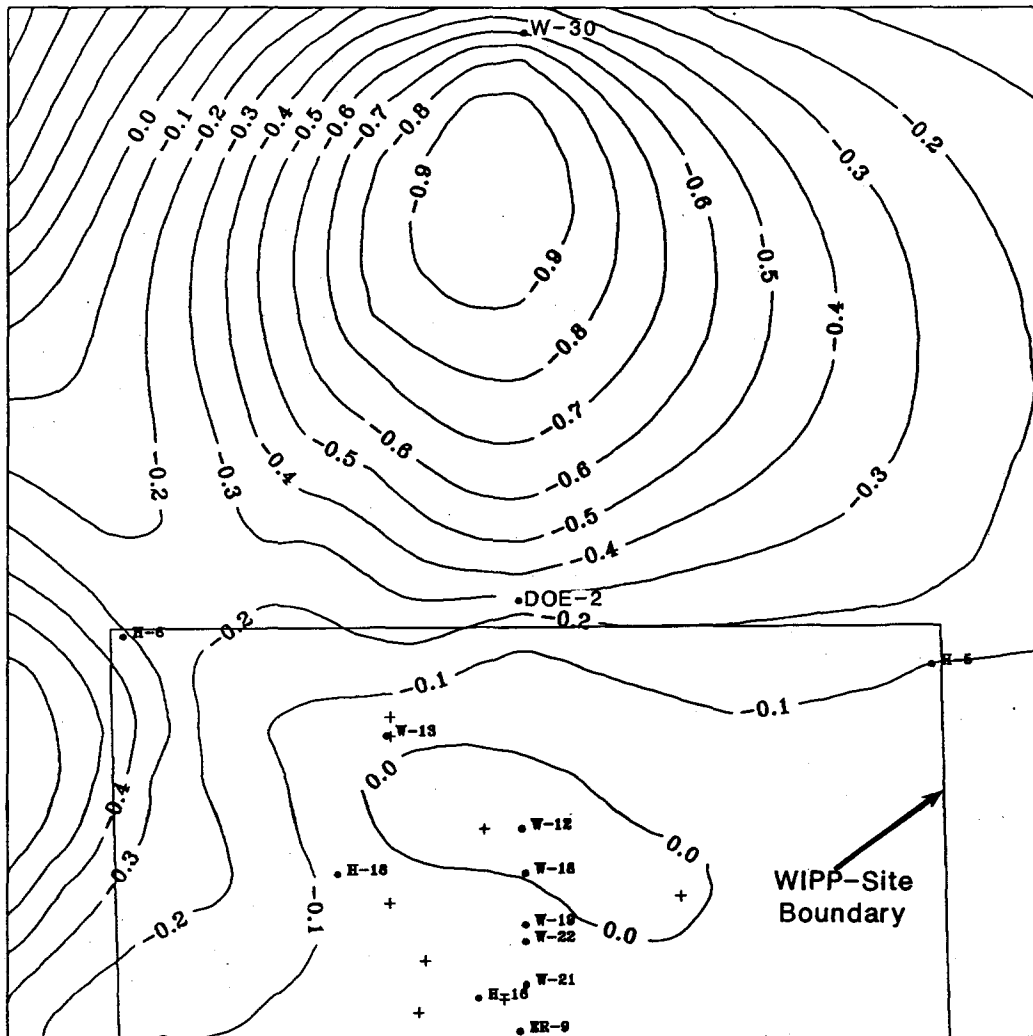
Figure 5.11

The next step in calibrating the model to the WIPP-13 pumping test focused on reducing the differences between the calculated and observed drawdowns at WIPP-30. A performance measure consisting of the steady-state head differences for the central WIPP-site boreholes and the transient head differences at WIPP-30, WIPP-13, DOE-2, and H-6 was selected. Figure 5.12 illustrates the normalized sensitivities determined by GRASP II. A large high-negative-sensitivity region is located south of WIPP-30. Two pilot points with higher transmissivities added to this region resulted in an increase in the drawdown at WIPP-30. However, the transient head differences were not sufficiently reduced until a higher transmissivity pilot point was also added to the WIPP-30 grid block (based upon a subsequent GRASP II calculation). Figure 5.13 illustrates the H-6, DOE-2, and WIPP-30 transient head plots after this step in the transient calibration. The calculated transient heads at DOE-2 and WIPP-30 agree well with the measured heads. The calculated absolute drawdown at H-6 agrees well with the observed drawdown; however, the calculated heads are generally higher than the observed heads during this entire simulation period, in part because the calculated steady-state head is higher than the observed head.

#### 5.2.6 Calibration to the Excavation of the Air-Intake Shaft

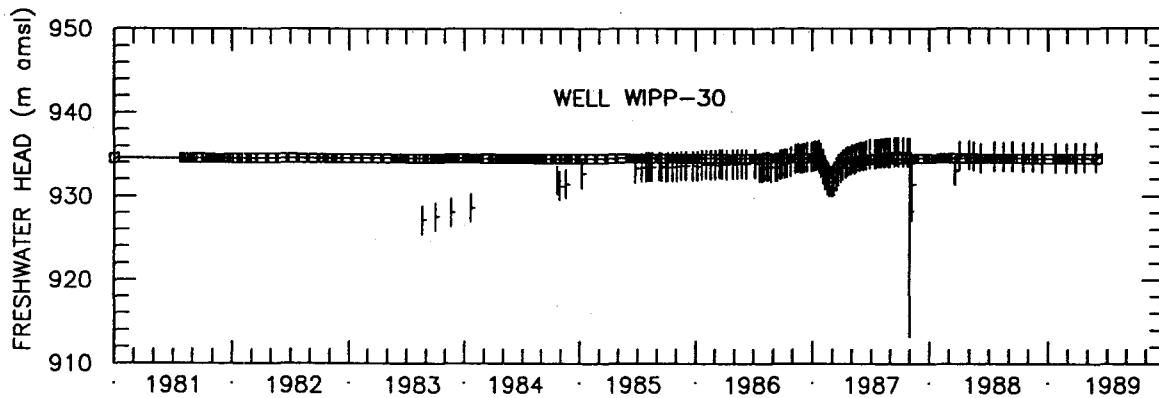
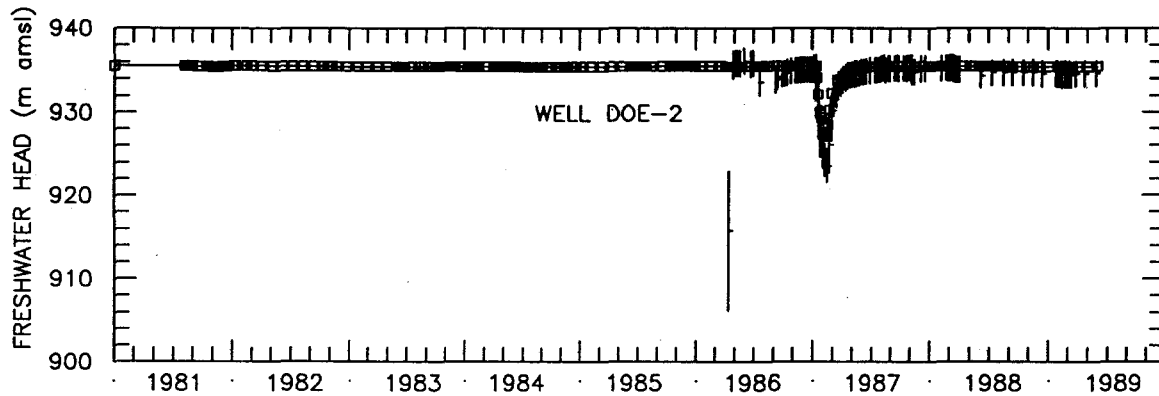
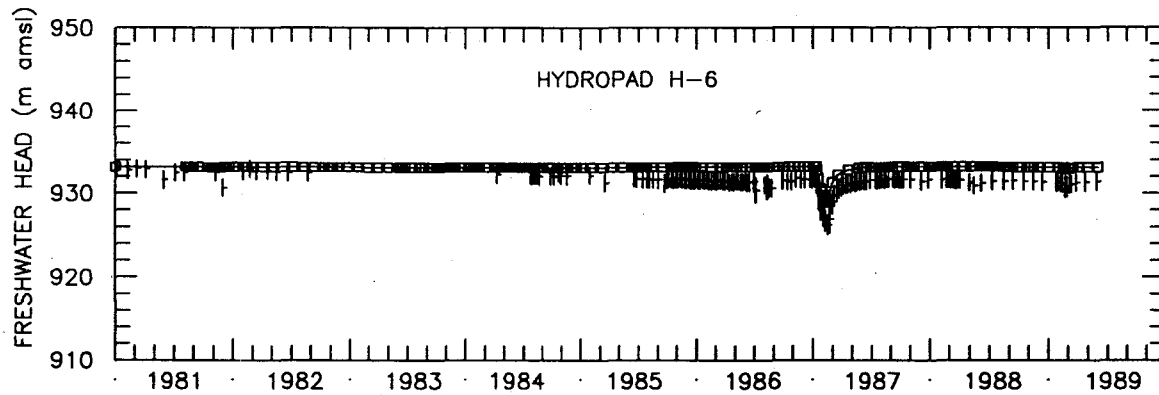
The excavation of the AIS at the Culebra horizon began on January 1, 1988. The major details of the excavation are described in Stensrud et al. (1990) and Cauffman et al. (1990). The boreholes in the central WIPP-site area that responded to the AIS excavation include H-1, H-2, H-16, WIPP-19, WIPP-21, WIPP-22, and ERDA-9, and to a lesser extent WIPP-18. Prior to calibrating to excavation at the AIS, the calculated drawdowns were less than the observed drawdown at H-1, WIPP-21, and ERDA-9 (Figure 5.14a), greater than the observed drawdown at WIPP-19 (Figure 5.14b), and approximately the same as the observed drawdowns at H-2 and WIPP-22 (Figure 5.14b). Thus, the calculated drawdowns near the AIS had to be increased without drastically increasing the drawdowns at H-2 and WIPP-22. Additional ground-water flow from the northern WIPP-site boundary was also needed to reduce the drawdown at WIPP-19.

A performance measure consisting of the transient head differences at WIPP-21 from January 1988 to January 1989 was used as a first step in improving the



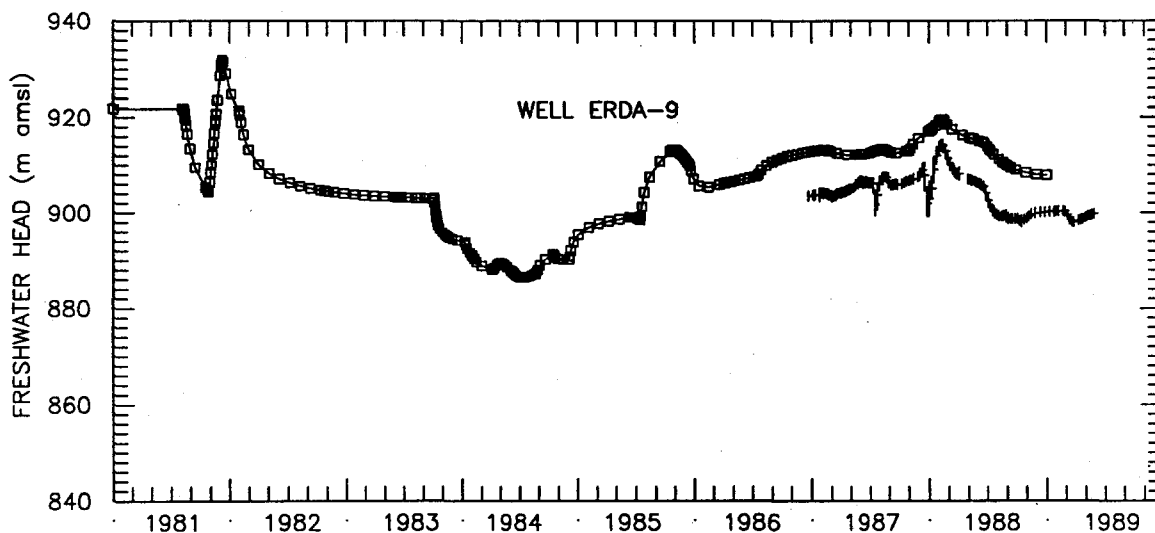
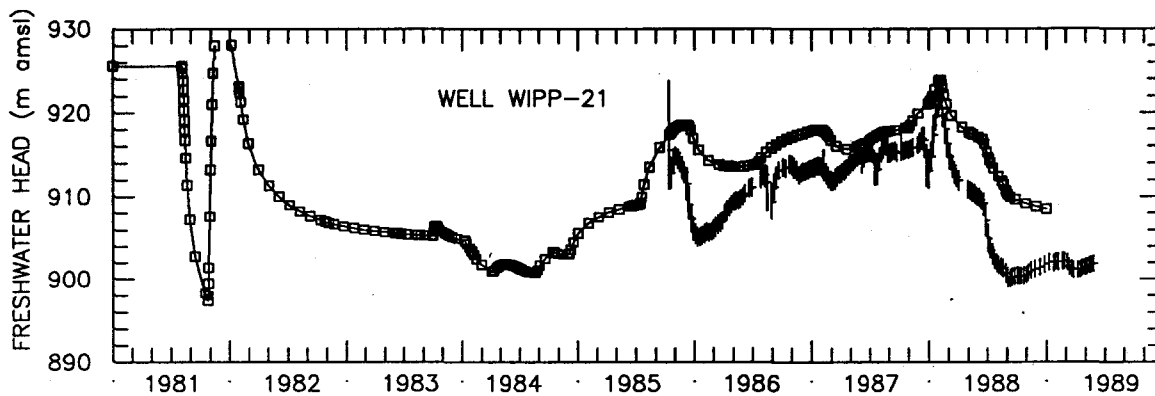
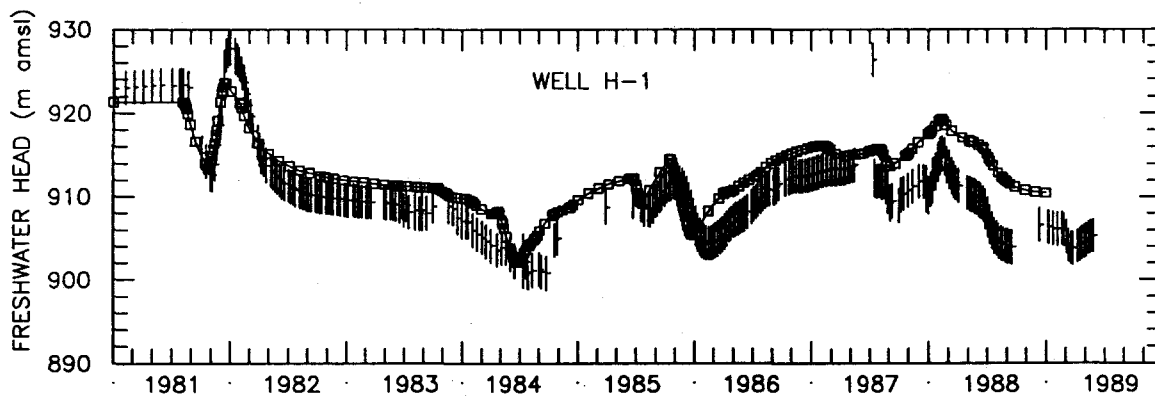
- Observation Well
- + Pilot-Point Location
- Contour Interval: 0.1
- Sensitivity Contours are Dimensionless

Drawn by ABW	Date 10/30/89	<b>Normalized Sensitivities of WIPP-30, WIPP-13, DOE-2, and H-6 Transient-Pressure Performance Measure to Changes in Transmissivities at Potential Pilot-Point Locations</b>
Checked by M.L.	Date 10/31/89	
Revisions	Date	
H09700R869	10/31/89	
<b>INTERA Technologies</b>		Figure 5.12



LEGEND: □—□ Calculated Freshwater Heads  
 | Observed Freshwater Heads

Drawn by	ABW	Date	10/30/89	<b>Calculated and Observed Transient Freshwater Heads          at H-6, DOE-2, and WIPP-30 After Calibrating to          the WIPP-13 Multipad Pumping Test</b>
Checked by	M.L.	Date	10/31/89	
Revisions		Date		
H09700R869		10/31/89		
<b>INTERA Technologies</b>				Figure 5.13



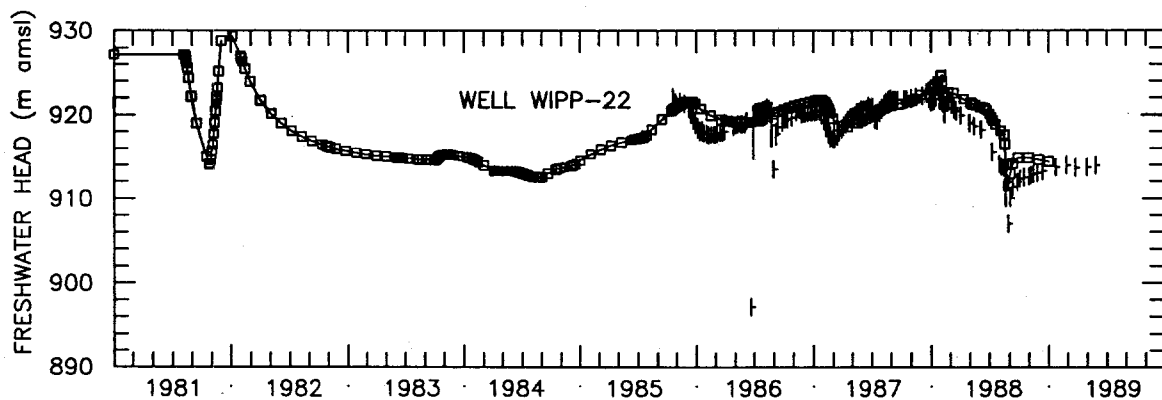
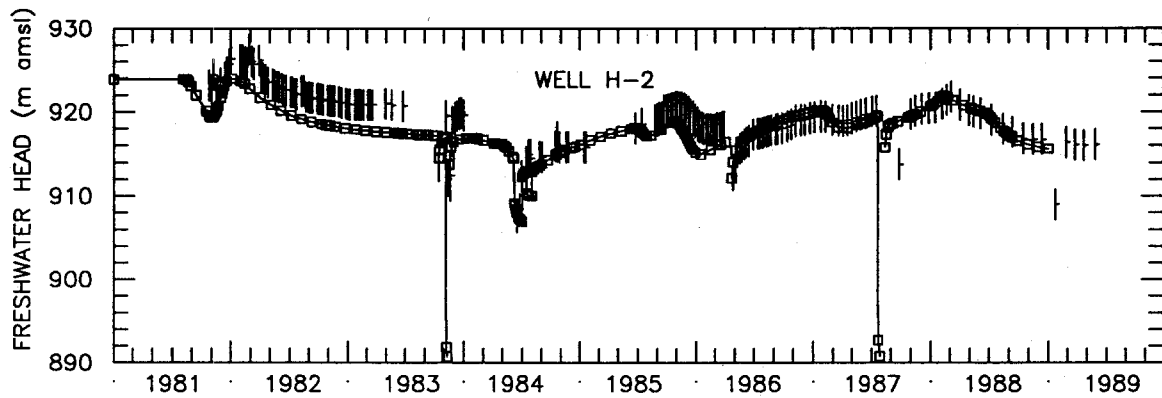
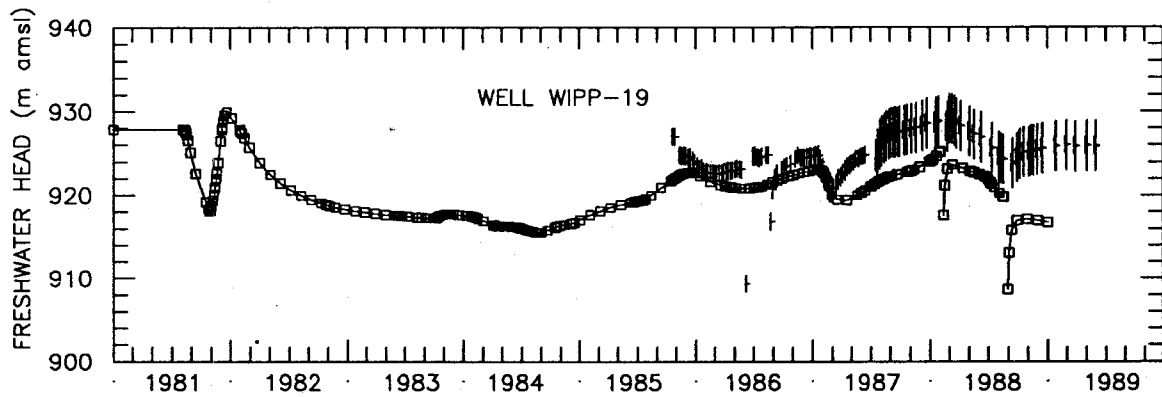
LEGEND: □—□ Calculated Freshwater Heads  
 | Observed Freshwater Heads

Drawn by	ABW	Date	10/30/89
Checked by	M.L.	Date	10/31/89
Revisions		Date	
H09700R869		Date	10/31/89

Calculated and Observed Transient Freshwater Heads at H-1, WIPP-21, and ERDA-9 After Calibrating to the WIPP-13 Multipad Pumping Test

**INTERA** Technologies

Figure 5.14a



LEGEND: □-□ Calculated Freshwater Heads  
 † Observed Freshwater Heads

Drawn by	ABW	Date	10/30/89
Checked by	M.L.	Date	10/31/89
Revisions		Date	
H09700R869		10/31/89	

Calculated and Observed Transient Freshwater Heads at WIPP-19, H-2, and WIPP-22 After Calibrating to the WIPP-13 Multipad Pumping Test

**INTERA** Technologies

Figure 5.14b

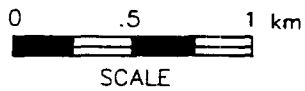
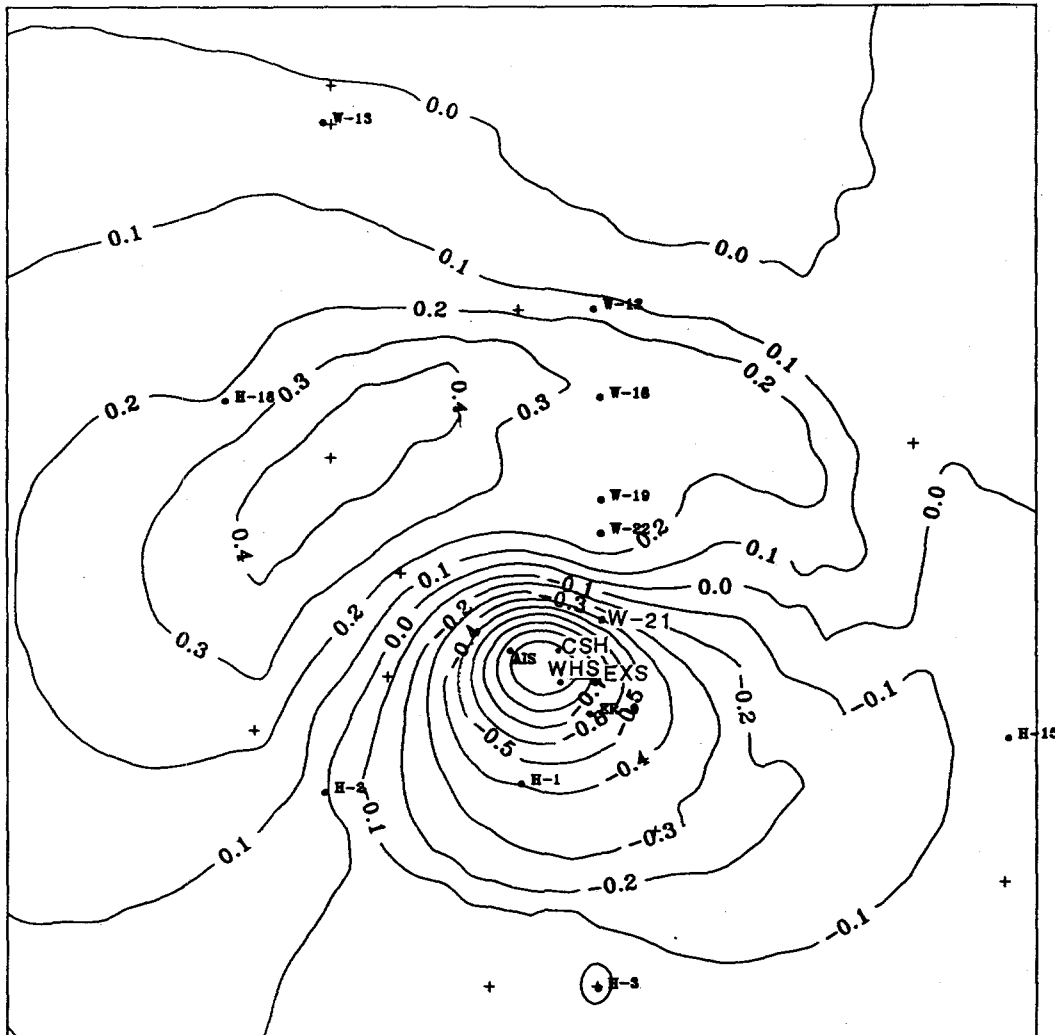
"near-field" transient fits due to construction of the AIS. It was assumed that increasing the drawdown at WIPP-21 would also improve the fit at ERDA-9. The GRASP II results, shown in Figure 5.15, depict a high-negative-sensitivity region near the AIS, WHS, and C&SH shaft. Two higher transmissivity pilot points were added to the high-sensitivity region; one within the grid block containing the AIS and one within the grid block that separates the AIS and the WIPP-21 grid blocks. After several increases to the assigned pilot-point transmissivities and the well index assigned to the AIS, no improvement in the transient head differences at WIPP-21 or ERDA-9 was observed (Figure 5.16). The increased transmissivities (1.0 order of magnitude) allowed more ground water to flow in this central region, which ultimately increased the differences between the calculated and observed heads because the lower transmissivities which occur south of ERDA-9 restricted ground-water flow southward and generated higher heads near the shafts.

The lack of improvement to the calculated drawdown due to excavating the AIS suggested that the calculated leakage rate at the AIS and/or other shafts must be raised to increase the local drawdown. Section 6.4 presents a set of sensitivity runs designed to address this issue. It is clear from the above attempt to improve the fit to the AIS-induced stresses, however, that neither changes in the skin transmissivity nor the grid-block transmissivities in the shaft region will improve the WIPP-21 and ERDA-9 transient head differences due to the AIS excavation.

One improvement to the transient fits of the AIS-excavation effects at WIPP-18 and WIPP-19 was achieved by the addition of a higher transmissivity pilot point west of WIPP-12. The location of this pilot point was based on judgement. The one-half order of magnitude increase in transmissivities in this area, caused by the addition of this pilot point, allowed more ground water to flow toward WIPP-19, which decreased the drawdown due to the AIS excavation and also improved the transient fit to the WIPP-13 pumping test in early 1987 (Figure 5.17).

#### 5.2.7 Calibration to the P-14 Pumping Test

The P-14 pumping test was conducted from February 14 to 17, 1989. During the transient calibration to the P-14 pumping test, the well index for P-14 was adjusted by approximately a factor of two to yield agreement between calculated and



- Observation Well
- + Pilot-Point Location
- Contour Interval: 0.1
- Sensitivity Contours are Dimensionless

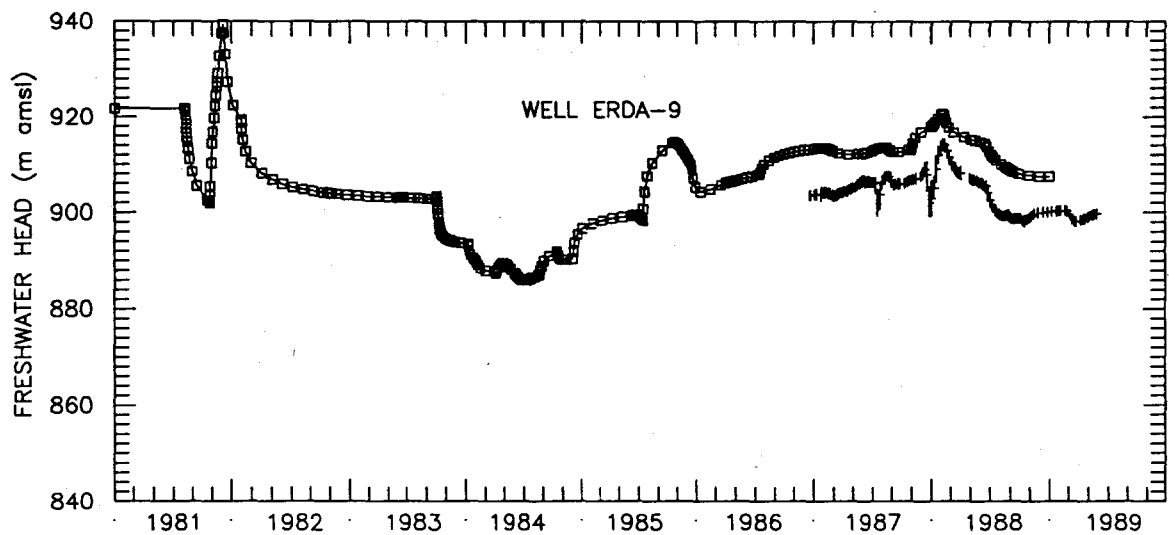
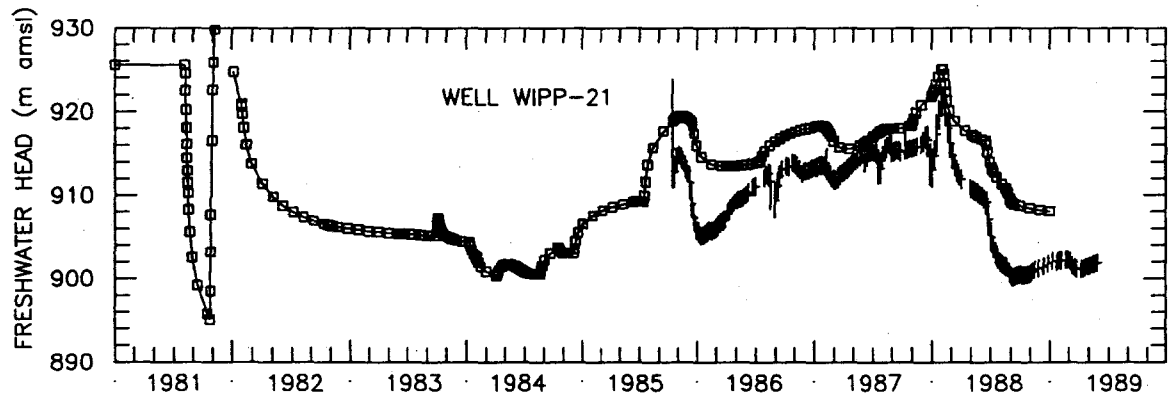
Drawn by ABW	Date 10/30/89
Checked by M.L.	Date 10/31/89
Revisions	Date
H09700R869	10/31/89

**Normalized Sensitivities of WIPP-21 Transient-Pressure Performance Measure to Changes in Transmissivities at Potential Pilot-Point Locations**

**INTERA Technologies**

Figure 5.15





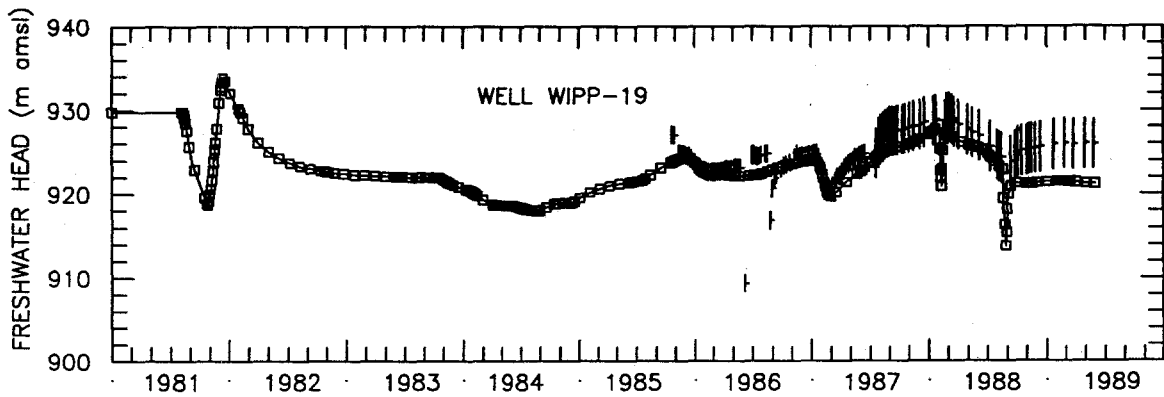
LEGEND: □—□ Calculated Freshwater Heads  
 + Observed Freshwater Heads

Drawn by	ABW	Date	10/30/89
Checked by	M.L.	Date	10/31/89
Revisions		Date	
H09700R869		10/31/89	

Calculated and Observed Transient Freshwater Heads at WIPP-19 and ERDA-9 After Adding Pilot Points Between AIS and WIPP-21

**INTERA** Technologies

Figure 5.16



LEGEND: □—□ Calculated Freshwater Heads  
 † Observed Freshwater Heads

Drawn by ABW	Date 10/30/89
Checked by M.L.	Date 10/31/89
Revisions	Date
H09700R869	10/31/89

Calculated and Observed Transient Freshwater Heads at WIPP-19 After Adding Pilot Point West of WIPP-12

**INTERA** Technologies

Figure 5.17

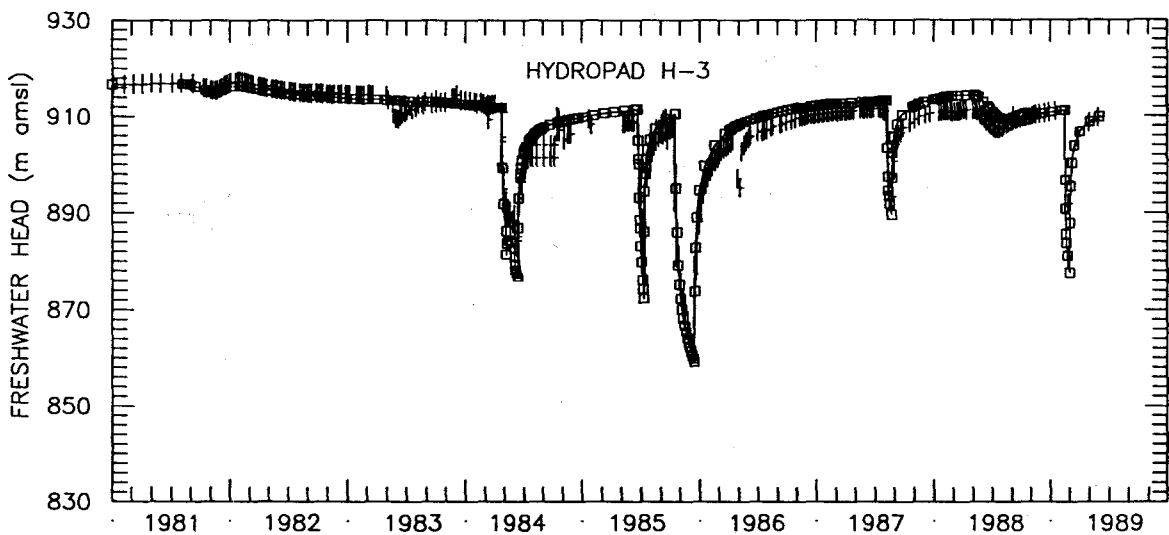
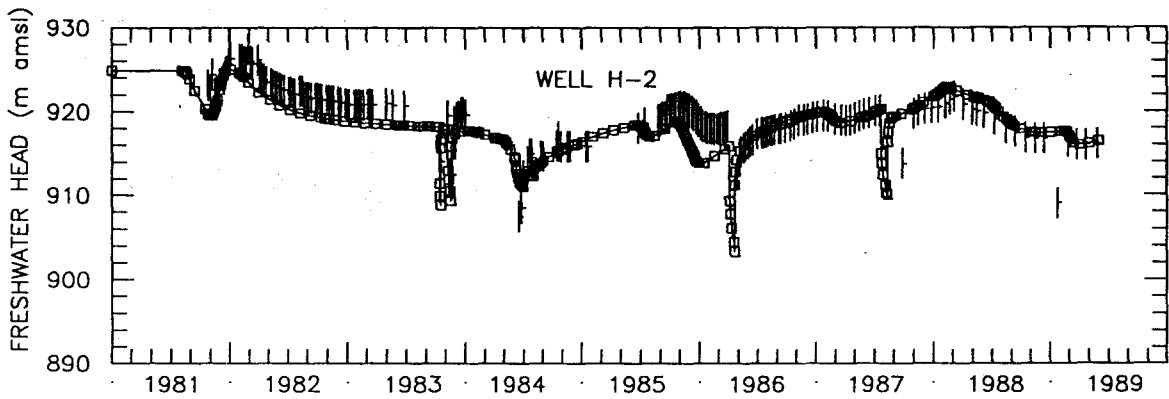
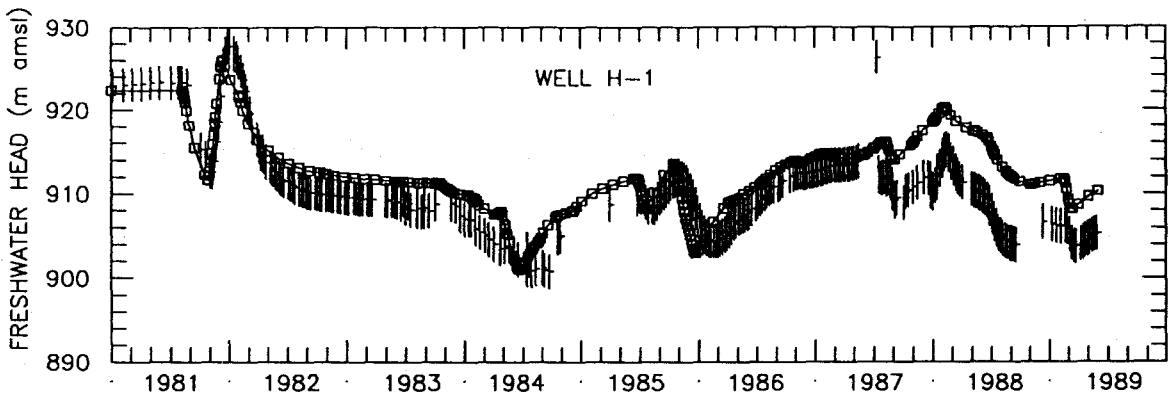
measured drawdowns (Figure 5.18d) at that location. Drawdowns of about 0.5 m were observed at H-6 and WIPP-25 due to the P-14 pumping test. The calculated drawdowns at H-6 and WIPP-25 are similar in magnitude to the observed drawdowns as shown in Figures 5.18b and 5.18g, respectively.

### 5.2.8 Calibration to Other Tests

Calibration to the activities at H-2 required a slight decrease in the well index at H-2. The most significant transient responses at H-2 were caused by the shaft activities and the well tests conducted at H-3. These H-2 responses were fit during calibration of the heads in the central model region to shaft activities and the H-3 events. Agreement between the calculated and observed responses at H-4 during the H-4 tracer test and at WIPP-19 during the WQSP pumping at WIPP-19 was achieved by increasing the well indices assigned to these two boreholes. The calculated and observed drawdowns at the H-4 borehole agree very well (Figure 5.18b) during the time of the H-4 tracer test (i.e., mid-1982 to late-1984). The calculated drawdowns during the two WQSP pumping periods at WIPP-19 during 1988 also agree well with the observed drawdowns (Figure 5.18f).

### 5.3 The Transient Calibrated Heads

Figures 5.18a through 5.18h contain the transient calibrated (TC) heads for the WIPP-area boreholes included in the transient simulations. The largest head differences occur for the calculated responses at ERDA-9 and for the wells which responded to the AIS excavation. The rates of recovery at H-15 and H-17 (Figure 5.18c), DOE-1 (Figure 5.18d), and P-17 (Figure 5.18e) due to H-11 pumping are also slower than the observed recovery rates. However, the calculated fits to other observed responses from the activities at the C&SH shaft, EXS, and WHS and the H-3, H-11, and WIPP-13 multipad pumping tests are good. The shaft-leakage rates for the transient calibrated model are shown in Figures 5.19a and 5.19b. Only minor differences exist between the final leakage rates for the transient calibrated model and the initial leakage rates calibrated prior to the introduction of any transmissivity modifications to the transient model (Section 5.2.2; Figures 5.3a and 5.3b). An increase in the leakage rate at the C&SH shaft from 1982 to 1987 was implemented to improve the transient fit at the H-1 borehole.



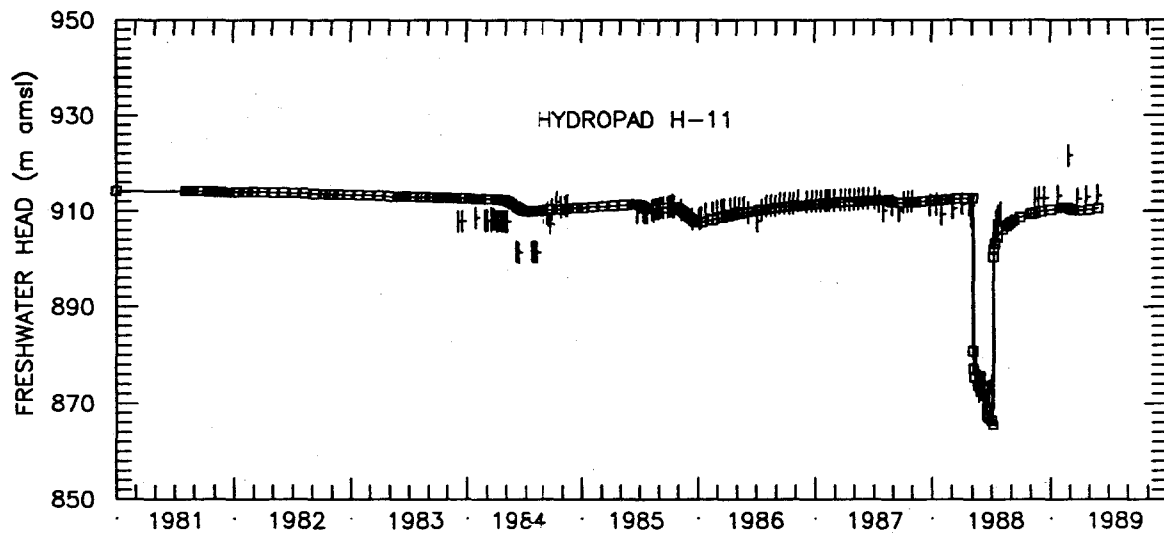
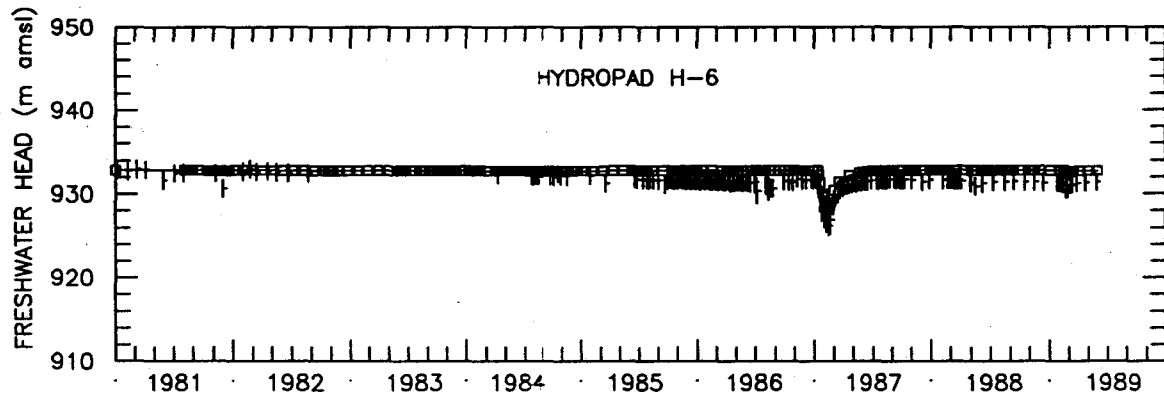
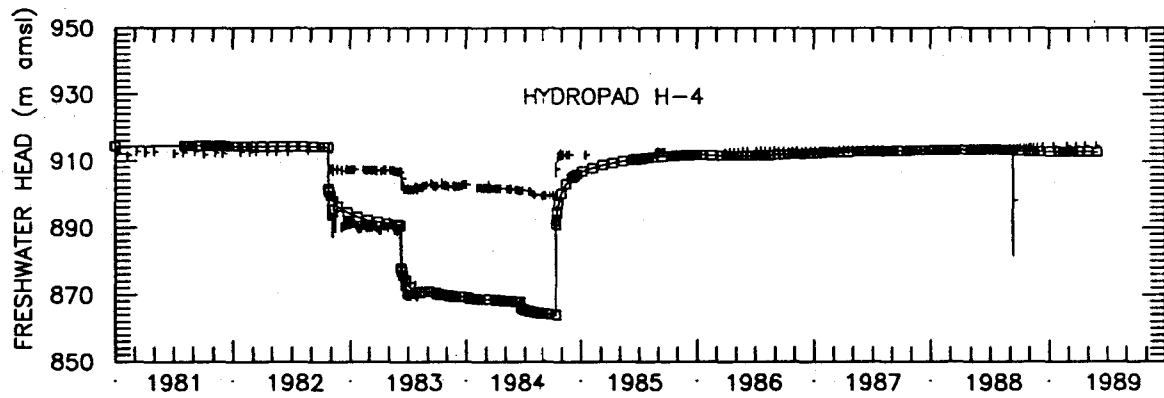
LEGEND:  $\square$ — $\square$  Calculated Freshwater Heads  
 | Observed Freshwater Heads

Drawn by ABW	Date 10/30/89
Checked by M.L.	Date 10/31/89
Revisions	Date
H09700R869	10/31/89

Calculated and Observed Transient Freshwater Heads at H-1, H-2, and H-3 Using the Transient Calibrated Transmissivity Field

**INTERA** Technologies

Figure 5.18a



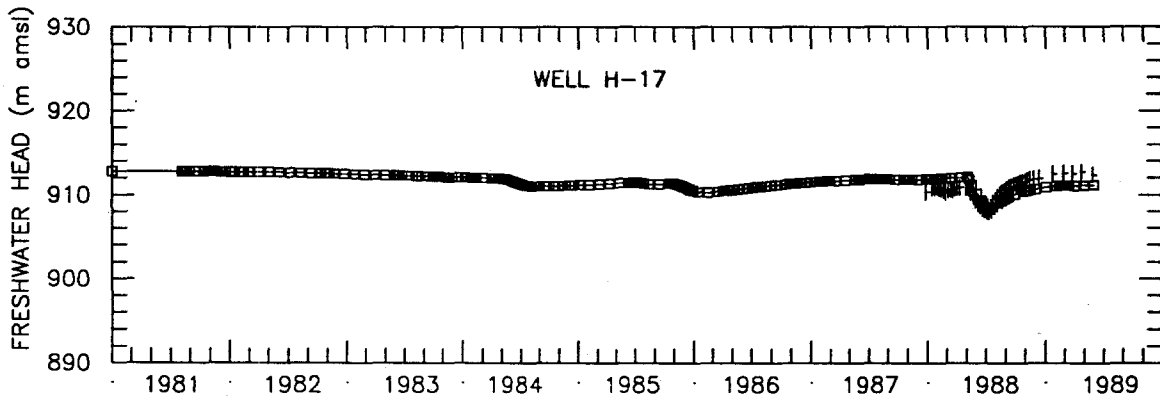
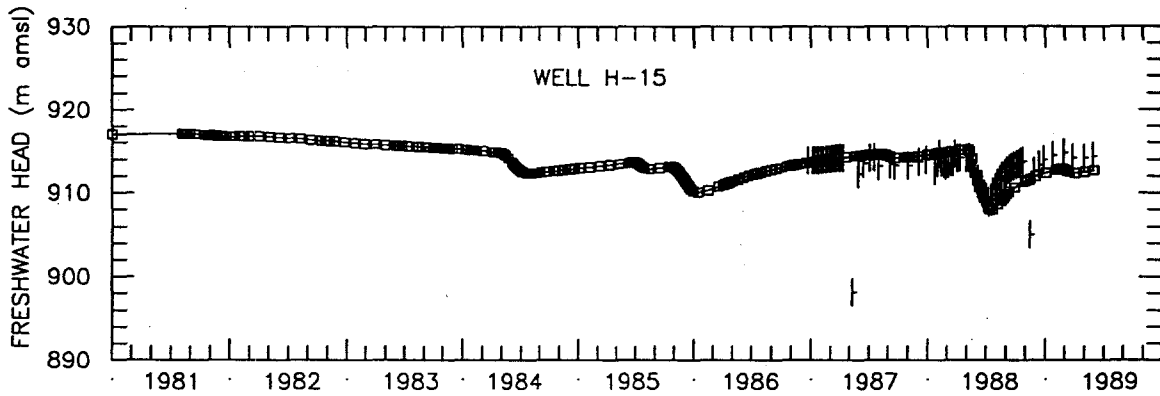
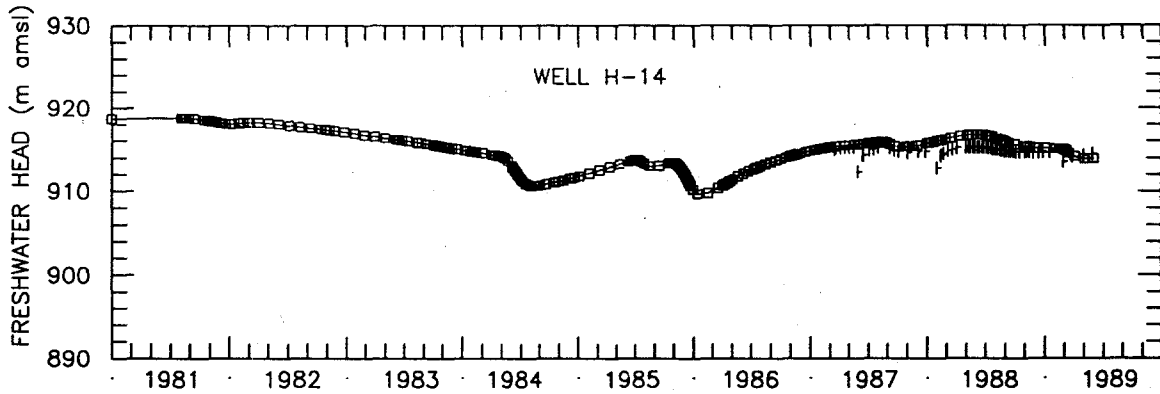
LEGEND: Calculated Freshwater Heads  
 Observed Freshwater Heads

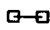

Drawn by	ABW	Date	10/30/89
Checked by	M.L.	Date	10/31/89
Revisions		Date	
H09700R869		10/31/89	

Calculated and Observed Transient Freshwater Heads at H-4, H-6, and H-11 Using the Transient Calibrated Transmissivity Field

**INTERA** Technologies

Figure 5.18b



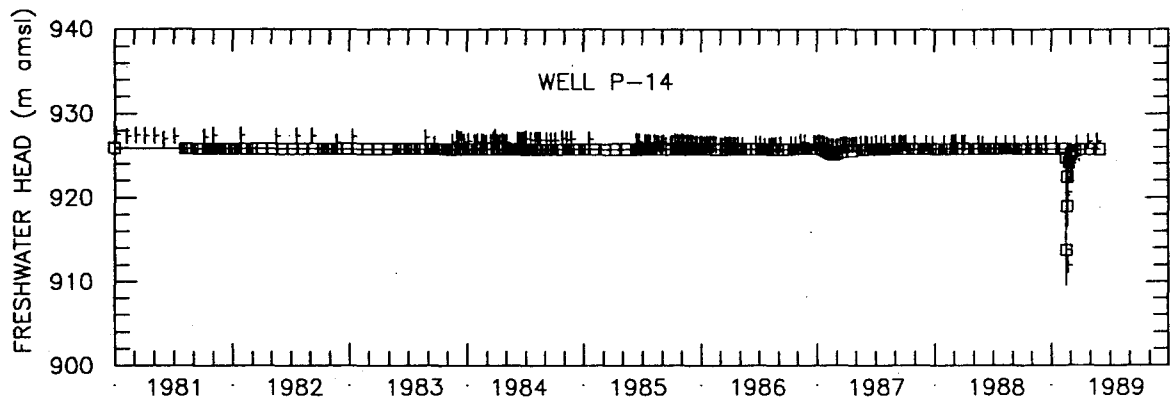
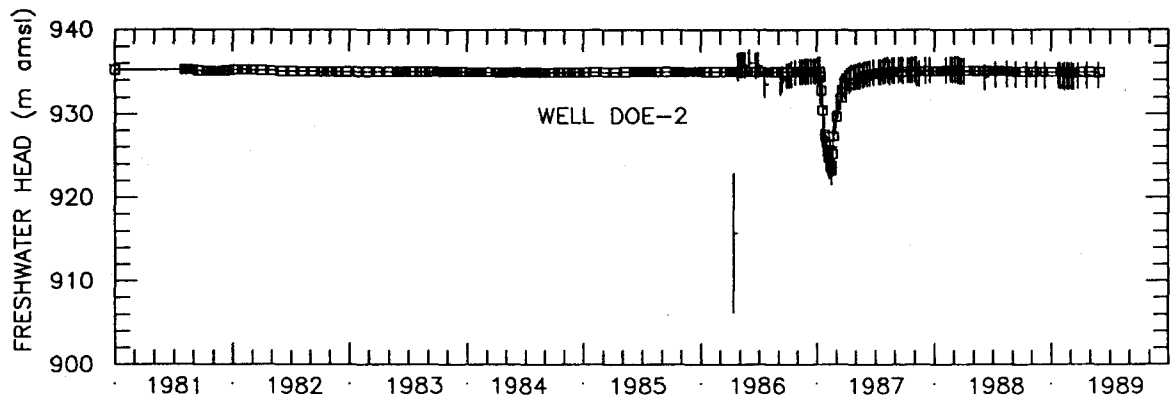
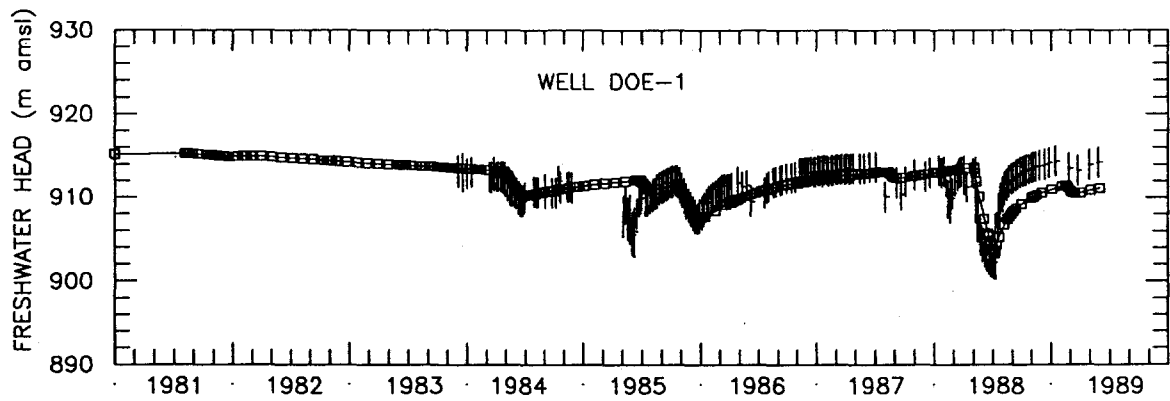
LEGEND:  Calculated Freshwater Heads  
 Observed Freshwater Heads

Drawn by	ABW	Date	10/30/89
Checked by	M.L.	Date	10/31/89
Revisions		Date	
H09700R869		10/31/89	

Calculated and Observed Transient Freshwater Heads  
 at H-14, H-15, and H-17 Using the Transient  
 Calibrated Transmissivity Field

**INTERA** Technologies

Figure 5.18c



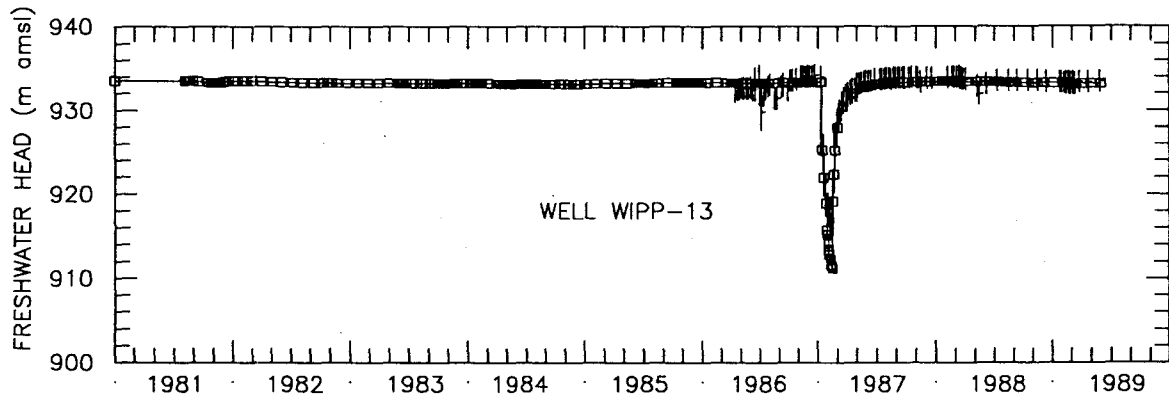
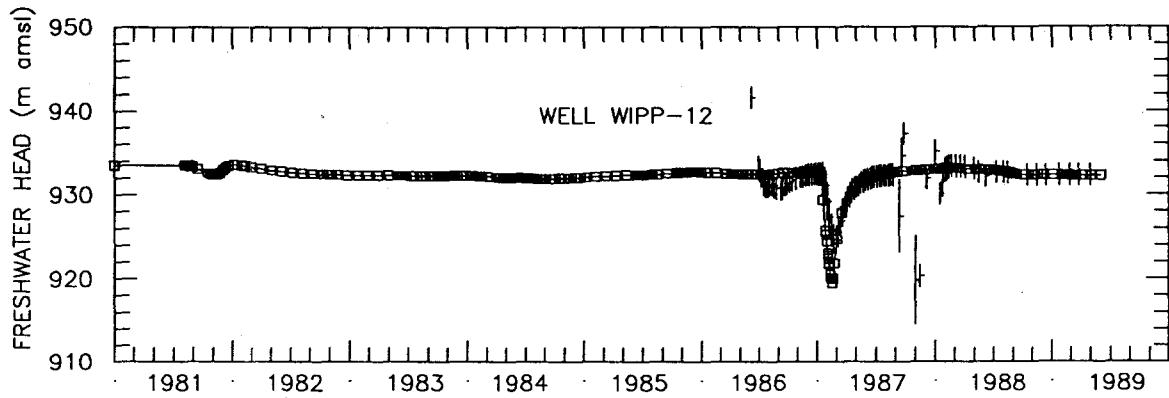
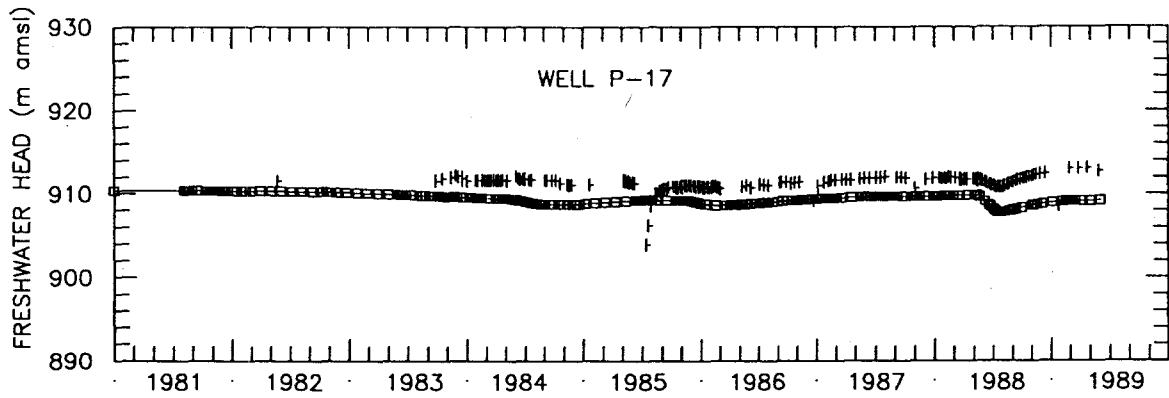
LEGEND: □—□ Calculated Freshwater Heads  
 | Observed Freshwater Heads

Drawn by ABW	Date 10/30/89
Checked by M.L.	Date 10/31/89
Revisions	Date
H09700R869	10/31/89

Calculated and Observed Transient Freshwater Heads  
 at DOE-1, DOE-2, and P-14 Using the Transient  
 Calibrated Transmissivity Field

**INTERA** Technologies

Figure 5.18d



LEGEND: □—□ Calculated Freshwater Heads  
 † Observed Freshwater Heads

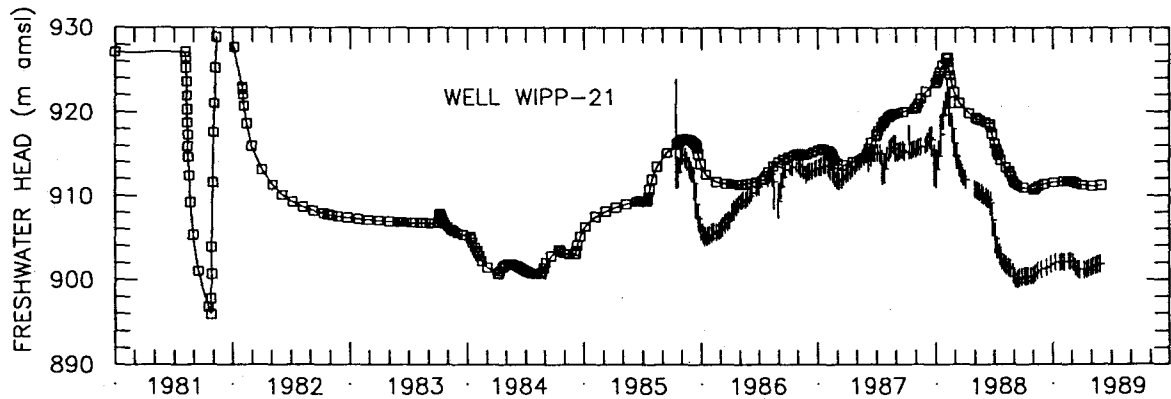
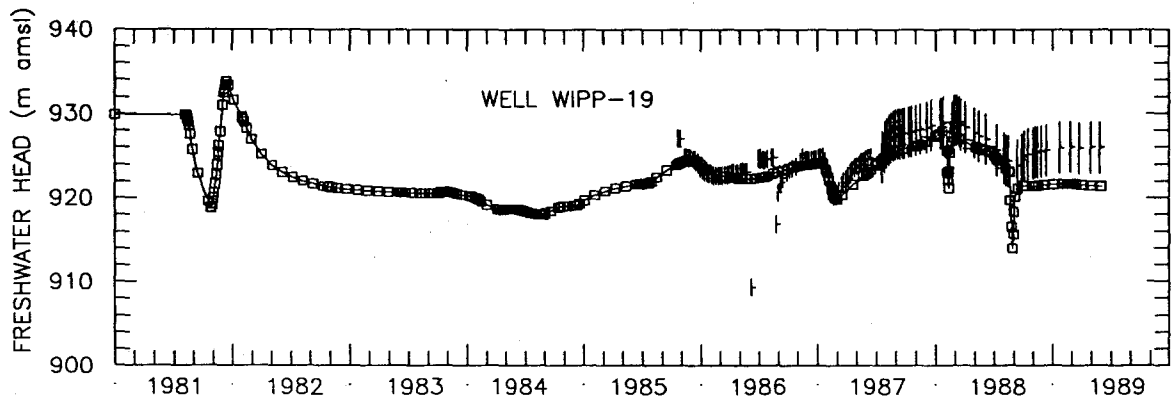
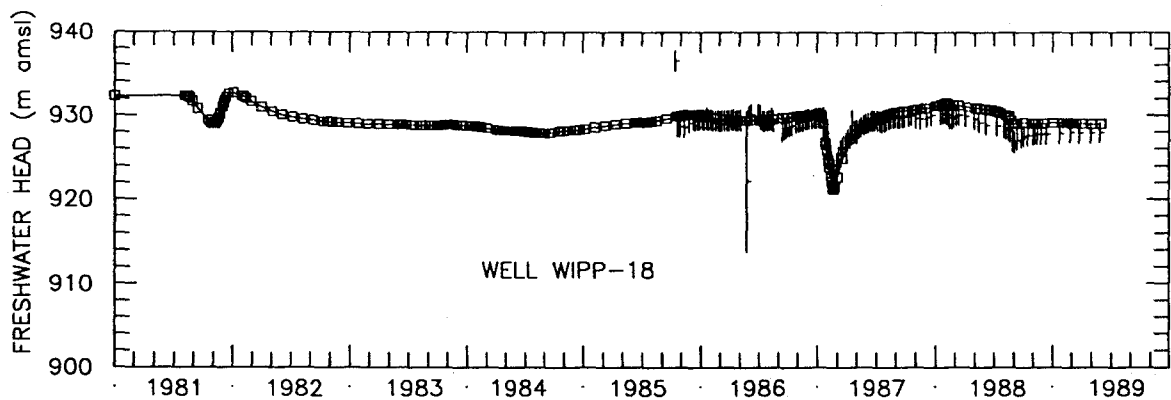
Drawn by ABW	Date 10/30/89
Checked by M.L.	Date 10/31/89
Revisions	Date
H09700R869	10/31/89

Calculated and Observed Transient Freshwater Heads at P-17, WIPP-12, and WIPP-13 Using the Transient Calibrated Transmissivity Field

**INTERA** Technologies

Figure 5.18e





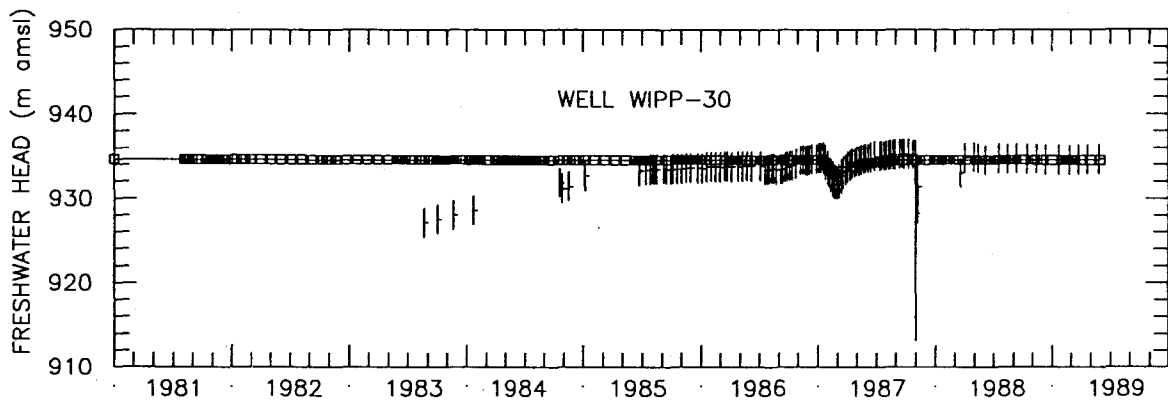
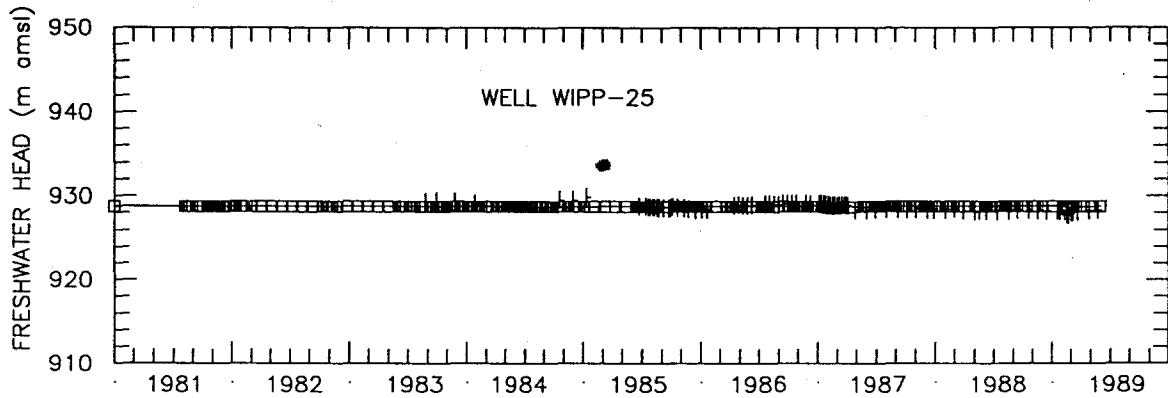
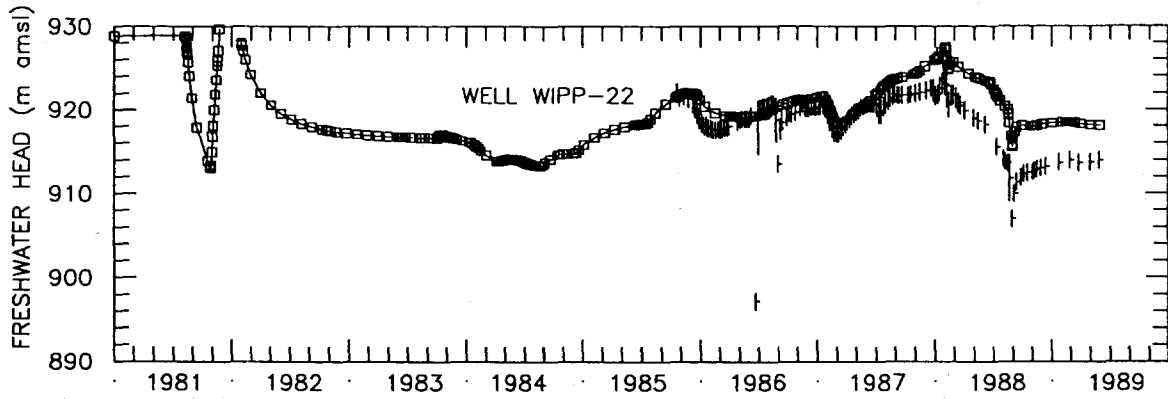
LEGEND: □-□ Calculated Freshwater Heads  
 † Observed Freshwater Heads

Drawn by ABW	Date 10/30/89
Checked by M.L.	Date 10/31/89
Revisions	Date
H09700R869	10/31/89

Calculated and Observed Transient Freshwater Heads  
 at WIPP-18, WIPP-19, and WIPP-21 Using the  
 Transient Calibrated Transmissivity Field

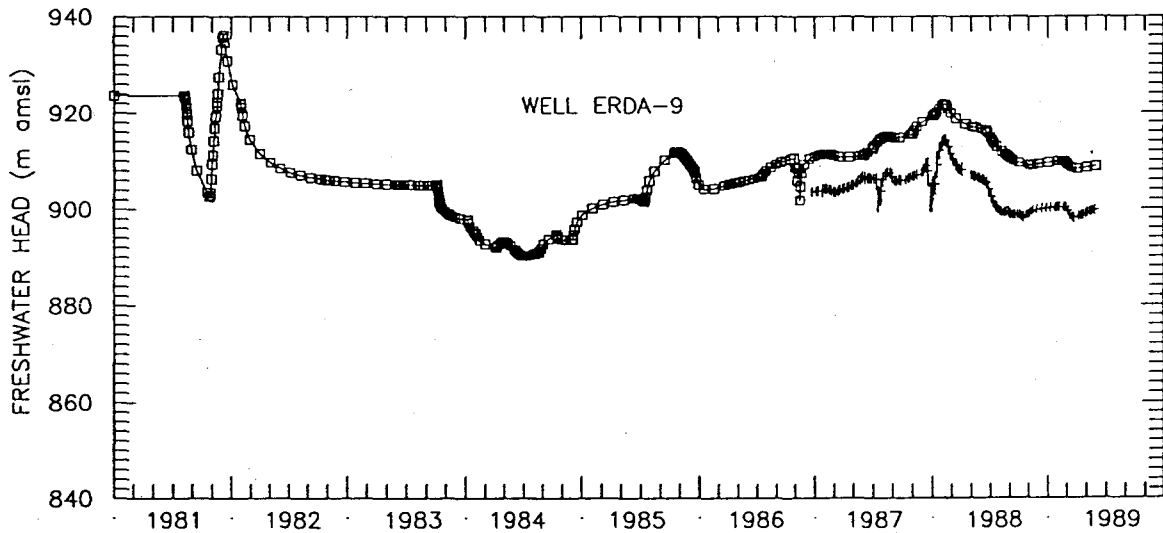
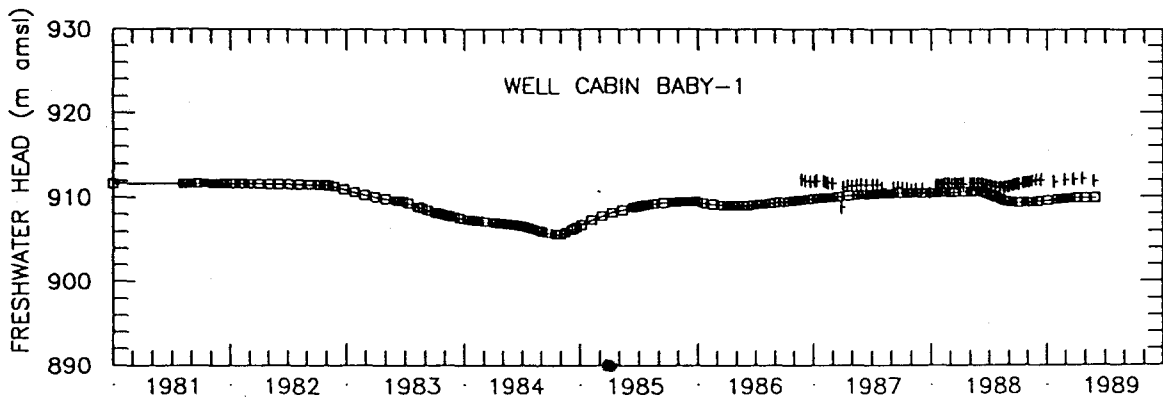
**INTERA** Technologies

Figure 5.18f



LEGEND: □—□ Calculated Freshwater Heads  
 | Observed Freshwater Heads

Drawn by ABW	Date 10/30/89	Calculated and Observed Transient Freshwater Heads at WIPP-22, WIPP-25, and WIPP-30 Using the Transient Calibrated Transmissivity Field
Checked by M.L.	Date 10/31/89	
Revisions	Date	
H09700R869	10/31/89	
<b>INTERA</b> Technologies		Figure 5.18g



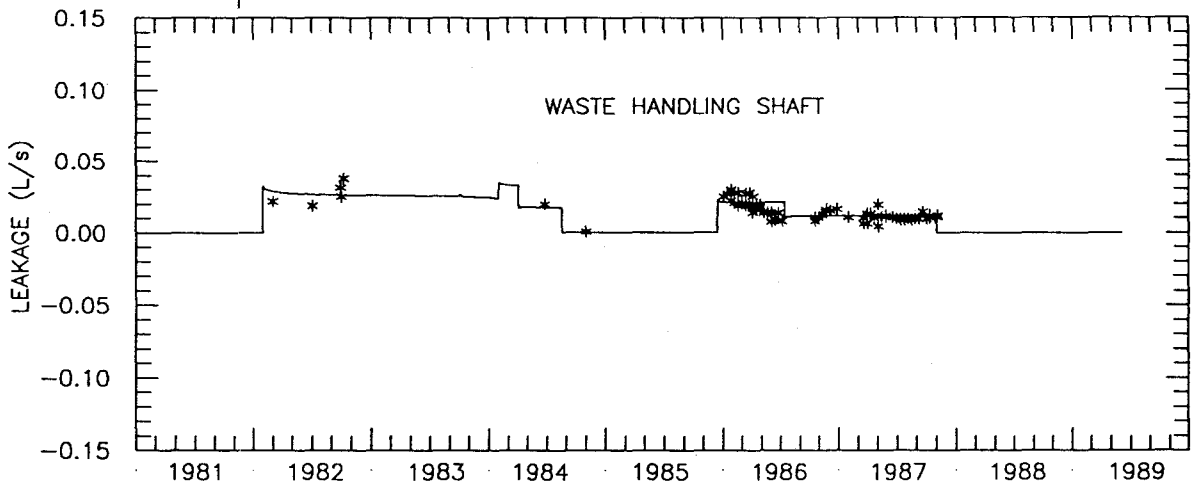
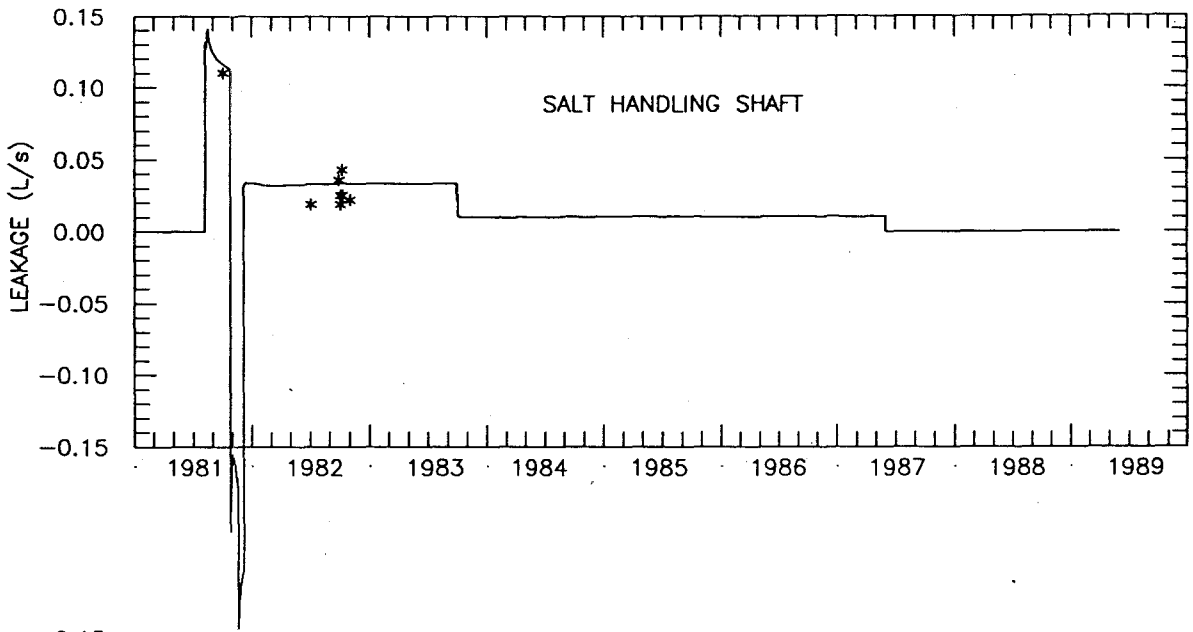
LEGEND: □—□ Calculated Freshwater Heads  
 † Observed Freshwater Heads

Drawn by ABW	Date 10/30/89
Checked by M.L.	Date 10/31/89
Revisions	Date
H09700R869	10/31/89

Calculated and Observed Transient Freshwater Heads at CB-1 and ERDA-9 Using the Transient Calibrated Transmissivity Field

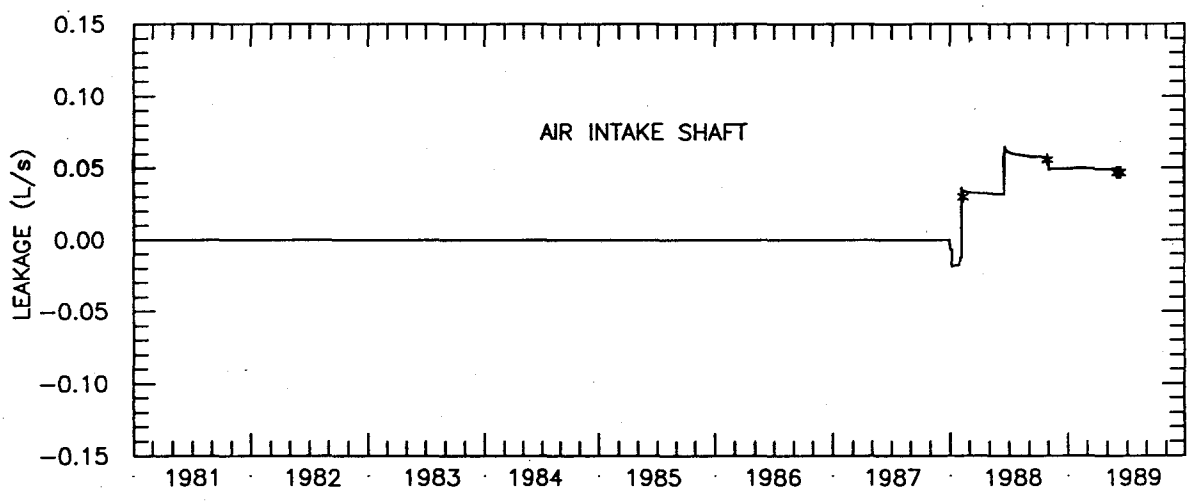
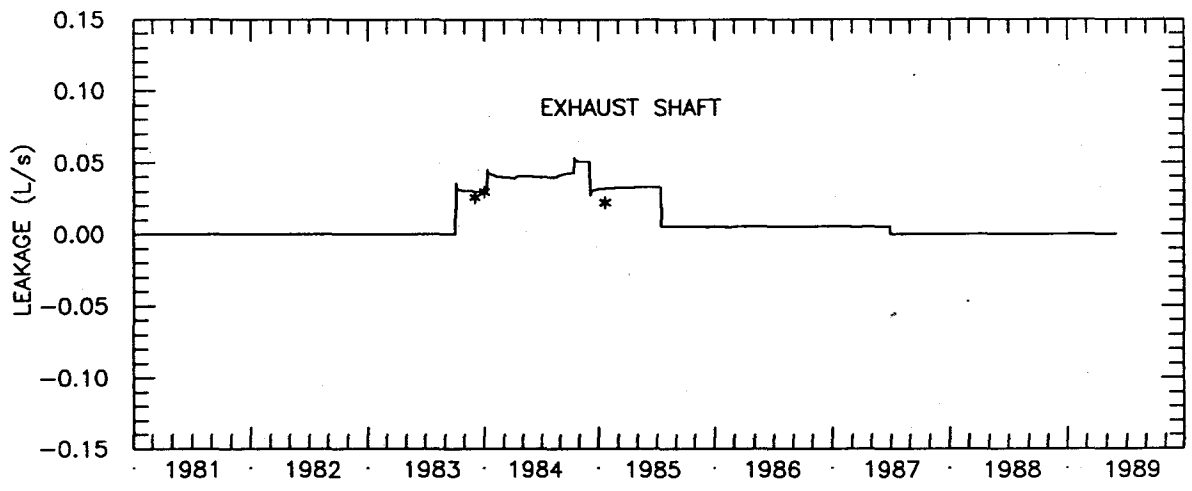
**INTERA** Technologies

Figure 5.18h



LEGEND: — Calculated Leakage Rate  
 \* Measured Leakage Rate

Drawn by ABW	Date 10/30/89	Calculated and Observed Leakage Rates at the C&SH and WHS Locations of the Transient Calibrated Model
Checked by M.L.	Date 10/31/89	
Revisions	Date	
H09700R869	10/31/89	



LEGEND: — Calculated Leakage Rate  
 \* Measured Leakage Rate

Drawn by ABW	Date 10/30/89
Checked by M.L.	Date 10/31/89
Revisions	Date
H09700R869	10/31/89

Calculated and Observed Leakage Rates at the EXS and AIS Locations of the Transient Calibrated Model

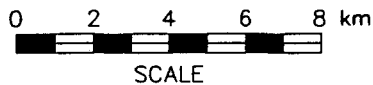
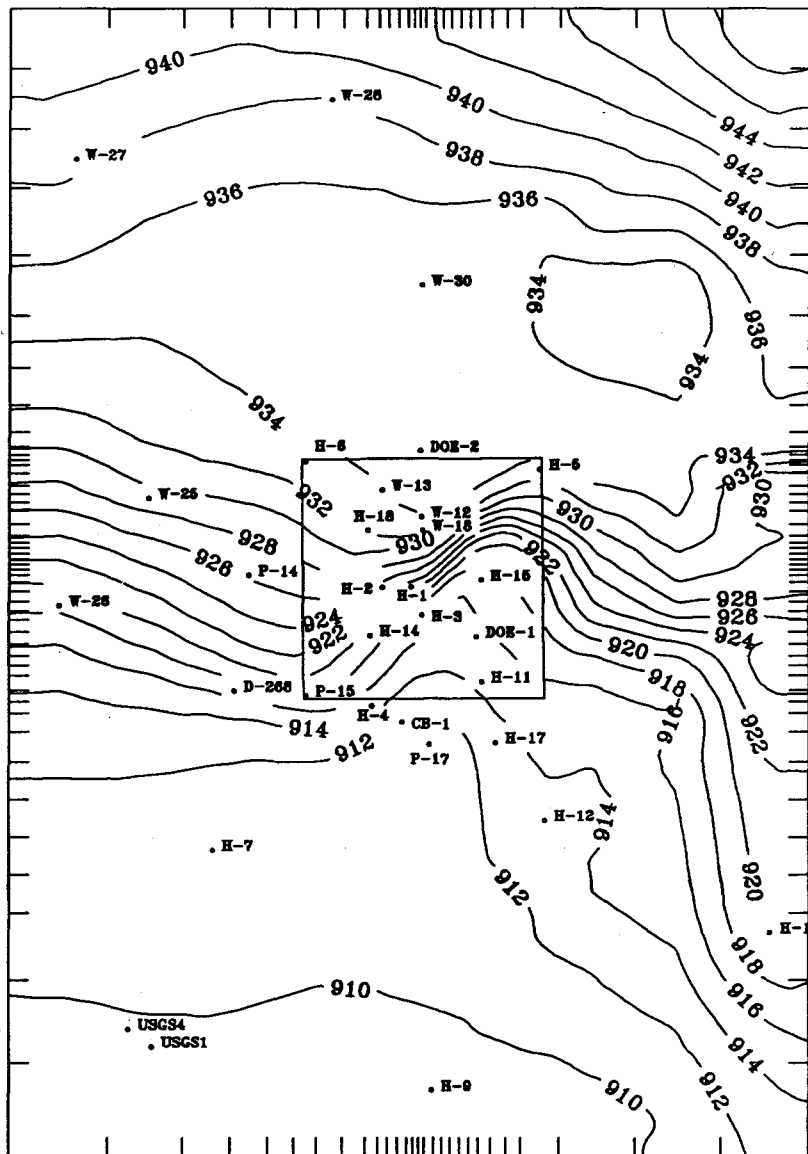
**INTERA** Technologies

Figure 5.19b

Steady-state heads were calculated using the TC transmissivity field developed during the calibration to the transient events as described in Section 5.2. Figure 5.20 shows these steady-state heads, referred to from hereon as the transient-calibrated (TC) steady-state heads, over the model region. The calculated heads are quite similar to the steady-state calibrated heads (Figure 3.10) and the observed head distribution (Figure 2.12). As in the observed head field, the TC head field has low gradients north and south of the WIPP-site boundary and an increased gradient within the WIPP-site boundary. Flow in the northern part of the WIPP site is generally from north to south. A large portion of the ground water within the WIPP-site boundary enters the high-transmissivity zone south of H-15 and exits the modeled region from the central part of the southern boundary.

The Darcy velocities of the TC steady-state heads are shown in Figure 5.21. The velocity directions and magnitudes are similar to those described for the steady-state calibrated (SSC) velocity field (Section 3.3.6). The greatest differences occur between H-1 and DOE-1 where the eastward components of the velocities in this region have increased because of the northern extension of the high-transmissivity zone. The velocities in this region range from  $3 \times 10^{-10}$  m/s near H-15 to  $2 \times 10^{-9}$  m/s between H-3 and H-11.

The head differences (the calculated heads minus the observed heads) for the transient-calibrated model are listed in Table 5.3. The differences between the calculated and observed heads are in general less than 1.5 m. The maximum head differences occur at H-14 and WIPP-18, where the calculated heads are 3.5 and 2.3 m higher than the observed heads, respectively. The observed heads at H-14 and WIPP-18 were estimated from short water-level records (Cauffman et al., 1990) which began after 1987 and 1985, respectively. Therefore, the large head differences at these locations could be due to long-term trends or other events which have affected the heads on a scale which is longer than the observed data available at these two boreholes. From examination of the transient calibrated heads at these locations (Figures 5.18c and 5.18f), it is evident that the calculated and observed heads are quite similar over the length of the measured head record which supports the conclusion that a discrepancy exists between the head value selected to represent the undisturbed conditions at these wells and the model-calculated hydrographs.



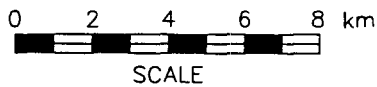
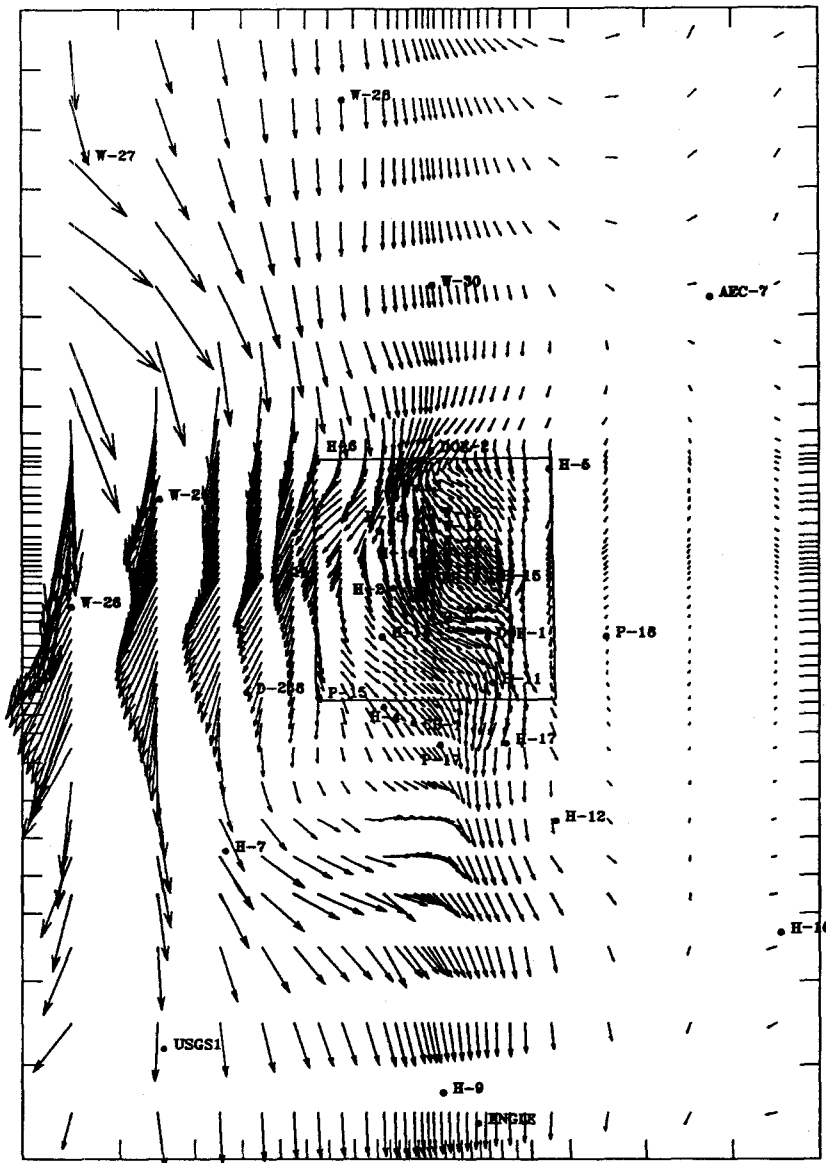
● Observation Well  
Freshwater Heads in m amsl  
Contour Interval: 2m

Drawn by	ABW	Date	10/30/89
Checked by	M.L.	Date	10/31/89
Revisions		Date	
H09700R869		10/31/89	

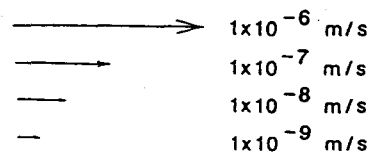
Freshwater Heads of the Transient Calibrated Model

**INTERA** Technologies

Figure 5.20



Darcy-Velocity Vector Scale



Drawn by ABW	Date 11/2/89
Checked by M.L.	Date 11/2/89
Revisions	Date
H09700R869	11/2/89

Darcy-Velocity Vectors of the Transient  
Calibrated Model

**INTERA** Technologies

Figure 5.21



<u>Location</u>	<u>Difference Between Calculated and Observed Freshwater Head (m)</u>
-----------------	---

H-1	-0.95
H-2	1.77
H-3	-0.33
H-4	1.62
H-5	-1.20
H-6	0.23
H-7	-1.69
H-9	0.78
H-10	-2.07
H-11	1.13
H-12	-0.44
H-14	3.52
H-15	1.33
H-17	1.81
H-18	0.09
P-14	-1.02
P-15	0.93
P-17	-1.23
WIPP-12	1.01
WIPP-13	-0.41
WIPP-18	2.29
WIPP-25	0.07
WIPP-26	-0.98
WIPP-27	0.38
WIPP-28	0.56
WIPP-30	-0.66
CB-1	0.01
DOE-1	0.92
DOE-2	-0.06
D-268	1.40
USGS-1	0.18
USGS-4	0.18

Drawn by	Date
Checked by	Date
Revisions	Date

Differences Between Calculated and Observed  
Freshwater Heads for the Transient Calibrated  
Model

**INTERA** Technologies

Table 5.3

Most of the boreholes located in the central WIPP-site area were not drilled until after the shaft activities had begun. The undisturbed freshwater heads at these boreholes (i.e., H-11, H-14, H-15, H-18, DOE-1, WIPP-12, WIPP-13, and WIPP-18) were, therefore, estimated from water-level records possibly affected by the shafts' construction. An attempt was made to reconcile the residual effects caused by the shafts' construction. Initially, only the H-11, H-15, H-18, and DOE-1 boreholes were believed to still be recovering from the drawdown caused by the shafts. Residual head values of 0.5, 1.5, 0.4, and 0.5 m were therefore added to the undisturbed heads picked from the recorded water levels at the H-11, H-15, H-18, and DOE-1 boreholes, respectively, to account for the drawdowns at these wells from shaft construction. The next two paragraphs examine the adequacy of the initial residual head values mentioned above and attempt to resolve the large head differences at the H-14 and WIPP-18 boreholes.

The discrepancies mentioned above between the H-14 and WIPP-18 steady-state head differences and their transient calibrated heads may stem from the inability to accurately account for residual effects because of the short water-level record at these locations. The H-14, and to a lesser extent WIPP-18, transient calibrated heads shown in Figures 5.18c and 5.18f depict a decline in the head values from 1981 to mid-1984. This decline is likely due to hydraulic stress generated by excavation of the C&SH shaft, WHS, and EXS after 1981. The calculated heads in Figure 5.18c also illustrate the response at H-14 due to H-3 pumping in 1984 and 1985. There is an approximate four-meter decrease in the calculated heads at H-14 from early 1981 to mid-1987. This decrease in the calculated heads after 1981 at both H-14 and WIPP-18 provides a good match to the observed water levels beginning in early 1987 for H-14 and 1986 for WIPP-18 (i.e., during the observed water-level records). The discrepancy between the steady-state head differences and the transient calibrated head fits at H-14 and WIPP-18 may, therefore, be due to inaccurate estimates of the residual effects present at these boreholes.

Table 5.4 reflects an adjustment of the central WIPP-site boreholes undisturbed heads based on the estimated residual effects as determined from the hydrographs of the calculated transient heads. This table attempts to improve the estimates at the boreholes which have short water-level records and which have been affected by the

Well	Initial Selected Undisturbed Freshwater Head (m)	Date of Selection	Model-Calculated Freshwater Head (m) @ t=0	Model-Calculated Freshwater Head (m) @ t=Selection Date	Difference Between Calculated Head (m) at t=0 and t=selection Date *	Initial Estimation of Residual Head at Borehole (m)	Adjusted Undisturbed Head (m)**	Difference Between Model-Calculated and Adjusted Undisturbed Head (m)
H-11	913.1	07/87	914.2	912.2	+2.0	+0.5	914.6	-0.4
H-14	915.2	05/87	918.7	915.5	+3.2	0.0	918.4	-0.3
H-15	915.7	04/87	917.0	914.1	+2.9	+1.5	917.1	-0.3
H-18	932.1	12/88	932.2	930.8	+1.4	+0.4	933.1	-0.9
DOE-1	914.2	07/87	915.2	913.0	+2.2	+0.5	915.9	-0.7
WIPP-12	932.5	01/87	933.5	932.6	+0.9	0.0	933.4	0.1
WIPP-13	934.0	09/87	933.6	933.3	+0.3	0.0	934.3	-0.7
WIPP-18	930.0	10/87	932.3	930.5	+1.8	0.0	931.8	0.5

\* This column may also be referred to as the model calculated residual head.

\*\* Adjusted undisturbed head = initial selected undisturbed head + (difference between model calculated residual head and initial estimation of residual head)

construction of the shafts. The columns in Table 5.4 contain the central WIPP-site boreholes in which an undisturbed-head value was estimated, the date for the estimate, the calculated steady-state head, and the transient calibrated head at the date of the undisturbed-head estimate. The difference between the columns containing the calculated steady-state head and the transient calibrated head represents the calculated residual head. The calculated residual heads at H-14 and WIPP-18 are equal to 3.2 and 1.8 m, respectively. The estimated residual heads from Cauffman et al. (1990) are also presented in Table 5.4. The difference between the calculated and estimated residual head is added to the original undisturbed head to achieve an adjusted undisturbed head. Thus, the adjusted undisturbed heads contain a residual effect which is probably much closer to the actual residual than that initially estimated in Cauffman et al. (1990) and which agrees well with the calculated steady-state heads. Adjustments in the undisturbed heads were also performed for other central WIPP-site boreholes including H-11, H-15, H-18, DOE-1, WIPP-12, and WIPP-13. Table 5.5 presents the revised undisturbed heads which includes updates for the boreholes which had adjusted undisturbed heads and the differences between the transient calibrated and revised undisturbed heads.

#### 5.4 The Transient Calibrated Transmissivity Field

The transient calibrated (TC) transmissivity field considered to reproduce the observed steady-state and transient freshwater heads adequately is shown over the model area in Figure 5.22a and within the WIPP-site boundary in Figure 5.22b. The TC transmissivity field is very similar to the steady-state calibrated (SSC) transmissivity field (Figure 3.9a) with the major differences occurring south of WIPP-30 and in the H-11 region (Figure 5.22c). The transmissivities between WIPP-30 and DOE-2 range from  $1 \times 10^{-4}$  to  $1 \times 10^{-5}$  m<sup>2</sup>/s, which is an increase of between 0.5 to 1.0 orders of magnitude. The increase in this region was required to improve the fit at WIPP-30 in response to the WIPP-13 multipad pumping test. The transmissivities between H-11 and DOE-1 range from  $1 \times 10^{-4}$  to  $3 \times 10^{-5}$  m<sup>2</sup>/s, which is an increase of approximately 0.5 order of magnitude. The transmissivities between DOE-1 and H-15 range from  $3 \times 10^{-5}$  to  $3 \times 10^{-6}$  m<sup>2</sup>/s, which is an increase of between 0.5 to 1.5 orders of magnitude. The increase in this region was required to improve the transient-head fits at DOE-1 and H-15 in response to the H-11 multipad pumping

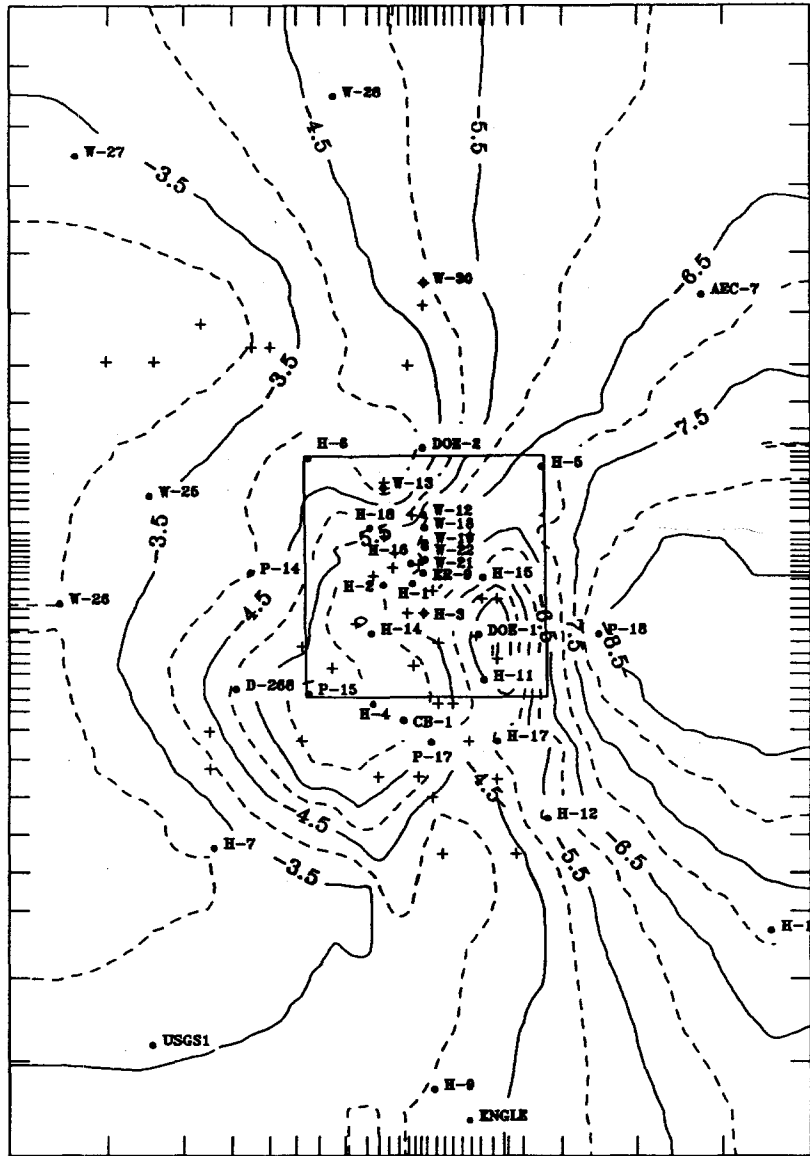
<u>Location</u>	<u>Revised Undisturbed Equivalent Freshwater Head (m amsl)</u>	<u>Differences Between Calculated and Revised Undisturbed Heads (m)</u>
H-1	923.3	-0.95
H-2	923.1	1.77
H-3	917.1	-0.33
H-4	912.8	1.62
H-5	934.0	-1.20
H-6	932.6	0.23
H-7	912.5	-1.69
H-9	907.6	0.78
H-10	921.4	-2.07
H-11	914.6	-0.40
H-12	913.7	-0.44
H-14	918.4	-0.30
H-15	917.1	-0.30
H-17	911.0	1.81
H-18	933.1	-0.90
DOE-1	915.9	-0.70
DOE-2	935.3	-0.06
P-14	926.9	-1.02
P-15	916.8	0.93
P-17	911.6	-1.23
WIPP-12	933.4	0.10
WIPP-13	934.3	-0.70
WIPP-18	931.8	0.50
WIPP-25	928.7	0.07
WIPP-26	919.3	-0.98
WIPP-27	938.1	0.38
WIPP-28	937.2	0.56
WIPP-30	935.3	-0.66
CB-1	911.6	0.01
USGS-1	909.7	0.18
USGS-4	909.7	0.18
USGS-8	911.1	0.18
D-268	915.0	1.40

Drawn by	Date
Checked by	Date
Revisions	Date

Revised Undisturbed Freshwater Heads and the Differences Between the Model-Calculated and Revised Undisturbed Freshwater Heads

**INTERA** Technologies

Table 5.5



● Observation Well  
 + Pilot-Point Location  
 Transmissivities in  $\log_{10} \text{ m}^2/\text{s}$   
 Contour Interval:  $0.5 \log_{10} \text{ m}^2/\text{s}$

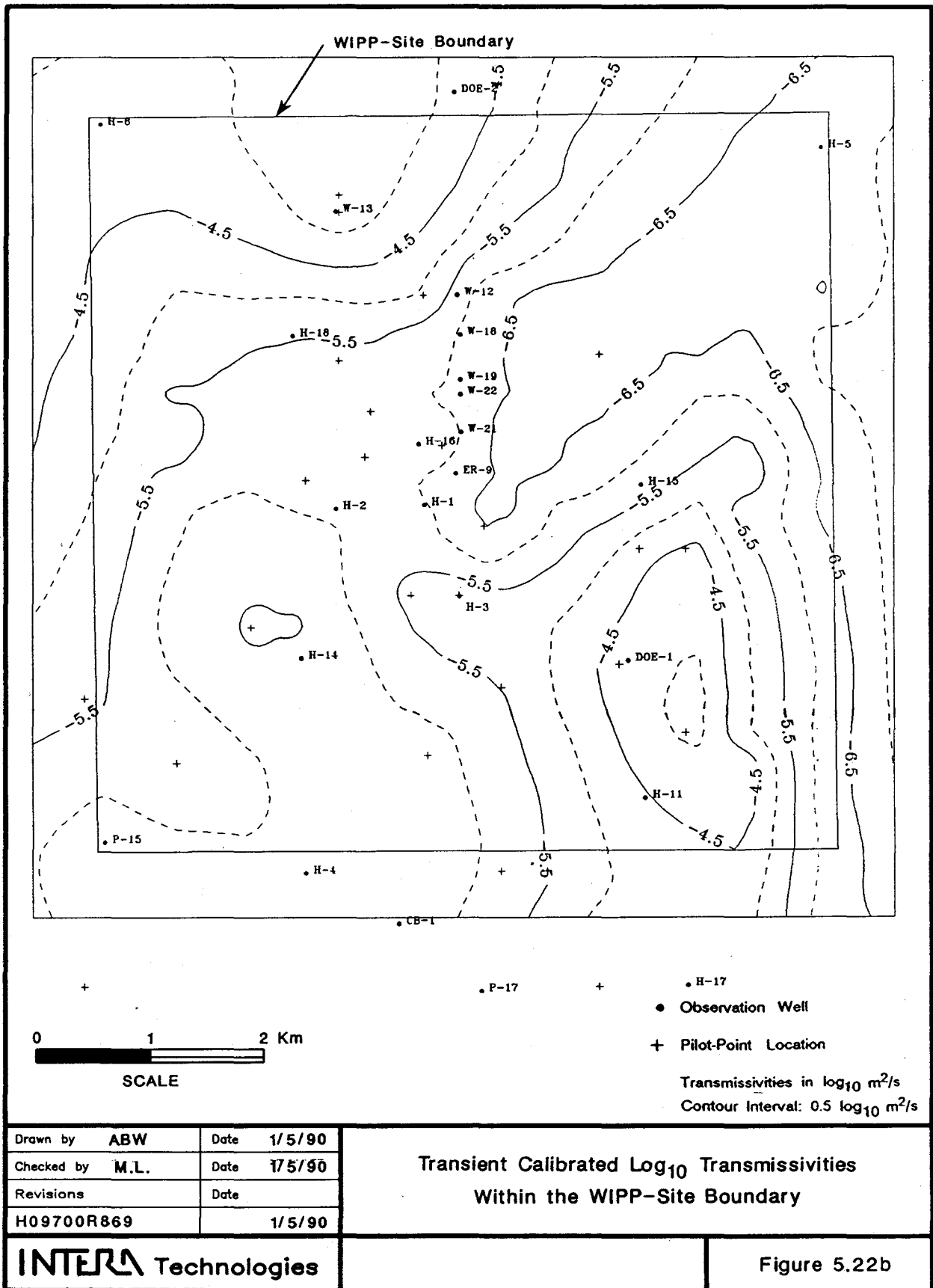
0 2 4 6 8 km  
 SCALE

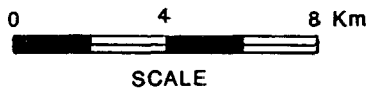
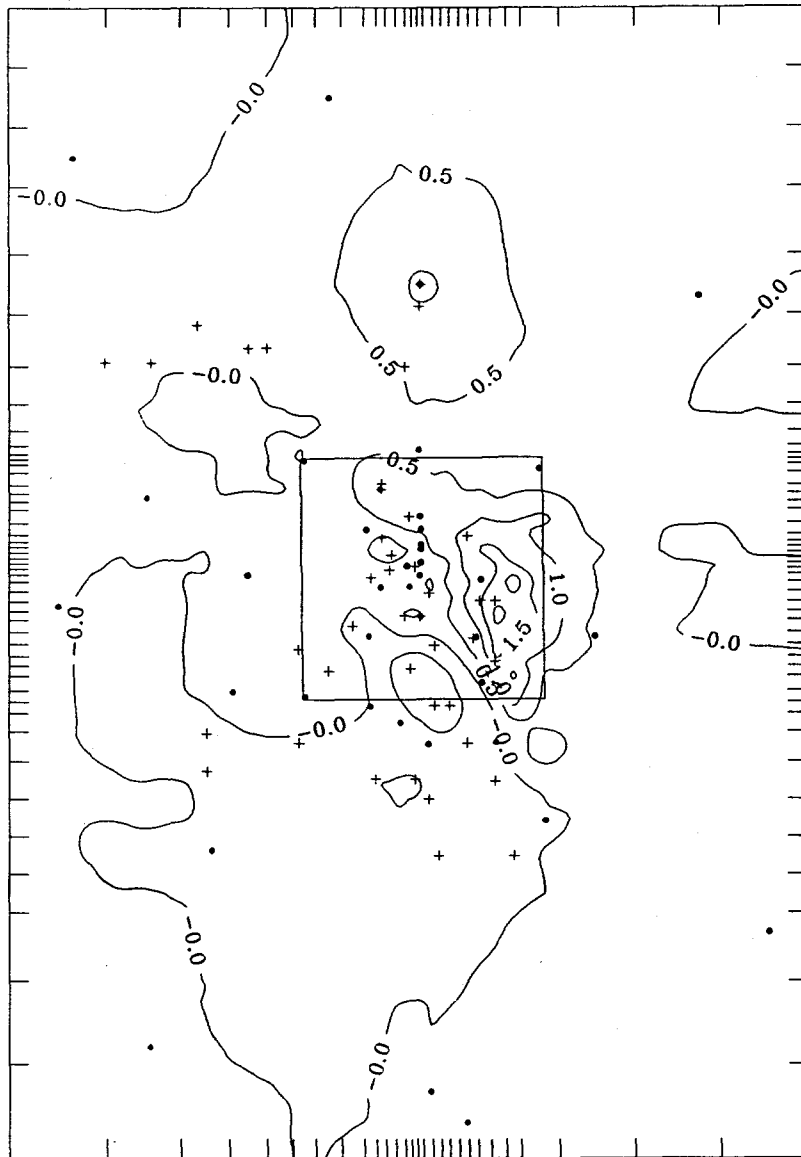
Drawn by ABW	Date 10/30/89
Checked by M.L.	Date 10/31/89
Revisions	Date
H09700R869	10/31/89

The Transient Calibrated  $\log_{10}$  Transmissivities

**INTERA** Technologies

Figure 5.22a





● Observation Well  
 + Pilot-Point Location  
 Contour Interval: 0.5 log<sub>10</sub> m<sup>2</sup>/s

Drawn by ABW	Date 1/5/90
Checked by M.L.	Date 1/5/90
Revisions	Date
H09700R869	1/5/90

Log<sub>10</sub> Transmissivity Differences Between  
 the Transient Calibrated and Steady-State  
 Calibrated Transmissivity Fields

**INTERA** Technologies

Figure 5.22c



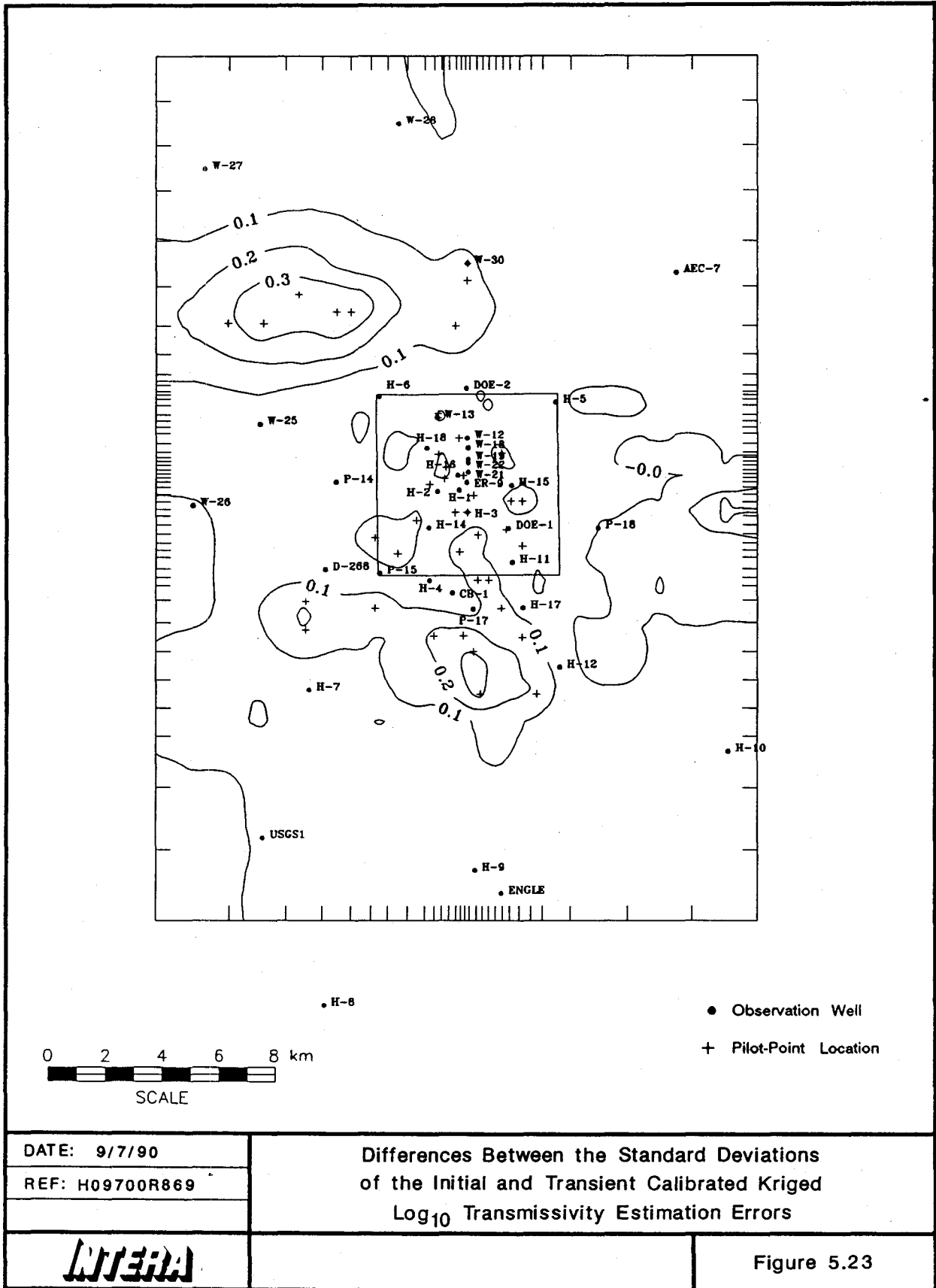
tests. The increase in the transmissivities south of H-15 have extended the high-transmissivity feature surrounding H-11 and DOE-1 to the north. This is the most significant change in the TC transmissivity field in comparison to the SSC transmissivity field.

The generalized covariance function (GCF) used to estimate grid-block transmissivities in this study was kept constant throughout steady-state and transient model calibration. The process used to determine the GCF was repeated to verify that the addition of the pilot points to the observed transmissivity data did not significantly change the covariance structure of the observed data. The zero-order GCF determined consistent with the observed data and the pilot points is:

$$K(h) = -3.6 \times 10^{-4}|h| \quad (5.2)$$

This model has a similar order (zero-order), form (linear), and coefficient ( $-3.6 \times 10^{-4}$ ) compared to Equation 2.5 which was used throughout this study. Considering that the determination of covariance structure performed in AKRIP is an automatic procedure and that there are over 20 different possible covariance models (in AKRIP), the difference between the coefficients in Equations 5.2 and 2.5 is not significant. Therefore, the addition of the pilot points did not significantly affect the covariance structure of the observed transmissivity field. In addition, the GCF listed in Equation 2.5 adequately represents the covariance of the observed transmissivity data and the pilot-point transmissivities.

The addition of the pilot points did however have an impact upon the standard deviations of the estimation errors of the block-averaged  $\log_{10}$  transmissivities. Figure 5.23 illustrates the difference between the initial standard errors (Figure 2.10b) and the standard errors obtained for the transient calibrated block-averaged  $\log_{10}$  transmissivities. The major differences between the standard deviations occur in the northwestern portion of the model area and south of the P-17 borehole location where the initial standard deviations are approximately 0.3 higher than the standard deviations of the calibrated  $\log_{10}$  transmissivity field. The differences are higher in these two areas due to the addition of several local pilot points. The standard-deviation differences within the WIPP-site boundary are small, 0.0 to 0.1, due to the number of observed transmissivity values in this area.



DATE: 9/7/90  
 REF: H09700R869

Differences Between the Standard Deviations  
 of the Initial and Transient Calibrated Kriged  
 Log<sub>10</sub> Transmissivity Estimation Errors



Figure 5.23

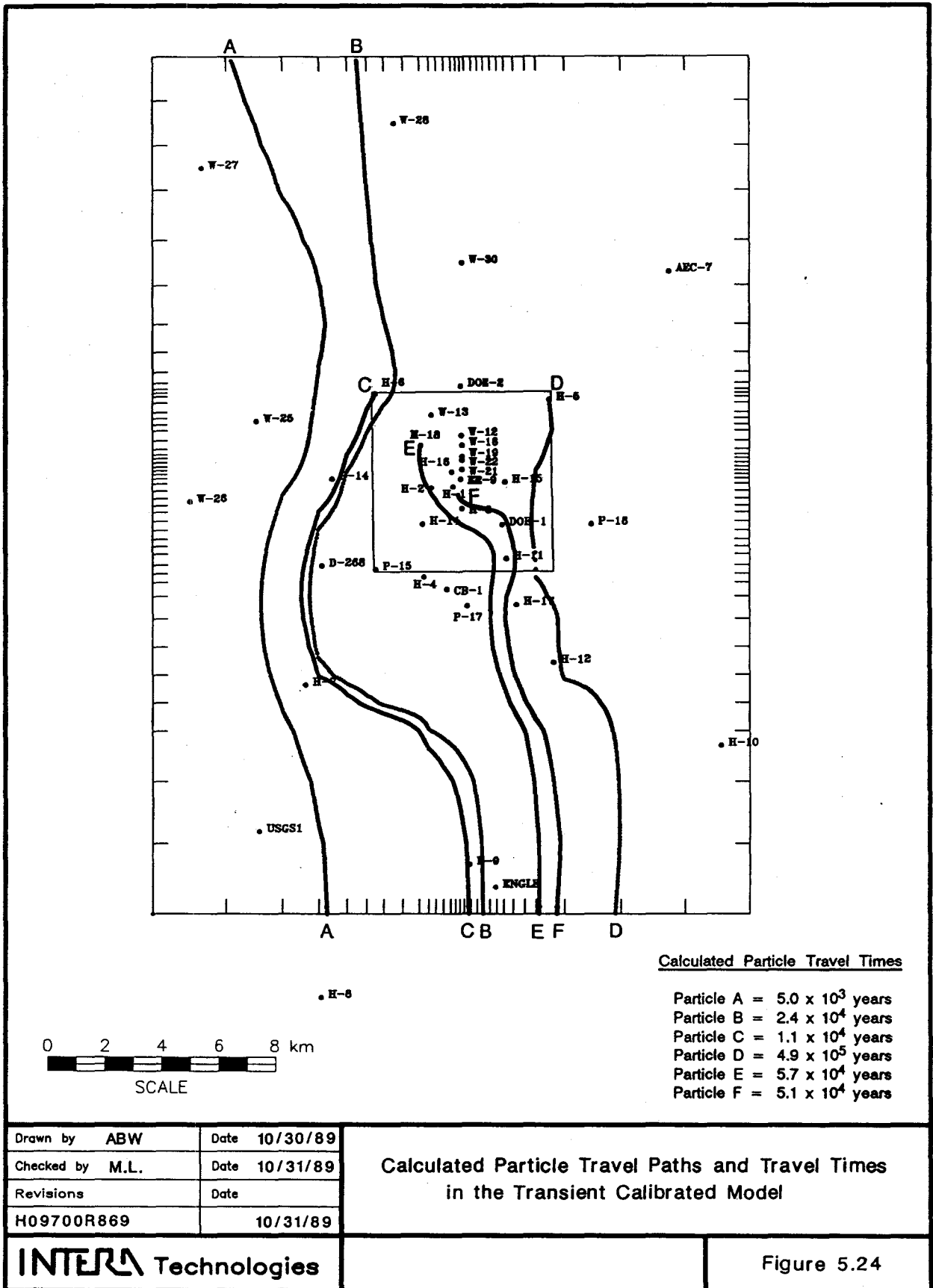
However, since the actual perturbations which were imposed upon the pilot point's  $\log_{10}$  transmissivity values are not incorporated into the calculation of the block-averaged standard errors, one must use caution in applying the standard errors calculated for the calibrated block-averaged  $\log_{10}$  transmissivity field for subsequent uncertainty analysis. An analysis of the actual changes to the grid-block transmissivity values should be investigated prior to using the mean estimates and their standard deviations in a stochastic framework.

### 5.5 Calculated Particle Travel Times in the Model Region

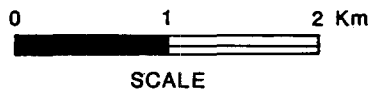
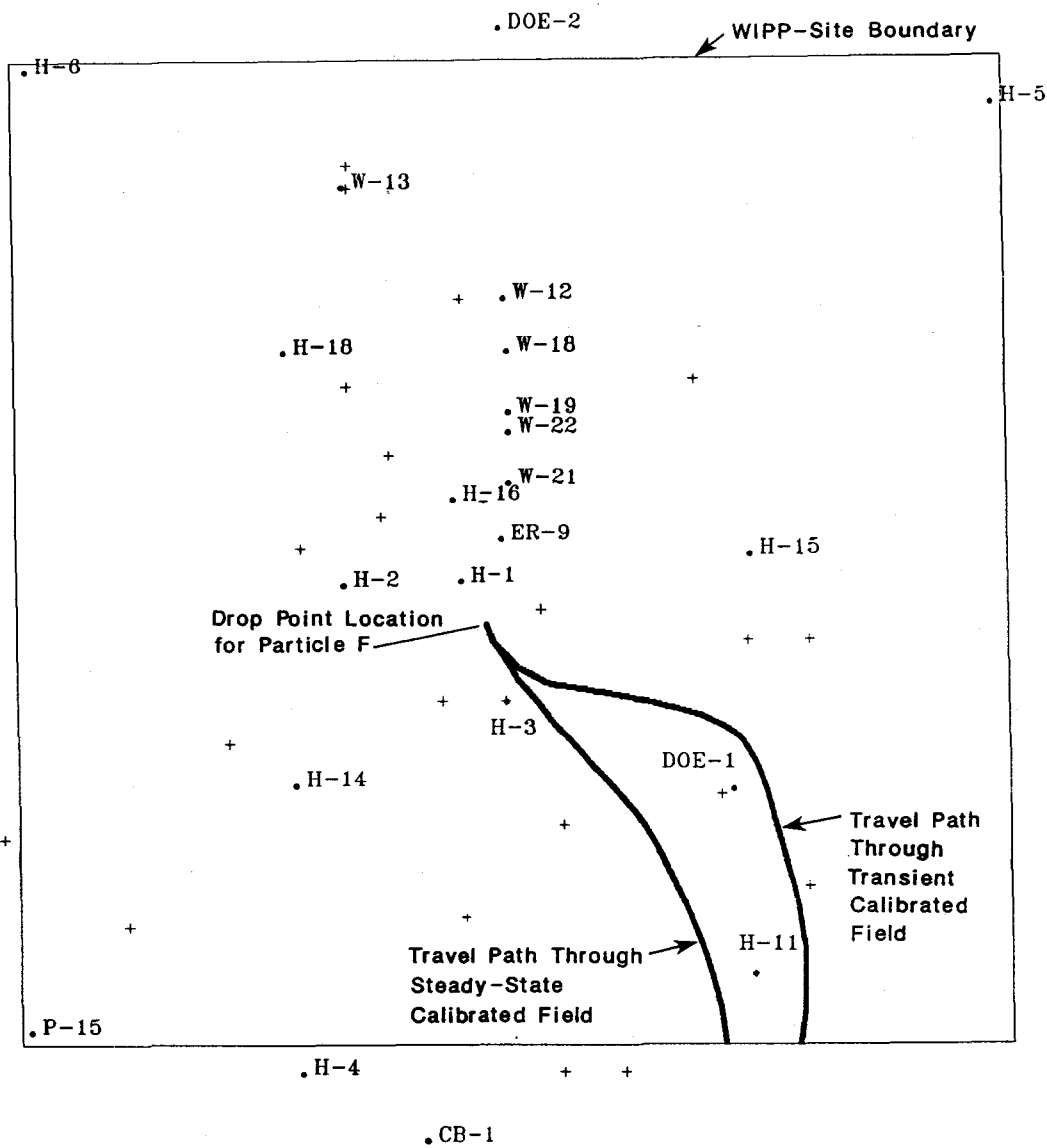
Calculations were performed for the release of the same six particles discussed in Section 3.3.7 in the flow field defined by the steady-state calibrated heads of the TC model. Figure 5.24 illustrates the particle travel paths for all six particles. The paths are consistent with the velocity vectors illustrated in Figure 5.21. The shortest travel times occur in the western part of the model area where Particles A and B have values of approximately  $5.0 \times 10^3$  and  $2.4 \times 10^4$  years, respectively. Both of these particles traveled directly south in the area representing Nash Draw where the Darcy velocities range from  $5 \times 10^{-8}$  to  $5 \times 10^{-7}$  m/s. Particle B initially travels southward but is redirected southwestward after passing near the H-6 borehole.

The travel path of Particle C, originating at H-6, is oriented southwest because the ground-water flow in this area is oriented away from the relatively low transmissivities south of H-6. The travel path is eventually redirected southeast starting near H-7 and exits the southern model boundary with a total particle travel time of  $1.1 \times 10^4$  years. Particle D was released from a location coincident with H-5 and exits the model area from the southern boundary in  $4.9 \times 10^5$  years. The calculated travel time for Particle D is long because of the low-calculated Darcy velocities ( $1 \times 10^{-11}$  to  $1 \times 10^{-10}$  m/s) near the eastern WIPP-site boundary and because Particle D does not enter the high-velocity zone between H-17 and P-17 which is generated by the high-transmissivity zone described in Section 3.3.5.

Particles E and F were released in the central part of the WIPP site. The release point for Particle E is slightly south of H-18. The particle then travels southeast toward H-3, enters the high-velocity zone near H-11 and reaches the southern model boundary in  $5.7 \times 10^4$  years. Particle F was released in the Culebra from a point



coincident with the centroid of the underlying repository area. This release point was used as the base-case release point in Reeves et al. (1987). The calculated particle travel time for Particle F to reach the southern WIPP-site boundary is approximately  $1.4 \times 10^4$  years, which is about one-quarter of the total travel time to the southern model boundary ( $5.1 \times 10^4$  years). The distance of the travel path for Particle F, 4140 m, increased relative to that determined using the SSC transmissivity field, 3370 m (Figure 5.25), while the total travel time decreased thirty percent (i.e., from  $2.1 \times 10^4$  to  $1.4 \times 10^4$  years). The decrease in travel time to the southern WIPP-site boundary is primarily due to the extension of the higher transmissivity feature north toward H-15. The travel time for Particle F is approximately the same as the travel time to the accessible environment (southern WIPP-site boundary) presented in LaVenue et al. (1988).



- Observation Well
- + Pilot-Point Location

Drawn by	ABW	Date	1/5/90
Checked by	M.L.	Date	1/5/90
Revisions		Date	
H09700R869		1/5/90	

Comparison of Particle Travel Paths Through the Steady-State Calibrated and Transient Calibrated Transmissivity Fields

**INTERA** Technologies

Figure 5.25

## 6.0 SENSITIVITY OF THE TRANSIENT CALIBRATED MODEL

Several sensitivity calculations were performed to determine the effect that general changes in the grid-block transmissivities or assigned boundary pressures have on the transient-calibrated steady-state heads and the calculated travel time to the southern WIPP-site boundary. GRASP II was used to conduct these calculations. In addition to the above GRASP II sensitivity calculations, several additional SWIFT II simulations were also performed to investigate the sensitivity of the calculated transient pressures at the H-1, WIPP-21, and ERDA-9 boreholes to shaft leakage.

The initial set of calculations, presented in Section 6.1, investigated the sensitivity of the calculated pressures over the model region to the model transmissivities. These sensitivities are useful in identifying which regions have the greatest impact on the calculated pressures over the model region. The subsequent set of sensitivity calculations focused on the sensitivity of the calculated pressures to the assigned boundary pressures (Section 6.2). These sensitivities are of interest because they provide insight to the effect the boundaries have on the steady-state pressures. The third set of calculations determined the sensitivity of the particle travel time to the model transmissivities and assigned boundary pressures and is presented in Section 6.3. The results of the sensitivity calculations for shaft leakage are presented in Section 6.4.

There are two objectives in performing the above sensitivity calculations. The first objective focuses on the determination of the most sensitive regions and parameters of the model area. However, even though the model results may be sensitive to a parameter within a specific region of the model, if the data (i.e., the sensitive parameter) certainty in the model region is high enough to restrict changes to the assigned values in the model, then the sensitivity of the parameter becomes less important from a site-characterization viewpoint. Thus, the second objective focuses on whether or not adequate data coverage and data certainty exists in the WIPP-site area.

### 6.1 Sensitivity of Calculated Pressures to Model Transmissivities

GRASP II allows for the determination of the sensitivity of various performance measures (i.e., pressure at a single location or a sum of the pressures at a number of

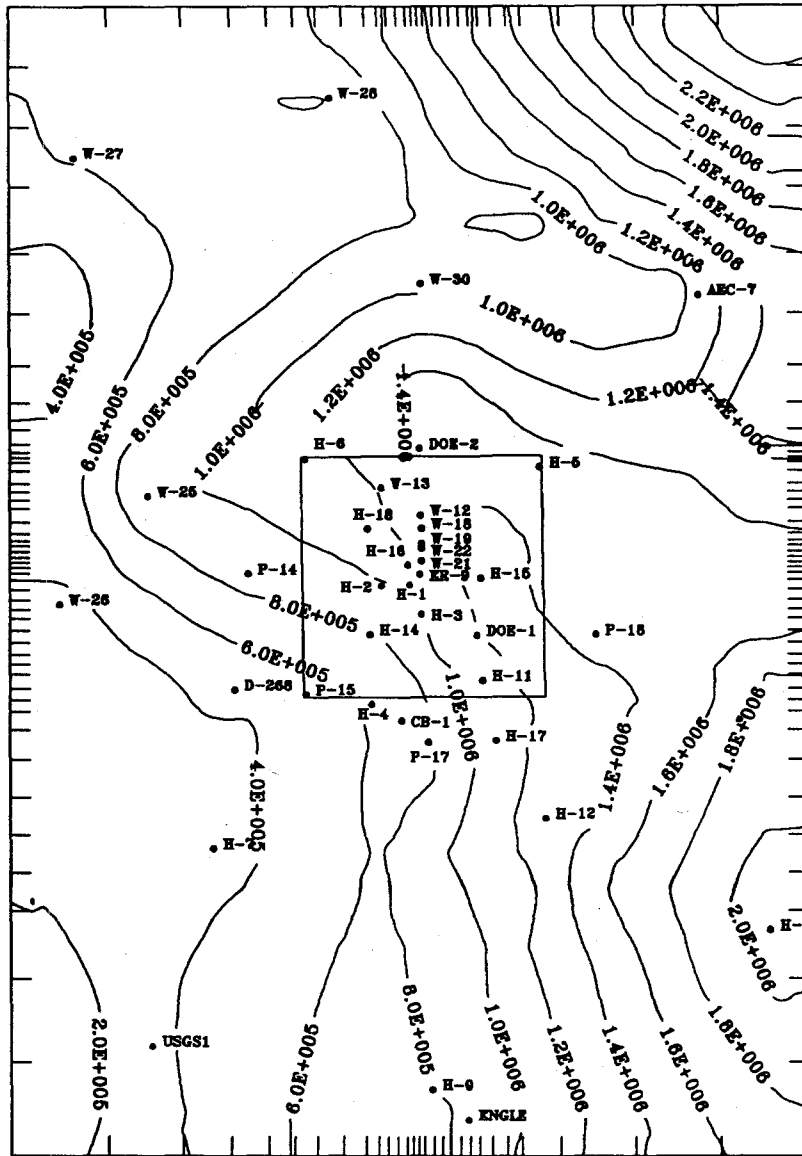
locations) to a selected sensitivity parameter (i.e., grid-block transmissivities or specified boundary pressures) by differentiating the matrix equations for flow contained in SWIFT II. The details of the sensitivity calculations performed by GRASP II are outlined in RamaRao and Reeves (1990).

The initial performance measures used during the sensitivity calculations described in Sections 6.1 and 6.2 focus on three major regions of the model, the northwestern model area, the southern model area, and the area within the WIPP-site boundary. The sensitivity of the pressures at the boreholes in these areas to changes in the model transmissivities is the topic of this section.

The pressures at grid-block elevation over the entire model area are shown in Figure 6.1. Figure 6.2 depicts the sensitivity to transmissivities of a performance measure consisting of the sum of the calculated steady-state pressures at grid-block elevation for the northwest boreholes (WIPP-25, WIPP-26, WIPP-27, WIPP-28, WIPP-30, H-6, P-14, and DOE-2),  $6.9 \times 10^6$  Pa. The contours depict dimensionless sensitivities (RamaRao and Reeves, 1990) which represent the percentage change in the performance measure (the sum of the grid-block pressures at grid-block elevation) for a one percent change in the value of the grid-block transmissivity. Figure 6.2 displays a high-sensitivity region in the northwest model region signifying the dependence of the calculated pressures at the northwest borehole locations to the local transmissivities. For example, if the transmissivities of the four grid blocks within the  $1 \times 10^{-3}$  contour were increased by 50 percent, the performance measure would be increased by approximately 0.32 percent (= sum of sensitivities x percentage change in sensitivity parameter), or  $2.2 \times 10^4$  Pa. This increase relates to an approximate total rise in freshwater head of 2.3 m, which would be distributed among the boreholes making up the performance measure.

In addition to the positive-sensitivity region to the northwest, a region of high-negative sensitivity exists between the WIPP-25 and WIPP-26 boreholes (Figure 6.2). This implies that if the transmissivities in this region are increased, additional ground-water flow would occur southward draining the pressures from the northern borehole locations and reducing the performance measure.

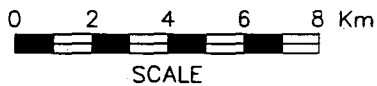




● Observation Well

Pressures in Pa

Contour Interval:  $2 \times 10^5$  Pa

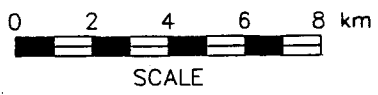
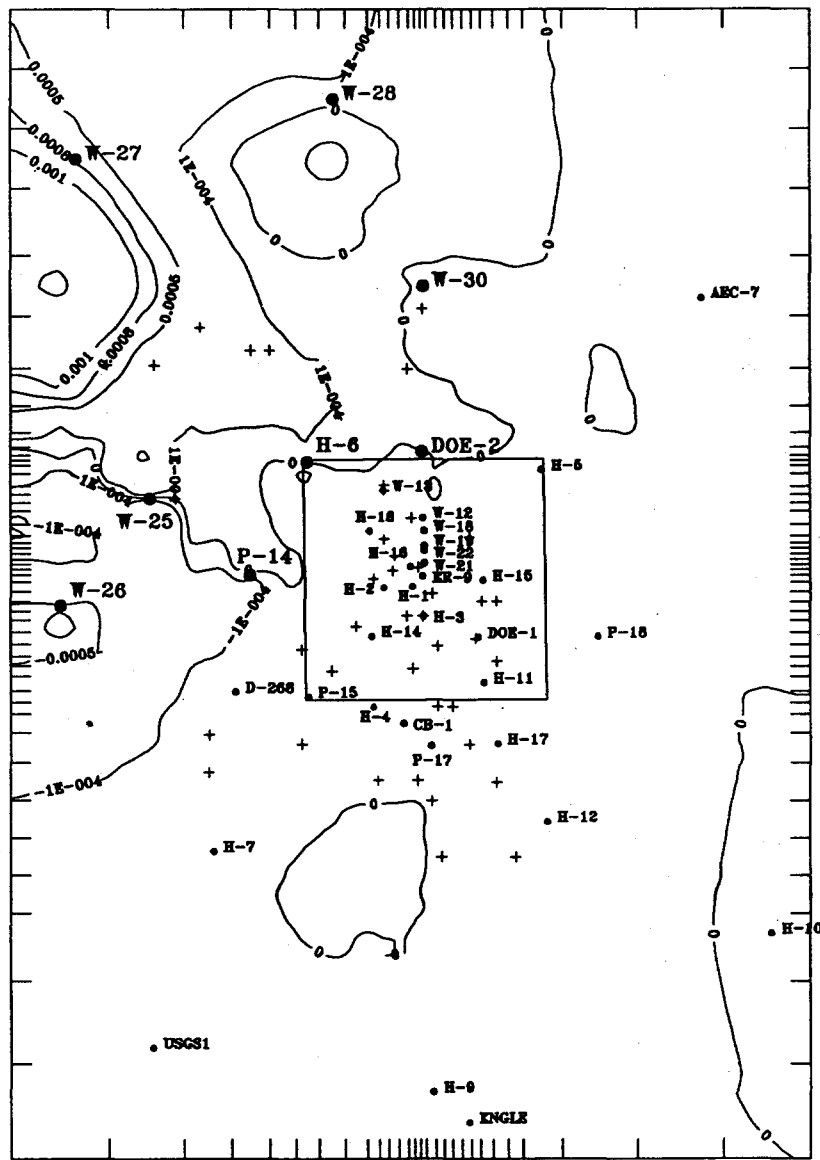


Drawn by ABW	Date 10/30/89
Checked by M.L.	Date 10/31/89
Revisions	Date
H09700R869	10/31/89

Steady-State Pressures at Grid-Block Elevation for the Transient Calibrated Model

**INTERA** Technologies

Figure 6.1



● Observation Well  
 + Pilot-Point Location  
 Contour Interval: Variable  
 Sensitivity Contours are Dimensionless

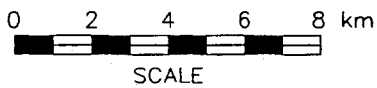
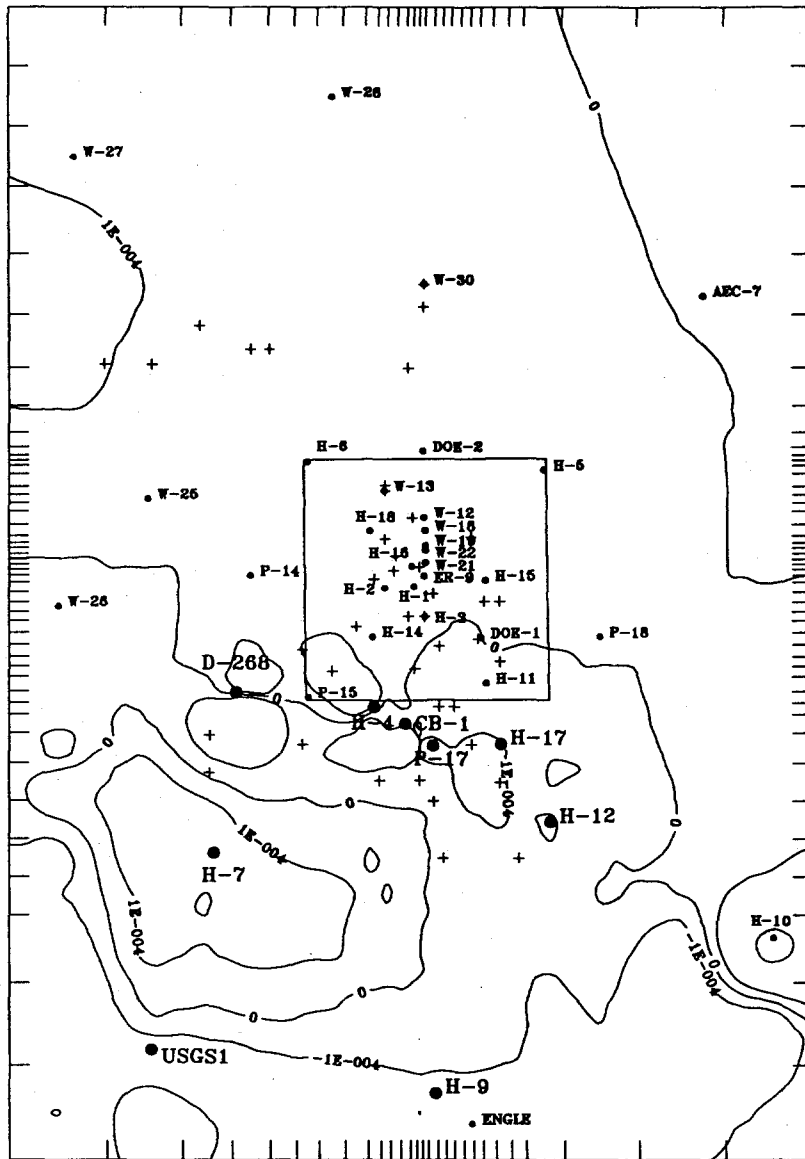
Drawn by ABW	Date 10/30/89	<b>Dimensionless Sensitivities of the Sum of the          Northwest Borehole Pressures at Grid-Block Elevation          to Grid-Block Transmissivities</b>
Checked by M.L.	Date 10/31/89	
Revisions	Date	
H09700R869	10/31/89	

<b>INTERA</b> Technologies		Figure 6.2
----------------------------	--	------------

The sum of the calculated pressures determined at the locations of the boreholes in the southern model area was selected as the next performance measure. The sum of the pressures was calculated to be  $6.3 \times 10^6$  Pa using the pressures within the grid blocks containing the H-4, H-7, H-9, H-12, H-17, P-17, D-268, CB-1, and USGS-1 boreholes. Figure 6.3 contains the sensitivities of this performance measure with respect to the model transmissivities. Two features illustrated in Figure 6.3 are of interest. First, the higher negative sensitivities coinciding with the southern and southwestern grid blocks imply that an increase in the transmissivities in these grid blocks would decrease the pressures at the above borehole locations by increasing the amount of ground water exiting the system.

The second feature of interest is the positive-sensitivity region surrounding the H-7 borehole. This region has positive sensitivities because of its proximity to the western and southern boundaries. A large amount of ground water flowing from the north (Figure 5.21) travels through this region and exits the system from the southern model boundary. If the transmissivities in this region were increased, additional ground water would flow toward the southern boundary. This increase in ground-water flux would raise the pressures within the southcentral model region which would also increase the performance measures. However, if the transmissivities within the H-7 area were reduced, less ground water from the western model region would exit the central southern boundary. The ground water exiting the system from the southcentral model region would be increased as a result of an increased hydraulic gradient, reducing the pressures and the performance measure.

The last performance measure used in this analysis consisted of the sum of pressures at the grid blocks containing the boreholes within the WIPP-site boundary which had estimated undisturbed freshwater heads, H-1, H-2, H-3, H-5, H-11, H-14, H-15, H-18, WIPP-12, WIPP-13, WIPP-18, DOE-1, and P-15. The performance measure using the grid-block pressures at the above locations is equal to  $1.4 \times 10^7$  Pa. The grid-block sensitivities of the performance measure to the model transmissivities are shown in Figure 6.4. The highest positive sensitivities,  $1 \times 10^{-3}$ , occur along the northern portion of the western boundary, implying that an increase in the transmissivities in this region would increase the calculated pressures by allowing more ground water to enter the flow system. For instance, a 50 percent increase in the transmissivity of the



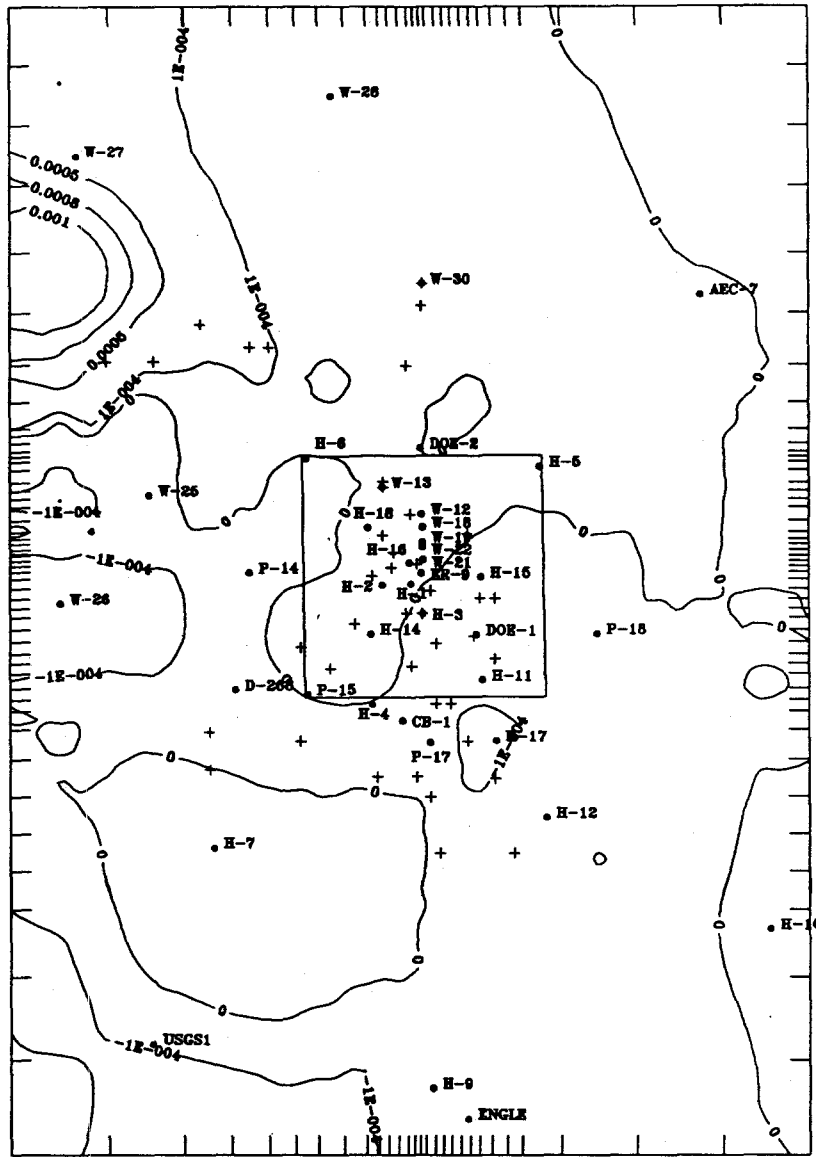
● Observation Well  
 + Pilot-Point Location  
 Contour Interval: Variable  
 Sensitivity Contours are Dimensionless

Drawn by ABW	Date 10/30/89
Checked by M.L.	Date 10/31/89
Revisions	Date
H09700R869	10/31/89

Dimensionless Sensitivities of the Sum of the Southern Borehole Pressures at Grid-Block Elevation to Grid-Block Transmissivities

**INTERA** Technologies

Figure 6.3



● Observation Well  
 + Pilot-Point Location  
 Contour Interval: Variable  
 Sensitivity Contours are Dimensionless

0 2 4 6 8 km  
 SCALE

Drawn by ABW	Date 10/30/89
Checked by M.L.	Date 10/31/89
Revisions	Date
H09700R869	10/31/89

Dimensionless Sensitivities of the Sum of the  
 WIPP-Area Borehole Pressures at Grid-Block Elevation  
 to Grid-Block Transmissivities

**INTERA** Technologies

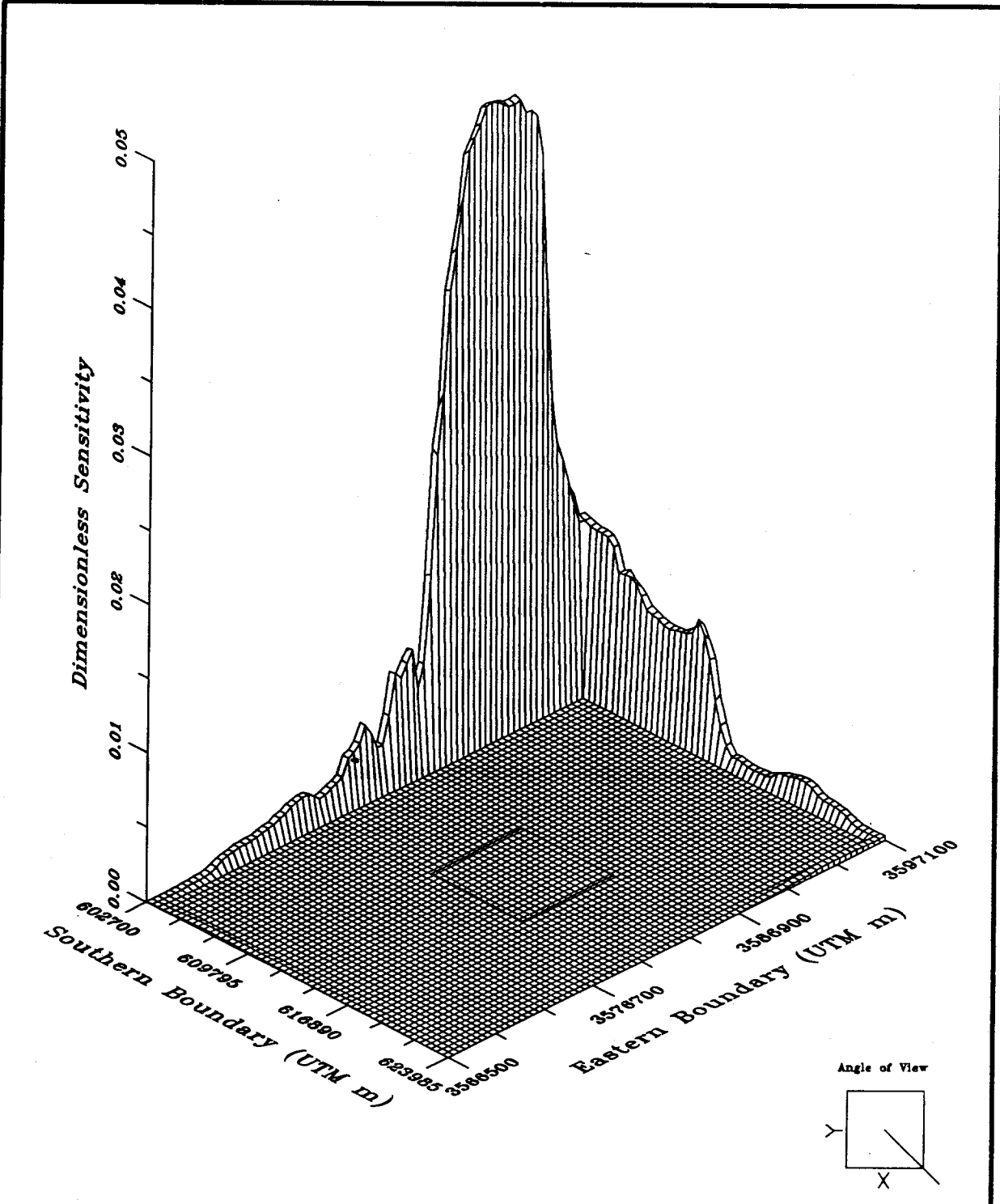
Figure 6.4

four grid blocks with the highest sensitivity would increase the performance measure by approximately 0.23 percent, or  $3.3 \times 10^4$  Pa (3.4 m). As Figure 6.4 illustrates, the magnitude of the sensitivities over most of the northwest region ranges from  $5 \times 10^{-4}$  to less than  $1 \times 10^{-4}$ . Sensitivities less than  $1 \times 10^{-4}$  (i.e., within the WIPP-site boundary) are probably insignificant.

## 6.2 Sensitivity of Calculated Pressures to Model Boundary Pressures

The dimensionless sensitivities of the sum of the pressures ( $6.9 \times 10^6$  Pa) at grid-block elevation for the northwest borehole locations (WIPP-25, WIPP-26, WIPP-27, WIPP-28, WIPP-30, H-6, P-14, and DOE-2) to changes in the pressures assigned to the boundaries of the model are shown in Figure 6.5. The magnitude of the sensitivities is higher than those in Figure 6.2 because a different sensitivity parameter has been selected. A percentage change in the transmissivities is often less noticeable in the calculated pressures than the same percentage change in the pressures assigned to the model boundaries. The change in the boundary pressures for the sensitivity calculations discussed in this section was, therefore, selected as 5 percent.

The magnitude of the highest sensitivity is 0.043, which occurs along the northern part of the western boundary. The high sensitivity indicates an increase in the pressures along the northwestern boundary would have a direct impact on the steady-state fit to the undisturbed heads in this area because of the increase in ground water which would enter the system through this northwest boundary. For instance, the specified pressure in the grid block with the highest sensitivity is  $3.3 \times 10^5$  Pa which, when the elevation of the grid block is accounted for, relates to a specified freshwater head of 937.0 m. Increasing the pressure in this grid block by 5 percent would increase the boundary pressure by  $1.7 \times 10^4$  Pa, raising the specified head to 938.7 m. The 5 percent increase in the boundary pressure would relate to a 0.21 percent increase in the performance measure, or approximately  $1.5 \times 10^4$  Pa (1.5 m). Thus, most of the increase in the boundary pressure would be directly imposed upon the calculated pressures in the northwest model region.



Drawn by	ABW	Date	10/30/89
Checked by	M.L.	Date	10/31/89
Revisions		Date	
H09700R869		10/31/89	

Dimensionless Sensitivities of the Sum of the Northwest Borehole Pressures at Grid-Block Elevation to Boundary Pressures

**INTERA** Technologies

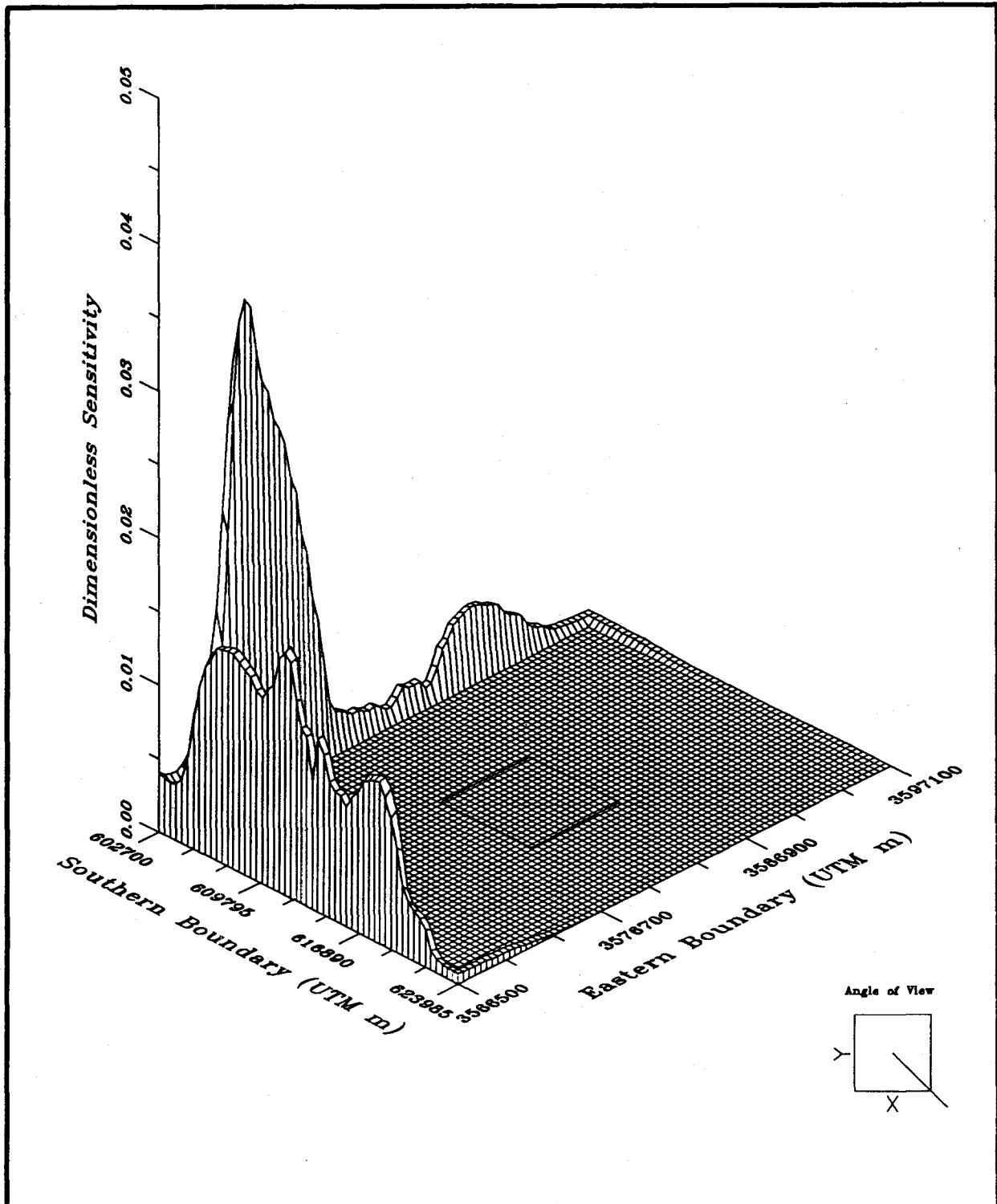
Figure 6.5

The sensitivities of the sum of the pressures ( $6.3 \times 10^6$  Pa) at the southern boreholes (H-4, H-7, H-9, H-12, H-17, P-17, D-268, CB-1, and USGS-1) to the boundary pressures (Figure 6.6) display a different profile than that seen in Figure 6.5. The southern borehole pressures are virtually insensitive to the northern and northwestern boundary pressures and are highly sensitive to the southern and southwestern boundary pressures. The highest sensitivities occur along the southern part of the western boundary where they range from a maximum of 0.03 to 0.015. Sensitivities over much of the southern boundary range from 0.015 to 0.01. These two regions along the western and southern boundaries have high sensitivities because of the large flux of ground water that exits the system at these locations. Increases in the pressures along these boundaries would reduce the hydraulic gradient over the southern model region and the calculated pressures at the southern boreholes would rise as a result. If the pressures which were specified (at grid-block elevation) along the entire southern model boundary were raised 5 percent, the performance measure ( $6.3 \times 10^6$  Pa) would increase by approximately 1.2 percent, or  $7.5 \times 10^4$  Pa. This is equivalent to a 7.7 m total rise in the freshwater heads which would be distributed among the southern boreholes making up the performance measure and would probably degrade the steady-state fit at several of these locations.

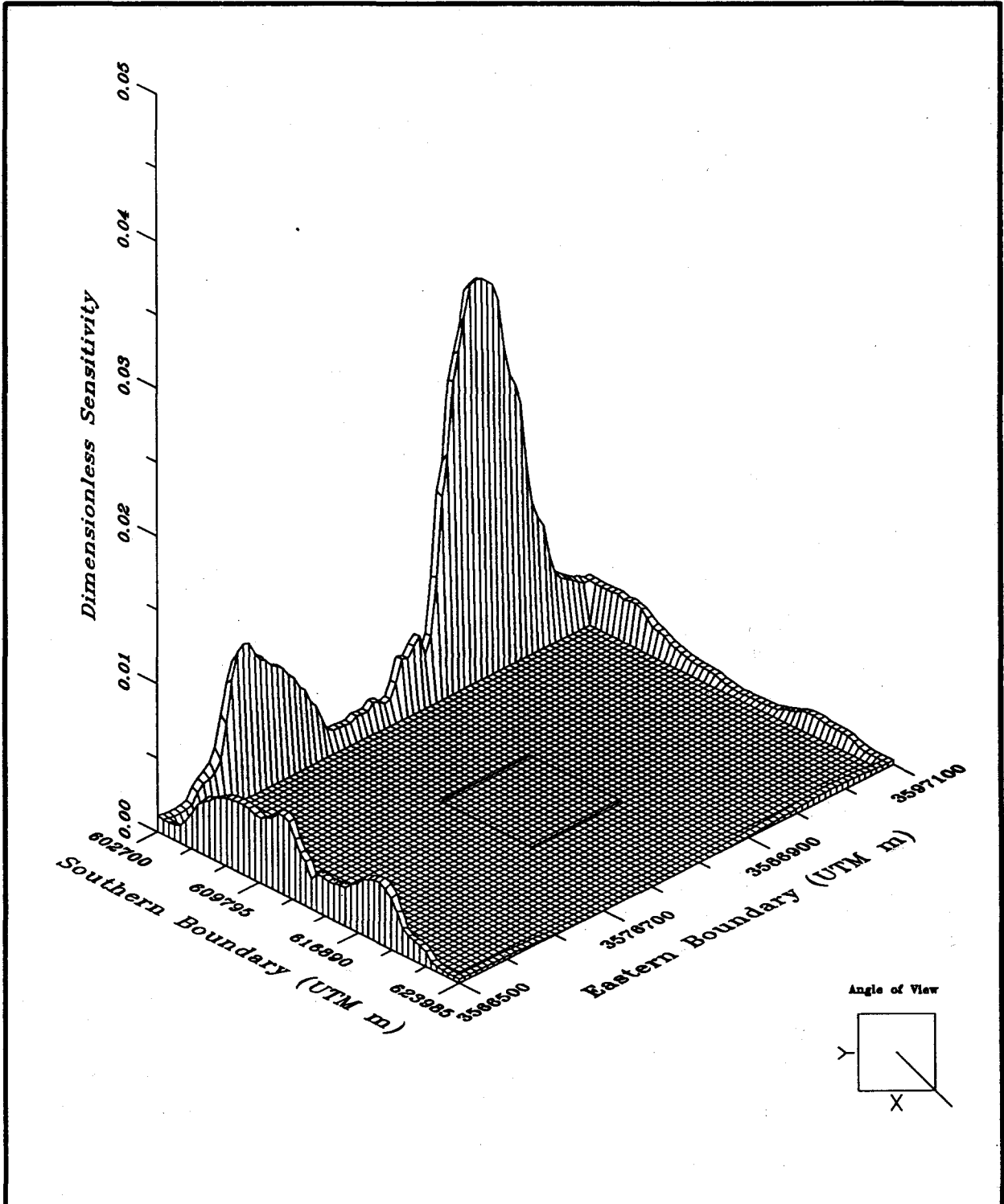
The sensitivity profile calculated using the sum of the calculated pressures at the borehole locations within the WIPP-site boundaries ( $1.4 \times 10^7$  Pa) as the performance measure (Figure 6.7) is observed to be a combination of Figures 6.5 and 6.6. The high-sensitivity regions discovered in Figures 6.5 and 6.6 are preserved in Figure 6.7, however, the magnitudes of the sensitivities have been reduced. The highest sensitivity, which occurs along the northwestern boundary, has been reduced from 0.043 (Figure 6.5) to 0.028. The highest sensitivities along the southern and southwestern boundaries have also been reduced and now range from 0.003 (along the southern boundary) to 0.012 (along the southwestern boundary). If the pressures at elevation along the entire southern boundary were raised 5 percent, the total increase in the freshwater heads at the WIPP-site borehole locations would be approximately 5 m.

If the pressure assigned to the northwest boundary grid block with the highest sensitivity was raised 5 percent, as previously described, the assigned freshwater head





Drawn by	ABW	Date	10/30/89	Dimensionless Sensitivities of the Sum of the Southern Borehole Pressures at Grid-Block Elevation to Boundary Pressures
Checked by	M.L.	Date	10/31/89	
Revisions		Date		
H09700R869		10/31/89		
<b>INTERA</b> Technologies				Figure 6.6



Drawn by	ABW	Date	10/30/89
Checked by	M.L.	Date	10/31/89
Revisions		Date	
H09700R869		10/31/89	

Dimensionless Sensitivities of the Sum of the WIPP-Area Borehole Pressures at Grid-Block Elevation to Boundary Pressures

**INTERA** Technologies

Figure 6.7.

would increase from 937.0 m to 938.7 m. The total increase in the freshwater heads at the locations of the WIPP-site boreholes due to this higher northwest boundary pressure would be 2 m.

In conclusion, the results determined in the above sensitivity calculations indicate the calculated pressures throughout the model area are most sensitive to the specified boundary pressures and grid-block transmissivities in the northwest region. A considerable amount of ground water enters the system through the northern part of the western boundary. Since the transmissivities within this region are among the highest in the modeled area, any increase in pressure along the northwestern boundary is transmitted to the interior model region. An increase in pressure can occur by raising the specified boundary pressure or by increasing the boundary grid-block's transmissivity which reduces the resistance between the boundary and the interior grid blocks. Thus, the high sensitivities determined for the northwest boundary pressures and transmissivities reflect the dependence of the system upon the flux of ground water entering the model area through the northwest region.

The question of data uncertainty and data coverage within the model should be discussed in light of the sensitivities just determined. As demonstrated above, the model-calculated pressures at the northwest and central borehole locations are most sensitive to changes in the transmissivities and/or boundary pressures in the northwest model area. The observed data within this area consist of estimated transmissivity values and water-level hydrographs (from which undisturbed heads were estimated) at the WIPP-25, WIPP-26, WIPP-27, WIPP-28, WIPP-30, DOE-2, P-14, and H-6 boreholes. As previously stated, the transmissivities in this area are the highest in the entire model region (Figure 2.9). The pumping and slug tests that have been performed at these boreholes are listed in Table C.1 of Cauffman et al. (1990). The two pumping-test transmissivity values at WIPP-27 have the highest range with values of  $2.6 \times 10^{-4}$  and  $7.0 \times 10^{-4}$  m<sup>2</sup>/s. The log<sub>10</sub> of these two values were averaged and assigned to the WIPP-27 borehole in this study (Table 2.4). It is clear from the above range that the transmissivity value at WIPP-27 could be factor of two to a factor of five different from that used in the model, which implies that the data certainty at the WIPP-27 borehole could allow for changes to the transmissivities in this area to occur and still be consistent with the observed data. In addition, there

is a wide region between WIPP-27 and WIPP-25 where no transmissivity measurements have been obtained. Thus, from a data-certainty and data-coverage perspective, the transmissivity measurements do not provide adequate restrictions on changes to the northwest region transmissivities.

In contrast to the transmissivity data, the head data in the northwest region does provide restrictions to the degree of change possible to both the boundary pressures and indirectly to the transmissivities of the northwest model region. This is mainly due to the uncertainties of the head data and the use of the heads as the calibration target in the model. The observed-head uncertainties for the northwest boreholes ranges from +0.9/-1.2 m at WIPP-28 to +1.0/-1.0 m at WIPP-25 (Table 2.6). These uncertainties are much less than those associated with the transmissivity data. In addition, the differences between the calculated and observed heads for the transient calibrated model at the northwest boreholes range from -1.0 m at WIPP-26 to -0.1 m at DOE-2 but are generally less than 0.5 m. Since the uncertainty values were used as a measure of head calibration at a borehole (i.e., the heads were considered calibrated when the differences between the calculated heads and observed heads were approximately equal to the uncertainties) and the differences between the calculated and observed heads are affected by changes in both the boundary conditions and model transmissivities, the degree of change possible in the northwest region to either of these parameters is restricted. Thus, even though the model is sensitive to transmissivity and boundary pressure in the northwest model region, the calibration to the steady-state heads in this area would be degraded if moderate changes to either parameter were implemented. In summary, the proximity of WIPP-25, WIPP-26, WIPP-27, and WIPP-28 to the model boundaries restricts the extent of change possible in the boundary pressures and the calibration to the heads at the other northwest borehole locations restricts the extent of change possible in the transmissivities.

### 6.3 Sensitivity of the Predicted Ground-Water Travel Time

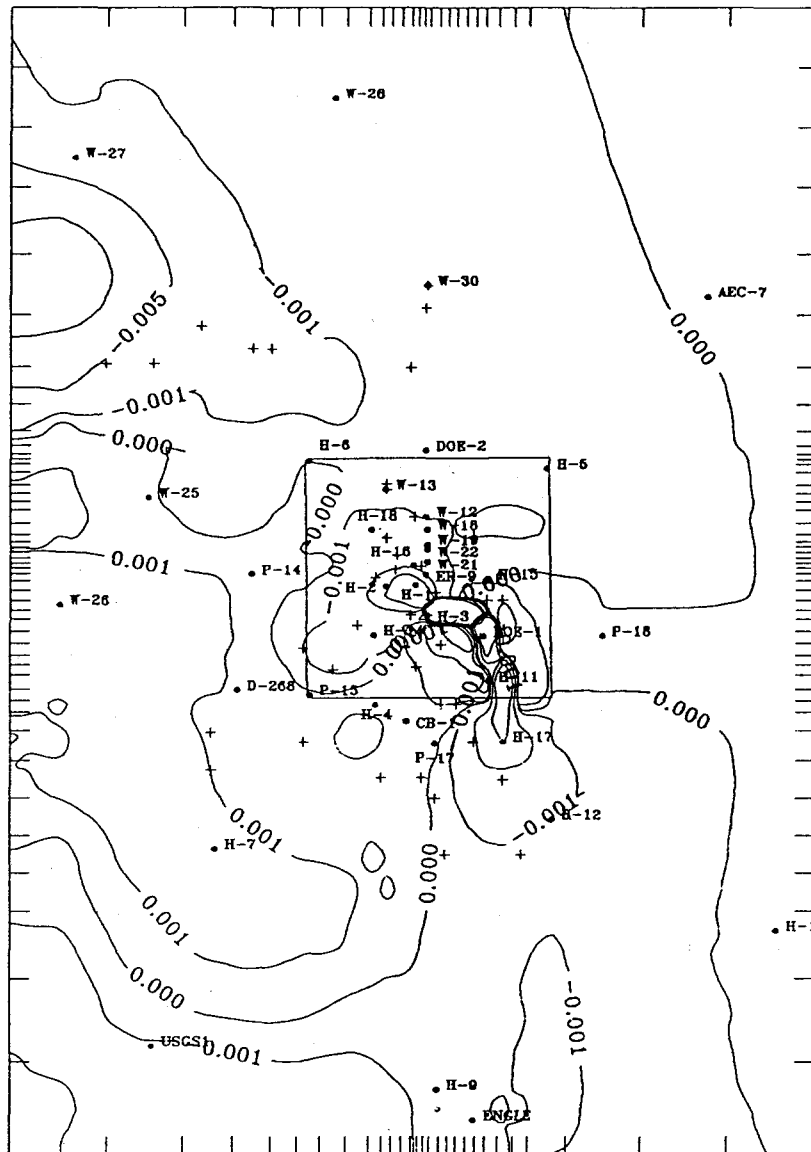
As stated in Sections 3.3.7 and 5.5, the particle travel times in this study were calculated using Darcy velocities and an assumed porosity of 16 percent. They are

good indicators of the travel times due strictly to the changes in permeability and hydraulic gradient over a particular area. These travel-time values may be much different from actual travel times due to the spatially constant porosity (16 percent) used in the calculations and also due to the uncertainties associated with the permeabilities and the hydraulic gradients. Since the permeabilities and the hydraulic gradient are not exactly known through the model region, it is important to determine the effect that changes in these parameters would have on the predicted travel time. An attempt has been made to address this problem by using GRASP II to calculate the sensitivities of particle travel time. The calculated sensitivities identify regions within the modeled area in which changes to the system parameters, i.e., grid-block transmissivities or pressures specified at the boundaries, would most greatly affect the performance-measure value.

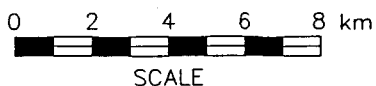
Caution must be used in using sensitivity magnitudes to predict the travel time for very large changes in the transmissivities (or boundary pressures). The reason for this is two-fold: first, the sensitivity derivatives are first order, meaning that if the actual response of the travel time due to increases or decreases in the transmissivities is not quasi-linear, the error of the travel-time prediction will increase as the assumed change in transmissivities increases. In addition, changes in the transmissivity field are assumed to not affect the flow field significantly, i.e., the travel path is assumed to remain the same. These points have been discussed in several publications (Andrews et al. (1986), Sykes et al. (1985), and LaVenue et al. (1989)), where the advantages and limitations of predicting travel times based on particle ground-water travel-time sensitivities are discussed.

The performance-measure value used throughout this section is equal to the particle travel time from a point within the Culebra coincident with the centroid of the underlying repository to the southern WIPP-site boundary,  $1.4 \times 10^4$  years (i.e., the trajectory determined using the transient calibrated model). The trajectory of the ground-water travel path to the edge of the WIPP-site boundary is shown in Figure 5.25 (Path F).

The dimensionless sensitivities of the predicted particle travel time to the grid-block transmissivities are depicted in Figures 6.8 and 6.9. The sensitivities in the



• H-8



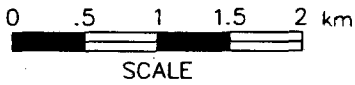
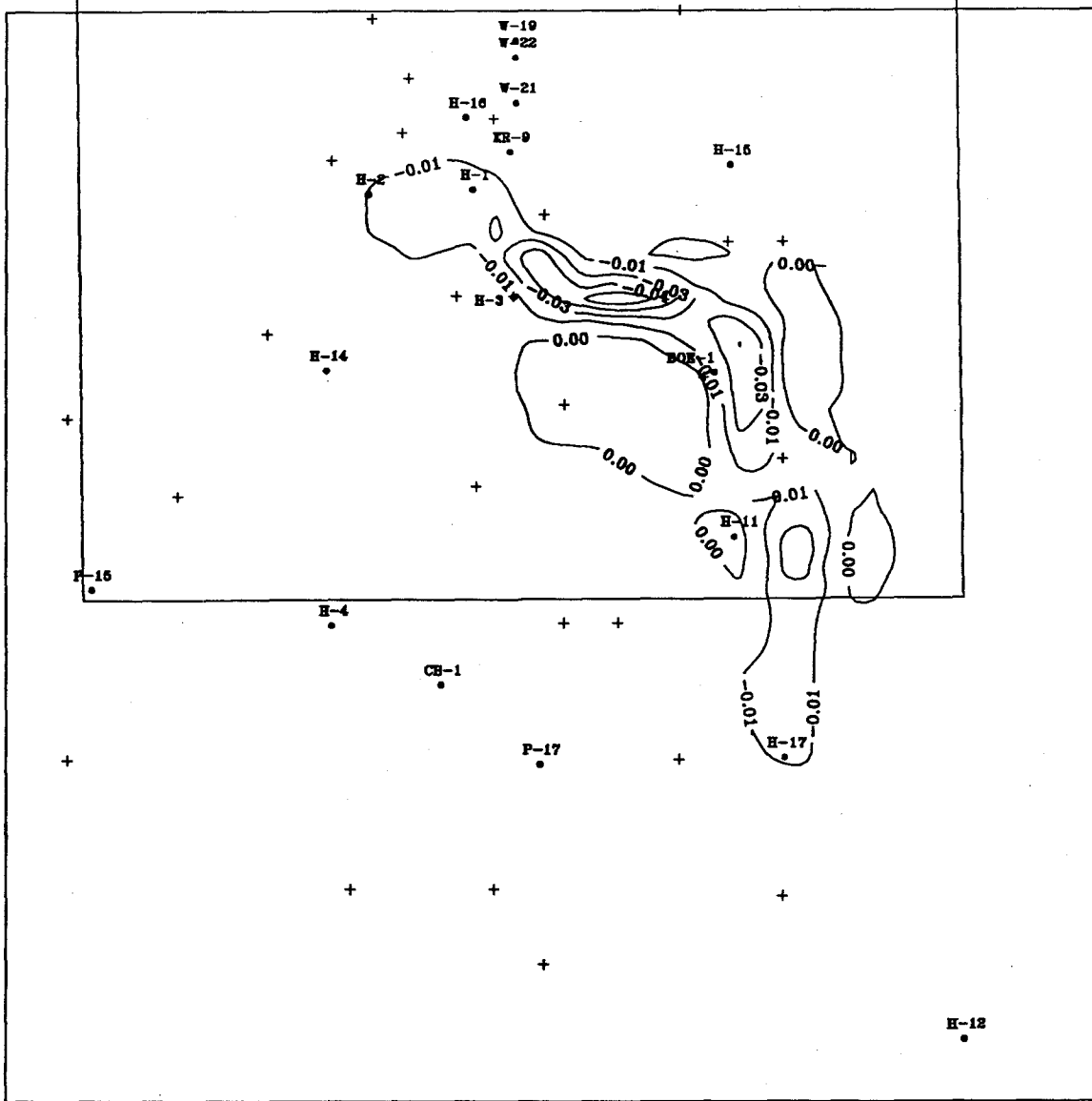
- Observation Well
- + Pilot-Point Location
- Contour Interval: Variable
- Sensitivity Contours are Dimensionless

Drawn by ABW	Date 10/30/89
Checked by M.L.	Date 10/31/89
Revisions	Date
H09700R869	10/31/89

### Dimensionless Sensitivities of Particle Travel Time to Grid-Block Transmissivities

**INTERA Technologies**

Figure 6.8



● Observation Well  
 + Pilot-Point Location  
 Contour Interval: Variable  
 Sensitivity Contours are Dimensionless

Drawn by ABW	Date 10/30/89	<b>Dimensionless Sensitivities in the Central Model          Region of Particle Travel Time to          Grid-Block Transmissivities</b>
Checked by M.L.	Date 10/31/89	
Revisions	Date	
H09700R869	10/31/89	

**INTERA** Technologies

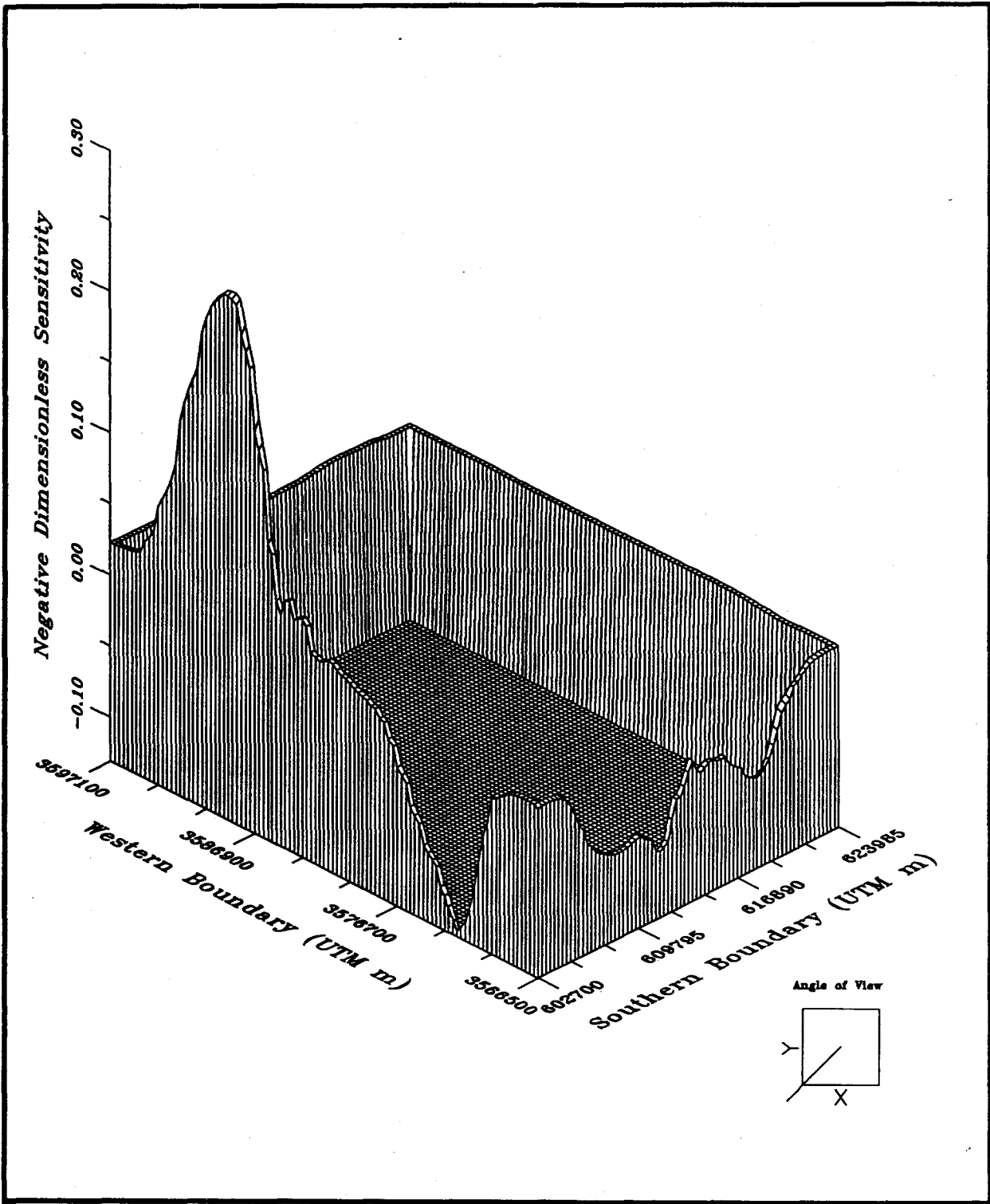
Figure 6.9

northwest model region range from -0.001 to -0.01 while those in the southern part of the model range from 0.005 to 0.001. Negative sensitivities indicate that if the transmissivities were increased, the travel time would decrease or conversely, that if the transmissivities were decreased, the travel time would increase. The highest sensitivities (-0.025 to -0.075) occur along the particle travel path (Figure 6.9) within the WIPP-site boundary. The maximum-sensitivity value, 0.075, lies approximately 800 m east of the H-3 borehole. If the sensitivities for each grid block along the travel path are summed, the resulting sensitivity total is -0.725. Thus, if the transmissivities along the travel path are uniformly increased by 25 percent, the travel time to the southern WIPP-site boundary would be reduced approximately 18 percent (= sum of the sensitivities x percentage change in sensitivity parameter), or 2500 to  $1.16 \times 10^4$  years. Conversely, if the transmissivities along the travel path were uniformly decreased by 25 percent, the travel time would increase by 2500 to  $1.66 \times 10^4$  years.

The uncertainties associated with the transmissivities within this central part of the WIPP-site area are less than those within the northwest model region due to (1) the higher number of observed transmissivity values from nearby boreholes, and (2) the calibration to the H-3 and H-11 multipad pumping-test responses. It is possible that a 25-percent change could occur within the grid blocks along the travel path without significantly affecting the steady-state heads or the responses to the H-3 or H-11 multipad tests. However, changes significantly higher than this would be restricted because they would degrade the steady-state and transient head fits in this region.

The sensitivities of the travel time to changes in the pressures assigned to the boundaries are illustrated in Figure 6.10. The negative dimensionless sensitivities are plotted in order for the highest sensitivity region to be oriented vertically upward, similar to the previous boundary-pressure plots. The highest sensitivity to a boundary pressure, -0.23, is located in the northwest region of the model where, as previously mentioned, a significant flux of ground water enters the modeled system (Figure 5.21). An increase in the pressure assigned to this portion of the western boundary would increase the volume of ground water entering the system and the hydraulic gradient within the system. The increased gradient would reduce the travel time to the southern WIPP-site boundary. However, as mentioned in





Drawn by ABW	Date 10/30/89
Checked by M.L.	Date 10/31/89
Revisions	Date
H09700R869	10/31/89

Dimensionless Sensitivities of Particle  
Travel Time to Boundary Pressures

**INTERA** Technologies

Figure 6.10

Section 6.2, the head-data uncertainty in the northwest region of the model restricts possible changes in the northwest boundary pressures and, therefore, the model is still fairly well constrained with respect to travel time.

#### 6.4 Sensitivity of the Calculated Pressures at Central WIPP-Site Boreholes to Shaft-Leakage Rates

The transient calibrated heads at the H-1, WIPP-21, WIPP-22 and ERDA-9 boreholes are illustrated in Figures 5.18a, f, g, and h, respectively. The calculated heads at H-1, from late 1987 to the end of the simulation time in mid-1989, range from 3 to 6 m higher than the observed heads. During the same time period, the calculated heads at the WIPP-21 and WIPP-22 boreholes range from 5 to 10 m and 2 to 4 m higher, respectively, than the observed heads. In addition, the calculated heads at the ERDA-9 borehole are approximately 8 m higher than the observed heads throughout the time period for which data is available at ERDA-9 (i.e., after 1986). The calculated heads at WIPP-19 (Figure 5.18f) agree well with the observed heads until mid-1988 when the calculated heads are approximately 4 m too low.

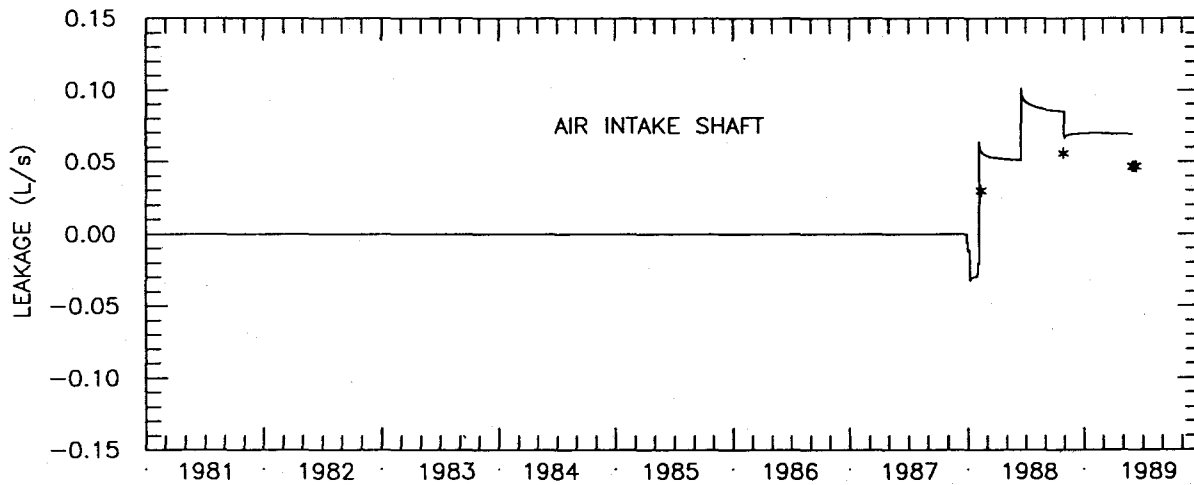
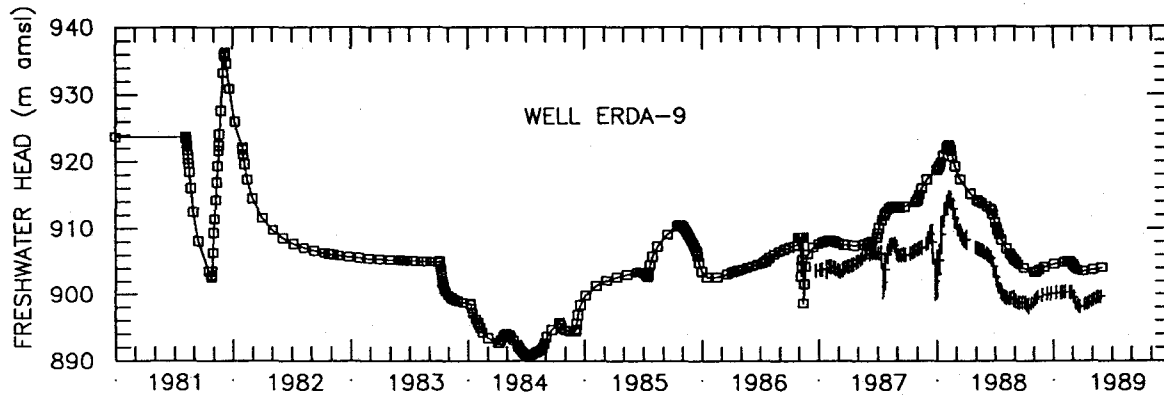
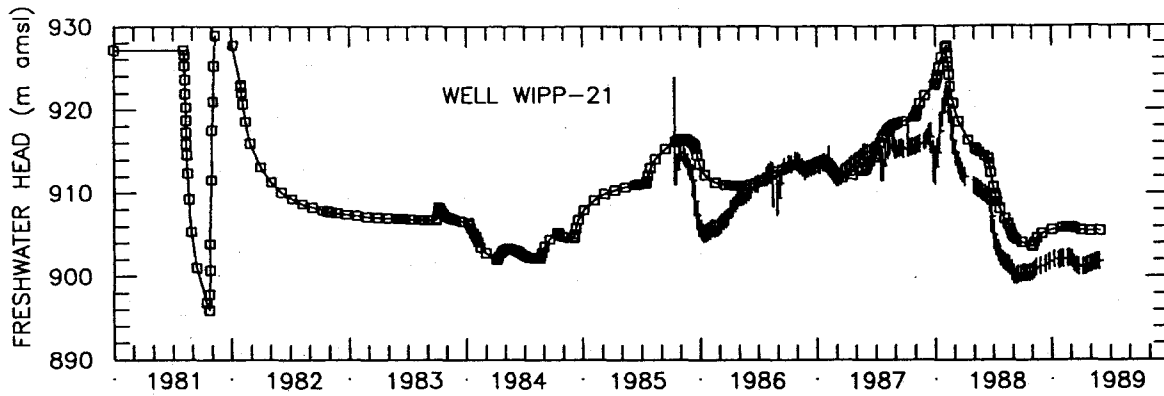
As discussed in Section 5.2.6, an attempt was made to improve the fits at these boreholes by increasing the transmissivities between WIPP-21 and the AIS and by increasing the transmissivity of the skin assigned to the AIS. Both of these changes were made in an attempt to increase the local drawdown due to the excavation of the AIS. However, neither of these changes improved the fit at these boreholes, suggesting that the calculated leakage rate at the AIS and/or another shafts must be raised to increase the local drawdown. This section will discuss the sensitivity of the calculated heads at these boreholes to changes in the leakage rates specified in the model.

The calculated leakage rates for the shafts, determined for the transient calibrated transmissivity field, are shown in Figures 5.19a and 5.19b. The leakage at the C&SH shaft, EXS, and WHS are assumed to be zero after 1987 because of a major grouting exercise performed in 1987 at each of these shafts. The AIS is the only shaft in which measured leakage rates are available after grouting of the other shafts was performed

in 1987. The amount of leakage occurring at the other shafts can only be hypothesized. In addition, the measured leakage rates at the AIS may be affected by ventilation occurring through the shaft which reduces the amount of inflow that is collected. Periodic inspections are performed at the WHS and the C&SH shaft, however, the results of these inspections have not been formally documented. Moreover, the EXS has not been inspected in over two years (P. Davies, personal communication). It is clear that the calculated leakage rates in one or all of the shafts may not represent the actual conditions in the shafts. Therefore, the calculated leakage rates were adjusted in two additional SWIFT II simulations in order to determine the amount of leakage necessary to match the transient heads at the H-1, WIPP-21, and ERDA-9 boreholes.

In the first SWIFT II simulation of this sensitivity analysis, the leakage at the AIS was increased by approximately 50 percent relative to the leakage in the transient calibrated model. Figure 6.11a shows the increased leakage rates calculated during this simulation along with the calculated heads at the WIPP-21 and ERDA-9 boreholes. The differences between the calculated and observed heads at these boreholes have been reduced to approximately 2 to 3 m from 1988 to mid-1989. The calculated heads just prior to shaft excavation (late 1987) still need to be reduced by 4 to 5 m in order to improve the match to the observed heads. However, the relative magnitudes of the calculated drawdowns at these boreholes due to the AIS excavation agree well with the observed drawdown. This implies that leakage from another shaft must be implemented in the model in order to reduce the head differences in late 1987. The increase leakage at the AIS also reduced the differences at the H-1 and WIPP-22 boreholes (Figure 6.11b). The calculated heads at WIPP-22 are now very similar to the observed heads while those at H-1 are now still about 1 to 2 m too high. However, the higher leakage rate increased the differences at the WIPP-19 borehole (Figure 6.11b).

Additional shaft leakage was introduced in a second sensitivity simulation by assigning a leakage rate of 0.012 L/s to the EXS after the grouting exercise was performed in 1987 (Figure 6.12). The leakage at the AIS was slightly reduced (Figure 6.12). This occurs because the AIS leakage is not directly specified but allowed to adjust according to the existence of atmospheric pressure in the shaft, and the specified properties of the shaft skin. The increased leakage at the EXS reduced



LEGEND: □—□ Calculated Freshwater Heads  
 † Observed Freshwater Heads

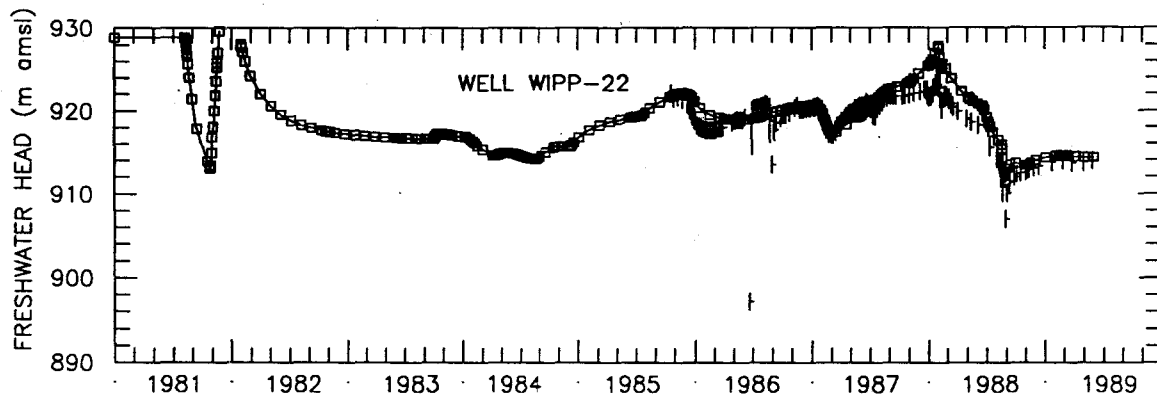
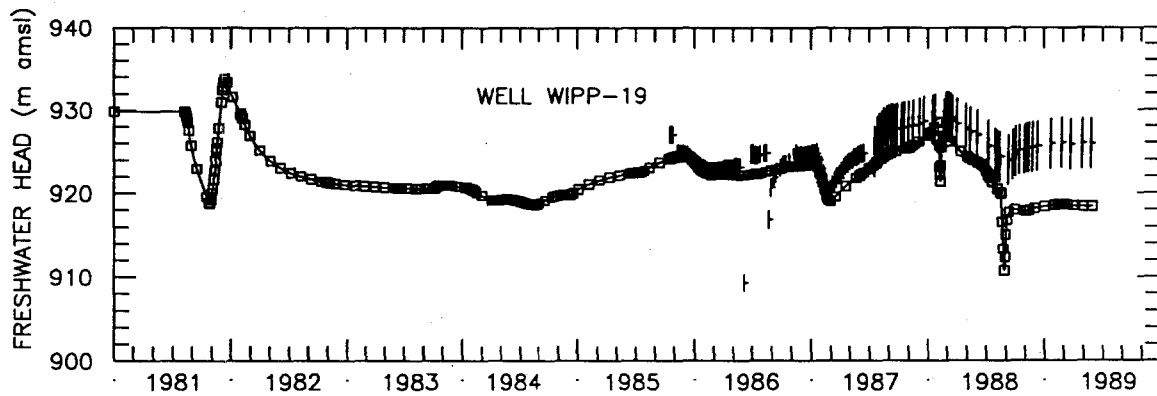
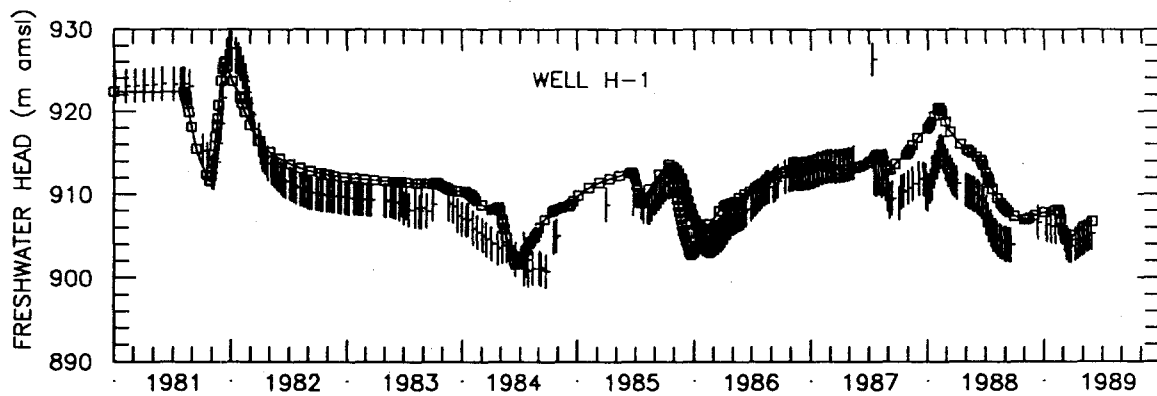
LEGEND: — Calculated Leakage Rate  
 \* Measured Leakage Rate

Drawn by ABW	Date 10/30/89
Checked by M.L.	Date 10/31/89
Revisions	Date
H09700R869	10/31/89

Calculated and Observed Transient Freshwater Heads at WIPP-21 and ERDA-9 and Increased Leakage Rate at the AIS Location

**INTERA** Technologies

Figure 6.11 a



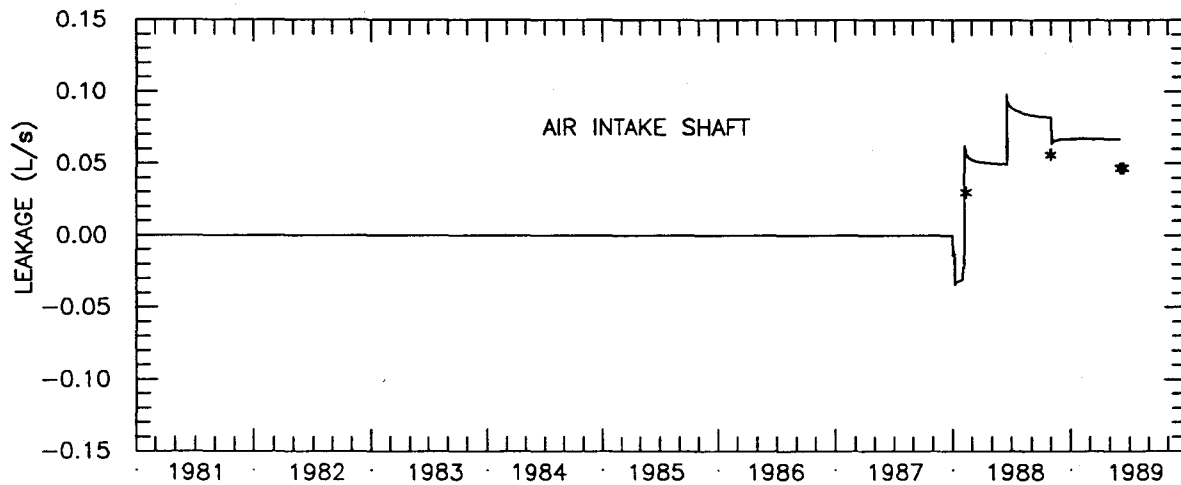
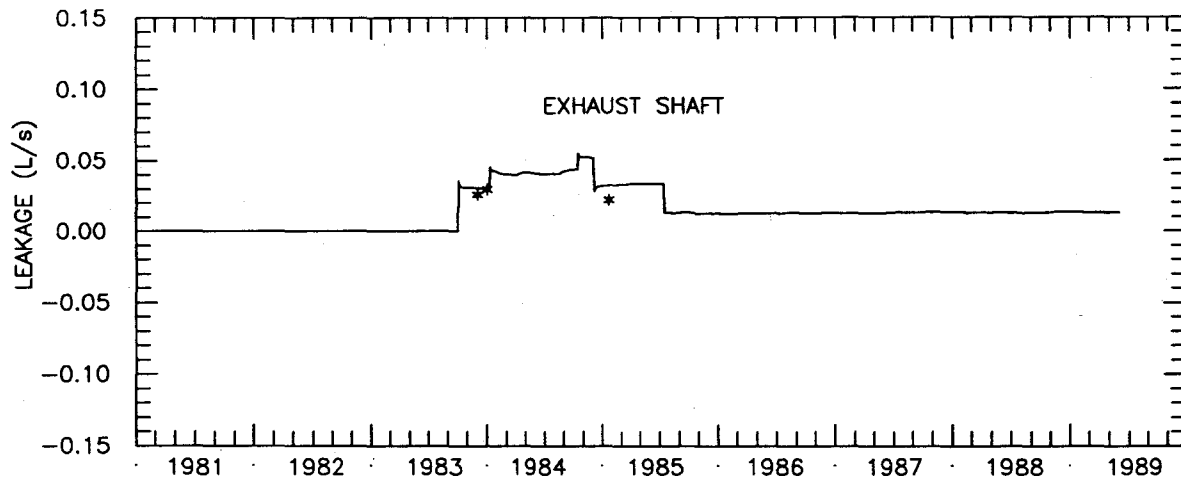
LEGEND: □-□ Calculated Freshwater Heads  
 † Observed Freshwater Heads

Drawn by ABW	Date 10/30/89
Checked by M.L.	Date 10/31/89
Revisions	Date
H09700R869	10/31/89

Calculated and Observed Transient Freshwater Heads at H-1, WIPP-19, and WIPP-22 Using Increased AIS Leakage

**INTERA** Technologies

Figure 6.11b



LEGEND: — Calculated Leakage Rate  
 \* Measured Leakage Rate

Drawn by ABW	Date 10/30/89
Checked by M.L.	Date 10/31/89
Revisions	Date
H09700R869	10/31/89

Increased Leakage Rates at the  
 EXS and AIS Locations

**INTERA** Technologies

Figure 6.12

the pressures in the central model area which reduced the amount of leakage into the AIS. Figures 6.13a and 6.13b contain the calculated and observed heads for the H-1, WIPP-21, WIPP-22, and ERDA-9 boreholes. The head differences at each of these boreholes have been significantly reduced such that the calculated heads virtually coincide with the observed values. The heads at WIPP-19 (Figure 6.13b) have been degraded relative to those in the previous simulation due to the increased drawdown around the shafts, which implies that there may be greater uncertainty in the WIPP-19 transient heads after 1987 (i.e., greater than  $\pm 3.0$  m).

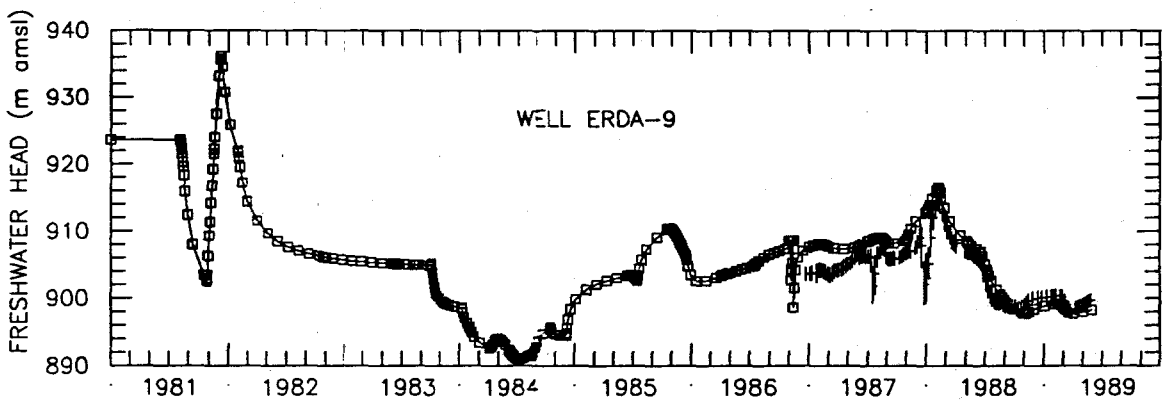
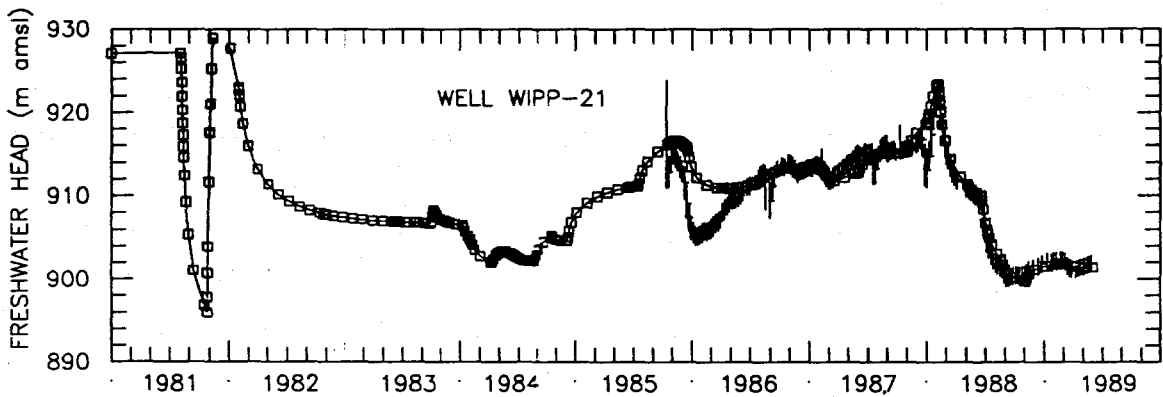
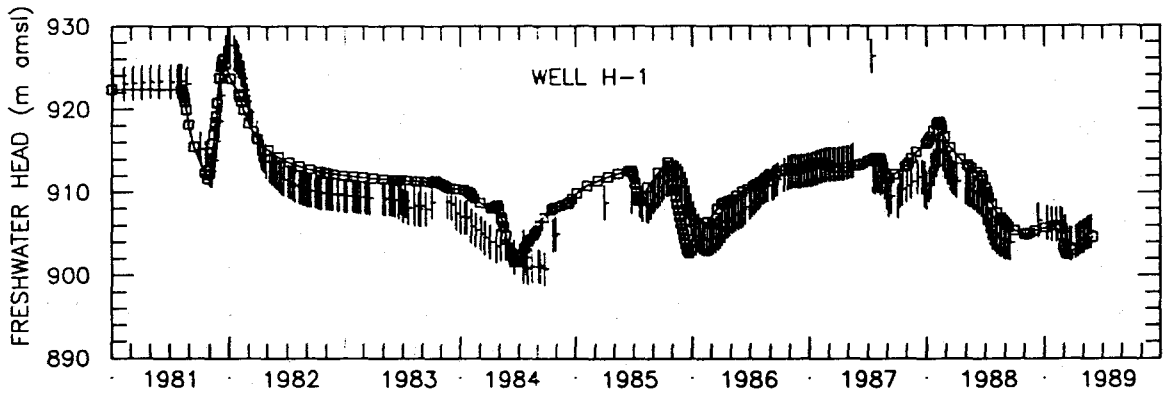
In conclusion, Figures 6.11a through 6.13b illustrate that leakage from the shafts has a significant effect upon the calculated heads in the central part of the WIPP site. The increased leakage implemented at the AIS and EXS to reduce the heads in this region may be realistic given the uncertainties associated with the measured (or lack of) data for these shafts. It is also possible that leakage is occurring at the WHS and C&SH shaft which would decrease the amount of leakage needed from the AIS to match the observed heads at the central WIPP-site boreholes successfully. However, as previously mentioned, the leakage from either the EXS, WHS, or C&SH shaft after 1987 (i.e., after final grouting) can only be hypothesized due to the absence of any visual observation of leakage occurring.

#### 6.5 Sensitivity of the Model Results to the Calibration Approach

The objective of this section is to address several questions which may arise about the approach used during calibration and the effect this approach may have on the calibrated transmissivity field. For example:

- If the model had been calibrated to the observed pressures within the WIPP-site boundary first and then to the observed pressures outside of the WIPP-site boundary next, would one have obtained the same calibrated transmissivity field?
- Is the transmissivity field obtained using the coupled adjoint-sensitivity and kriging technique unique?

As mentioned in Section 3.3.1, the steady-state heads in regions which lie outside of the WIPP-site boundary were calibrated prior to matching the heads inside the



LEGEND: □-□ Calculated Freshwater Heads  
 + Observed Freshwater Heads

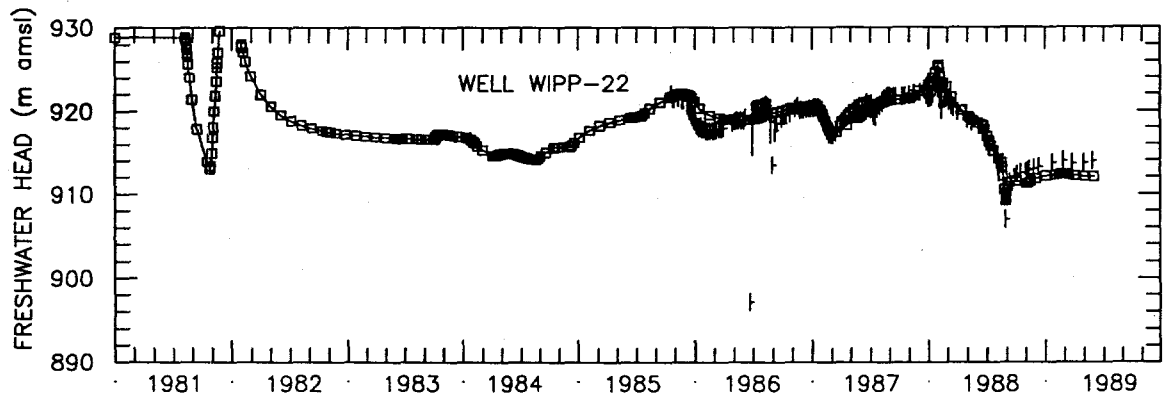
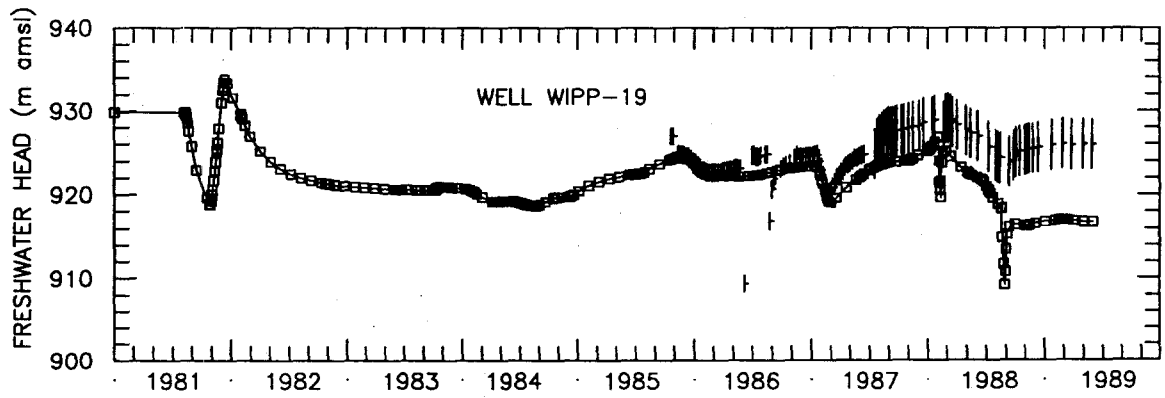
Drawn by ABW	Date 10/30/89
Checked by M.L.	Date 10/31/89
Revisions	Date
H09700R869	10/31/89

Calculated and Observed Transient Freshwater Heads at H-1, WIPP-21, and ERDA-9 Using Increased AIS and EXS Leakage

INTERA Technologies

Figure 6.13a





LEGEND: □—□ Calculated Freshwater Heads  
 † Observed Freshwater Heads

Drawn by ABW	Date 10/30/89
Checked by M.L.	Date 10/31/89
Revisions	Date
H09700R869	10/31/89

Calculated and Observed Transient Freshwater Heads at WIPP-19 and WIPP-22 Using Increased AIS and EXS Leakage

**INTERA** Technologies

Figure 6.13b

WIPP-site boundary. This approach was used in order to reproduce the regional hydraulic gradient north and south of the WIPP-site boundary prior to matching the local hydraulic gradient within the WIPP-site boundary and is similar to the modeling technique of using model-calculated heads determined in a regional model to provide boundary conditions for subsequent local-scale modeling. Because the calculated local-scale (i.e., within the WIPP-site boundary) results are sensitive to the calculated regional conditions (i.e., changes to ground-water flux on the regional scale), the regional heads should be matched first.

If one attempts to match the local-scale heads first, the changes to the transmissivity field at the local scale will probably need subsequent modification once the regional heads are matched, a process which is much less efficient from a calibration viewpoint than matching the regional heads first. However, even if one attempted the local-scale calibration and then performed the regional-scale calibration, the transmissivity field obtained within the WIPP-site boundary would probably not contain significantly different results due to the large degree of transient pressure data obtained from the multiwell pumping tests. Using this alternate approach, the regional transmissivities may have some small differences assuming the boundary conditions were the same. This is not meant to imply uniqueness, though. There is a large difference between the reproduceability of a calibrated transmissivity field given a particular calibration technique and the uniqueness of the results. For instance, the width and nature of the zone of higher transmissivity extending southward from H-15 is not well known. The grid blocks in this area of the model have a minimum width of 250 m which is too wide to fully investigate the minimum dimensions of a feature necessary to match the pressure responses at the H-15 and DOE-1 boreholes due to H-11 pumping.

In conclusion, the calibrated transmissivity field is not unique; however, given the technique used to calibrate the model, it is believed to be reproduceable and defensible due to the extensive transient pressure data available from within the WIPP-site boundary.

## 7.0 CONCLUSIONS

This hydrogeologic modeling study has been performed as part of the regional hydrologic characterization of the Waste Isolation Pilot Plant (WIPP) Site in southeastern New Mexico. The study has produced an estimation of the transmissivity and Darcy-velocity distributions in the Culebra Dolomite Member of the Permian Rustler Formation at the WIPP site. These results are intended to provide support for performance-assessment calculations being performed by Sandia National Laboratories. The main conclusions are presented below:

- The transient-calibrated transmissivity distribution contains the same general trend over the model area as the observed transmissivities with predominantly lower transmissivities ( $< 1 \times 10^{-7} \text{ m}^2/\text{s}$ ) east of the WIPP-site boundary, intermediate transmissivities in the central part of the model area ( $1 \times 10^{-6}$  to  $1 \times 10^{-4} \text{ m}^2/\text{s}$ ), and high transmissivities ( $> 1 \times 10^{-3} \text{ m}^2/\text{s}$ ) in the western part of the model area representing Nash Draw. Local differences to the general trend are present in the H-11 area where a higher transmissivity zone is needed to reduce the differences between the calculated and observed heads for both steady-state and transient conditions at the H-11, H-14, H-15, H-17, DOE-1, and P-17 borehole locations. The high-transmissivity feature has approximately the same magnitude of transmissivities near the H-11 borehole as a similar feature proposed in LaVenue et al. (1988). However, the transmissivities just south of the H-15 borehole have been increased approximately one order of magnitude relative to the transmissivities presented in LaVenue et al. (1988) in order to reproduce the observed response to H-11 pumping.
- The steady-state freshwater heads of the transient calibrated model illustrate low hydraulic gradients ( $1 \times 10^{-4} \text{ m/m}$ ) north of the WIPP-site boundary between WIPP-28 and DOE-2 and south of the WIPP-site boundary between H-17 and H-7. Higher gradients ( $4 \times 10^{-3} \text{ m/m}$ ) occur in the central part of the model area.
- The model-calculated ground-water-flow directions are predominantly south to southwest. The largest volume of ground water enters the model area through the northern portion of the western model boundary and enters the high-transmissivity

area along the western part of the model representing Nash Draw. A significant portion of the ground water within the WIPP-site boundaries passes through the high-transmissivity zone south of H-15 and exits the southern boundary of the model area near H-9. The model-calculated flow directions support conclusions from previous modeling and isotopic studies that the ground-water chemistry is not at steady state with respect to ground-water flow.

- The calculated Darcy velocities range over six orders of magnitude in the model area. The highest velocities ( $5 \times 10^{-7}$  to  $5 \times 10^{-8}$  m/s) occur in the western portion of the model area representing Nash Draw. Darcy velocities within the WIPP-site boundary range from approximately  $1 \times 10^{-10}$  m/s in the vicinity of the shafts to  $1 \times 10^{-9}$  m/s in the high-transmissivity zone south of H-11. Darcy velocities of  $1 \times 10^{-12}$  m/s occur east of the WIPP-site boundary.
- The transient calibrated transmissivities reproduce the observed transient heads reasonably well. The calculated drawdowns are quite close to the drawdowns observed during the multipad pumping tests and shaft excavations. The transient calibrated transmissivities do not adequately reproduce the observed transient responses generated from the air-intake shaft excavation. Sensitivity analyses indicate that a 50-percent increase in leakage into the air-intake shaft greatly reduces the differences between the observed and calculated transient heads for the central WIPP-site boreholes. The increase in leakage at the air-intake shaft is about 30 percent higher than the measured data. However, the effects of ventilation in the air-intake shaft could reduce the amount of inflow measured. The transient heads at the central boreholes virtually coincide with the observed heads if an additional leakage of 0.012 L/s is specified at the exhaust shaft from late 1987 to the present. There are no inflow data available during this time to determine whether leakage at the exhaust shaft is in fact occurring.
- The particle travel time to the WIPP-site boundary from a point in the Culebra coincident with the centroid of the waste panels, assuming porous-media flow and a porosity of 16 percent, is approximately  $1.4 \times 10^4$  yrs, which is very similar to the

travel time presented in LaVenue et al. (1988). Even though the transmissivities are higher along the flow path determined in this study, the length of the flow path is longer than that determined in LaVenue et al. (1988).

- Sensitivity analyses indicate that (1) the calculated steady-state heads within the WIPP-site boundary are most sensitive to changes in the transmissivities and specified boundary pressures in the northwest part of the model, and (2) the particle travel time to the southern WIPP-site boundary from a point in the Culebra coincident with the centroid of the waste panels is sensitive to changes in the transmissivities along the flow path and the pressures assigned to the northwest boundary. However, the extent of data coverage and the magnitude of data uncertainty within the model provides bounds to the flexibility one has in changing the transmissivities and specified boundary pressures in the northwest part of the model area. That is, even though the model is sensitive to the parameters in the northwest model region, the calibration to the steady-state heads in this area would be degraded if significant changes to either the transmissivities or boundary pressures were implemented. Therefore, the existing data set provides a high level of confidence in the calibrated transmissivity distribution and steady-state Darcy velocity distribution.

## 8.0 REFERENCES

- Andrews, R.W., V.A. Kelley, J.A. McNeish, A.M. LaVenue, and J.E. Campbell, 1986. Travel Path/Travel Time Uncertainties at Salt Sites Proposed for High-Level Waste Repositories. Prepared for Office of Nuclear Waste Isolation, Battelle Memorial Institute, Columbus, Ohio, 379 p.
- Avis, J.D. and G.J. Saulnier, Jr., 1990. Analysis of the Fluid-Pressure Responses of the Rustler Formation at H-16 to the Construction of the Air-Intake Shaft at the Waste Isolation Pilot Plant (WIPP) Site. Sandia National Laboratories, Contractor Report SAND89-7067.
- Bachman, G.O., 1980. Regional Geology and Cenozoic History of Pecos Region, South-Eastern, New Mexico. U.S. Geological Survey, Open-File Report 80-1099, 116 p.
- Bachman, G.O., 1985. Assessment of Near-Surface Dissolution at and Near the Waste Isolation Pilot Plant (WIPP), Southeastern New Mexico, Sandia National Laboratories, SAND84-7178, 33 p.
- Bachman, G.O., 1987. Karst Evaporites in Southwestern New Mexico. Sandia National Laboratories, SAND86-7078, 82 p.
- Barr, G.E., W.B. Miller, and D.D. Gonzalez, 1983. Interim Report on the Modeling of the Regional Hydraulics of the Rustler Formation. Sandia National Laboratories, SAND83-0391, 58 p.
- Bear, J., 1972. Dynamics of Fluids in Porous Media. American Elsevier Publishing Company, New York, 764 p.
- Beauheim, R.L., 1986. Hydraulic-Test Interpretations for Well DOE-2 at the Waste Isolation Pilot Plant (WIPP) Site. Sandia National Laboratories, SAND86-1364, 89 p.
- Beauheim, R.L., 1987a. Analysis of Pumping Tests of the Culebra Dolomite Conducted at the H-3 Hydropad at the Waste Isolation Pilot Plant (WIPP) Site. Sandia National Laboratories, SAND86-2311, 154 p.

- Beauheim, R.L., 1987b. Interpretations of Single-Well Hydraulic Tests Conducted at and Near the Waste Isolation Pilot Plant (WIPP) Site, 1983-1987. Sandia National Laboratories, SAND87-0039, 169 p.
- Beauheim, R.L., 1987c. Interpretation of the WIPP-13 Multipad Pumping Test of the Culebra Dolomite at the Waste Isolation Pilot Plant (WIPP) Site. Sandia National Laboratories, SAND87-2456, 171 p.
- Beauheim, R.L., 1988. "Scale Effects in Well Testing in Fractured Media." Proceedings: Fourth Canadian/American Conference on Hydrogeology: Fluid Flow, Heat Transfer and Mass Transport in Fractured Rocks, Banff, Alberta, Canada, June 21-24, 1988. Ed. B. Hitchon and S. Bachu. Dublin, Ohio: National Water Well Association, p. 152-159.
- Beauheim, R.L., 1989. Interpretation of H-11b4 Hydraulic Tests and the H-11 Multipad Pumping Test of the Culebra Dolomite at the Waste Isolation Pilot Plant (WIPP) Site. Sandia National Laboratories, SAND89-0536.
- Benjamin, J.R., and C.A. Cornell, 1970. Probability Statistics and Decisions for Civil Engineers, McGraw-Hill, New York.
- Carrera, J. and S.P. Neuman, 1986a. Estimation of aquifer parameters under transient and steady state conditions, 1, Maximum likelihood method incorporating prior information, Water Resources Research, Vol. 22, No. 2, p. 199-210.
- Carrera J. and S.P. Neuman, 1986b. Estimation of aquifer parameters under transient and steady state conditions, 2, Uniqueness, stability, and solution algorithms, Water Resources Research, Vol. 22, No. 2, p. 211-227.
- Cauffman, T.L., A.M. LaVenue, and J.P. McCord, 1990. Ground-Water Flow Modeling of the Culebra Dolomite: Volume II - Data Base. Sandia National Laboratories, Contractor Report SAND89-7068/2.
- Chapman, J.B., 1986. Stable Isotopes in Southeastern New Mexico Groundwater: Implications for Dating Recharge in the WIPP Area. New Mexico Environmental Evaluation Group, EEG-35, 76 p.

- Chaturvedi, L. and J.K. Channell, 1985. *The Rustler Formation as a Transport Medium for Contaminated Groundwater*. New Mexico Environmental Evaluation Group, EEG-32, 85 p.
- Chaturvedi, L. and K. Rehfeldt, 1984. *Groundwater Occurrence and the Dissolution of Salt at the WIPP Radioactive Waste Repository Site*. American Geophysical Union, EOS, July 3, 1984, p. 457-459.
- Chavent, G., 1971. *Analyse fonctionnelle et identification de coefficients repartis des les equations aux derivees partielles*. These de Docteur es Sciences, University of Paris, VI.
- Chavent, G., Dupuy, M., and P. Lemonier, 1975. *History matching by use of optimal control theory*, Soc. Pet. Eng. J., 15(1), p. 74-86.
- Cole, C.R. and F.W. Bond, 1980. *Assessment of Effectiveness of Geologic Isolation Systems: Comparison of INTERA and WISAP Consequence Model Application*. Report prepared by Pacific Northwest Laboratory for Office of Nuclear Waste Isolation under contract to U.S. Department of Energy, PNL-3070, 50 p.
- Cooper, J.B. and V.M. Glanzman, 1971. *Geohydrology of Project Gnome Site, Eddy County, New Mexico*. U.S. Geological Survey, Professional Paper 712-A, 24 p.
- D'Appolonia Consulting Engineers, Inc., 1981. *Modeling Verification Studies: Long-Term Waste Isolation Assessment*. Report prepared for Westinghouse Electric Corporation under contract to U.S. Department of Energy.
- David, M., 1977. *Geostatistical Ore Reserve Estimation*, Elsevier, New York.
- David, M., 1988. *Handbook of Applied Advanced Geostatistical Ore Reserve Estimation*. Elsevier, New York, NY, 216 p.
- Davies, P.B., 1989. *Variable-Density Ground-Water Flow and Paleohydrology in the Waste Isolation Pilot Plant (WIPP) Region, Southeastern New Mexico*. U.S. Geological Survey, Open-File Report 88-490, 139 p.



- de Marsily, G., 1978. De l'identification des systemes hydrogeologiques, These d'Etat, University of Paris VI, 900 p.
- de Marsily, G., G. Lavedan, M. Boucher, and G. Fasanino, 1984. Interpretation of interference tests in a well field using geostatistical techniques to fit the permeability distribution in a reservoir model, Second NATO Advanced Study Inst., GEOSTAT 1983 - Tahoe, CA, in proceedings "Geostatistics for Natural Resources Characterization" edited by G. Verly, M. David, A.G. Journel, and A. Marechal, pp. 831-849, D. Reidel, Hingham, Mass.
- de Marsily, G., 1986. Quantitative Hydrogeology. Academic Press, Inc., Orlando, Florida, 440 p.
- Delfiner, P., 1976. Linear estimation of nonstationary spatial phenomena in Advanced Geostatistics in the Mining Industry. edited by M. Guarascio, M. David, and C. Huijbregts, pp. 49-68, D. Reidel, Hingham, Mass.
- Delhomme, J.P., 1978. Kriging in the hydrosiences, Advan. Water Resour., 1(5), p. 251-266.
- Delhomme, J.P., 1979. Spatial variability and uncertainty in groundwater flow parameters: A geostatistical approach, Water Resour. Res., 15(2), p. 269-280.
- Deshler, R. and R. McKinney, 1988. Construction and Water Inflow Histories for the Shafts at the Waste Isolation Pilot Plant. Report prepared by IT Corporation.
- Dettinger, M.D., and J.L. Wilson, 1981. First-order analysis of uncertainty in numerical models of groundwater flow, 1, Mathematical development, Water Resour. Res., 17(1), p. 149-161.
- Finley, N.C. and M. Reeves, 1981. SWIFT Self-Teaching Curriculum: Illustrative Problems to Supplement the User's Manual for the Sandia Waste-Isolation Flow and Transport Model (SWIFT). Sandia National Laboratories, NUREG/CR-1968, SAND81-0410, 169 p.

- Freeze, R.A. and J.A. Cherry, 1979. *Groundwater*. Prentice-Hall, Inc., Englewood Cliffs, New Jersey, 604 p.
- Gonzales, M.M., 1989. *Compilation and Comparison of Test-Hole Location Surveys in the Vicinity of the Waste Isolation Pilot Plant (WIPP) Site*. Sandia National Laboratories, SAND88-1065.
- Haug, A., V.A. Kelley, A.M. LaVenue, and J.F. Pickens, 1987. *Modeling of Ground-Water Flow in the Culebra Dolomite at the Waste Isolation Pilot Plant (WIPP) Site: Interim Report*. Sandia National Laboratories, Contractor Report SAND86-7167.
- Hoeksema, R.J., and P.K. Kitanidis, 1984. *An application of the geostatistical approach to the inverse problem in two-dimensional ground-water modeling*, *Water Resources Res.*, 20(7), p. 1003-1020.
- Holt, R.M. and D.W. Powers, 1984. *Geotechnical Activities in the Waste Handling Shaft, Waste Isolation Pilot Plant (WIPP) Project, Southeastern New Mexico*. U.S. Department of Energy, WTSD-TME-038.
- Holt, R.M. and D.W. Powers, 1988. *Facies Variability and Post-Depositional Alteration Within the Rustler Formation in the Vicinity of the Waste Isolation Pilot Plant, Southeastern New Mexico*. U.S. Department of Energy, DOE/WIPP-88-04.
- Hydro Geo Chem, Inc., 1985. *WIPP Hydrology Program, Waste Isolation Pilot Plant, SENM, Hydrologic Data Report #1*. Sandia National Laboratories, Contractor Report SAND85-7206, 710 p.
- INTERA Environmental Consultants, Inc., 1983. *Adjoint sensitivity theory for steady-state ground-water flow*, Prepared for Office of Nuclear Waste Isolation, Battelle Memorial Institute, Columbus, Ohio, BMI/ONWI-515.
- INTERA Environmental Consultants, Inc., 1984a. *First status report on regional and local ground-water flow modeling for the Richton Dome, Mississippi*, prepared for Office of Nuclear Waste Isolation, Battelle Memorial Institute, Columbus, Ohio, BMI/ONWI-502.

**INTERA Environmental Consultants, Inc., 1984b. First status report on regional and local ground-water flow modeling for the Paradox Basin, Utah, prepared for Office of Nuclear Waste Isolation, Battelle Memorial Institute, Columbus, Ohio, BMI/ONWI-503.**

**INTERA Environmental Consultants, Inc., 1984c. First status report on regional and local ground-water flow modeling for the Palo Duro Basin, Texas, prepared for Office of Nuclear Waste Isolation, Battelle Memorial Institute, Columbus, Ohio, BMI/ONWI-504.**

**INTERA Technologies, Inc., 1986. WIPP Hydrology Program, Waste Isolation Pilot Plant, SENM, Hydrologic Data Report #3. Sandia National Laboratories, Contractor Report SAND86-7109.**

**INTERA Technologies, Inc. and Hydro Geo Chem, Inc., 1985. WIPP Hydrology Program, Waste Isolation Pilot Plant, SENM, Hydrologic Data Report #2. Sandia National Laboratories, Contractor Report SAND85-7263.**

**Izette, G.A. and R.E. Wilcox, 1982. Map Showing Localities and Inferred Distributions of the Huckleberry Ridge, Mesa Falls and Lava Creek Ash Beds (Pearlette Family Ash Beds) of Pliocene and Pleistocene Age in the Western United States and Southern Canada. U.S. Geological Survey, Miscellaneous Investigations Series Map I-1325.**

**Jones, C.L., 1959. Thickness, Character, and Structure of the Upper Permian Evaporites in Part of Eddy County, Southeast New Mexico. U.S. Geological Survey, Trace Elements Memorandum Report #1033, 19 p.**

**Jones, C.L., 1973. Salt Deposits of Los Medaños Area, Eddy and Lea Counties, New Mexico. U.S. Geological Survey, Open-File Report 4339-7, 67 p.**

**Jones, C.L., 1975. Potash Resources in Part of Los Medaños Area of Eddy and Lea Counties, New Mexico. U.S. Geological Survey, Open-File Report 75-407, 37 p.**

- Jones, C.L., 1978. Test Drilling for Potash Resources: Waste Isolation Pilot Plant Site, Eddy County, New Mexico. U.S. Geological Survey, Open-File Report 78-592, V. 1 & 2, 431 p.
- Journel, A.G., and C.T. Huijbregts, 1978. Mining Geostatistics, 600 p., Academic, New York.
- Kafritsas, J. and R.L. Bras, 1981. The Practice of Kriging, Technical Report 263, Ralph M. Parsons Lab., Mass. Inst. of Technol., Cambridge, 107 p.
- Kitanidis, P.K., and E.G. Vomvoris, 1983. A geostatistical approach to the inverse problem in groundwater modeling (steady state) and one-dimensional simulations, Water Resour. Res., 19, p. 677-690.
- Kelley, V.A. and J.F. Pickens, 1986. Interpretation of the Convergent-Flow Tracer Tests Conducted in the Culebra Dolomite at the H-3 and H-4 Hydropads at the Waste Isolation Pilot (WIPP) Site. Sandia National Laboratories, Contractor Report SAND86-7161.
- Kelley, V.A. and G.J. Saulnier, Jr., 1990. Core Analysis for Selected Samples From the Culebra Dolomite at the Waste Isolation Pilot Plant (WIPP) Site. Sandia National Laboratories, Contractor Report SAND90-7011. In review.
- Kuchling, H., 1982. Taschenbuch der Physik. Verlag Harri Deutsch, Thun und Frankfurt, 678 p.
- Lambert, S.J., 1987. Feasibility Study: Applicability of Geochronologic Methods Involving Radiocarbon and Other Nuclides to the Groundwater Hydrology of the Rustler Formation. Sandia National Laboratories, SAND86-1054.
- Lambert, S.J. and J.A. Carter, 1987. Uranium-Isotope Systematics in Groundwaters of the Rustler Formation, Northern Delaware Basin, Southeastern New Mexico. Sandia National Laboratories, SAND87-0388.

- Lambert, S.J. and D.M. Harvey, 1987. Stable Isotope Geochemistry of Groundwaters in the Delaware Basin of Southeastern New Mexico. Sandia National Laboratories, SAND87-0138.
- Langguth, H.R. and R. Voigt, 1980. Hydrogeologische Methoden. Springer-Verlag, New York, 486 p.
- Lappin, A.R., R.L. Hunter, D.P. Garber, and P.B. Davies, 1989 (Editors). Systems Analysis, Long-Term Radionuclide Transport, and Dose Assessments, Waste Isolation Pilot Plant (WIPP), Southeastern New Mexico; March 1989. Sandia National Laboratories, SAND89-0462.
- LaVenue A.M., A. Haug, and V.A. Kelley, 1988. Numerical Simulation of Ground-Water Flow in the Culebra Dolomite at the Waste Isolation Pilot Plant (WIPP) Site: Second Interim Report. Sandia National Laboratories, Contractor Report SAND88-7002.
- LaVenue A.M., R.W. Andrews, and B.S. RamaRao, 1989. Groundwater Travel Time Uncertainty Analysis Using Sensitivity Derivatives. Water Resources Research, Vol. 25, No. 7, p 1551-1566.
- Lerman, A., 1979. Geochemical Processes. John Wiley and Sons, New York, 481 p.
- Lowenstein, T.K., 1987. Post Burial Alteration of the Permian Rustler Formation Evaporites, WIPP Site, New Mexico: Textural, Stratigraphic and Chemical Evidence. New Mexico Environmental Evaluation Group, EEG-36, 56 p.
- Lyon, M.L., 1989. Annual Water Quality Data Report for the Waste Isolation Pilot Plant, April 1989. DOE/WIPP 89-001.
- Matheron, G., 1971. The Theory of Regionalized Variables and its Applications, Ecole des Mines, Fontainebleau, France.
- Matheron, G., 1976. A simple substitute for conditional expectation: The disjunctive kriging. in M. Guarascio, et al. (Eds.), Advanced Geostatistics in the Mining Industry, D. Reidel: Dordrecht, p. 221-236.

- Mercer, J.W., 1983. Geohydrology of the Proposed Waste Isolation Pilot Plant Site, Los Medaños Area, Southeastern New Mexico. U.S. Geological Survey, Water-Resources Investigations 83-4016, 113 p.
- Mercer, J.W., R.L. Beauheim, R.P. Snyder, and G.M. Fairer, 1987. Basic Data Report for Drilling and Hydrologic Testing of Drillhole DOE-2 at the Waste Isolation Pilot Plant (WIPP) Site. Sandia National Laboratories, SAND86-0611.
- Metcalf, D.E., J.E. Campbell, B.S. RamaRao, and W.V. Harper, 1985. Geostatistical and adjoint sensitivity techniques applied to a conceptual model of ground-water flow in the Paradox Basin, Utah, paper presented at Waste Management '85, Univ. of Arizona, Tucson.
- Myers, D.E., 1982. Matrix formulation of co-kriging. *Mathematical Geology*, 14, p. 249-257.
- Myers, D.E., 1984. Co-kriging-New developments. in G. Verly et al. (Eds.), *Geostatistics for Natural Resources Characterization*. D. Reidel: Dordrecht, p. 295-305.
- Narasimhan, T.N., and B.Y. Kanehiro, 1980. A Note on the Meaning of Storage Coefficient. *Water Resources Research*, Vol. 16, No. 2, p. 423-429.
- Neuman, S.P., 1980a. Adjoint-state finite element equations for parameter estimation, paper presented at 3rd International Conference on Finite Elements in Water Resources, Univ. of Miss., Oxford, May 19-23.
- Neuman, S.P., 1980b. A statistical approach to the inverse problem of aquifer hydrology, 3, Improved solution method and added perspective, *Water Resources Research*, Vol. 16, No. 2, p. 331-346.
- Neuman, S.P., 1982. Statistical characterization of aquifer heterogeneities: An overview, in *Recent Trends in Hydrogeology*, Geol. Soc. Am. Spec. Pap., 184, p. 81-102.

Niou, S. and J. Pietz, 1987. A Statistical Inverse Analysis of the H-3 Hydropad Pumping Test. Report prepared by IT Corporation, Inc. for Westinghouse Electric Corporation.

Olea, R.A., 1975a. Optimum mapping techniques using regionalized variable theory, Ser. Spatial Anal. 2, 137 pp., Kans. Geol. Surv., Lawrence.

Olea, R.A., 1975b. Measuring spatial dependence with semivariograms, Ser. Spatial Anal. 3, 24 pp., Kans. Geol. Surv., Lawrence.

Powers, D.W., and R.M. Holt, 1984. Depositional environments and dissolution in the Rustler Formation (Permian), southeastern New Mexico. (Abs.) Geol. Soc. Amer., 97th Annual Meeting Abstracts with Program, V. 16, No. 6, p. 627.

Powers, D.W., S.J. Lambert, S.E. Shaffer, L.R. Hill, and W.D. Weart, 1978 (Editors). Geologic Characterization Report, Waste Isolation Pilot Plant (WIPP) Site, Southeastern New Mexico. Volumes I and II. Sandia National Laboratories, SAND78-1596.

RamaRao, B.S., and M. Reeves, 1990. Theory and verification for the GRASP II code for adjoint-sensitivity analysis of steady-state and transient ground-water flow. Sandia National Laboratories, Contractor Report SAND89-7143.

Randall, W.S., M.E. Crawley, and M.L. Lyon, 1988. 1988 Annual Water Quality Data Report for the Waste Isolation Pilot Plant, March 1988. Westinghouse Electric Corporation, Report DOE-WIPP-88-006.

Reeves, M., D.S. Ward, N.D. Johns, and R.M. Cranwell, 1986a. Theory and Implementation for SWIFT II, the Sandia Waste-Isolation Flow and Transport Model, Release 4.84. Sandia National Laboratories, NUREG/CR-3328 and SAND83-1159, 189 p.

- Reeves, M., D.S. Ward, N.D. Johns, and R.M. Cranwell, 1986b. Data Input Guide for SWIFT II, the Sandia Waste-Isolation Flow and Transport Model for Fractured Media, Release 4.84. Sandia National Laboratories, NUREG/CR-3162 and SAND83-0242, 144 p.
- Reeves, M., V.A. Kelley, and J.F. Pickens, 1987. Regional Double-Porosity Solute Transport in the Culebra Dolomite: An Analysis of Parameter Sensitivity and Importance at the Waste Isolation Pilot Plant (WIPP) Site. Sandia National Laboratories, Contractor Report SAND87-7105.
- Richey, S.F., 1989. Geologic and Hydrologic Data for the Rustler Formation Near the Waste Isolation Pilot Plant, Southeastern New Mexico. U.S. Geological Survey, Open File Report 89-32.
- Roberts, D.L., 1985. Waste Shaft Grouting Report. Report prepared by Bechtel National, Inc.
- Robinson, K.L., 1987. Analysis of Solutes in Groundwaters from the Rustler Formation at and Near the WIPP Site. Sandia National Laboratories, SAND86-0917.
- Robinson, T.W. and W.B. Lang, 1938. Geology and Ground-Water Conditions of the Pecos River Valley in the Vicinity of Laguna Grande de la Sal, New Mexico. New Mexico State Engineer, 12th & 13th Biennial Reports, p. 77-100.
- Samper, F.J. and S.P. Neuman, 1986. Adjoint state equations for advective-dispersive transport, in Finite Elements in Water Resources, Proc. 6th Int. Conf., Lisbon, Portugal, p. 423-438.
- Sandia Laboratories and U.S. Geological Survey, 1979a. Basic Data Report for Drillhole WIPP 13 (Waste Isolation Pilot Plant - WIPP). Sandia Laboratories, SAND79-0273, 16 p.
- Sandia Laboratories and U.S. Geological Survey, 1979b. Basic Data Report for Drillhole WIPP 25 (Waste Isolation Pilot Plant - WIPP). Sandia Laboratories, SAND79-0279, 26 p.



Sandia Laboratories and U.S. Geological Survey, 1979c. Basic Data Report for Drillhole WIPP 26 (Waste Isolation Pilot Plant - WIPP). Sandia Laboratories, SAND79-0280, 31 p.

Sandia Laboratories and U.S. Geological Survey, 1979d. Basic Data Report for Drillhole WIPP 27 (Waste Isolation Pilot Plant - WIPP). Sandia Laboratories, SAND79-0281, 20 p.

Sandia Laboratories and U.S. Geological Survey, 1979e. Basic Data Report for Drillhole WIPP 28 (Waste Isolation Pilot Plant - WIPP). Sandia Laboratories, SAND79-0282, 33 p.

Sandia Laboratories and U.S. Geological Survey, 1979f. Basic Data Report for Drillhole WIPP 29 (Waste Isolation Pilot Plant - WIPP). Sandia Laboratories, SAND79-0283, 19 p.

Sandia Laboratories and U.S. Geological Survey, 1980a. Basic Data Report for Drillhole WIPP 18 (Waste Isolation Pilot Plant - WIPP). Sandia Laboratories, SAND79-0275, 18 p.

Sandia Laboratories and U.S. Geological Survey, 1980b. Basic Data Report for Drillhole WIPP 19 (Waste Isolation Pilot Plant - WIPP). Sandia Laboratories, SAND79-0276, 27 p.

Sandia Laboratories and U.S. Geological Survey, 1980c. Basic Data Report for Drillhole WIPP 21 (Waste Isolation Pilot Plant - WIPP). Sandia Laboratories, SAND79-0277, 18 p.

Sandia Laboratories and U.S. Geological Survey, 1980d. Basic Data Report for Drillhole WIPP 22 (Waste Isolation Pilot Plant - WIPP). Sandia Laboratories, SAND79-0278, 21 p.

Sandia Laboratories and U.S. Geological Survey, 1980e. Basic Data Report for Drillhole WIPP 30 (Waste Isolation Pilot Plant - WIPP). Sandia Laboratories, SAND79-0284, 19 p.

Sandia National Laboratories, 1982. Simulated-Waste Experiments Planned for the Waste Isolation Pilot Plant (WIPP). Sandia National Laboratories, SAND82-0547, 62 p.

Sandia National Laboratories and D'Appolonia Consulting Engineers, 1982a. Basic Data Report for Drillhole WIPP 12 (Waste Isolation Pilot Plant - WIPP). Sandia National Laboratories, SAND82-2336, 62 p.

Sandia National Laboratories and D'Appolonia Consulting Engineers, 1982b. Basic Data Report for Deepening of Drillhole WIPP 13 (Waste Isolation Pilot Plant - WIPP). Sandia National Laboratories, SAND82-1880, 54 p.

Sandia National Laboratories and D'Appolonia Consulting Engineers, 1982c. Basic Data Report for Drillhole WIPP 14 (Waste Isolation Pilot Plant - WIPP). Sandia National Laboratories, SAND82-1783, 36 p.

Sandia National Laboratories and D'Appolonia Consulting Engineers, 1983a. Basic Data Report for Drillhole AEC 7 (Waste Isolation Pilot Plant - WIPP). Sandia National Laboratories, SAND79-0268, 96 p.

Sandia National Laboratories and D'Appolonia Consulting Engineers, 1983b. Basic Data Report for Drillhole AEC 8 (Waste Isolation Pilot Plant - WIPP). Sandia National Laboratories, SAND79-0269, 100 p.

Sandia National Laboratories and D'Appolonia Consulting Engineers, 1983c. Basic Data Report for Drillhole ERDA 10 (Waste Isolation Pilot Plant - WIPP). Sandia National Laboratories, SAND79-0271, 78 p.

Sandia National Laboratories and U.S. Geological Survey, 1980. Basic Data Report for Drillhole WIPP 32 (Waste Isolation Pilot Plant - WIPP). Sandia National Laboratories, SAND80-1102, 25 p.

Sandia National Laboratories and U.S. Geological Survey, 1981a. Basic Data Report for Drillhole WIPP 33 (Waste Isolation Pilot Plant - WIPP). Sandia National Laboratories, SAND80-2011, 27 p.

Sandia National Laboratories and U.S. Geological Survey, 1981b. Basic Data Report for Drillhole WIPP 34 (Waste Isolation Pilot Plant - WIPP). Sandia National Laboratories, SAND81-2643, 52 p.

Sandia National Laboratories and U.S. Geological Survey, 1982. Basic Data Report for Drillhole WIPP 11 (Waste Isolation Pilot Plant - WIPP). Sandia National Laboratories, SAND79-0272, 28 p.

Sandia National Laboratories and U.S. Geological Survey, 1983a. Basic Data Report for Drillhole ERDA 6 (Waste Isolation Pilot Plant - WIPP). Sandia National Laboratories, SAND79-0267, 64 p.

Sandia National Laboratories and U.S. Geological Survey, 1983b. Basic Data Report for Drillhole ERDA 9 (Waste Isolation Pilot Plant - WIPP). Sandia National Laboratories, SAND79-0270, 54 p.

Sandia National Laboratories and University of New Mexico, 1981. Basic Data Report for Drillhole WIPP 15 (Waste Isolation Pilot Plant - WIPP). Sandia National Laboratories, SAND79-0274, 31 p.

Saulnier, G.J., Jr., 1987. Analysis of Pumping Tests of the Culebra Dolomite Conducted at the H-11 Hydropad at the Waste Isolation Pilot Plant (WIPP) Site. Sandia National Laboratories, Contractor Report SAND87-7124.

Saulnier, G.J., Jr., G.A. Freeze, and W.A. Stensrud, 1987. WIPP Hydrology Program, Waste Isolation Pilot Plant, Southeastern New Mexico, Hydrologic Data Report #4. Sandia National Laboratories, Contractor Report SAND86-7166.

Snyder, R.P., 1985. Dissolution of Halite and Gypsum, and Hydration of Anhydrite to Gypsum, Rustler Formation in the Vicinity of the Waste-Isolation Pilot Plant, Southeastern New Mexico. U.S. Geological Survey, Open-File Report 85-229, 11 p.

Stensrud, W.A., M.A. Bame, K.D. Lantz, A.M. LaVenue, J.B. Palmer, and G.J. Saulnier, Jr., 1987. WIPP Hydrology Program, Waste Isolation Pilot Plant, Southeastern New Mexico, Hydrologic Data Report #5. Sandia National Laboratories, Contractor Report SAND87-7125.

- Stensrud, W.A., M.A. Bame, K.D. Lantz, T.L. Cauffman, J.B. Palmer, and G.J. Saulnier, Jr., 1988a. WIPP Hydrology Program, Waste Isolation Pilot Plant, Southeastern New Mexico, Hydrologic Data Report #6. Sandia National Laboratories, Contractor Report SAND87-7166.
- Stensrud, W.A., M.A. Bame, K.D. Lantz, J.B. Palmer, and G.J. Saulnier, Jr., 1988b. WIPP Hydrology Program, Waste Isolation Pilot Plant, Southeastern New Mexico, Hydrologic Data Report #7. Sandia National Laboratories, Contractor Report SAND88-7014.
- Stensrud, W.A., M.A. Bame, K.D. Lantz, J.B. Palmer, and G.J. Saulnier, Jr., 1990. WIPP Hydrology Program, Waste Isolation Pilot Plant, Southeastern New Mexico, Hydrologic Data Report #8. Sandia National Laboratories, Contractor Report SAND89-7056.
- Stevens, K. and W. Beyeler, 1985. Determination of Diffusivities in the Rustler Formation from Exploratory Shaft Construction at the Waste Isolation Pilot Plant in Southeastern New Mexico. U.S. Geological Survey Water-Resources Investigations Report 85-4020, 32 p.
- Sykes, J.F. and J.L. Wilson, 1984. Adjoint sensitivity theory for the finite element method, paper presented at 5th International Conference on Finite Elements in Water Resources, Burlington, Vermont, U.S.A.
- Sykes, J.F., J.L. Wilson, and R.W. Andrews, 1985. Sensitivity Analysis for Steady State Groundwater Flow Using Adjoint Operators. Water Resources Research, Vol. 21, No. 3, p. 359-371.
- Townley, L.R. and J.L. Wilson, 1985. Computationally efficient algorithms for parameter estimation and uncertainty propagation in numerical models of groundwater flow, Water Resources Research, Vol. 21, No. 1, p. 1581-1860.
- Uhland, D.W. and W.S. Randall, 1986. 1986 Annual Water Quality Data Report for the Waste Isolation Pilot Plant, September 1986. Westinghouse Electric Corporation Report DOE-WIPP-86-006.

Uhland, D.W., W.S. Randall, and R.C. Carrasco, 1987. 1987 Annual Water Quality Data Report for the Waste Isolation Pilot Plant, March 1987, Westinghouse Electric Corporation Report DOE-WIPP-87-006.

U.S. Department of Energy, 1980a. Final Environmental Impact Statement, Waste Isolation Pilot Plant, DOE/EIS-0026, Volume 2, U.S. Government Printing Office, Washington, D.C.

U.S. Department of Energy, 1980b. Waste Isolation Pilot Plant, Safety Analysis Report. Volumes 1-5.

U.S. Department of Energy, 1986. Design Validation Final Report: U.S. Department of Energy Report DOE-WIPP 86-010.

Vine, J.D., 1963. Surface Geology of the Nash Draw Quadrangle, Eddy County, New Mexico. U.S. Geological Survey, Bulletin 1141-B, 46 p.

Wackernagel, H., 1989. Overview of methods for coregionalization analysis. in M. Armstrong (ed.), Geostatistics, Kluwer Academic Publishers: Dordrecht, p. 409-420.

Ward, D.S., M. Reeves, and L.E. Duda, 1984. Verification and Field Comparison of the Sandia Waste-Isolation Flow and Transport Model (SWIFT). Sandia National Laboratories, NUREG/CR-3316 and SAND83-1154, 155 p.

Wilson, J.L. and D. Metcalfe, 1985. Illustration and verification of adjoint sensitivity theory for steady-state groundwater flow, Water Resources Research, Vol. 21, No. 3, p. 1602-1610.

Wilson, J.L., B.S. RamaRao, and J.A. McNeish, 1986. GRASP: A Computer Code to Perform Post-SWENT Adjoint Sensitivity Analysis of Steady State Groundwater Flow, BMI/ONWI-625. Prepared for Office of Nuclear Waste Isolation, Battelle Memorial Institute, Columbus, Ohio.

Yeh, W.W.-G., 1986. Review of parameter identification procedures in groundwater hydrology: Inverse problem, Water Resources Research, Vol. 22, No. 2, p. 95-108.

**FEDERAL AGENCIES**

U. S. Department of Energy, (5)  
Office of Civilian Radioactive Waste  
Management

Attn: Deputy Director, RW-2  
Associate Director, RW-10  
Office of Program Administration  
and Resources Management  
Associate Director, RW-20  
Office of Facilities Siting  
and Development  
Associate Director, RW-30  
Office of Systems Integration  
and Regulations  
Associate Director, RW-40  
Office of External Relations  
and Policy

Forrestal Building  
Washington, DC 20585

U. S. Department of Energy (3)  
Albuquerque Operations Office

Attn: J. E. Bickel  
R. Marquez, Director  
Public Affairs Division

P.O. Box 5400  
Albuquerque, NM 87185

U. S. Department of Energy  
Attn: National Atomic Museum Library  
Albuquerque Operations Office  
P. O. Box 5400  
Albuquerque, NM 87185

U. S. Department of Energy (9)  
WIPP Project Office (Carlsbad)

Attn: A. Hunt (4)  
V. Daub (2)  
J. A. Mewhinney  
R. Batra  
J. Carr

P.O. Box 3090  
Carlsbad, NM 88221

U. S. Department of Energy  
Research & Waste Management Division

Attn: Director  
P. O. Box E  
Oak Ridge, TN 37831

U.S. Department of Energy  
Richland Operations Office  
Nuclear Fuel Cycle & Production  
Division  
Attn: R. E. Gerton  
P.O. Box 500  
Richland, WA 99352

U. S. Department of Energy (1)  
Attn: Edward Young  
Room E-178  
GAO/RCED/GTN  
Washington, DC 20545

U. S. Department of Energy (6)  
Office of Environmental Restoration  
and Waste Management  
Attn: Jill Lytle, EM30  
Mark Frei, EM-34 (3)  
Mark Duff, EM-34  
Clyde Frank, EM-50  
Washington, DC 20585

U. S. Department of Energy (3)  
Office of Environment, Safety  
and Health  
Attn: Ray Pelletier, EH-231  
Kathleen Taimi, EH-232  
Carol Borgstrom, EH-25  
Washington, DC 20585

U. S. Department of Energy (2)  
Idaho Operations Office  
Fuel Processing and Waste  
Management Division  
785 DOE Place  
Idaho Falls, ID 83402

U.S. Department of Energy  
Savannah River Operations Office  
Defense Waste Processing  
Facility Project Office  
Attn: W. D. Pearson  
P.O. Box A  
Aiken, SC 29802

U.S. Environmental Protection Agency (2)  
Attn: Ray Clark  
Office of Radiation Programs (ANR-460)  
Washington, DC 20460

U.S. Geological Survey  
Branch of Regional Geology  
Attn: R. Snyder  
MS913, Box 25046  
Denver Federal Center  
Denver, CO 80225

U.S. Geological Survey  
Conservation Division  
Attn: W. Melton  
P.O. Box 1857  
Roswell, NM 88201

U.S. Geological Survey (1)  
Water Resources Division  
Attn: Kathy Peter  
Suite 200  
4501 Indian School, NE  
Albuquerque, NM 87110

U.S. Nuclear Regulatory Commission (4)  
Attn: Joseph Bunting, HLEN 4H3 OWFN  
Ron Ballard, HLGP 4H3 OWFN  
Jacob Philip  
NRC Library  
Mail Stop 623SS  
Washington, DC 20555



Boards

Defense Nuclear Facilities Safety Board  
Attn: Dermot Winters  
Suite 675  
600 E Street, NW  
Washington, DC 20004

U. S. Department of Energy  
Advisory Committee on Nuclear  
Facility Safety  
Attn: Merritt E. Langston, AC21  
Washington, DC 20585

Nuclear Waste Technical  
Review Board (2)  
Attn: Dr. Don A. Deere  
Dr. Sidney J. S. Parry  
Suite 910  
1100 Wilson Blvd.  
Arlington, VA 22209-2297

Richard Major  
Advisory Committee  
on Nuclear Waste  
Nuclear Regulatory Commission  
7920 Norfolk Avenue  
Bethesda, MD 20814

George M. Hornberger  
Board on Radioactive Waste Management  
Department of Environmental Engineering  
Clark Hall  
University of Virginia  
Charlottesville, VA 22903

STATE AGENCIES

Environmental Evaluation Group (3)

Attn: Library

Suite F-2

7007 Wyoming Blvd., N.E.

Albuquerque, NM 87109

New Mexico Bureau of Mines

and Mineral Resources (2)

Attn: F. E. Kottolowski, Director

J. Hawley

Socorro, NM 87801

NM Department of Energy & Minerals

Attn: Librarian

2040 S. Pacheco

Santa Fe, NM 87505

NM Environmental Improvement Division

Attn: Deputy Director

1190 St. Francis Drive

Santa Fe, NM 87503

LABORATORIES/CORPORATIONS

**Battelle Pacific Northwest Laboratories (6)**

Attn: D. J. Bradley, K6-24  
J. Relyea, H4-54  
R. E. Westerman, P8-37  
S. Bates, K2-57  
H. C. Burkholder, P7-41  
L. Pederson, K6-47

Battelle Boulevard  
Richland, WA 99352

**Savannah River Laboratory (6)**

Attn: N. Bibler  
E. L. Albenisius  
M. J. Plodinec  
G. G. Wicks  
C. Jantzen  
J. A. Stone

Aiken, SC 29801

**George Dymmel**

SAIC

101 Convention Center Dr.  
Las Vegas, NV 89109

**INTERA Inc. (9)**

Attn: G. E. Grisak  
J. F. Pickens (7)  
A. Haug

Suite #300  
6850 Austin Center Blvd.  
Austin, TX 78731

**INTERA Inc. (3)**

Attn: Wayne Stensrud  
P.O. Box 2123  
Carlsbad, NM 88221

**INTERA Inc. (3)**

Attn: Marsh LaVenue  
8100 Mountain Road  
Suite #204D  
Albuquerque, NM 87110

IT Corporation (4)  
Attn: R. F. McKinney  
J. Myers  
P. Drez  
H. Dove  
Regional Office - Suite 700  
5301 Central Avenue, NE  
Albuquerque, NM 87108

IT Corporation (2)  
Attn: D. E. Deal  
P.O. Box 2078  
Carlsbad, NM 88221

Charles R. Hadlock  
Arthur D. Little, Inc.  
Acorn Park  
Cambridge, MA 02140-2390

Los Alamos Scientific Laboratory  
Attn: B. Erdal, CNC-11  
Los Alamos, NM 87545

Oak Ridge National Laboratory (4)  
Attn: T. F. Lomenick  
Box 2009  
Oak Ridge, TN 37831

RE/SPEC, Inc. (3)  
Attn: W. Coons  
P. F. Gnirk  
M. Wallace  
P.O. Box 14984  
Albuquerque NM 87191

RE/SPEC, Inc. (7)  
Attn: L. L. Van Sambeek  
G. Callahan  
T. Pfeifle  
J. L. Ratigan  
P. O. Box 725  
Rapid City, SD 57709

Center for Nuclear Waste  
Regulatory Analysis (4)  
Attn: P. K. Nair  
Southwest Research Institute  
6220 Culebra Road  
San Antonio, TX 78228-0510

Science Applications  
International Corporation  
Attn: Howard R. Pratt,  
Senior Vice President  
10260 Campus Point Drive  
San Diego, CA 92121

Science Applications  
International Corporation  
Attn: Michael B. Gross  
Ass't. Vice President  
Suite 1250  
160 Spear Street  
San Francisco, CA 94105

Systems, Science, and Software (2)  
Attn: E. Peterson  
P. Lagus  
Box 1620  
La Jolla, CA 92038

Westinghouse Electric Corporation (7)  
Attn: Library  
Lamar Trego  
W. P. Poirer  
W. R. Chiquelin  
V. F. Likar  
D. J. Moak  
R. F. Kehrman  
P. O. Box 2078  
Carlsbad, NM 88221

Weston Corporation (1)  
Attn: David Lechel  
Suite 1000  
5301 Central Avenue, NE  
Albuquerque, NM 87108

Durham Geological Association  
908 Town & Country Blvd.  
Suite 120  
Houston, TX 77024

GRAM, Inc.  
Attn: D. A. Zimmerman  
1709 Moon NE  
Albuquerque, NM 87111

UNIVERSITIES

University of Arizona  
Attn: J. G. McCray  
Department of Nuclear Engineering  
Tucson, AZ 85721

University of New Mexico (2)  
Geology Department  
Attn: D. G. Brookins  
Library  
Albuquerque, NM 87131

Pennsylvania State University  
Materials Research Laboratory  
Attn: Della Roy  
University Park, PA 16802

Texas A&M University (4)  
Center of Tectonophysics  
Attn: R. Carlson  
B. Johnson  
J. Russell  
E. Hoskins  
College Station, TX 77840

Texas A&M University  
Department of Geology  
Attn: P. A. Domenico  
College Station, TX 77840

New Mexico Tech (3)  
Department of Geoscience  
Attn: J. Wilson  
A. Gutjahr  
F. Phillips  
Socorro, NM 87801

G. Ross Heath  
College of Ocean  
and Fishery Sciences  
University of Washington  
Seattle, WA 98195

INDIVIDUALS

Dennis W. Powers  
Star Route Box 87  
Anthony, TX 79821

LIBRARIES

Thomas Brannigan Library  
Attn: Don Dresp, Head Librarian  
106 W. Hadley St.  
Las Cruces, NM 88001

Hobbs Public Library  
Attn: Ms. Marcia Lewis, Librarian  
509 N. Ship Street  
Hobbs, NM 88248

New Mexico State Library  
Attn: Ms. Ingrid Vollenhofer  
P.O. Box 1629  
Santa Fe, NM 87503

New Mexico Tech  
Martin Speere Memorial Library  
Campus Street  
Socorro, NM 87810

Pannell Library  
Attn: Ms. Ruth Hill  
New Mexico Junior College  
Lovington Highway  
Hobbs, NM 88240

WIPP Public Reading Room  
Attn: Director  
Carlsbad Public Library  
101 S. Halagueno St.  
Carlsbad, NM 88220

Government Publications Department  
General Library  
University of New Mexico  
Albuquerque, NM 87131

THE SECRETARY'S BLUE RIBBON PANEL ON WIPP

Dr. Thomas Bahr  
New Mexico Water Resources Institute  
New Mexico State University  
Box 3167  
Las Cruces, NM 88003-3167

Mr. Leonard Slosky  
Slosky and Associates  
Suite 1400  
Bank Western Tower  
1675 Tower  
Denver, Colorado 80202

Mr. Newal Squyres  
Eberle and Berlin  
P. O. Box 1368  
Boise, Idaho 83701

Dr. Arthur Kubo  
Vice President  
BDM International, Inc.  
7915 Jones Branch Drive  
McLean, VA 22102

Mr. Robert Bishop  
Nuclear Management Resources Council  
Suite 300  
1776 I Street, NW  
Washington, DC 20006-2496



NATIONAL ACADEMY OF SCIENCES, WIPP PANEL

Dr. Charles Fairhurst, Chairman  
Department of Civil and  
Mineral Engineering  
University of Minnesota  
500 Pillsbury Dr. SE  
Minneapolis, MN 55455

Dr. John O. Blomeke  
Route 3  
Sandy Shore Drive  
Lenoir City, TN 37771

Dr. John D. Bredehoeft  
Western Region Hydrologist  
Water Resources Division  
U.S. Geological Survey (M/S 439)  
345 Middlefield Road  
Menlo Park, CA 94025

Dr. Karl P. Cohen  
928 N. California Avenue  
Palo Alto, CA 94303

Dr. Fred M. Ernsberger  
250 Old Mill Road  
Pittsburgh, PA 15238

Dr. Rodney C. Ewing  
Department of Geology  
University of New Mexico  
200 Yale, NE  
Albuquerque, NM 87131

B. John Garrick  
Pickard, Lowe & Garrick, Inc.  
2260 University Drive  
Newport Beach, CA 92660

John W. Healy  
51 Grand Canyon Drive  
Los Alamos, NM 87544

Leonard F. Konikow  
U.S. Geological Survey  
431 National Center  
Reston, VA 22092

Jeremiah O'Driscoll  
505 Valley Hill Drive  
Atlanta, GA 30350

Dr. Christopher G. Whipple  
Electric Power Research Institute  
3412 Hillview Avenue  
Palo Alto, CA 94303

Dr. Peter B. Myers, Staff  
Director  
National Academy of Sciences  
Committee on Radioactive  
Waste Management  
2101 Constitution Avenue  
Washington, DC 20418

Dr. Geraldine Grubb  
Board on Radioactive  
Waste Management  
GF462  
2101 Constitution Avenue  
Washington, DC 20418

FOREIGN ADDRESSES

Studiecentrum Voor Kernenergie  
Centre D'Energie Nucleaire  
Attn: Mr. A. Bonne  
SCK/CEN  
Boeretang 200  
B-2400 Mol  
BELGIUM

Atomic Energy of Canada, Ltd. (2)  
Whiteshell Research Estab.  
Attn: Peter Haywood  
John Tait  
Pinewa, Manitoba, CANADA  
R0E 1L0

Dr. D. K. Mukerjee  
Ontario Hydro Research Lab  
800 Kipling Avenue  
Toronto, Ontario, CANADA  
M8Z 5S4

Mr. Francois Chenevier, Director (2)  
ANDRA  
Route du Panorama Robert Schumann  
B.P.38  
92266 Fontenay-aux-Roses Cedex  
FRANCE

Mr. Jean-Pierre Olivier  
OECD Nuclear Energy Agency  
Division of Radiation Protection  
and Waste Management  
38, Boulevard Suchet  
75016 Paris, FRANCE

Claude Sombret  
Centre D'Etudes Nucleaires  
De La Vallee Rhone  
CEN/VALRHO  
S.D.H.A. BP 171  
30205 Bagnols-Sur-Ceze  
FRANCE

Bundesministerium fur Forschung und  
Technologie  
Postfach 200 706  
5300 Bonn 2  
FEDERAL REPUBLIC OF GERMANY

Bundesanstalt für Geowissenschaften  
und Rohstoffe  
Attn: Michael Langer  
Klaus Schelkes  
Postfach 510 153  
3000 Hannover 51  
FEDERAL REPUBLIC OF GERMANY

Gesellschaft für Reaktorsicherheit  
Attn: Peter Bogorinski  
Schwertnergasse 1  
5000 Köln 1  
FEDERAL REPUBLIC OF GERMANY

Gesellschaft für Strahlen-und Umweltforschung mbH  
Attn: Richard Storck  
Theodor-Heuss-Str. 4  
D-3300 Braunschweig  
FEDERAL REPUBLIC OF GERMANY

Hahn-Meitner-Institut für Kernforschung  
Attn: Werner Lutze  
Glienicke Strasse 100  
100 Berlin 39  
FEDERAL REPUBLIC OF GERMANY

Institut für Tief Lagerung (4)  
Attn: K. Kuhn  
Theodor-Heuss-Strasse 4  
D-3300 Braunschweig  
FEDERAL REPUBLIC OF GERMANY

Kernforschung Karlsruhe  
Attn: K. D. Closs  
Postfach 3640  
7500 Karlsruhe  
FEDERAL REPUBLIC OF GERMANY

Physikalisch-Technische Bundesanstalt  
Attn: Peter Brenneke  
Postfach 33 45  
D-3300 Braunschweig  
FEDERAL REPUBLIC OF GERMANY

D. R. Knowles  
British Nuclear Fuels, plc  
Risley, Warrington, Cheshire WA3 6AS  
1002607 GREAT BRITAIN

Shingo Tashiro  
Japan Atomic Energy Research Institute  
Tokai-Mura, Ibaraki-Ken  
319-11 JAPAN

Netherlands Energy Research Foundation  
ECN (2)  
Attn: Tuen Deboer, Mgr.  
L. H. Vons  
3 Westerduinweg  
P.O. Box 1  
1755 ZG Petten  
THE NETHERLANDS

Rijksinstituut Voor Volksgezondheid en Milieuhygiene (RIVM) (2)  
Attn: Peter Glasbergen  
Seyed M. Hassanizandeh  
P. O. Box 1  
3720 BA Bilthoven  
THE NETHERLANDS

Svensk Karnbransleforsorjning AB  
Attn: Fred Karlsson  
Project KBS  
Karnbranslesakerhet  
Box 5864  
10248 Stockholm  
SWEDEN

NAGRA  
Attn: Stratis Vomvoris  
Parkstr. 23  
CH-5401 Baden  
SWITZERLAND

COLENCO  
Attn: Olivier Jaquet  
Parkstr. 27  
CH-5401 Baden  
SWITZERLAND

SANDIA INTERNAL

400 L. D. Tyler  
1510 J. W. Nunziato  
1520 C. W. Peterson  
1521 J. G. Arguello  
1521 H. S. Morgan  
3141 S. A. Landenberger (5)  
3141-1 C. L. Ward, (8) for DOE/OSTI  
3151 Supervisor (3)  
6000 V. L. Dugan, Acting  
6232 W. R. Wawersik  
6233 J. C. Eichelberger  
6233 J. L. Krumhansl  
6300 T. O. Hunter, Acting  
6310 T. E. Blejwas, Acting  
6313 T. Blejwas  
6340 W. D. Weart  
6340 S. Y. Pickering  
6341 R. C. Lincoln  
6341 Staff (7)  
6341 Sandia WIPP Central Files (10)  
6342 D. R. Anderson  
6342 Staff (11)  
6343 T. M. Schultheis  
6343 Staff (2)  
6344 E. Gorham  
6344 Staff (8)  
6344 P. B. Davies (7)  
6344 M. LaVenue  
6345 A. R. Lappin  
6345 Staff (9)  
6346 J. R. Tillerson  
6346 Staff (7)  
6350 W. C. Luth  
6416 E. J. Bonano  
6416 J. McCord  
6416 S. Conrad  
7223 C. Gotway  
8524 J. A. Wackerly (SNLL Library)  
9300 J. E. Powell  
9310 J. D. Plimpton  
9320 M. J. Navratil  
9325 R. L. Rutter  
9325 J. T. McIlmoyle  
9330 J. D. Kennedy  
9333 O. Burchett  
9333 J. W. Mercer  
9334 P. D. Seward



8232-2/070871



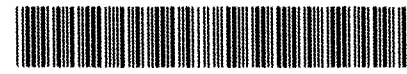
00000001 -



8232-2/070871



00000001 -



8232-2/070871



00000001 -

8524

8524-2